New drug therapies to kill TSC2-deficient cell lines

Henry Denis McCann

1467575

2019

Thesis submitted to Cardiff University in fulfilment of the of the requirements for the degree of Doctor of Philosophy

This thesis is dedicated to Dr. Padraic O'Neill, for all the support given throughout the years.

Publications

1. Johnson, Charlotte E., Dunlop, Elaine A., Seifan, Sara, **McCann, Henry D.**, Hay, Trevor, Parfitt, Geraint J., Jones, Ashley T., Giles, Peter J., Shen, Ming H., Sampson, Julian R., Errington, Rachel J., Davies, David Mark and Tee, Andrew R. 2018. Loss of tuberous sclerosis complex 2 sensitizes tumours to nelfinavir−bortezomib therapy to intensify endoplasmic reticulum stress-induced cell death. *Oncogene* 37, pp. 5913-5925

2. **McCann, Henry**, Johnson, Charlotte, Errington, Rachel, Davies, D. Mark, Dunlop, Elaine and Tee, Andrew 2018. Energy stress-mediated cytotoxicity in tuberous sclerosis complex 2-deficient cells with nelfinavir and mefloquine treatment. *Cancers* 10 (10), 375.

Contents

Figures and Tables

Figures

Tables

Declaration

STATEMENT 1

This thesis is being submitted in partial fulfilment of the requirements for the degree of ... (insert PhD, MD, MPhil, etc., as appropriate)

Signed

_____

Date

_____

STATEMENT 2

This work has not been submitted in substance for any other degree or award at this or any other university or place of learning, nor is it being submitted concurrently for any other degree or award (outside of any formal collaboration agreement between the University and a partner organisation).

Signed

_____

Date

_____

STATEMENT 3

I hereby give consent for my thesis, if accepted, to be available in the University's Open Access repository (or, where approved, to be available in the University's library and for inter-library loan), and for the title and summary to be made available to outside organisations, subject to the expiry of a University-approved bar on access if applicable.

Signed

_____

Date

_____

STATEMENT 4

This thesis is the result of my own independent work, except where otherwise stated, and the views expressed are my own. Other sources are acknowledged by explicit references. The thesis has not been edited by a third party beyond what is permitted by Cardiff University's Use of Third-Party Editors by Research Degree Students Procedure.

Signed

_____

Date

_____

WORD COUNT

_____

(Excluding summary, acknowledgements, declarations, contents pages, appendices, tables, diagrams and figures, references, bibliography, footnotes and endnotes

Acknowledgements

First and foremost, I would like to thank my supervisors, Dr. Andrew Tee, and Dr. David Davies for all their training, support and advice throughout this PhD and for giving me the opportunity to do this work. I would like to thank the Tuberous Sclerosis Association (TSA) for funding me and this project for the last 3 years.

I would also like to thank the members (present and former) of the Tee lab, Dr. Elaine Dunlop, Dr. Charlotte Johnson, Dr. Sara Seifen, Dr. Kayleigh Dodd and Dr. Ellie Rad for teaching me the techniques I needed for this project, and for all their advice and support throughout this PhD.

I would like to thank fellow PhD students, Ashley, Rachel and Elena, who were in the trenches with me during this thesis. Thank you for the support and friendship throughout the years and for the spontaneous games of poker and exploding kittens, and for the other randomness (Christmas decorations, fantasy football etc). I also like to thank to all the other PhD students who I have had the honour of calling friends during the last 3 years. Thank you all for your friendship and support.

I also need to thank my family and friends for all their love and support throughout the last three years. I would be nowhere without them and hope to make them proud in the future.

Special thanks go to my wonderful girlfriend, Anna. Thank you for all the love, support and advice throughout the years. Thank you for making those long trips from Nottingham/London to see me. Thank you for letting me live with you while I wrote this thesis.

Finally, I would like to thank Scott “Colt Cabana” Colton and Phil “CM Punk” Brooks – I wasn’t happy, so I made myself happy.

Abstract

Tuberous sclerosis complex (TSC) is a rare autosomal dominant genetic disorder which results in the global formation of hamartomas, along with epilepsy, autism and learning difficulties. TSC is caused by mutations in TSC1 and/or TSC2 genes, which are involved in regulating the mTOR pathway, an essential pathway involved in cell cycling, proliferation, survival and growth.

For non-surgically viable tumours, the use of mTOR inhibitors such as rapamycin (and rapalogs) have been shown to reduce tumour size and incidence of seizures and to improve intellectual and social development. However, these tumours will grow back rapidly when treatment ceases

Research has shown that mTOR-hyperactive cells have increased basal levels of endoplasmic reticulum (ER) stress compared to wildtype cells which could be seen as a potential drug target. Several combinations containing nelfinavir, a known ER stress enhancer, have been shown to selectively target *Tsc2*-/- mouse embryonic fibroblasts (MEFs) and mTOR-hyperactive sporadic cancer cells while being well tolerated by wildtype cells.

In this thesis, the key findings were the identification of three nelfinavir-based combinations (mefloquine, Bortezomib and cepharanthine). Results showed that optimised combinations caused selective cytotoxicity in *Tsc2*-/- MEFs and mTOR-hyperactive sporadic cancer cells while being tolerated by wildtype control cells (measured by DRAQ7 staining). All combinations caused cytotoxicity in a 3D environment (using tumour spheroids). The mechanism of action for each combination was investigated via several method including western blot analysis, rescue assays and RNA sequencing. Results show that mefloquine/nelfinavir and cepharanthine/nelfinavir combinations caused cell death via combined energy stress (cell death was rescued by the addition of methyl pyruvate) and potentially prolonged ER stress while the Bortezomib/nelfinavir combination caused cell death via prolonged ER stress and proteasome inhibition. This work highlights critical vulnerabilities in cancer cells with hyperactive mTORC1 activity that lack flexibility in homeostatic pathways.

Abbreviations

4E-BP1 – Eukaryotic translation initiation factor 4E (eIF4E)-binding protein 1

ACC1 – Acetyl-CoA carboxylase 1

ADHD – Attention-deficit/hyperactivity disorder

AKT – Acutely transforming retrovirus AKT8 in rodent T cell lymphoma

AMBRA1 – Autophagy/beclin 1 regulator 1

AML – Angiomyolipomas

AMPK – 5' adenosine monophosphate-activated protein kinase

ATF3 – Activating transcription factor 3

Atg13 – Autophagy-related protein 13

Atg101 – Autophagy-related protein 101

ATP – Adenosine triphosphate

ASD – Autism Spectrum Disorder

Baf – Bafilomycin A1

Bcl2 – B-cell lymphoma 2

BiP – Binding immunoglobulin protein

BSA – Bovine serum albumin

BTZ - Bortezomib

bZIP – Basic leucine zipper

CAD – Carbamoyl-phosphate synthase 2, aspartate transcarbamoylase and dihydroorotase

CASP – Caspase

CBD – Cannabidiols

CC – Chelerythrine chloride

CDK2 – Cyclin dependent kinase 2

Ceph - Cepharanthine

CHOP – CCAAT-enhancer-binding protein homologous protein

CK1 – Casein kinase 1

CPT1 – Carnitine palmitoyltransferase 1

COX-2 – Cyclooxygenase-2

CReP – Constitutive Repressor of eIF2α Phosphorylation

DCFDA – 2', 7' –dichlorofluorescin diacetate

DEPDC5 – DEP domain-containing protein 5

Deptor – DEP-domain-containing mTOR-interacting protein

DMEM – Dulbecco's Modified Eagle's Medium

DMSO – Dimethyl sulfoxide

Dox – Doxorubicin hydrochloride

DR5 – Death receptor 5

DTT – Dithiothreitol

eEF2K – Elongation factor 2 kinase

eIF2α – Eukaryotic initiation factor 2

eIF4E – Eukaryotic translation initiation factor 4E

ELT3 – Eker rat leiomyoma-derived cells

EMT – Epithelial-mesenchymal transition

ER – Endoplasmic reticulum

ERα – Estrogen receptor alpha

ERAD – ER associated degradation

ERK – Extracellular signal-regulated kinase

Eto – Etoposide

EXIST – EXamining everolimus In a Study of Tuberous Sclerosis Complex

FBS – Foetal bovine serum

FDA – Food and Drug Administration

FGF – Fibroblast Growth Factor

FLCN – Folliculin

FKBP12 – 12-kDa FK506-binding protein

FNIP – Folliculin interacting protein

FRB – FKBP12/rapamycin-binding

G6PD – Glucose-6-phosphate dehydrogenase

GADD34 – Growth arrest and DNA damage-inducible protein 34

GATOR - Gap Activity TOward Rags

GβL – G protein β-subunit like protein

GJIC – Gap junction protein alpha 1 (GJA1) gap junction intercellular communication

γH2AX – Gamma H2A histone family member X

GEF – Guanine nucleotide-exchange factor

GLUT4 – Glucose transporter type 4

GSK3β – Glycogen synthase kinase 3 beta

GRP94 – Glucose-regulated protein 94

HBXIP – Hepatitis B Virus X-interacting protein

HER2 – Human epidermal growth factor receptor 2

HIF – Hypoxia inducible factor

HRP – Horse radish peroxidase

HSP90 – Heat shock protein 90

ID – Intellectual Disability

IκKβ – Inhibitor of nuclear factor kappa-B kinase subunit beta

IRE-1α – Inositol-requiring enzyme 1 alpha

IRS-1 – Insulin receptor substrate 1

ISR – Integrated stress response

JAK2 – Janus kinase 2

LAM – Lymphangioleiomyomatosis

LAMTOR – Late endosomal/lysosomal adaptor

LKB1 – Liver-kinase-B1

Lut – Luteolin

MAM – Mitochondria-associated ER-membrane

MAPK – Mitogen activated protein kinase

MEF – Mouse embryonic fibroblasts

MITF – Melanogenesis Associated Transcription Factor

mLST8 – Mammalian lethal with Sec13 protein 8

MMP-2 – Matrix metalloproteinase-2

MP – Methyl pyruvate

MP1 – MAPK scaffold protein 1

MQ – Mefloquine

mTOR – Mechanistic Target of Rapamycin

mSIN1 – Mammalian stress-activated protein kinase interacting protein

NaCl – Sodium Chloride

NaF – Sodium Fluoride

NGS – Next Generation Sequencing

NFV – Nelfinavir

NMI – No mutation identified

NPRL2 – Nitrogen permease regulator 2-like protein

NRAS – Neuroblastoma RAS viral oncogene homolog

NSCLC – Non-small cell lung cancer

p53BP1 – p53-binding protein 1

PARP – Poly ADP ribose polymerase

Paro – Paroxetine hydrochloride hemihydrate

PBS – Phosphate buffered saline

PDAC – Pancreatic ductal adenocarcinoma

PDCD4 – Programmed Cell Death 4

PDI – Protein disulphide isomerase

PDK1 – Phosphoinositide-dependent kinase 1

PERK – Protein kinase RNA-like endoplasmic reticulum kinase

PFKFB3 – 6-phosphofructo-2-kinase/fructose-2,6-biphosphatase 3

PGC1α – Peroxisome proliferator-activated receptor gamma, coactivator 1α

PI3K – Phosphoinositide 3-kinase

PIP_3 – Phosphatidylinositol-3, 4, 5-trisphosphate

PKCα – Protein kinase Cα

PML – Progressive multifocal leukoencephalopathy

PMSF – Phenylmethane sulfonyl fluoride

PP1 – Protein phosphatase 1

PTEN – Phosphatase and tensin homolog deleted on chromosome 10

PR – Progesterone receptor

PRAS40 – Proline-rich AKT substrate 40 kDa

Protor-1 – Protein observed with Rictor-1

PSC – Pancreatic stellate cells

PVDF – Polyvinylidene fluoride

RAG – Rag guanosine triphosphatases

Rap – Rapamycin

Raptor – Regulatory-associated protein of mammalian target of rapamycin

Rheb – Ras homolog enriched in brain

Rictor – Rapamycin-insensitive companion of mTOR

rpS6 – Ribosomal protein S6

ROS – Reactive oxygen species

RPMI – Roswell Park Memorial Institute

S1P – Site 1 protease

S6K1 – p70 ribosomal protein S6 kinase 1

SDS – Sodium dodecyl sulfate

SEGA – Subependymal giant cell astrocytoma

SEN – Subependymal nodules

SGK1 – Serum- and glucocorticoid-induced protein kinase 1

Sirt1 - Sirtuin 1

SRPK2 – SR protein kinase 2

SREBP-1 – Sterol regulatory element-binding protein-1

STAT3 – Signal transducer and activation of transcription 3

TAND - TSC-associated neuropsychiatric disorders

TBC1D7 – Tre2-Bub2-Cdc16 (TBC) 1 Domain Family Member 7

TBS – Tris-buffered saline

TFEB – Transcription factor EB

Tre – Trequinsin

Tri – Trifluoperazine

TRAIL – Tumour Necrosis Factor-related Apoptosis-inducing Ligand

TSC – Tuberous sclerosis

TSH – Thyroid stimulating hormone

TXNIP – Thioredoxin-interacting protein

ULK1 – Unc-51-like kinase 1

UPR – Unfolded protein response

VEGF – Vascular endothelial growth factor

YAP – Hippo-Yes-associated protein 1

XBP1 – X-box binding protein 1

Chapter 1: General Introduction

1.1 Tuberous Sclerosis Complex (TSC)

1.1.1 History and General Introduction

1.1.1.1 General Introduction

Tuberous Sclerosis Complex (TSC) (previously known as Bournville-Pringle disease (Verma and Radhakrishnan 2011)) is an autosomal dominant neurocutaneous (second most common behind neurofibromatosis (K *et al*. 2015) and progressive syndrome (Nathan *et al.* 2016; Rosset *et al.* 2017), which is characterized by the presence of benign tumours (called hamartomas) in multiple organ systems including the brain, lungs, heart, the kidneys and skin (Dodd and Dunlop 2016; Peron *et al*. 2016). TSC is also associated with various neurological and psychiatric symptoms, such as epilepsy (70–90% of TSC cases), autism spectrum disorder (ASD; 20–50%), attention-deficit/hyperactivity disorder (ADHD; 30–50 %), intellectual disability (ID; 50%), depression and anxiety disorders (30–60%) (Both *et al.* 2018). The underlying pathomolecular mechanism of tumour growth that is also linked to neurological conditions involves hyperactivation of the mechanistic target of rapamycin (mTOR) pathway, caused by heterozygous loss of function mutations of *TSC1* or *TSC2* (Kwiatkowski *et al.* 2010).

TSC is a rare condition that was previously underdiagnosed until the 1980s as cases were originally reported in 1 in 100,000-200,000 live births (Northrup and Krueger 2013). However, with increased understanding of the disease, the number of cases reported with TSC is now 1 in 6000-9,000 live births with at least 2 million people affected worldwide by the disease with 8,000 cases in the United Kingdom and 40,000 cases in the United States of America. TSC affects all ethnic groups and is equally identified in both sexes (Nasuti *et al*. 2016; Kaneda 2017).

1.1.1.2 History of TSC

The first recorded descriptions of TSC were in the 19th century. The first description was done in 1835 by Pierre Francois Olive Rayer in an atlas of skin diseases where angiofibromas were described as "*végétations vasculaires"* around the mouth and nose. Further references to the disease were seen in 1850 by Thomas Addsion and William Gull who called angiofibromas "vitiligoidea tuberosa" and between 1862-1864 by Friedrich Daniel von Recklinghausen and Rudolf Virchow who reported a child who died with tumours of the heart and several scleroses of the brain. Virchow later observed that a child with tuberous sclerosis had a sister who also died of a cerebral tumour.

It wasn't until 1880 that the first true report of TSC was reported by Désiré-Magloire Bourneville (from whom the disease got its original name). He observed and documented a 15-year-old girl called Marie who had psychomotor retardation, epilepsy, a "confluent vascular-papulous eruption of the nose, the cheeks and forehead" and a history of seizures since infancy. The post-mortem examination disclosed hard, dense tubers in the brain, which Bourneville named "Sclérose tubéreuse des circonvolutions cérébrales" and whitish hard masses were found in both kidneys (Gómez 1995).

Throughout the remainder of the 19th and into the 20th Century, important discoveries about TSC were made, such as the first diagnostic criteria (1906 by Campbell and 1908 by Vogt). Also, it was established that the disease was not only genetic (Kirpicznick in 1910) but could also be hereditary (Berg in 1913). The first reported cases of lymphangioleiomyomatosis (LAM) - rare, progressive and systemic disease that typically results in cystic lung destruction caused by mutations in TSC1 and TSC2 and often reported in female TSC patients was also described by Lutembacher in 1918 (Gómez 1995). In 1942, Moolten proposed the name 'Tuberous Sclerosis Complex' for the disease and introduced the terms hamartial (basic lesion), hamartoma (tumour-like lesion) and hamartoblastoma (truly neoplastic) (Moolten 2011). In 1979, Gomez described the first clinical spectrum for TSC and developed a diagnostic criteria (Sancak 2005). These diagnostic criteria was revised in 1998 (Roach *et al.* 1998) and revised again to its current version in 2012 (Northrup and Krueger 2013).

1.1.1.3 TSC diagnosis criteria

In 2012, the International Tuberous Sclerosis Complex Consensus Group updated the diagnostic criteria for TSC. The criteria consist of two parts; genetic and clinical. The genetic criteria consist of identification of either a *TSC1* or *TSC2* pathogenic mutation (mutation that clearly inactivates the function of the TSC1 or TSC2 proteins, respectively) in DNA from normal tissue and is sufficient evidence to make a definite diagnosis of TSC. However, mutations of either *TSC1* or *TSC2*, whose effect on function is less certain do not meet these criteria and are not sufficient alone to make a definite diagnosis of TSC. It is also important to note that 10-25% of TSC patients have no mutation identified by conventional genetic testing (which will be discussed later), and a normal result does not exclude TSC, or have any effect on the use of clinical diagnostic criteria to diagnose TSC.

The second part of the criteria is clinical based as patients must have two major TSC features or one major feature and more than two minor TSC features. A possible diagnosis can be made if the patient has either a major TSC feature or two or more minor TSC features. The major TSC features include: hypomelanotic macules (>3, at least 5-mm diameter), angiofibromas (>3) or fibrous cephalic plaque, ungual fibromas (>2), shagreen patch, multiple retinal hamartomas, cortical dysplasias, subependymal nodules, subependymal giant cell astrocytoma (SEGA), cardiac rhabdomyoma, LAM and angiomyolipomas (>2). The minor features of TSC are defined as: “confetti” skin lesions, dental enamel pits (>3), intraoral fibromas (>2), retinal achromic patch, multiple renal cysts and nonrenal hamartomas. Each feature will be explained in detail in later sections of this chapter (Northrup and Krueger 2013).

1.1.1.4 Mutations associated with TSC

As previously mentioned, TSC is caused by loss of function mutations in either *TSC1* and/or *TSC2* (Verma and Radhakrishnan 2011). Disease causing mutations can be identified in up to 85% of TSC patients tested with between 500 to 2000 different mutations reported in both the *TSC1* and *TSC2* genes, respectively (Williams *et al*. 2007; Kwiatkowski *et al*. 2015). A third of identifiable mutations can be hereditary (K *et al*. 2015; Lam *et al*. 2017a), although 60% of TSC cases are caused by sporadic mutations (Hoelz *et al.* 2018). TSC-associated tumours follow

the classical Knudson's two-hit inactivation model, where loss of heterozygosity occurs.

Typically, the first inactivating mutation is germline and TSC patients are born heterozygous *TSC1*+/- or *TSC2*+/-. Homozygous deletion of either gene is embryonically lethal (as shown in Eker rats, a TSC rat model) (Aizawa *et al.* 2016). The second mutational hit is somatic and can be the result of several causes, including loss of heterozygosity through large gene deletion or mutation as well as promoter methylation (Rosset *et al.* 2017).

TSC2 mutations are around four times more common than *TSC1* (Lim *et al*. 2016; Kaneda 2017). Mutations in TSC1 are usually small insertions or deletions causing nonsense and frameshift mutations (Dabora *et al*. 2001; Franz *et al*. 2001). Many *TSC2* mutations contain missense mutations (25-32%) and large deletions or rearrangements (12-17%) (Cheadle *et al.* 2000). In general, patients with *TSC2* mutations are more likely to have a more severe phenotype than *TSC1* mutations. Patients with *TSC2* mutations often present with symptoms at a younger age and are more likely to have seizures, cognitive impairment, infantile spasms, autism spectrum disorder and have been reported to have a greater risk for renal malignancy. Patients with *TSC1* variants are less likely to have intellectual disability, renal abnormalities, and retinal abnormalities but are more likely to have shagreen patches (Domanska-Pakiela *et al*. 2002; Sancak *et al*. 2005; Goedbloed *et al*. 2006; Algra *et al*. 2007; Kothare *et al*. 2014; Mortaji *et al*. 2017; Rosset *et al*. 2017).

10-15% of TSC patients have mutations that cannot be detected by conventional genetic testing and are referred to as no mutation identified (NMI) patients. Tyburczy *et al.* (2015) used next generation sequencing (NGS) to identify mutations in 45 out of 53 patients. Mosaicism (small insertions and deletions, larger genomic deletions, and nonsense, splice site, and missense mutations) was observed in 26 out of 45 of patients, and intronic mutations were also unusually common, seen in 18 of these 45 subjects. 82% of these mutations were detected in the *TSC2* gene and 18% in the *TSC1* gene, like the general distribution of mutations. Heterozygous non-mosaic mutations in coding exons and consensus splice sites were identified in 11% of the remaining samples, which had been previously missed with NGS. Mutations in the introns, non-coding regions of the genes, were detected in 40% of the NMI samples, 33% of which were mutations that had not been previously reported.

The incidence and severity of TSC manifestations can vary widely between individuals, and even between identical twins. This phenotypic heterogeneity is likely due to differences in mutations occurring in *TSC1* versus *TSC2*, and other poorly defined factors (Sahin *et al.* 2016). There are no identifiable risk factors making someone susceptible to developing tuberous sclerosis. A parent with TSC has a 50% chance of passing the disease on to their child, while sporadic TSC patients likely have a "second hit" phenomenon (a fundamental concept that sequential insults, which are individually innocuous, can lead to overwhelming physiologic reactions (Lasanianos *et al.* 2010)).

With regards to Tre2-Bub2-Cdc16 (TBC) 1 domain family member 7 (TBC1D7), mutations in this protein are not associated with TSC. However, mutations within TBC1D7 are associated with several diseases including intellectual disability, macrocrania, patellar dislocation and coeliac disease (Chrast *et al.* 2014).

1.1.1.5 TSC - tumour suppressor protein complex

The two causative genes of TSC form a multiprotein complex. The 130 kDa TSC1 protein (hamartin) and the 200 kDa protein TSC2 (tuberin) associate with each other as a protein complex with another core subunit, TBC1D7 (Asara *et al*. 2012; Zech *et al*. 2016). TSC1 is responsible for TSC2 stabilisation, preventing ubiquitin-mediated degradation of TSC2. TSC2 contains a C-terminal GAP domain, which is required for its tumour suppressor role. Through this GAP domain, TSC1/TSC2 negatively controls mTORC1 activity via converting the small G protein, Ras homolog enriched in brain (Rheb), to its inactive GDP-bound form (Tee *et al.* 2005). Rheb is a member of the RAS-family of small G proteins that directly binds to and activates mTORC1 when Rheb is GTP-bound (Sarbassov *et al.* 2005; Groenewoud and Zwartkruis 2013). Therefore, the tumour suppressor role of TSC1/TSC2 is to inactivate mTORC1 through conversion of active GTP-bound Rheb to an inactive GDP-bound state (Groenewoud and Zwartkruis 2013).

Growth signalling inputs are known to activate mTORC1 through repression of TSC2. For instance, AKT in the PI3K signalling pathway can directly phosphorylate and inactivate TSC2 at five residues (Ser^{939}, Ser^{981} Ser^{1130}, Ser^{1132} and Thr^{1462} - all of which exist outside of the GAP domain of TSC2) (Dibble and Cantley 2015), which causes an increase of Rheb-GTP and mTORC1 activation. There are multiple signalling inputs towards the TSC1/TSC2 complex, such as;

through activation of the MAPK pathways (which results in ERK phosphorylates TSC2) (Ma *et al.* 2005), phosphorylation by IκKβ, phosphorylation on Ser^{644} or by WNT pathway inhibition of glycogen synthase kinase 3 (GSK3) beta. GSK3 phosphorylates TSC2 on Ser^{1341} and Ser^{1337}, in conjunction with phosphorylation by AMPK activates TSC2 to downregulate mTORC1 signalling (Sulaimanov *et al.* 2017; Wataya-Kaneda, 2015).

1.1.2 Clinical management of TSC

TSC is a complex disease with pathological features of multiple organs that needs careful clinical management. The current therapy for TSC uses mTORC1 inhibitors, with the idea to restore the pathological defect of hyperactive mTORC1 signalling to restore disease state. mTORC1 promotes cell growth and is thought to be the main driver of hamartomas (benign tumour growth), but may also contribute to other aspects of disease, such as enhanced cell motility and differentiation states. In the sections below, different pathological features of TSC will be described with their clinical management. Therapy with mTORC1 inhibitors has markedly improved the clinical care of TSC patients and will also be summarised below for each organ type. Yet there are also aspects of TSC that are not cured with mTORC1 inhibitors, revealing that there is a clinical need to find better therapies.

1.1.2.1 Renal manifestations

Renal angiomyolipomas (AMLs) are a very common manifestation of TSC patients. 80% of TSC patients develop at least one AML in their lifetime (Ikarashi *et al.* 2017; Warncke *et al.* 2017). AMLs are benign mesenchymal tumours which are composed of various tissue types including adipose tissue, spindle and epithelioid smooth muscle cells and abnormal vessels (Champagnac *et al.* 2016; Ikarashi *et al.* 2017) and occur as multiple and bilateral lesions (Rabenou and Charles 2015) (Figure 1.1).

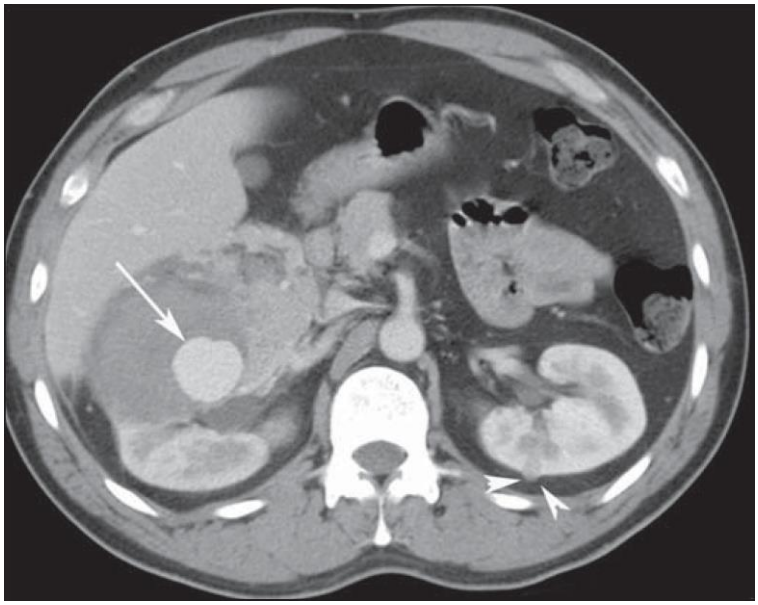

Figure 1.1 CT scan of Angiomyolipoma (AML). White arrows indictate the locations of AMLs in patients kidneys. Image taken from (von Ranke *et al*. 2015).

Adverse effects of AML include acute injuries such as haemorrhage of a lesion (also referred to as Wunderlich syndrome) in which the risk of a bleed correlates with the size of the tumours. This is because vasculature of AMLs is characterized by thick-walled blood vessels that contain little or no elastin, making them prone to rupture. Long term effects of AMLs include progressive loss of normal renal parenchyma leading to reduced kidney function and eventually kidney failure. AMLs are the second leading cause of morbidity and mortality (behind epilepsy) in TSC patients (Sheperd *et al.* 1991).

In terms of AMLs, dysfunctional mTORC1 activity plays an important role in tumour development. mTORC1 regulates the nuclear entry of lipin-1, a phosphatidic acid phosphatase, which is involved in activating SREBP-1 (sterol regulatory element-binding protein-1), a transcription factor which is a master regulator of *de novo* lipogenesis (Laplante and Sabatini 2009; Peterson *et al.* 2011). Increased *de novo* lipid synthesis is a hallmark of proliferating cancer cells by providing the lipids required for membrane synthesis (Laplante and Sabatini 2009) and since mTORC1 is constitutively active in AMLs, there are increased levels of lipid production (hence why AMLs are considered as fatty tumours).

Hypoxia inducible factors (HIFs) play a role in vascularisation and angiogenesis and regulates vascular endothelial growth factor (VEGF) – a biomarker involved in angiogenesis. mTORC1 causes an accumulation of HIF1α via

direct phosphorylation and activation of signal transducer and activation of transcription 3 (STAT3) (Dodd *et al*. 2015). Hyperactive mTORC1 results in overexpression of VEGF and HIF1α which leads to hypervascularisation and is a common trait found on tumours, especially TSC-associated tumours such as AMLs (Dodd *et al*. 2015).

Given the links of mTORC1 hyperactivity to drive tumour growth in AMLs, mTORC1 inhibitors have been shown efficacy to shrink tumours. Rapamycin and everolimus have both undergone extensive *in vitro* and *in vivo* investigation in models of TSC. Rapamycin was shown to have antitumour properties as first reported in 2002 (Guba *et al.* 2002). Rapamycin was shown to be able to inhibit primary and metastatic tumour growth via antiangiogenesis (decreased vascular epithelial growth factor (VEGF) production).

mTOR inhibitors have been shown to decrease the phosphorylation of downstream effectors of mTOR, resulting in decreased DNA synthesis and cellular proliferation in TSC patient–derived tumour cell lines, including angiomyolipomas (Krymskaya *et al*. 2002; Lesma *et al*. 2005). In *Tsc1*-null and *Tsc2*-null MEFs, rapamycin caused VEGF levels to rapidly decrease *in vitro* (El-Hashemite *et al.* 2003).

A meta-analysis of 4 clinical trials and 4 case reports showed that in the presence of rapamycin and rapalogs (analogues of rapamycin, such as everolimus), there was a significant reduction in the size of renal AMLs and SEGAs (Sasongko *et al.* 2015). ‘EXamining everolimus In a Study of Tuberous Sclerosis Complex-2’ (EXIST-2) was a randomized, double-blind, placebo-controlled trial in 118 TSC or sporadic LAM patients aged >18 years old with at least one AML >3 cm diameter. The angiomyolipoma response rate was 42% for everolimus compared to 0% for patients treated with a placebo control (Bissler *et al.* 2015; Budde *et al.* 2016). In a 2-year, nonrandomized, open-label trial consisting of 18 patients of AML, with at least one AML ≥3 cm diameter, the proportion of patients who achieved ≥50% reduction from baseline in the sum of volumes of target lesions increased from 52.94% at 3 months, to 58.82% and 66.67% at months 6 and 12 (Cai *et al.* 2018). In 8 patients tested, everolimus treatment had a statistically significant effect on AML volume reduction that ranged from 10.5-45.3% reduction in four patients with everolimus at 2.5 mg daily and 40.7-73.1% in four patients with everolimus at 5.0 mg daily (Tsai *et al.* 2017).

However, the main problem with using mTORC1 inhibitors is that while the use of these drugs can reduce tumour volume and angiogenesis when patients are on treatment, tumours regrow cessation of treatment. In other words, these drugs are cytostatic rather than being cytotoxic (Sheth *et al.* 2016). Along with this are several known side effects include mTOR inhibitors-related pneumonitis, immunosuppression, and high incidences of hyperglycaemia, new-onset diabetes, hyperlipidaemia and hypercholesterolemia.

The use of mTORC1 inhibitors reduces the need to operate on AML which (according to international guidelines) is recommended when AML grows to 30-40 mm in diameter. Approximately one-quarter of adult TSC patients have experienced renal embolization or partial nephrectomy (Krueger *et al*. 2013; Bissler *et al.* 2015; Curatolo *et al.* 2016). However, due to the complex nature of TSC-associated AMLs, tumours may regrow and require recurring intervention resulting in progressive loss of functioning kidney tissue and even end stage renal disease (O'Callaghan *et al.* 2004).

While mTORC1 inhibitors are sufficient to prevent AML growth and reduce the need to remove these tumours, TSC patients would be required to take mTORC1 treatment for life. This is due to the cytostatic drug activity of mTORC1 inhibitors. Therefore, there is a clinical need to find an alternative therapy that might completely remove the tumour through a cytotoxic activity.

1.1.2.2 Skin

Between 81-95% of TSC patients will have at least one TSC-associated skin condition (Lim *et al.* 2017). These can be painful, disfiguring, emotionally distressful, or prone to bleeding (Nathan *et al.* 2015). Angiofibromas (reddish-brown papules which primarily affect the nasolabial folds, cheeks and chin, bilaterally and symmetrically or unilaterally and mosaic (Rodrigues *et al.* 2012)) are the most recognized cutaneous manifestations of TSC (Figure 1.2B). Other forms of TSC-associated skin conditions include hypopigmented macules (found on nearly all of patients and present as white lesions (Rabito and Kaye 2014)) (Figure 1.2A), Shagreen patches (fibrotic plaque with irregular margins and raised, greyish-green or light brown roughened surfaces (often referred to as "orange-peel''), generally appearing on the trunk (most specifically in the lumbosacral area) and present in approximately 20–54% of TSC patients (Rodrigues *et al.* 2012; Northrup and

Krueger 2013; Rabito and Kaye 2014) (Figure 1.2C). Ungual fibroma (Koenen tumours) (skin-coloured or reddish nodules adjacent to or underneath the nails, present in approximately 15–20% of TSC patients (Rabito and Kaye 2014) (Figure 1.2D). Fibrous cephalic plaques (thickened bundles of reticular collagen with little or no elastic fibres) stereotypically develop on the forehead (about 40% of cases - but can also occur in non-forehead sections of the face and scalp mostly on the left-hand side) of TSC patients and are found in 36% of TSC patients.

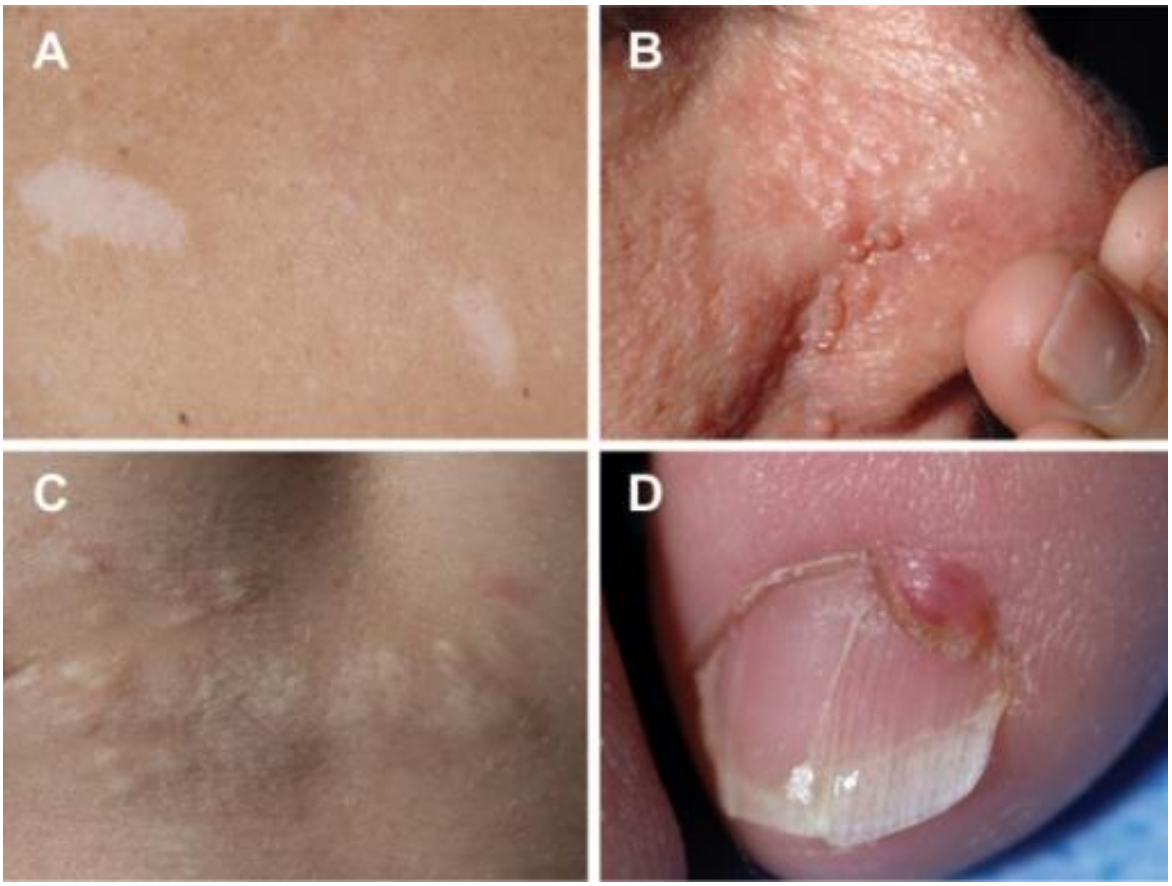

Figure 1.2 Skin Manifestations of TSC. A selection of skin manifestations of TSC including (A) hypomelanotic macules, (B) angiofibromas, (C) Shagreen patch and (D) Ungual fibroma. Image taken from Taveira-DaSilva and Moss (2015)

During clinical trials using mTORC1 inhibitors in TSC patients, it was noticed that facial angiofibromas were markedly reduced in size upon treatment. This has led to topical skin applications with mTORC1 inhibitors, which recently showed promise in clinical trials (Koenig *et al*. 2012). Different pharmaceutical formulations of treatment were tried at different rapamycin concentrations (0.003–1%), from crushed tablets to oral solution, where all formulations were reported to cause

patient improvement to facial angiofibromas (cosmetic results) with minimal side effects (Madke 2013; Neri *et al.* 2014; Bouguéon *et al.* 2015). However, there were several problems caused through inconsistent percutaneous absorption and systemic diffusion. A 0.1% (w/v) rapamycin topical cream was later developed for the treatment of angiofibromas (Bouguéon *et al.* 2016).

Loss of either *TSC1* or *TSC2* heterozygosity within angiofibromas was discovered to be associated with UV-induced DNA damage of the remaining allele (Tyburczy *et al.* 2014), which would cause hyperactivation of mTORC1. This has a huge impact on the care of TSC patients, where reducing sun exposure as a preventative would reduce the formation of angiofibromas. Given the current therapy (reducing fibrous growth and erythema, (Salido-Vallejo *et al.* 2014)) finding additional treatments for the skin is less of a research priority. DNA-damage from UV has been found to be sufficient in causing the formation of angiofibromas. This finding would also argue against the use of genotoxic chemotherapy to treat TSC-associated tumours, as DNA-damaging agents such as oxaliplatin and doxorubicin would likely promote further tumour formation through loss of heterozygosity of either *TSC1* or *TSC2*.

1.1.2.3 Brain

1.1.2.3.1 Neurological manifestations of TSC

Epilepsy is one of the most common neurological complication associated with TSC and occurs in up to 90% of TSC patients. Epilepsy can occur within the first year of life (a critical timepoint in neurological development) with the average age of seizures onset being around 5.6 months (Williams *et al*. 2017). Around 45% of TSC patients have mild-to-profound intellectual disability (ID), with up to 50% of patients having Autism Spectrum Disorder (ASD) symptoms (Sahin 2012). For TSC patients with intellectual disability/ASD, epilepsy may be a leading cause of mental retardation as 67.39% of infants with infantile spasms developed mental retardation (Wang *et al.* 2017).

TSC-associated neuropsychiatric disorders (TAND) is a term that was coined by the Neuropsychiatry Panel at the 2012 Tuberous Sclerosis Complex International Consensus Conference to help recognize the complex cognitive and behavioural manifestations of TSC and generate screening guidelines (de Vries *et al.* 2015). The

most common neuropsychiatric conditions associated with TSC are depression, anxiety, attention-deficit and hyperactivity disorder and aggressive/disruptive disorders. Behavioural manifestations of TSC can range from mild (poor eye contact) to severe with the most common being aggression (45% of cases) and self-injury (10%) (Gipson and Johnston 2017).

Epilepsy becomes refractory to medical therapy over time (Wei *et al.* 2018), with refraction rates ranging from 25% - 60% (Cardamone *et al.* 2014; French *et al.* 2016) with refraction typically developing at the age of 2 (Evans *et al.* 2012). TSC2 mutations are associated with a more severe epilepsy phenotype compared to TSC1 mutations (Zeng *et al.* 2011) while the presence of cortical tubers (described later in this chapter) with TSC2 mutations are associated with refractory epilepsy (Chu-Shore *et al.* 2009). The type of seizure also plays a role in epilepsy refraction as in patients with focal epilepsy, drug resistance was reported in 59.6% of cases, with focal seizure onset prior to age 1 year while infantile spasms were incompletely responsive to therapy and associated with an increased likelihood of refraction (Jeong *et al.* 2017).

However, mTORC1 inhibitors have shown to reduce the severity of seizures. EXIST-3 was randomised double-blind, placebo-controlled phase III trial designed to assess the efficacy and safety of two trough exposure concentrations of Everolimus, 3–7 ng/mL (low exposure) and 9–15 ng/mL (high exposure), compared to placebo as adjunctive therapy for treatment-resistant focal-onset seizures in TSC patients. Results showed that treatment significantly reduced seizure frequency (14.9% with placebo versus 29.3% with low-exposure everolimus and 39.6% with high-exposure everolimus) with a tolerable safety profile compared to placebo in patients (French *et al*. 2016). In TSC patients with refractory epilepsy, the target concentration of everolimus to use was shown to be 5-7 ng/ml initially but possibly 5-15 ng/ml in cases of an inadequate clinical response but patients have a favourable risk-benefit profile (Franz *et al.* 2016).

TSC-associated seizures are highly responsive to Vigabatrin, an antiepileptic drug used in the US (since 2009). Vigabatrin was shown to have an approximate 95% efficacy at stopping infantile spasms (Curatolo *et al.* 2001). Cannabidiols (CBD) may also be useful for the treatment of TSC-associated seizures. After 3 months of treatment, patients with TSC-associated refractory seizures were shown to have a decrease in the weekly frequency of seizures (in all seizure types of patients in the

study) and improved cognitive ability (85.7%) and behaviour (66.7%) (in patients with baseline cognitive and/or behavioural problems) (Hess *et al.* 2016). Cytotoxic agents are clinically less likely to be used for this indication, while drugs that restore disease state would be better. While it is currently unclear what pathways might trigger seizures, endoplasmic reticulum (ER) stress and inflammatory signals have been suggested as possible mechanisms.

1.1.2.3.2 Brain Tumours

Brain lesions are found in approximately 90% of TSC patients and manifest in several different types (Mühlebner *et al.* 2016); cortical tubers, subependymal nodules (SENs) and subependymal giant astrocytomas (SEGAs).

Cortical tubers have been reported in up to 90% of patients (Katz *et al.* 2017). Tubers are focal developmental abnormalities. They can form as single or multiple lesions (Crino 2013). They may be found in any cortical region but found predominately in frontal and temporal regions. Tubers can also be detected during foetal life. Foetal tubers have been identified as early as 20 weeks gestation (Park *et al*. 2002) and in older children and adults. Tubers may calcify and undergo cystic degeneration. The presence of cortical tubers is often associated developmental delays, autism and treatment-resistant epilepsy (Katz *et al.* 2017)

SENs are asymptomatic periventricular nodular lesions (Figure 1.3), which may evolve postnatally and throughout early adulthood into SEGAs (Zordan *et al.* 2018). SENs have been reported in between 80% to nearly 100% of patients *(*Hu *et al.* 2016). SENs frequently show calcifications, particularly at an early stage. They are typically less than 1 cm in diameter and are better detected by computerized tomography (CT) (Çelenk *et al.* 2005; Hu *et al.* 2016).

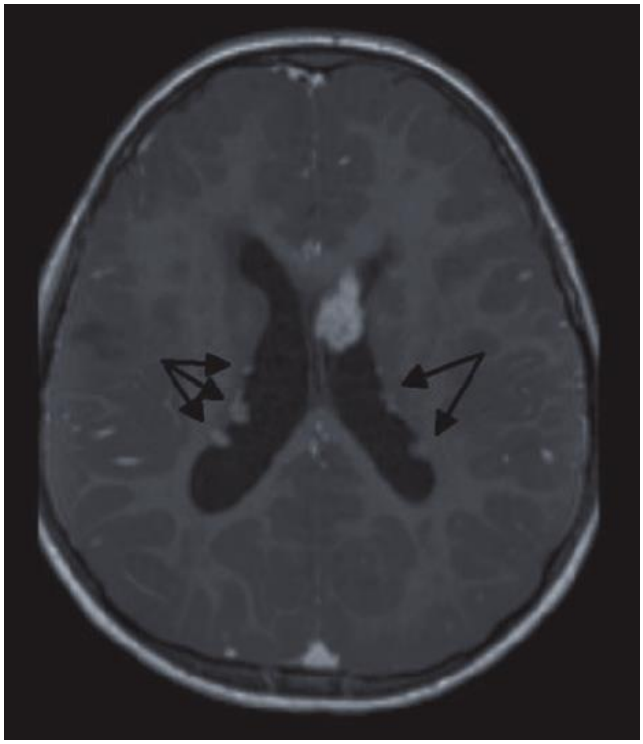

Figure 1.3 CT Scan of subependymal nodules (SENs). Black arrows indicate the locations of the SENs in the patient's brain. Image taken from (Samueli *et al*. 2015).

SEGAs are a rare slow growing glioneuronal tumours which develop from SENs in about 20% of TSC patients with a peak of incidence in the second decade of life (Franz *et al.* 2013; Cardamone *et al.* 2014) (Figure 1.4). SEGAs tend to occur in the wall of the lateral ventricle and foramen of Monro and, rarely, in the third ventricle. While SEGAs are defined as low-grade tumours (WHO grade I) or even benign (Weidman *et al.* 2015; Dadey *et al.* 2016), growth and location of tumours can result in obstructive hydrocephalus and intracranial pressure, sequelae including seizures and focal neurological deficits which can result in death *(*Cuccia *et al. 2003;* Appalla *et al.* 2016; Katz *et al.* 2017; Zordan *et al.* 2018). SEGAs are not responsive to chemotherapy or radiation therapy. Currently, standard treatment for SEGAs involves resection, however 48.9% of patients suffer from postoperative complications which have been associated with the extent of dissection required to access the deep location of SEGAs (Beaumont *et al.* 2012; Sun *et al.* 2012). Incomplete resection of SEGAs will typically lead to recurrence (Roszkowski *et al.* 1995).

Figure 1.4 CT Scan of subependymal giant astrocytoma (SEGA). White arrow indicates the location of the SEGA into patient's brain. Image taken from (Franz *et al*. 2013).

mTORC1 inhibitors have some shown clinical promise for the treatment of brain tumours. In 3 TSC patients with large intracranial SEGAs, the use of oral rapamycin as a pre-treatment prior to surgery was shown to allow for easier resection of tumours as the border between tumour and healthy tissue became well-differentiated because of tumour size reduction (Du *et al*. 2017). Rapamycin was hypothesized to decrease the flow of blood to the tumours and as a result reduce the risk of postsurgical cerebrospinal fluid diversion.

EXIST-1 was a multicentre, randomized, double-blind, placebo-controlled phase III trial with an open-label extension evaluating the efficacy and tolerability of Everolimus in 117 patients with TSC-associated SEGA. 27 (35%) patients in the Everolimus cohort had at least 50% reduction in the volume of SEGAs versus none in the control placebo cohort. Adverse events were mostly grade 1 or 2 (fever, fatigue, stomatitis (aphthous ulcers of the mouth), mucositis, rash, loss of appetite, diarrhoea, arthralgias, thrombocytopenia and blood lipid abnormalities) and no patients discontinued treatment because of adverse events (Franz *et al.* 2013). Additional analysis of data has shown Everolimus to be a safe therapeutic option for patients aged <3 years (as Everolimus was initially approved for patients >3 years of age) (Jóźwiak *et al.* 2016) and prolonged usage was shown to lead to sustained reduction in tumour volume, and new responses were observed for SEGA and renal angiomyolipoma (Franz *et al.* 2016).

Investigations were carried out into using Everolimus as a maintenance therapy after a higher dose of therapy caused a reduction in SEGA tumour volume (Trelinska *et al*. 2017). To reach a trough concentration of 5-15 ng/ml in patients, Everolimus was administered 3 times a week (rather than administering daily, as done in standard therapy). This EMINENTS study involved 10 patients with TSC-associated SEGAs. Observations over a period of 360 days (with checks on days 0, 90, 120 and 360) showed no regrowth of tumours. Adverse effects were also noted as being significantly less severe and less frequent during maintenance compared with the standard therapy.

1.1.2.4 Lung

LAM (Figure 1.5) is a rare multisystem neoplastic disease characterized by the proliferation of oestrogen receptor alpha (ERα)- and progesterone receptor (PR)-positive abnormal smooth muscle like cells (LAM cells). This leads to cystic destruction of the lungs, and the formation of lymphatic tumours such as chylous effusions and lymphangioleiomyomas (Chu *et al.* 1999; Matsui *et al.* 2000; Johnson *et al.* 2010; Gao *et al.* 2014; Taveira-DaSilva and Moss 2015). LAM can occur in two forms; sporadic or as a pulmonary manifestation of TSC (Seyama *et al*. 2016).

Figure 1.5 CT scan of lymphangiomyomatosis (LAM). White arrows indicate sample of the LAM lesions found in the patients lung. Image taken from (Badawi and Geddes 2003).

LAM predominately affects women of child-bearing age (average age of diagnosis is approximately 35 years). There are very few case of male TSC patients developing LAM (Costello *et al.* 2000; Ryu *et al.* 2006; Johnson *et al.* 2010; Oprescu *et al.* 2013). The prevalence of TSC-associated LAM is an issue of debate as it initially thought to affect 1-4% of female patients (Dwyer *et al.* 1971; Sheperd *et al.* 1991; Castro *et al.* 1995). However, in the 2000s, studies into LAM demonstrated a prevalence of 28-38% in female patients *(Costello et al.* 2000; Franz *et al.* 2001; Moss *et al.* 2001). This may also be a further underrepresentation, as one study reported that prevalence may be as high as 80% of female TSC patients (Adriaensen *et al.* 2011).

LAM affects the lung function of patients as decline in function rates are two to four times higher than rates seen typically associated with age (Johnson and Tattersfield 1999; Urban *et al.* 1999; Taveira-DaSilva *et al.* 2004). Respiratory failure is a principal cause of death in sporadic and TSC-associated LAM patients (Courtwright *et al.* 2017). The median transplant-free survival is approximately 29 years from the onset of symptoms, with a 10-year transplant-free survival of 86% (Ryu *et al*. 2006; Galvin *et al*. 2007; Oprescu *et al*. 2013). Clinical symptoms of this progressive disease includes dyspnoea, cough, recurrent pneumothorax, haemoptysis and chylothorax with most patients requiring oxygen supplementation within 10 years of symptom onset (McCormack *et al.* 2016; Moir 2016). LAM patients also appear to be at an increased risk of respiratory infections (Courtwright *et al.* 2017)(McCormack *et al*. 2011; Chang *et al*. 2014; Radzikowska *et al*. 2015a).

LAM patients who receive lung transplants can still developed LAM lesions post-transplant (Karbowniczek *et al.* 2003). This indicates that LAM cells do not originate in the lungs but instead originate in a different organ before travelling to the lungs (Gao *et al.* 2014). The original source of LAM cells remains unknown (Prizant and Hammes 2016). The predominant histological features of LAM are the abundance of lymphatic vessels and the proliferation of LAM cells (Seyama *et al*. 2016). Research by Kumasaka *et al.* (2005) suggested that lymphangiogenesis-mediated fragmentation of LAM lesions and shedding of LAM cell clusters (LCCs) in the lymphatic stream may play a role in the metastatic progression of LAM.

On the molecular level, LAM cells have very specific defects. LAM cells have mutations in either *TSC1* or *TSC2* (Prizant and Hammes 2016). Sporadic LAM is caused by two acquired mutations while TSC-associated LAM is caused by one

germline mutation and one acquired mutation (Moir 2016). Approximately 60% of women with sporadic LAM also have renal AMLs (Ryu *et al.* 2012) and in these cases mutations (loss of heterozygosity) were only found in *TSC2* and in many cases these TSC2 mutations were identical in both kidney and lung samples (Yu *et al*. 2001; Carsillo *et al*. 2002). Mutations in *TSC1*/*2* also causes increased Rho-A GTPase activity and likely contributes to enhanced cellular migration and proliferation (Li *et al*. 2011).

Hormones, such as estradiol, play an important pathological role in LAM. LAM which is found nearly exclusively in women of child bearing age, can progress during pregnancy or treatment with oestrogen. LAM is stabilised or disease progress slowed in postmenopausal women (Radzikowska 2015). Metabolomic profiling identified an estradiol-enhanced prostaglandin biosynthesis signature in *Tsc2*-deficient cells. Estradiol increased the expression of cyclooxygenase-2 (COX-2), a rate-limiting enzyme in prostaglandin biosynthesis, which was also increased at baseline in *Tsc2*-deficient cells and was not affected by mTORC1 inhibition with rapamycin treatment (Li *et al*. 2014). In *Tsc2*-deficient cells, estradiol was found to reactivate ambra signalling and increased levels of glucose-6-phosphate dehydrogenase (G6PD), the rate limiting enzyme of the pentose phosphate pathway (Sun *et al.* 2014). Oestrogen is also known to activate mitogen-activated protein kinase (MAPK) and promoted the survival of TSC2-null LAM-like cells as well as to enhance the expression of matrix metalloproteinase-2 (MMP-2), which attributes to the invasiveness of LAM cells (Li *et al.* 2013). Progesterone involvement has been shown to have varied results. For instance, Sun *et al.* (2014) showed that progesterone alone (and synergistically with estradiol) activated AKT and ERK pathways and increased proliferation in ELT-3 cells (a rat TSC model cell line) and could cause lung metastasis and invasiveness *in vivo*. However, Glace *et al.* (2009) and Hodges *et al.* (2002) showed in ELT3 cells that progesterone suppressed the oestrogen-induced gene expression and inhibited oestrogen-induced cell proliferation.

mTOR inhibitors are used as a treatment for LAM, with rapamycin being FDA approved for LAM. Rapamycin has been shown to inhibit cell growth and the production of VEGF, while at the same time stabilizing lung function. Problems can arise in this scenario based on the cytostatic nature of rapamycin. Whether or not rapamycin can also prevent LAM migration is also unknown. As a result, further research into cytotoxic alternatives are needed to treat LAM.

1.2 mTORC1 in tumour growth

1.2.1 mTOR

1.2.1.1 mTORC1 and mTORC2

mTOR is a downstream target of TSC1/TSC2 and is a drug target for the treatment of TSC. mTOR is an evolutionary preserved atypical serine/threonine kinase that acts as a master regulator of several key functions including growth, proliferation and metabolism (Laplante and Sabatini 2009b), which are processes linked to the pathology of TSC. In the 2000s, mTOR was found to function as a core protein of at least two distinct multi-protein complexes, mTOR complex 1 (mTORC1) and mTOR complex 2 (mTORC2) and will be further discussed in this chapter (Laplante and Sabatini 2009; Blenis 2017).

mTORC1 is a multi-protein complex composed of several components that interact with the mTOR kinase. mTORC1 is known for its control of cellular growth, translation, transcription and autophagy (Sulaimanov *et al.* 2017). mTORC1 adopts a cage-like, dimeric architecture with the mTOR kinase domain located near the centre of the assembly (Aylett *et al.* 2016). Rapamycin has been shown to be selective for mTORC1 inhibition. Rapamycin inhibits mTORC1 via formation of a gain-of-function complex with 12-kDa FK506-binding protein (FKBP12), that binds to the FKBP12/rapamycin-binding (FRB) domain of mTOR in mTORC1 only. When this occurs the rapamycin/FKBP12 complex causes dissociation of Raptor from the mTOR causing loss of contact between mTORC1 and it substrate, resulting in pathway shutdown (Ehninger and Silva 2011; Chiarini *et al.* 2015). The components of mTORC1 that interact with mTOR are found in Table 1.1.

Table 1.1 Components of mTORC1 complex. List of the component and their function of the mTORC1 complex

Regulatory-associated protein of mammalian target of rapamycin (Raptor)	150 kDa protein found exclusive in mTORC1 and functions as a scaffold protein that interacts with downstream substrates, S6K1 and 4E-BP1 - which will be discussed later in the chapter. mTORC1 substrates, contain mTOR signalling (TOS) motifs that helps with mTORC1-dependent phosphorylation of those substrate. Raptor is also needed to assist with the localization of the mTORC1 to the lysosome (Chong, 2015; Tee, Sampson, Pal, & Bateman, 2016).
Proline-rich AKT substrate 40 kDa (PRAS40)	mTORC1 exclusive protein with a TOS motif that is a negative regulator of mTORC1. PRAS40 interacts with Raptor and competitively binds to S6K1 and 4E-BP1. AKT phosphorylates PRAS40 causing PRAS40 to bind to protein 14-3-3 (causing PRAS40 inactivation) resulting in increased mTORC1 activity (Cho, 2011; Chong, 2015)
mLST8	See Table 1.2.
Deptor	See Table 1.2.

mTORC2 is found to be proximally located to the endoplasmic reticulum (ER) (close to the ribosomes), mitochondria, mitochondria-associated ER-membrane (MAM) and the nucleus in mammalian cells (Liu *et al*. 2015c). mTORC2 was initially defined for its role in regulating cell skeletal organisation but mTORC2 also promotes cell proliferation and survival through the phosphorylation of AKT (Liu *et al.* 2013).While rapamycin may be regarded as an mTORC1 selective inhibitor (as rapamycin/FKBP12 complex does allosterically inhibit mTORC2) rapamycin is able to inhibit mTORC2 activity after prolonged exposure (over 24 h), when high concentrations of rapamycin are used, or due to variation in the expression levels of FK506 binding proteins (especially FKBP12 and FKBP51) (Sarbassov *et al.* 2006; Efeyan and Sabatini 2010; Li *et al.* 2014b; Schreiber *et al.* 2015). TSC2 positively regulates mTORC2 in a manner independent of the GTPase-activating protein activity the complex has towards Rheb and can physically associate with mTORC2 but not mTORC1 (Huang *et al*. 2008). mTORC2 also promotes survival in *TSC2*-

null cell proliferation and survival through RhoA GTPase and Bcl2 proteins (Li *et al*. 2011). The components of mTORC2 (including mTOR) are found in Table 1.2.

Table 1. 2 Components of mTORC2 complex. List of the component and their function of the mTORC2 complex

Rapamycin-insensitive companion of mTOR (Rictor)	An mTORC2 exclusive component that is involved in the activation of AKT via direct phosphorylation of Ser^{473}, a priming site that enables PDK1 to phosphorylate Thr^{308} (Sarbassov *et al.* 2005).
Mammalian stress-activated protein kinase interacting protein (mSIN1)	A negative regulator exclusive to the mTORC2 complex that prevents mTOR kinase activity by interacting with and inhibiting the mTOR kinase domain. mSIN1 is regulated by PIP_3 (Liu *et al*. 2015c).
Protein observed with Rictor-1 (Protor-1)	Protor-1 is a Rictor-binding subunit required for the activation of serum- and glucocorticoid-induced protein kinase 1 (SGK1) (Chong 2015)
Mammalian lethal with Sec13 protein 8 (mLST8)	Also called G protein β-subunit like protein (GβL). mLST8 structurally has seven WD-40 repeats and is located on endosomal or Golgi membranes. mLST8/GβL associates with mTORC2 by binding to the kinase domain of mTOR and plays several roles in stability, assembly, and mTOCR2 activity towards AKT and protein kinase Cα (PKCα) (Cho 2011).
DEP domain containing mTOR interacting protein (Deptor)	A negative regulator of mTORC2, which binds to the FAT domain of mTOR (Chong, 2015).

1.2.1.2 Signalling upstream of mTOR

Upstream of mTOR is the Phosphoinositide 3-kinase (PI3K)/acutely transforming retrovirus AKT8 in rodent T cell lymphoma (AKT, also known as protein kinase B) pathway. PI3K is a class IA member of the lipid kinase family which is activated by tyrosine kinase receptors which is activated by insulin (or insulin-like growth factor), which generates phosphatidylinositol-3, 4, 5-trisphosphate (PIP_3) from phosphatidylinositol-4, 5 bisphosphate (PIP_2) (Hassan *et al*. 2013; Huang and Fingar 2014).

PIP_3 is an important lipid messenger that is used to allosterically regulate several components upstream of mTOR. Activated PIP_3 recruits and allows phosphoinositide-dependent kinase 1 (PDK1 – a serine/threonine kinase) to phosphorylate AKT. PIP_3 also interacts with the mTORC2 complex via mSIN1interaction that causes mSIN1 to release its inhibition of the mTOR kinase domain leading to activation of mTORC2. PIP_3 is negatively regulated by phosphatase and tensin homolog deleted on chromosome 10 (PTEN), which dephosphorylates PIP_3 back to PIP_2 (Huang and Fingar 2014; Dibble and Cantley 2015; Liu *et al*. 2015; Zhang *et al*. 2016).

AKT is a serine/threonine protein kinase that is a key intracellular mediator of diverse cellular processes (Cho, 2011). AKT becomes fully activated via direct phosphorylation by mTORC2 and PDK1. AKT activates mTORC1 via direct phosphorylation of TSC2 at five residues (Ser^{939}, Ser^{981} Ser^{1130}, Ser^{1132} and Thr^{1462} - all of which exist outside of the GTPase activating protein (GAP) domain of TSC2) (Dibble and Cantley 2015). AKT also regulates cellular levels of ATP. Activated AKT maintains a high level of ATP by promoting glucose metabolism through hexokinase phosphofructokinase activity stimulation and translocation of glucose transporters (Glut1 and Glut4) to the cell surface. This triggers a decrease in the AMP/ATP ratio, resulting in AMPK inactivation and as a result, prevents activation of TSC2 (Figure 1.6) (Hahn-windgassen *et al.* 2005; Perluigi *et al.* 2015; Hung *et al.* 2017)

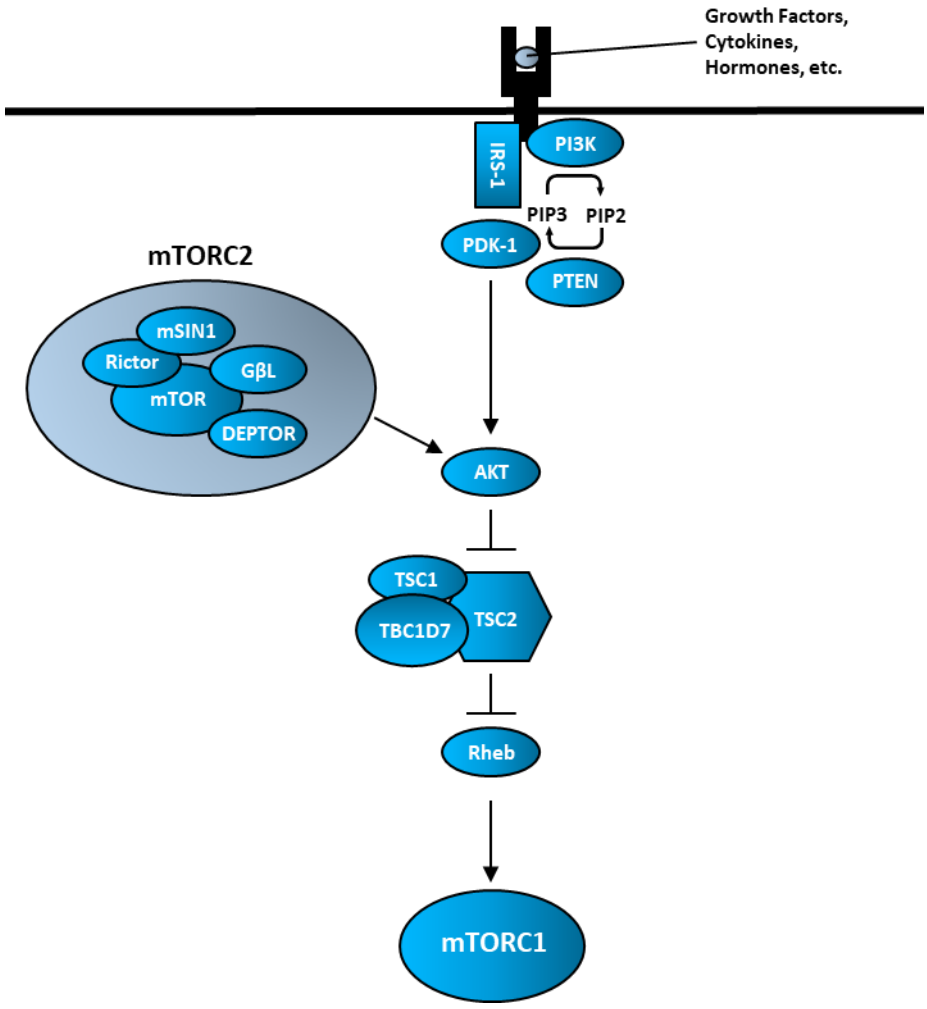

Figure 1.6 Upstream activation of the mTORC1. Growth factors/Insulin activates PI3K which catalyses the transformation of PIP_2 to PIP_3. PIP_3 allows mTORC2 and PDK1 to interact with AKT and causes AKT to become phosphorylated. Phosphorylated AKT disrupts TSC complex via phosphorylation of TSC2. The TSC complex regulates Rheb via GTPase activity which converts Rheb to an inactive GDP-bound state. Phosphorylation of TSC2 by activated AKT prevents GTPase activity, which allows for the activation of mTORC1

1.2.1.3 Downstream of mTORC1 complex

mTORC1 has 2 main downstream mediators p70 ribosomal protein S6 kinase 1 (S6K1) and eukaryotic translation initiation factor 4E (eIF4E)-binding protein 1 (4E-BP1) (Qin *et al.* 2016; Calkins *et al.* 2018) (Figure 1.7).

S6K1 is a serine/threonine kinase and is a member of the AGC kinase family (Tavares *et al.* 2015). The main target of S6K1 is ribosomal protein S6 (rpS6) which is a component of the 40S ribosomal subunit (Tavares *et al.* 2015). S6K1 can also enhance *de novo* synthesis of pyrimidines via phosphorylation of carbamoyl-phosphate synthase 2, aspartate transcarbamoylase and dihydroorotase (CAD)

(Ben-Sahra *et al.* 2013). Direct S6K1 phosphorylation (at Thr^{389}) by mTORC1 activates S6K1 which, in turn, phosphorylates several downstream targets involved in mRNA translation including eIF4B (a positive regulator of the 5'-cap binding eIF4F complex) and PDCD4 (an inhibitor of eIF4B which is degraded following phosphorylation) (Saxton and Sabatini 2017).

4E-BP1 in a hypo-phosphorylated state, prevents translation initiation by binding to the translation factor, eukaryotic initiation factor 4E (eIF4E). eIF4E interacts with the 7-methyl-guanosine 5′-cap structure, m7GpppX (where X is any nucleotide) at the 5-end of the mRNA. eIF4E regulates cap-mediated mRNA translation by forming a multi-subunit complex called eIF4F (eIF4E associated with eIF4G (a scaffold protein), eIF4B and eIF4A (which unwinds the secondary structure in the 5'-untranslated regions (5'-UTR) of mRNAs)). The eIF4F complex is involved in the recruitment of 40S ribosomal subunits to the 5'-cap of the mRNA. mTORC1 activation phosphorylates 4E-BP1 and causes dissociation of 4E-BP1 from eIF4E, allowing the recruitment of eIF4G to form the eIF4F complex that then promotes translation initiation (Morita *et al.* 2015; Qin *et al.* 2016; Tee *et al.* 2016; Calkins *et al.* 2018). While mTORC1 controls global protein synthesis by regulating eIF4F assembly, eIF4E preferentially stimulates the translation of select groups of mRNAs through "eIF4E-sentitive" mRNAs (Koromilas *et al*. 2018). These eIF4E-sensitive mRNAs include several mRNAs encoding proteins involved in cell survival and proliferation, such as cyclins, ornithine decarboxylase (ODC), VEGF and Myc (Nandagopal and Roux 2014).

Protein synthesis is essential for cell growth and proliferation. However, aberrant levels of protein synthesis can cause the accumulation of unfolded, misfolded, insoluble, or otherwise damaged proteins. Accumulation of unfolded protein can cause cell stress. If cells cannot accommodate the increased demand of newly synthesised proteins (either by increasing the capability to fold proteins or by getting rid of damaged proteins via autophagy and the proteasome), recovery of stress caused from this accumulation of unfolded proteins occurs in the endoplasmic reticulum (ER). This stressed condition is discussed in detail later in this chapter. Protein synthesis is also the largest consumer of ATP. As a result, energy stress can occur if protein synthesis is enhanced and cells cannot find other means to ensure a sufficient replenishment of energy.

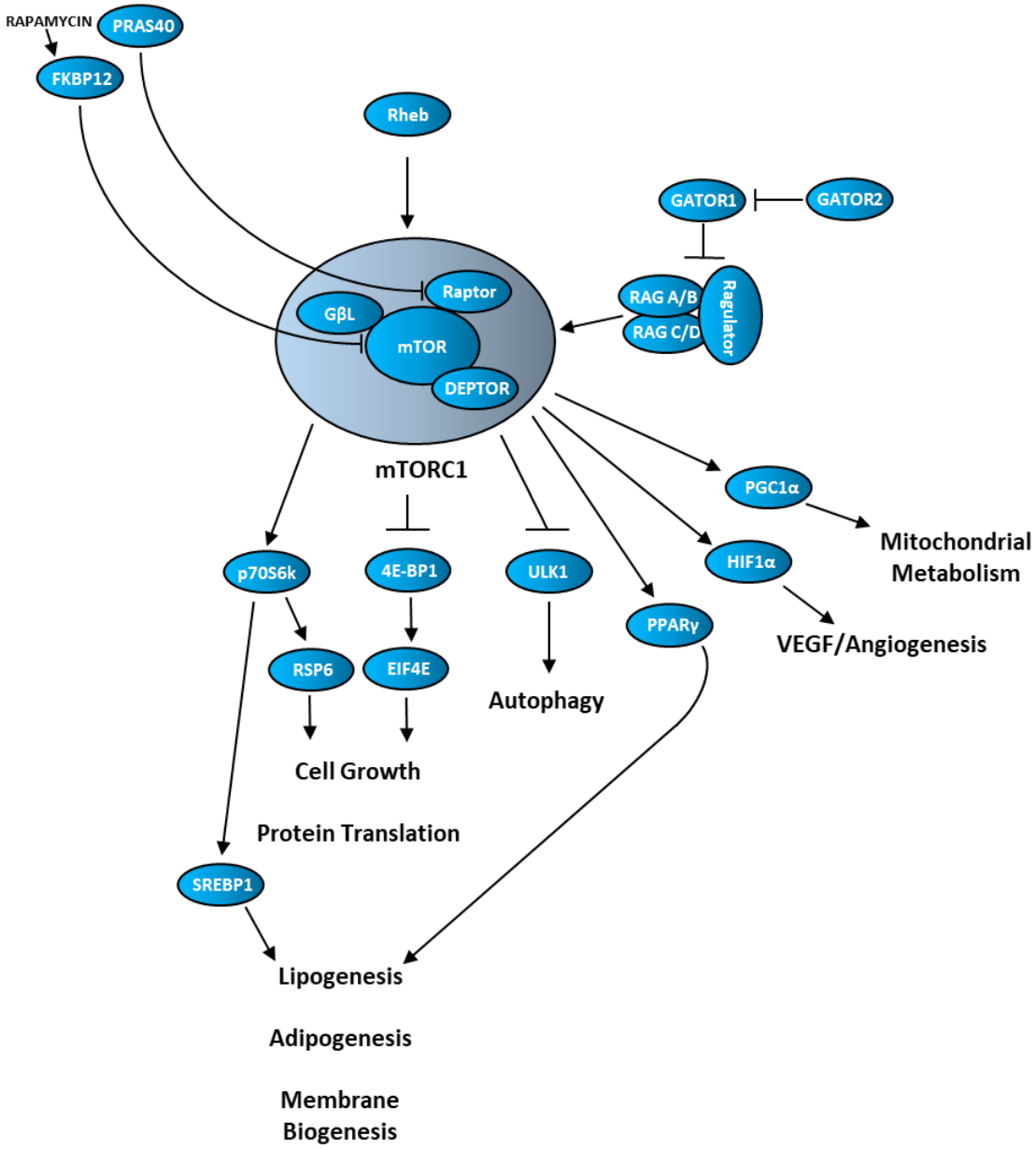

Figure 1.7 The mTORC1 pathway. Inactive mTORC1 is translocated to the surface of the lysosome (via with Rag guanosine triphosphatases (Rag GTPases or RAGs)). At the lysosome, mTORC1 interacts with Rheb (in its GTP-bound state) causing activation of the mTORC1 complex. Activated mTORC1 has several downstream effects. These include increased protein translation (via inhibition of 4E-BP1), increased mRNA biogenesis (via S6K1), decreased autophagy (via inhibition of ULK1), increased angiogenesis (via HIF1α activation), lipogenesis/adipogenesis, and membrane biogenesis.

1.2.2 mTORC1 and angiogenesis

As previously mentioned above, HIF1α plays a role in vascularisation and angiogenesis and is defined as a master transcriptional factor of cellular and developmental response to hypoxia. In normoxic conditions, HIF1α undergoes ubiquitination and proteasomal degradation, while HIF1α accumulates and plays a

role in transcription during hypoxia (Zhang *et al.* 2015). When mTORC1 is hyperactive, HIF1α drives VEGF gene-expression to high levels. TSC patients have been shown to have elevated baseline levels of VEGF-D in their blood. This data can be used as a diagnostic biomarker to demonstrate a sensitivity to mTORC1 inhibitor therapy. (Dabora *et al*. 2011; Malinowska *et al*. 2013). mTORC1 activation causes an accumulation of HIF1α via direct phosphorylation of STAT3 on Ser^{727} (Dodd *et al*. 2015), resulting in VEGF accumulation (Figure 1.7).

Different components of mTORC1 control protein expression of HIF1α and VEGF (Dodd et al. 2015). Protein translation of HIF1α is regulated by S6K1 and 4E-BP1, while VEGF is primarily under the control of 4E-BP1 and eIF4E. The relationship between mTORC1 and HIF1α is also important in foetal lung development, as Scott *et al.* (2010) showed HIF1α-driven vasculogenesis is linked to the cross-talk between mTORC1 and the fibroblast growth factor (FGF) 10/FGF-receptor2b/Spry2 regulator of airway branching.

mTOR inhibitors effectively blocked Ser^{727} phosphorylation of STAT3, and abolishment of HIF-1α expression was achieved by targeting JAK2-mediated Tyr^{705} phosphorylation site and mTORC1-mediated Ser^{727} site on STAT3 (Dodd *et al*. 2015).

1.2.3 mTORC1 and lipogenesis

mTORC1 plays a role in lipogenesis (Figure 1.7). Lipid biosynthesis is essential for the maintenance of cellular homeostasis. The lipids produced by cells (glycerolipids, fatty acids, phospholipids, cholesterol, spingolipids) are used in different ways; as an energy source/reserve, as building blocks for membrane biosynthesis, as precursor molecules for the synthesis of various cellular products and also as signalling molecules (Laplante and Sabatini 2009). Following their activation, mTORC1 facilitates the accumulation of triglycerides by promoting adipogenesis and lipogenesis and by shutting down catabolic processes such as lipolysis and β-oxidation (Caron *et al.* 2015).

mTORC1 controls lipogenesis via regulation of Lipin-1 entry into the nucleus. Lipin-1 is a phosphatidic acid phosphatase involved in the cleavage of phosphatidic acid, an integral step in triacylglycerol synthesis (Huffman *et al.* 2002). Lipin-1 also regulates sterol regulatory element binding protein 1 (SREBP1) activity. SREBP1 is a transcription factor that is critical for the regulation of fatty acid and cholesterol

biosynthetic gene expression (Horton *et al*. 2002). While located in the nucleus, Lipin-1 inhibits lipogenesis by SREBP1 (Peterson *et al.* 2011). When mTORC1 is activated, mTORC1 directly phosphorylates Lipin-1 preventing translocation of Lipin-1 into the nucleus, allowing SREBP1 activity to proceed in *de novo* lipogenesis.

mTORC1 also contributes to lipogenesis via SR protein kinase 2 (SRPK2), a key regulator of RNA-binding SR proteins. S6K1 phosphorylates SRPK2 at Ser^{494}, which primes Ser^{497} phosphorylation by Casein kinase 1 (CK1). Activated SRPK2 is then translocated to the nucleus and activates SR proteins and U1-70K to promote splicing of lipogenic transcripts (Chavez *et al*. 2017).

Significant lysophosphatidylcholine (LPC) – a lysoglycerophospholipid accumulation was found in TSC2-deficient cells relative to TSC2-expressing control cells (Priolo *et al.* 2015). These changes occurred alongside changes in other phospholipid and neutral lipid species. mTORC1 shuts down catabolic processes involved in lipid metabolism such as lipolysis and β-oxidation (Caron *et al.* 2015) while at the same time, autophagy regulating intracellular lipid stores via macrolipophagy (Singh *et al.* 2009). Constitutive activation of mTORC1 (via TSC1/2 mutation) prevents lipid metabolism and inhibits autophagy causing an accumulation of lipids in the cell which in turn could lead to an energy crisis as cells cannot utilise lipid components to generate much needed energy to compensate for protein biogenesis. The regulation of energy crisis is regulated in TSC1/2-deficient cells is discussed later in this chapter.

1.2.4 mTORC1 and autophagy

Autophagy is a conserved self-degrading process which is a well-established survival mechanism to maintain cellular homeostasis in both a normal and stressed environment (Wataya-Kaneda 2015). Unc-51-like kinase 1 (ULK1) is a serine/threonine kinase that functions in a complex with Atg13, FIP200 and Atg101 to form the highest upstream component of the mammalian autophagy pathway (Dunlop and Tee 2013). In stressed conditions (e.g. nutrient starvation) autophagy is activated by the phosphorylation of Atg13 and FIP200 and by the autophosphorylation (at Ser^{1047}) of ULK1 (Dunlop and Tee 2013; Dunlop and Tee 2014).

mTORC1 inhibits autophagy via phosphorylation of ULK1 on Ser^{758} (Kim and Guan 2015; Gallagher *et al.* 2016) (Figure 1.7). Interestingly, different types of mTORC1 inhibition affect dephosphorylation of ULK1. Nutrient starvation causes a complete dephosphorylation of ULK1 compared to mTORC1 inhibitors such as rapamycin (Wong *et al.* 2015). This is possibly because nutrient starvation causes a complete shutdown of mTORC1 while mTOR inhibitors can only cause a partial mTORC1 inhibition. However ULK1 is also known to phosphorylate Raptor in a form of signal feedback at Ser^{696}, Thr^{706}, Ser^{855}, Ser^{859}, Ser^{863}, Ser^{877} and Ser^{792} that can potently block mTORC1 activity (Dunlop and Tee 2013).

Another possible mechanism of mTORC1-mediated ULK1 regulation is via the disruption of ULK1 stability through inhibitory phosphorylation of autophagy/beclin 1 regulator 1 (AMBRA1) (Nazio *et al.* 2013). mTORC1 also regulates autophagy at the transcriptional level by modulating the localisation of transcription factor EB (TFEB), a master transcriptional regulator of lysosomal biogenesis and autophagy genes (Kim and Guan 2015).

Depending on the cellular context, autophagy can either promote or inhibit tumorigenesis. In terms of TSC, It was proposed that the AMPK/p27 axis might be promoting a survival mechanism in *Tsc2*-null cells as AMPK stabilises p27 and p27-dependent activation of autophagy is involved in *Tsc2*-null cell survival under rapamycin treatment (Campos *et al.* 2016). Inhibition of AMPK and p27 depletion were observed to reduce activation of autophagy by rapamycin in *Tsc2*-null cells (Campos *et al.* 2016). Parkhitko *et al.* (2011) observed inhibiting both mTORC1 and autophagy inhibition was more effective than either treatment alone in terms of inhibiting the survival of *TSC2*-null cells, growth of *TSC2*-null xenograft tumours (which also trigger large amounts of necrosis), and development of spontaneous renal tumours in *Tsc2*(+/-) mice. The authors also showed that down regulation of p62 (the autophagic substrate that accumulates in TSC2-deficient cells has its expression reduced via autophagic inhibition. Hippo-Yes-associated protein 1 (YAP) was shown to accumulate in TSC1/TSC2-deficient cells due to impaired degradation of the protein by the autophagosome/lysosome system. The data also showed that YAP inhibition blunts abnormal proliferation and induces apoptosis of TSC1–TSC2-deficient cells, both in culture and in mosaic *Tsc1* mutant mice (Liang *et al.* 2014).

Autophagy inhibition combined with enhanced protein synthesis and the inability to use lipids as an energy source, causes *TSC1/2*-null cells to become

energy stressed. In the next two sections of this chapter, how energy stress is managed will be discussed.

1.2.5 mTORC1 and energy metabolism

mTORC1 responds to intracellular and environmental stresses that are incompatible with growth such as reduction in cellular energy charge (e.g. during glucose deprivation or in low ATP environments). Energy starvation is the result of protein and lipid biosynthesis in TSC. This activates the stress responsive metabolic regulator AMPK, which inhibits mTORC1 both indirectly, through phosphorylation of TSC2 leading to GAP activity, as well as directly, through the phosphorylation of Raptor at Ser^{722} and Ser^{792}, leading to 14-3-3 protein binding and mTORC1 inhibition (Dunlop and Tee 2013; Saxton and Sabatini 2017).

5' adenosine monophosphate-activated protein kinase (AMPK) is a trimeric complex that acts as a highly conserved master regulator of metabolism, which restores energy balance during metabolic stress both at the cellular and physiological levels (Garcia and Shaw 2017). AMPK becomes activate in the presence of high AMP: ATP and ADP: ATP ratios, via allosteric binding of AMP and ADP to the γ-subunit of AMPK. This confirmation change of AMPK then promotes Thr^{172} phosphorylation in the activation loop of the kinase domain by the serine/threonine kinase LKB1 (liver-kinase-B1) (Hawley *et al.* 2003; Woods *et al.* 2003; Shaw *et al.* 2004). AMPK promotes glucose uptake by phosphorylating TBC1D1 (TBC domain family, member 1) and TXNIP (thioredoxin-interacting protein), which controls the translocation and cell-surface levels of glucose transporters GLUT4 and GLUT1. AMPK also acutely regulates glycolysis in some tissue types by phosphorylating PFKFB3 (6-phosphofructo-2-kinase/fructose-2,6-biphosphatase 3) (Hardie 2013; Wu *et al.* 2013). At the same time, AMPK controls overall cellular lipid metabolism through direct phosphorylation of ACC1 (acetyl-CoA carboxylase 1) and ACC2, resulting in the suppression fatty acid synthesis while simultaneously promoting fatty acid oxidation by relieving the suppression of CPT1 (carnitine palmitoyltransferase 1) by malonyl-CoA (Ahmadian *et al*. 2011; Abbott *et al*. 2016) (Figure 1.8).

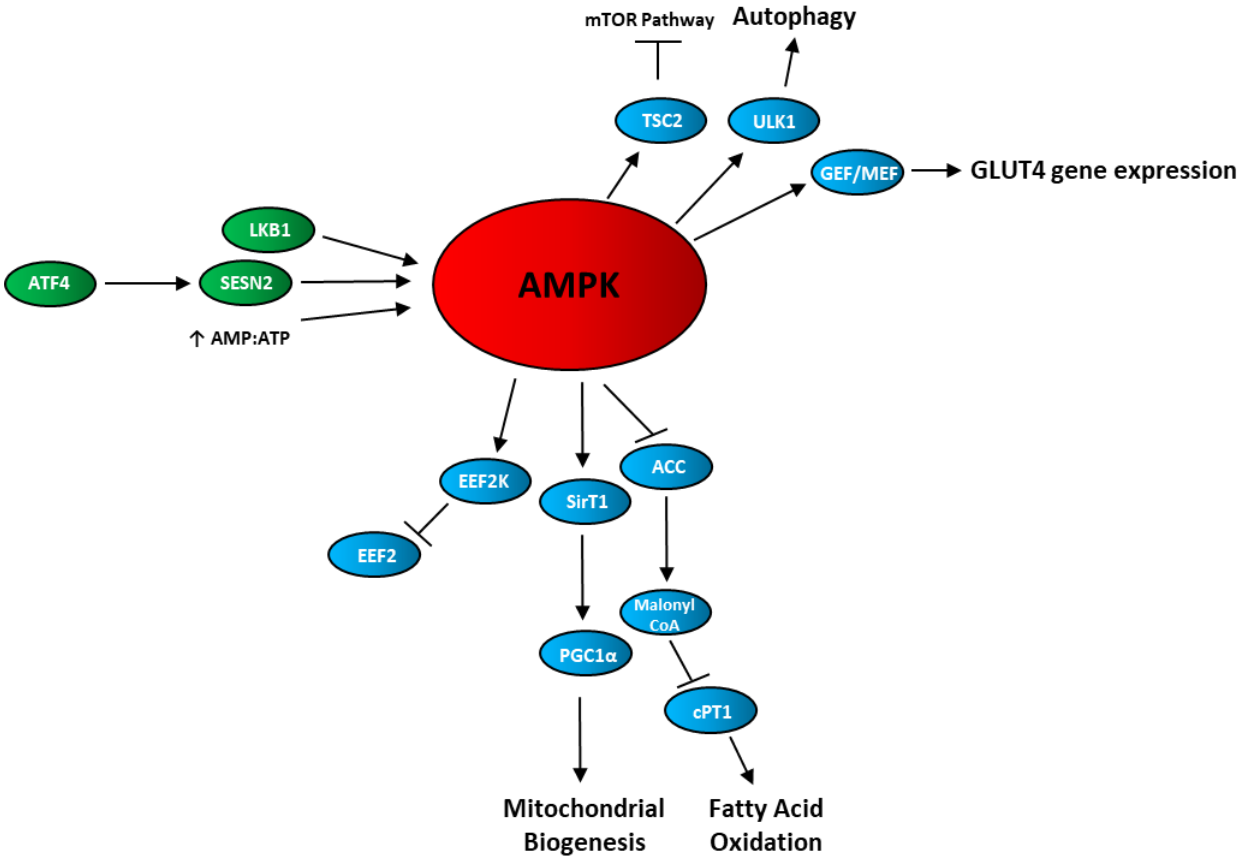

Figure 1.8 Energy metabolism. In the presence of low energy levels, AMPK is activated by several factors including SESN2 and LKB1. Activated AMPK causes increased mitochondrial biogenesis (via PGC1α), increases glucose uptake (via increase GLUT4), regulates lipid metabolism by promoting fatty acid oxidation (via cPT1) and suppresses mTOR pathway (via TSC2).

1.2.6 mTORC1 and mitochondrial biogenesis

To compensate for the high energy demand caused by protein synthesis and lipogenesis, TSC1/2-null cells enhance ATP generation by increasing mitochondrial biogenesis. mTORC1 controls mitochondrial activity and biogenesis by selectively promoting translation of nucleus-encoded mitochondria-related mRNAs via inhibition of 4E-BP1. The translation of nucleus-encoded mitochondria-related mRNAs stimulates an increase in the generation of ATP, which is a required energy source for translation (Morita *et al.* 2013). AMPK (activated as a result of low ATP levels) is also responsible for the activation of PGC1α (peroxisome proliferator-activated receptor gamma, coactivator 1α), a master regulator of mitochondrial biogenesis, via direct phosphorylation of PGC1α and by promoting NAD+-dependent activation of PGC1α by Sirt1 (sirtuin 1) (Speer *et al*. 2012) (Figure 1.8).

1.2.7 Potential vulnerabilities of TSC

Understanding the pathophysiology of TSC-diseased cells gives potential insights into signalling pathways that could be therapeutically targeted to restore disease status. Understanding the key signalling pathways involved in homeostatic balance in TSC-diseased cells might also reveal potential avenues of therapy that could have cytotoxic effect.

1.2.7.1 TSC and the lysosome

While inactive, mTORC1 is found in the cytoplasm, in the presence of amino acids, mTORC1 is translocated to the surface of the lysosome, where Rheb (in its GTP-bound state) is located, which in turns activates mTORC1. This is due to mTORC1 association with Rag guanosine triphosphatases (Rag GTPases or RAGs) (Wataya-Kaneda 2015). RAGs (identified by Kim *et al.* (2008) and Sancak *et al.* (2008)) exist as heterodimers of either RagA or RagB bound to either RagC or RagD that in turn binds to Raptor in mTORC1 (Chong 2015). Association only occurs if RagA/B is in a GTP-bound state (and RagC/D is in a GDP-bound state) (Shimobayashi and Hall 2016) (Figure 1.7).

Rags don't contain a membrane-targeting sequence but are able to bind to the lysosomal surface due to the presence of the Ragulator complex (Groenewoud and Zwartkruis 2013). The Ragulator complex is a pentametric complex that is comprised of LAMTOR (late endosomal/lysosomal adaptor, MAPK (mitogen activated protein kinase) and mTOR activator)1,2 and 3 (also known as p18, p14 and MP1 (MAPK scaffold protein 1)), HBXIP (hepatitis B virus X-interacting protein) and C7orf59 (Groenewoud and Zwartkruis 2013; Saxton and Sabatini 2017). The Ragulator complex also acts as an amino acid-stimulated GEF (guanine nucleotide-exchange factor) for RagA/B that brings these GTPases to their active GTP-bound state.

The GAP for RagA/B is the Gap Activity TOward Rags (GATOR) complex. This complex is involved in amino acid sensing activity and is composed of two subcomplexes, GATOR1 and GATOR2 function as negative and positive regulators of mTORC1, respectively. GATOR1 is the GAP component of the complex and is composed of DEPDC5 (DEP domain-containing protein 5, which is the GAP subunit), NPRL2 (nitrogen permease regulator 2-like protein) and NPRL3 (nitrogen permease regulator 3-like protein). Proteins that regulate the GATOR complex

include sestrin2 (which releases, GATOR1 from GATOR2), (Baldassari *et al.* 2016; Shimobayashi and Hall 2016). The amino acid leucine is especially important for GATOR complex as leucine binds to the GATOR complex, which causes the GATOR complex to become tethered to the lysosome (Saxton and Sabatini 2017).

The GAP for RagC/D is folliculin (FLCN), that promotes the active conformation of RagC/D. FCLN is bound to the lysosome in an amino acid-starved environment when RagA/B is inactive. When RagA/B is active, FLCN disassociates from the lysosome with FLCN-interacting protein (FNIP) that promotes mTORC1 translocation to the lysosome (Shimobayashi and Hall 2016).

Chloroquine-induced inhibition of lysosomal function caused an upregulation in the expression of cholesterol homeostasis genes in *TSC2*-deficient cells while simultaneous inhibition of the lysosome and endosomal trafficking (using chloroquine and SAR405) inhibits the proliferation of *TSC2*-deficient cells (Valvezan *et al*. 2017). Accumulation of chloroquine in the lysosome contributed to cytotoxicity of a chloroquine/nelfinavir combination against *Tsc2*-/- MEFs (Johnson *et al*. 2015).

1.2.7.2 TSC and energy stress

Tsc1/2-null cells are hypersensitive to glucose deprivation. mTORC1 inhibition during glucose deprivation prevented cell death (Choo *et al.* 2010). It was also found that mTORC1 hyperactive cells became highly dependent on glutamate dehydrogenase-dependent glutamine metabolism via the TCA cycle for survival. In TSC-diseased cells, constitutive activation of mTORC1 causes cells to become sensitised to glucose starvation and DNA damage (which in this case was triggered by the introduction of DNA-alkylating agent methyl methane sulfonate (MMS), which causes base mispairing and replication blocks) (Lee *et al.* 2007). The combined starvation and DNA damage resulted in enhanced p53 activation (via stabilising phosphorylation), leading to cell death.

2-deoxy-D-glucose (2-DG) which is a glucose analog missing in which the 2-hydroxyl group has been replaced by hydrogen, preventing it from undergoing glycolysis leading to reduced cellular ATP levels and cell growth and a carbohydrate-free diet were tested on LEF2 cells from a Tsc2-null rat tumour in mice (Jiang *et al*. 2011). The authors showed that exposure of these cells to 2-DG resulted in a decreased cell viability at low glucose concentration. This analysis

shows that cells lacking TSC2 are vulnerable to conditions that result in energy stress.

1.2.7.3 TSC and ER stress

1.2.7.3.1 ER stress

The endoplasmic reticulum (ER) is a multifunctional organelle which is involved in several key roles such as lipid biosynthesis, calcium storage and protein folding and processing. It has two different surfaces: the ribosomal stubbed outer layer (or rough ER), which is involved in protein synthesis and secretion. The smooth ER layer that has no ribosomes and is mostly involved in the synthesis of proteins, fatty acids and phospholipids synthesis, assembly of lipid bilayers, the metabolism of carbohydrates, and the regulation of calcium homeostasis (Schönthal 2012).

Several physiological and pathological conditions and a variety of pharmacological agents can disturb the proper function of the ER resulting in ER stress. Several adaptive mechanisms bring the folding capacity of the ER and its unfolded protein burden into line and return the ER to its normal physiological state: (1) upregulation of ER folding capacity through induction of ER-resident molecular chaperones and foldases; (2) increase the ER size through membrane expansion; (3) down-regulation of the biosynthetic load of the ER through inhibition of protein synthesis at a transcriptional and translational level; (4) and increased clearance of unfolded proteins from the ER through the upregulation of ER associated degradation (ERAD) (Harding *et al*. 1999; Friedlander *et al*. 2000; Travers *et al*. 2000; Martínez and Chrispeels 2003; Pakula *et al*. 2003; Zúñiga *et al*. 2004). Endoplasmic-reticulum-associated protein degradation (ERAD) can occur in two different ways. The first is where damaged proteins are exported back into the cytoplasm and delivered to the proteasome for degradation. The second way is via aggresome formation, where damaged proteins are compacted together with other cellular debris into juxtanuclear complexes and then recycled via autophagy (Schönthal 2012).

The accumulation of unfolded, misfolded, insoluble, or otherwise damaged proteins can irreparably damage cellular functions and thus pose a proteotoxic threat to the survival of the cell. Due to this cytotoxic risk several cellular sensors and pathways have evolved to respond to this threat

1.2.7.3.2 PERK pathway

Protein kinase RNA-like endoplasmic reticulum kinase (PERK) is a type I transmembrane protein and is activated by the release by the release of binding immunoglobulin protein (BiP also called GRP78) from its ER luminal domain (Schröder and Kaufman 2005). Upon BiP release, PERK undergoes homodimerization and autophosphorylation before phosphorylating the α subunit of eukaryotic initiation factor 2 (eIF2α) at Ser^{51} (Rojas *et al.* 2015). Phosphorylation of eIF2α converts eIF2-GDP into a competitive inhibitor of eIF2B (guanine nucleotide exchange factor). This prevents the recycling of eIF2 between successive rounds of protein synthesis and results in the inhibition of the protein translation initiation pathway (Hinnebusch 2000; Clemens 2013; Bogorad et al. 2017).

Phosphorylation of eIF2α also triggers the promotion of mRNA translation for mRNA encoding specific stress response factors such as activating transcription factor 4 (ATF4) which in turn leads to the transcription of downstream CCAAT-enhancer-binding protein homologous protein (CHOP) and growth arrest and DNA damage-inducible protein 34 (GADD34, also called PPP1R15A) and activating transcription factor 3 (ATF3), which also contributes to the expression of CHOP and GADD34 (Jiang *et al.* 2004; Rojas *et al.* 2015).

CHOP is an important proapoptotic transcription factor. Expression of CHOP in ER stress is up-regulated by ATF6, and preferential synthesis of ATF4 (Ma *et al.* 2002). In normal cells, CHOP levels are kept very low level, however, increased expression and accumulation of CHOP occurs in as a response to unfolded protein response (UPR) and integrated stress response (ISR) (CHOP levels can also be increased by growth arrest, DNA damage, nutrient deprivation, hypoxia and genotoxic agents) (Li *et al.* 2014c; Yang *et al.* 2017). The full pro-apoptotic effects of CHOP won't occur unless ER stress is constitutive and cannot be subdued. If ER stress cannot be subdued, CHOP will upregulate proapoptotic members of the Bcl-2 family such as Bim and the down regulation of the of Bcl-2 transcription (McCullough *et al.* 2001; Tabas and Ron 2011). CHOP also upregulates expression of death receptor 5 (DR5) which sensitizes cells to apoptotic stimulation by a variety of conditions that cause ER stress (Yamaguchi and Wang 2004) GADD34 expression is stimulated by CHOP (Kojima *et al.* 2003) and is expressed late in ER stress. GADD34 regulates the phosphatase activity of protein phosphatase 1 (PP1) via its C-terminal domain. GADD34 acts as a scaffold for PP1 accepts eIF2α as substrate and causes dephosphorylation of eIF2α (Figure 1.9).

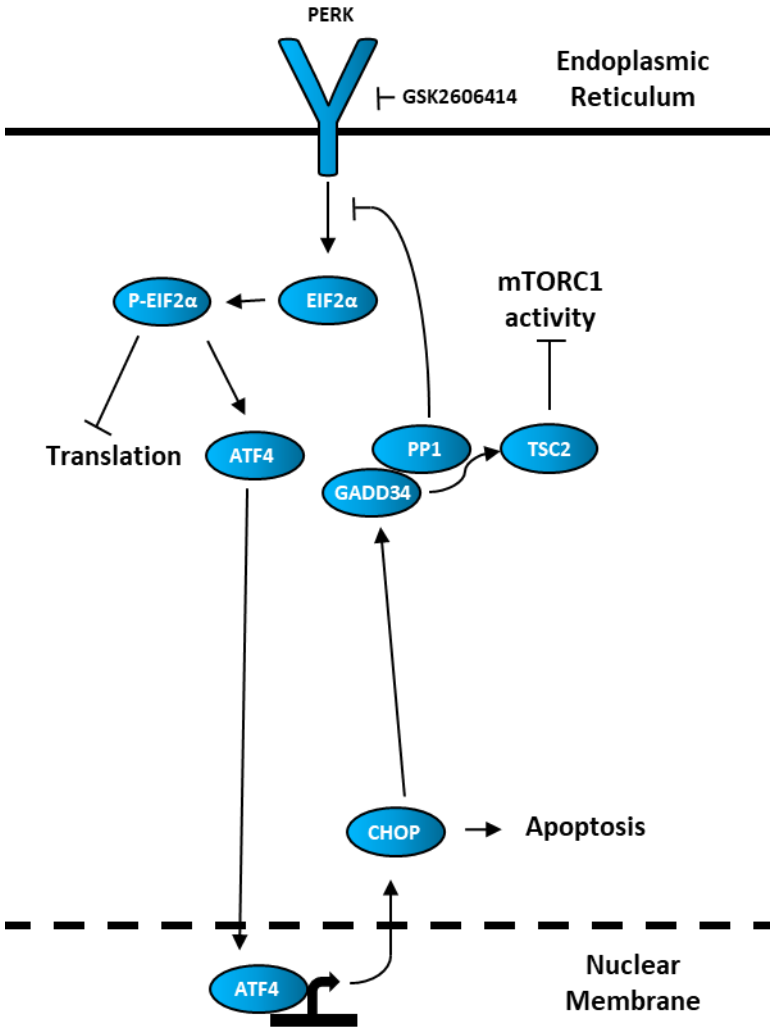

Figure 1.9 PERK pathway. Activation of the PERK pathway phosphorylates EIF2α which inhibits protein translation. EIF2α phosphorylation triggers the promotion of mRNA translation for mRNA encoding specific stress response factors such as ATF4. ATF4 production, in turn, leads to the transcription of downstream products such as CHOP and GADD34.

1.2.7.3.3 ATF6

Cyclic AMP-dependent transcription factor ATF-6 (ATF6) exists as two homologous proteins ATF6α and ATF6β. ER transmembrane-localized ATF6 contains a basic leucine zipper (bZIP) motif and has transcriptional properties. Upon the release of BiP, the Golgi localization sequence is unmasked and ATF6 is translocated to the Golgi complex. At the Golgi complex, ATF6 is modified by two separate enzymes; the luminal domain of ATF6 is cleaved by serine protease site-1 protease (S1P) while the N-terminal (which is anchored in the Golgi membrane) is cleaved by metalloprotease site-2 protease (S2P). The N-terminal cleavage results in the release of the cytosolic bZIP transcription factor domain from the Golgi membrane

and translocates to the nucleus. ATF6 is responsible for the stimulation of several genes whose protein products contribute to protein folding, protein secretion, and ERAD include BiP and Glucose-regulated protein 94 (GRP94 – a HSP90-like protein that specialised in protein folding and ER quality control), protein disulphide isomerase (PDI – ER chaperone), x-box binding protein 1 (XBP1), and C/EBP homologous protein (CHOP) (Schröder and Kaufman 2005; Schönthal 2012) (Figure 1.10).

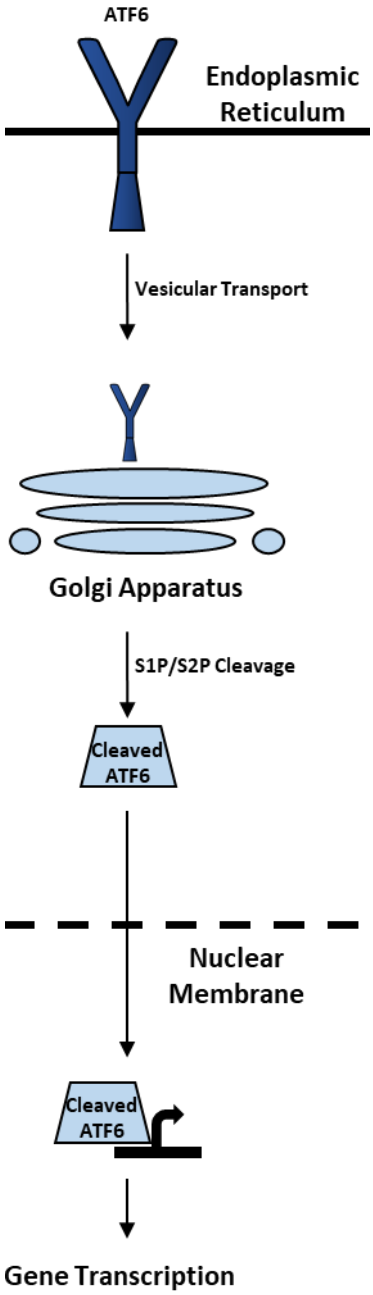

Figure 1.10 The ATF6 pathway. ATF6 is translocated to the Golgi Apparatus and cleaved by S1P and S2P. Cleaved ATF6 translocates to the nucleus and stimulates several genes involved in protein folding, protein secretion, and ERAD.

1.2.7.3.4 IRE-1α pathway

Inositol-requiring enzyme 1 (IRE1) pathway regulates chaperone induction, ERAD and ER expansion in times of ER stress and exist as two paralogues in mammals; IRE-1α and IRE-1β (where expression is limited to the gut) (Schröder and Kaufman 2005; Tsuru *et al.* 2016). IRE-1α signalling is the most conserved signalling branch of ER stress (Patil and Walter 2001; Kohno 2010). It possesses a luminal sensor

domain and a cytosolic effector domain containing kinase and RNase subdomains (Tsuru *et al.* 2016). IRE-1α is suppressed by BiP and upon release from BiP, IRE-1α will undergo homodimerization and autophosphorylation as part of its activation process (Parmar and Schröder 2012).

Activated IRE-1α cleaves a 26-base fragment from the mRNA encoding XBP1, resulting in a spliced product called XBP1s (a frameshift that generates an alternative C-terminus of XBP1 with enhanced transcriptional activation potential (Walter and Johnson 1994)). XBP1 is a potent transcription factor controlling the expression of genes involved in ERAD and protein folding, and the synthesis of phospholipids that are required for the expansion of ER membranes during ER stress (Schönthal 2012). The XBP-1 splicing is also dependent of the PERK pathway as ATF4 influences the expression of IRE-1α (i.e., the higher the ATF4 expression, the higher the IRE-1α which in turn leads to higher XBP-1 splicing) (Tsuru *et al.* 2016) (Figure 1.11).

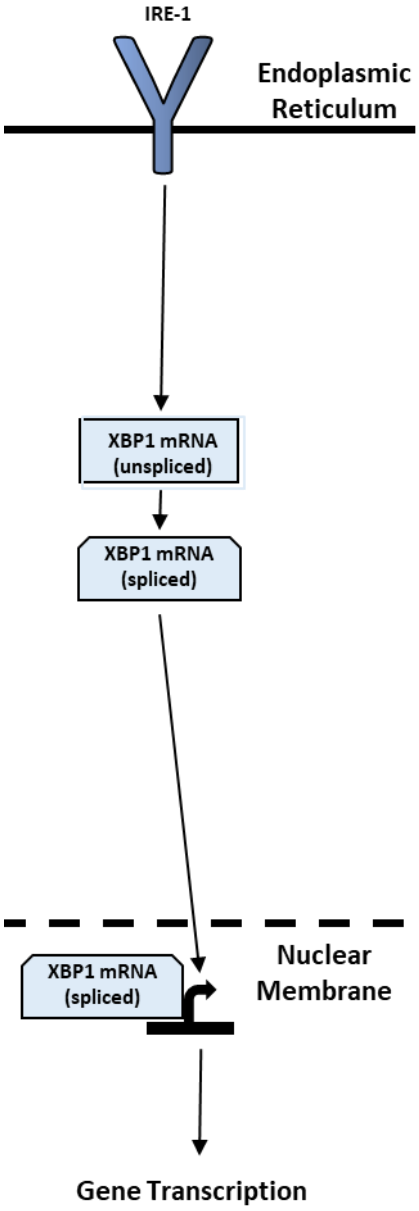

Figure 1.11 The IRE-1α pathway. Activated IRE-1α cleaves XBP1 (a transcription factor) resulting in a spliced product with enhanced transcriptional activation potential.

1.2.7.3.5 TSC and ER stress

Loss of *TSC1* or *TSC2* causes ER stress and activates the unfolded protein response (UPR) (Ozcan *et al.* 2008). mTORC1 further enhances the burden of ER stress through autophagy repression, as autophagy removes unfolded protein aggregates to restore the protein folding environment within the ER (Høyer-Hansen and Jäättelä 2007). Crosstalk between autophagy and ER homeostasis showed that induction of ER stress by thapsigargin was through impairment of autophagosome–lysosome fusion (Ganley *et al.* 2011). Insulin is major stimulus for many biosynthetic

pathways including protein synthesis, the action of feedback inhibition of insulin in the presence of ER stress is likely to represent an adaptive response and might even be considered part of the UPR. ER stress and activation of the UPR pathway are important pathological feature of TSC and contributes to critical functional abnormalities in insulin/IGF1 action and cell survival. UPR contributes to a negative feedback signal in TSC-deficient cells, at least in part, through the activation of c-Jun NH2-terminal kinases (JNK), which plays a role in inhibition of IRS-1 activity and the development of insulin resistance both *in vitro* and *in vivo* (Chang *et al*. 2002; Hotamisligil 2005).

Elevated cell stress is common in cancer cells and could be exploited (Hanahan and Weinberg 2011) as compromised stress recovery pathways in cancer cells may confer sensitivity to stress-inducing drugs as many cancer cell lines are sensitive to ER stress-inducers, where excessive or prolonged ER stress leads to cell death (Johnson *et al*. 2015).

TSC1/2-null cells are naturally ER stressed because of the enhanced protein synthesis and the inhibition of autophagy. The introduction of known ER stress inducers/enhancers could be a potentially viable treatment to investigate. In the next section of this chapter, one such ER stress enhancer, nelfinavir will be discussed as potential treatment for TSC after it was observed to have success in enhancing ER stress in several cancer cell lines

1.3 Nelfinavir

1.3.1 General Introduction

Nelfinavir is a clinical approved retroviral aspartic proteasome inhibitor which has been approved the treatment of HIV approved by the FDA in 1997. Kaldor *et al.* (1997) showed that Nelfinavir was able to prevent the proteolytic cleavage of viral precursor proteins to their mature forms. Nelfinavir forms part of the highly active antiretroviral therapy (HAART) (Brüning 2011).

Nelfinavir has been shown to cause ER stress (although this was only a partial response as there was an absence of detectable PKR-like endoplasmic reticulum kinase (PERK) or ATF6 activation or accumulation of misfolded proteins within the ER. By interfering with proteostasis, nelfinavir triggers ER stress. Nelfinavir has been shown to cause a decrease in protein translation and cause

promotion of transcriptional program which is characteristic of the integrated stress response (ISR). Nelfinavir activates elongation factor 2 kinase (eEF2K) through phosphorylation, leading to the phosphorylation and inhibition of the elongation factor eEF2, resulting in a reduction in mRNA translation. At the same time, nelfinavir contributes to phosphorylation of eIF2α which in turn leads to the translation of ER stress markers, ATF4 and GADD34 (which dephosphorylates eIF2α via interactions with protein phosphatase-1 (PP1c)). However, nelfinavir does not cause direct activation of the eIF2α stress kinases but instead relies on the inhibition of the constitutive eIF2α dephosphorylation and down-regulation of the phosphatase cofactor CReP (Constitutive Repressor of eIF2α Phosphorylation; also known as PPP1R15B) to cause phosphorylation of eIF2α (Martinon *et al*. 2015; De Gassart and Martinon 2017).

1.3.2 Nelfinavir controversy

Between May 2007 and July 2008, nelfinavir production was accidentally polluted with ethyl methyl sulfone. This is a highly toxic compound which has been shown to have mutagenic, carcinogenic, and teratogenic effects by reacting with guanine in DNA, forming O-6-ethylguanine which, during DNA replication, causes DNA polymerases to place thymine, instead of cytosine, opposite O-6-ethylguanine) (Gocke *et al.* 2009). The risks of adverse outcomes such as cancer in this patient cohort were measured and found to be statistically insignificant when compared to patients treated with the drug in other years (Boettiger *et al.* 2016) while in *in utero* exposure, incidence of malformation was similar to that in the cohort as a whole with different drug exposures and no children developed cancer after 9 years of follow-up (Blanche *et al*. 2016).

1.3.3 Nelfinavir and cancer

Nelfinavir has been shown to have a variety of anticancer properties. Nelfinavir has been shown to inhibit the PI3K/AKT/mTOR pathway especially in the case of solid tumours reported by (Blumenthal *et al.* 2014). It has also been shown to inhibit HSP90 via inhibiting the association between AKT and HSP90 (Choi *et al*. 2016b). Nelfinavir was shown to be able to cause two types of cell death in non-small cell lung cancer (NSCLC); caspase-dependent apoptosis and caspase independent

death that was characterized by induction of ER stress and autophagy (Gills *et al.* 2007).

Nelfinavir was shown to be able to inhibit the proliferation of primary human melanoma cell lines as it induced cell cycle arrest at the G_1 phase (via inhibition of cyclin dependent kinase 2 (CDK2) and concomitant dephosphorylation of retinoblastoma tumour suppressor) and promoted apoptosis (Jiang *et al* .2007). Inhibition of CDK2 was shown to be caused by proteasome-dependent degradation of Cdc25A phosphatase. Nelfinavir was able to profoundly sensitize BRAF and NRAS mutant melanoma cells to MAPK-pathway inhibitors via suppressions of MITF (the melanoma survival oncogene) expression (Smith *et al.* 2016).

Nelfinavir was able to cause cell death in a variety of malignant glioma cell lines via potent stimulation of ER stress (as observed in the increased expressions of CHOP and GRP78) which lead to activation of caspase 4-mediated cell death (Pyrko *et al.* 2007). Inhibition of glioma growth via ER stress was also observed *in vivo*, as nelfinavir inhibited the growth of a xenografted human malignant glioma, with concomitant induction of CHOP. Nelfinavir enhanced ER stress in glioblastoma multiforme cells (as seen with increased expression of CHOP and ATF4), which lead to an increase in DR5 receptor expression. This increased receptor expression caused cells to be sensitized to Tumour Necrosis Factor-related Apoptosis-inducing Ligand (TRAIL) and induced apoptosis (Tian *et al.* 2011).

In thyroid cancer cell lines FT133, BCPAP and SW1736, at 10 μM, nelfinavir increased the time required for cell passage through the phases of cell cycle (as seen in accumulation of cells in G0/G1 phase, downregulation of cyclin D1 and cyclin-dependent kinase 4 (CDK4)) and induced DNA fragmentation (as seen in the expression of γH2AX and p53BP1) (Jensen *et al.* 2017). At 20 μM, nelfinavir was shown to cause apoptosis (via caspase-3 cleavage) and decreased the levels of total and phosphorylated AKT in PTEN-deficient FTC133 cells. Nelfinavir was shown to have no significant effects on total ERK and p-ERK in BRAF-positive BCPAP and SW1736 cells or on the expression of EMT markers (Twist, Vimentin, E- and N-Cadherin), but inhibited the migration and decreased the abilities of thyroid cancer cells to survive in non-adherent conditions. In medullary thyroid cancer, at 10 μM, nelfinavir was shown down regulate RET tyrosine kinase signalling pathway, cause cell cycle arrest and trigger caspase 3 cleavage. Nelfinavir also induced

metabolic stress, AMPK activation and increased autophagic flux (Kushchayeva *et al.* 2014).

Nelfinavir (along with ritonavir, saquinavir and lopinavir) was able to induce proteotoxic stress in human monocytic leukaemia cell lines, THP-1, HL-60 and U937 (Kraus *et al.* 2014). It could also sensitise cells to proteasome inhibitors such as bortezomib and carfilzomib at low molecular micromolar drug concentrations as nelfinavir reduced proteasome activity by 50% at concentrations of 20-40 μM. Nelfinavir was shown, in *vitro*, to be able to induce apoptosis and necrosis in ovarian cancer cell lines SKOV-3, OVCAR-3, and A2780 while being well tolerated by fibroblasts or peripheral blood mononuclear leukocytes used as controls. They also showed that nelfinavir was able to cause an upregulation of the tumour necrosis factor-related apoptosis-inducing ligand (TRAIL) receptor DR5. Nelfinavir sensitized ovarian cancer cells to treatment with an apoptosis-inducing TRAIL receptor antibody as in a phase I trial for liposarcoma, nelfinavir was well-tolerated with minimal toxicities and 6 out of 10 patients were observed to clinical benefit in terms of complete response, partial response and stable disease (Pan *et al.* 2012).

In a phase III clinical trial, nelfinavir, as a single agent, used to treat patients with recurrent adenoid cystic carcinomas no patient showed partial or complete response (Hoover *et al.* 2015). Nelfinavir was shown to be able to selectively inhibit HER2-positive breast cancer cells (including trastuzumab and lapatininb-resistant) *in vitro* and *in vivo* via HSP90 inhibition (Shim *et al.* 2012). Nelfinavir inhibited proliferation and induced apoptosis of castration-resistant prostate cancer through inhibition of site-2 protease (S2P) activity, which leads to suppression of regulated intramembrane proteolysis (Guan *et al.* 2015). Nelfinavir has selective anticancer effects such as induction of autophagy and apoptosis possibly through the induction of ER stress as well as interfering with cell signalling pathways, including mTOR across a range of leukaemia cell lines (SEM, C1, Molt3, TIB202, Molm13, and MV4-11). (Kattel *et al.* 2015).

As seen with the above-mentioned trials and tests, nelfinavir has limited use as a single agent for the treatment of tumour cells. However, the use of nelfinavir, in a combination therapy (be it with other drugs or treatment types), against tumour cells is promising/has potential.

1.3.4 Nelfinavir and radiotherapy

The introduction of nelfinavir to radiotherapy has shown success across a range of cancer cell types. In a phase I trial for rectal cancer, nelfinavir 750 mg BID (bis in die) was shown to be the recommended phase II dose in combination with capecitabine and 50.4 Gy pre-operative radiotherapy as the first tumour response evaluations were observed to be promising as 3 patients (out of 11) achieved a pathological complete response (pCR) (Buijsen *et al.* 2013). The use of oral nelfinavir before and during radiotherapy was well tolerated by patients with advanced rectal cancer (Hill *et al.* 2016). 5 out of 9 patients tested in this trial exhibited good tumour regression on MRI (assessed by tumour regression grade (mrTRG)).

Nelfinavir sensitized pancreatic ductal adenocarcinoma (PDAC) cells (Panc-1, MiaPaCa-2, PSN-1) alone and cocultured with pancreatic stellate cells (PSC) to radiotherapy (Al-Assar *et al.* 2016). The presence of PSCs played a role in how strong the sensitization was as in Panc-1 and PSN-1 cells radiosensitization was larger when cells were in the presence of PSCs. PSCs were also sensitized by NFV via reduced p-FAK levels. In PSN-1 xenografts, the presence of PSC led to faster tumour regrowth after radiation compared to just tumour cells. The regrowth delay effect of nelfinavir after radiation was dramatically larger in the presence of PSCs (time to reach 250 mm^3 183% vs 22%). In a phase II trial, a combination of nelfinavir and chemoradiation showed acceptable toxicity and promising survival rates in patients with locally advanced inoperable pancreatic cancer (Wilson *et al.* 2016).

1.3.5 Nelfinavir and TSC

Nelfinavir selectively targets TSC2-deficient angiomyolipoma-derived cells (621-101) (Medvetz *et al*. 2015). Previous work within the research group of nelfinavir-based combinations have shown these combinations can be very successful against cell lines which are mTORC1 hyperactive, especially cells with *TSC2* mutations. A combination of salinomycin and nelfinavir selectively caused cell death in *TSC2-null* cells while being while being well-tolerated by control cells. This combination targeted the cells by tipping the protein homeostasis balance of the already metabolically stressed *TSC2*-deficient cells in favour of cell death. The salinomycin and nelfinavir combination was also able to cause cell death in sporadic cancer cell lines with mTORC1 hyperactivity (NCI-H460 and HCT116) (Dunlop *et al*. 2017).

A combination of chloroquine and nelfinavir caused selective cell death in TSC2-null cells while being while being well-tolerated by control cells and able to cause cell death in several cell line models with hyperactive mTORC1. The chloroquine/nelfinavir combination was also shown to enhance ER stress and entrapment of chloroquine to acidified lysosomal/endosomal compartments was necessary for cytotoxicity (Johnson *et al*. 2015).

1.4 Aims of Thesis

As previously mentioned, the current drug therapies available for TSC have been shown to excel at shrinking tumours and decreasing vascularisation while at the same time improving neurological aspects of the disease (such as epilepsy). However, these drugs are cytostatic in nature and tumours regrow upon cessation of treatment. Because of this, there is a strong demand to develop cytotoxic treatments, that can eradicate tumours and prevent the need for long-term treatment (and the side effects that come with such treatment). its rarity within the global population (1:6000) means that it is not currently seen as a high research priority. This status means there are reduced resources available to develop new TSC-exclusive treatments. As a result, finding already clinical approved drugs (that can selectively target mTORC1 hyperactive cells, while being tolerated by normal healthy cells) is a good starting point for identifying potential treatments for TSC.

As mentioned in this chapter, nelfinavir enhances cell death when used in combination with other drugs (such as chloroquine and salinomycin). Data from multiple studies indicates that enhancing ER stress is an incredibly valid target for the treatment of mTORC1 hyperactive cells. Nelfinavir and ER stress enhancement alone is not enough to generate the desired levels of cytotoxicity in mTORC1 hyperactive cells. While nelfinavir is less effective as a single agent, there is evidence that nelfinavir has more cytotoxicity when combined in drug combination targeting mTORC1 hyperactive cells.

As a result, two main unanswered research questions need to be asked: 1) what signalling pathways can be targeted (in combination with nelfinavir) to cause cytotoxicity? and 2) can these drug combinations also selectively target the diseased mTORC1 hyperactive cell lines while also being tolerated by the normal healthy cells?

In terms of potential pathways, several have been discussed in this chapter such as the autophagy (which has already been shown to be sensitive to drugs in *Tsc2*-/- cells) and energy stress (i.e., *Tsc2-/-* cells have already been shown to be sensitive to glucose starvation). But what about other pathways such as proteasomal degradation, reactive oxygen species (ROS) management or perhaps other forms of cellular drug accumulation (e.g., P-glycoprotein)? Could drugs be identified that target mTORC1 itself and can these drugs be useful for the TSC treatment?

Because of these questions, the main aims of this thesis are defined as follows:

1. Identifying novel drug combinations (with nelfinavir) which can selectively target *Tsc2*-/- cells while being well tolerated by healthy control cells.
2. Upon identifying novel combinations, optimising these combinations and determining if the combinations are synergistic.
3. Testing this combination in a 3D environment (i.e., tumour spheroids) to prevent the establishment of new tumours and can to target previously established tumours.
4. Considering that mTORC1 hyperactivity can also occur in a wide variety of sporadic tumours, can these novel drug combinations also be used to cause cytotoxicity is mTORC1 hyperactive sporadic cancer cell lines.
5. Identify the mechanism(s) of drug action that causes cytotoxicity in *Tsc2*-/- cells. Such fundamental understanding is required to determine the vulnerabilities of TSC-diseased cells that could lead to better therapies. Techniques used to do this include RNA sequencing.

Over the next several chapters, a series of nelfinavir-based drug combinations will be tested with these aims in mind to determine the answers to these questions mentioned above.

Chapter 2: Materials and Methods

2.1 Materials:

2.1.1 Cell culture

Tsc2+/+ *p53*-/- and *Tsc2*-/- *p53*-/- mouse embryonic fibroblasts (MEFs) were kindly provided by David J. Kwiatkowski (Harvard University, Boston, USA). *Tsc2*-/- ELT3 (Eker rat leiomyoma-derived cells) and ELT3-*Tsc2* cells with *Tsc2* re-expression (to use as control cells) were kindly provided by Cheryl Walker (M.D. Anderson Cancer Centre, Houston, USA). Human breast cancer cells (MCF7), human colorectal cancer cells (HCT116) and human lung carcinoma cells (NCI-H460) cells were purchased from American Type Culture Collection (ATCC), (Middlesex, U.K.). MEFs, ELT3, HCT116 and NCI-H460 cell lines were cultured in Dulbecco's Modified Eagle's Medium (DMEM) (Lonza™ BioWhittaker™ DMEM high glucose with Ultra Glutamine, catalogue number: BE12-604F). The MCF7 cell line was incubated in Roswell Park Memorial Institute (RPMI) 1640 medium (Lonza™ RPMI 1640, with L-Glutamine, catalogue number: BE12-702F). All media types were supplemented with 10% (v/v) foetal bovine serum (FBS) and 1% (v/v) Penicillin/Streptomycin (Pen/Strep). All cell lines were incubated at 37 ^{o}C, 5% (v/v) CO_2 in a humidified incubator. All media types, FBS and Pen/Strep were purchased from Life Technologies Ltd. (Paisley, UK).

2.1.2 Drugs

Nelfinavir mesylate hydrate, chloroquine di-phosphate salt, mefloquine hydrochloride, bafilomycin-A1, piperlogumine, paroxetine hydrochloride, hemihydrate, trifluoperazine dihydrochloride, BPTES, luteolin, cepharanthine, 17-AAG, trequinsin, rapamycin, etoposide dimethyl sulfoxide (DMSO) and thapsigargin were purchased from Sigma–Aldrich Company Ltd. (Dorset, UK). Chelerythrine Chloride and doxorubicin hydrochloride were purchased from Merck Millipore (Hertfordshire, UK). Etoposide was dissolved in DMSO at 100 mM stock solution. Mefloquine was dissolved in DMSO at 50 mM stock solution. Nelfinavir, piperlongumine, paroxetine, trifluoperazine, BPTES and luteolin were dissolved in DMSO at 30 mM stock solutions. Chelerythrine chloride and cepharanthine were

dissolved in DMSO at 15 mM stock solution. Thapsigargin was dissolved in DMSO at 10 mM stock solution. 17-AAG was dissolved in DMSO at 1 mM stock solutions. Trequinsin was dissolved in water at 30 mM stock solution. Doxorubicin was dissolved in water at 10 mM stock solution. Rapamycin was dissolved in ethanol at 100 µM stock solution. Chloroquine was dissolved in fresh culture medium to a 100 mM stock and further diluted in culture medium to the required concentrations for use. All solutions (except doxorubicin) were aliquoted and stored at -20 ^{o}C. Doxorubicin was aliquoted and stored at 4 ^{o}C.

2.2 Methods:

2.2.1 Cell proliferation assay

To determine the level of cell proliferation in the presence of drugs, a CyQUANT cell proliferation assay was performed. The CyQUANT assay is a highly sensitive fluorescence-based method for quantifying cells and assessing cell proliferation and cytotoxicity by measuring DNA content to directly quantify cells without relying on metabolic activity. 5000 cells in 180 µl of media were added into the wells of a 96-well plate and incubated for over several h to allow the cells the adhere to the plate. The outer layer of wells was filled with 200 µl media per well to reduce evaporation occurring within the inner wells. 20 µl of media containing 10 x concentration of chosen drug or DMSO was added to each well giving a total volume of 200 µl per well and a final 1x concentration of DMSO or drug in each well. Cells were returned to the incubator for 48 h. After 48 h, all the media was removed, and the plate was snap frozen at -80 ^{o}C until needed. Proliferation assays were carried out using the CyQUANT Cell Proliferation Assay kit (Life Technologies). While the 96-well plates were being thawed at room temperature, 40 ml of CyQUANT GR working solution was made by adding 2 ml of the 20 X cell-lysis buffer stock solution to 38 ml of nuclease-free distilled water before 100 µl of the CyQUANT GR stock solution was added and mixed thoroughly. Working solution was protected from light during preparation. To each well, 200 µl of working solution was added and incubated for 2–5 min at room temperature, protected from light. The fluorescence was read using a FLUOstar OPTIMA fluorimeter (BMG LABTECH, Buckinghamshire, UK)) set at 480 nm excitation and 520 nm emission. To confirm the proliferation assay was

working, a range of serial dilutions (50000, 25000, 10000, 5000, 2500, 1000, 500, 250 and 0 cells per well) were also testing alongside test samples.

2.2.2 Flow cytometry

Trypsinised cells were plated onto a 24–well plate. 500 µl of media was added to each well. Cells were returned to incubator overnight to allow cells to adhere to the wells. Culture media was removed and 1 ml of media containing either drug or DMSO was added to wells. Cells were returned to the incubator for either 24 or 48 h (depending on the length of the experiment). After the time point, media was transferred into labelled 5 ml polystyrene round-bottom tubes (Corning, Amsterdam, Netherlands). Cells were washed in 250 µl of trypsin and the wash was transferred into designated tubes. Cells were trysinised by adding 250 µl of trypsin per well and returning cells to the incubator for 5 mins at 37 ^{o}C. After incubation, add 500 µl of media to wells to neutralise trypsin. Cells were collected and transferred to tubes. Tubes were then centrifuged at 900 RCF for 5 min. Supernatant was removed, and pellet was loosened by gentle flicking. Cell pellet was resuspended in 500 µl of media. 5µl of 300 µM DRAQ7 (far-red emitting, anthraquinone compound that stains nuclei in dead and permeabilized cells) (final concentration 3 µM) (Biostatus, Leicestershire, UK)) was added to cells and incubated at room temperature for 10 min. Flow cytometry was performed using a FACS Calibur flow cytometer (available from Becton Dickinson, Cowley, UK)) with excitation set at 488 nm and detection of fluorescence in log mode at wavelengths greater than 695 nm. Cell Quest Pro software was used for signal acquisition. A minimum of 10,000 events were collected. Data was analysed using FlowJo software (FlowJo LLC). Data was first analysed in Front scatter (FSC) versus Side scatter (SSC) were data was gated to eliminate cell debris and fragments from final analysis. Revised data was then analysed in FSC (x axis) versus FL4 (sensor with a 675 nm band pass filter which is used to detect far red fluorescent dyes) (Y axis) and data was gated in viable and non-viable populations using 10^{1} on the Y axis as an approximate cut off point between the populations.

2.2.3 Drug synergy assay

Trypsinised *Tsc2+/+* and *Tsc2-/-* MEFs were plated into each well of a 24 –well plate. 500 µl of media was added to each well. Cells were returned to incubator overnight to allow cells to adhere to the wells. After overnight incubation, media was removed, and 1 ml of media was added containing the following:

Mefloquine (in µM):

- For mefloquine/nelfinavir testing; 0.1, 1, 10, 100
- For mefloquine/17AAG testing; 2.5, 5, 10, 20, 40

17AAG (in µM); 0.25, 0.5, 1, 2, 4

Cepharanthine (in µM); 0.625, 1.25, 2.5, 5, 10

Nelfinavir (in µM):

- For mefloquine/nelfinavir testing; 0.1, 1, 10, 100
- For cepharanthine/nelfinavir testing; 2.5, 5, 10, 20, 40

Cells were returned to incubator for 48 h. Flow Cytometry was carried out as previously mentioned. Synergy was determined using the Chou-Talalay Method (Ting-Chao Chou 2010). CI value (which determines the level of synergy) were calculated using CompuSyn programme (CompuSyn is available from CombuSyn Inc) using a non-constant ratio (except for mefloquine and 17AAG testing which used a constant ratio).

2.2.4 Western blotting

Antibodies used in western blotting are listed in Table 2.1.

Table 2.1: List pf primary antibodies, molecular weight and suppliers. All primary antibodies have a stock concentration of 1 mg/ml.

Antibody	Molecular Weight	Supplier
Ribosomal protein S6 (rpS6)	32	Cell Signalling Technology (Danvers, USA)
Phospho-rpS6 ($Ser^{235/236}$)	32	Cell Signalling Technology
p70-S6 kinase 1 (S6K1)	70, 85	Cell Signalling Technology
Phospho-S6K1 (Th^{389})	70, 85	Cell Signalling Technology
Inositol-requiring and ER-to-nucleus signalling protein 1α (IRE1α)	130	Cell Signalling Technology
C/EBP homologous protein (CHOP)	27	Cell Signalling Technology
Caspase-3	17, 19 (cleaved), 35 (uncleaved)	Cell Signalling Technology
Caspase-7	20 (cleaved), 35 (uncleaved)	Cell Signalling Technology
Caspase-8	18, 43 (cleaved), 57 (uncleaved)	Cell Signalling Technology
Caspase-9	35, 37 (cleaved), 47 (uncleaved)	Cell Signalling Technology
Poly ADP ribose polymerase (PARP)	89 (cleaved), 116 (uncleaved)	Cell Signalling Technology
Growth arrest and DNA damage-inducible protein (GADD34)	75	Cell Signalling Technology
Activating transcription factor 4 (ATF4)	49	Cell Signalling Technology
TSC2	200	Cell Signalling Technology
β-actin	45	Cell Signalling Technology
Sestrin 2	56	Cell Signalling Technology
Acetyl-CoA Carboxylase (ACC)	280	Cell Signalling Technology
Phospho-ACC (Ser^{79})	280	Cell Signalling Technology
AMP-activated protein kinase (AMPKα)	62	Cell Signalling Technology
Phospho-AMPKα (Thr^{172})	62	Cell Signalling Technology
LC3	19	Novus Ltd. (Cambridge, UK)
Ubiquitin-binding protein p62 (p62)	47	Progen Biotecknik (Heidelberg, Germany)

444,444 *Tsc2*+/+ and 333,333 *Tsc2*-/- MEF cells were plated onto 35 mm^2 plates (TTP, Switzerland). 2 ml of media was added to each plate. Plates incubated overnight to allow cells to adhere to plates. After incubation, media was removed and replaced with 2 ml of media containing DMSO or drug. Plates were then incubated for a designated time period (3, 6, 16, 24, 48 h depending on whether target protein expression is being analysed for a specific time point or being analysed over several time points). After designated incubation period, media was removed. Cells were washed in ice-cold phosphate buffered saline (PBS) and then lysed in cell lysis buffer (20 mM Tris (pH 7.5), 125 mM Sodium Chloride (NaCl), 50 mM Sodium Fluoride (NaF), 5% (v/v) glycerol, 0.1% (v/v) Triton X-100. Lysis buffer was supplemented with 1 mM dithiothreitol (DTT), 1 µg/ml pepstatin, 20 µM leupeptin, 1 mM benzamidine, 2 µM antipain, 0.1 mM phenylmethane sulfonyl fluoride (PMSF), 1 mM sodium orthovanadate and 1 nM okadaic acid prior to cell lysis). and left to incubate in buffer for approximately 5 min on ice. Cells were scrapped off and transferred to labelled 1.5 ml Eppendorf tube and stored at -80 ^oC until needed. With regards to samples which were incubated for 24 h or longer, removed media and washes were transferred to labelled 15 ml tube and centrifuged at 1,500 RCF for 10 min. Supernatant was discarded, and pellet was resuspended in lysis buffer from Eppendorf tubes and transfer back to tubes. Samples were sonicated at high power using a diagenade bioruptor (Diagenade, Seraing, Belgium) three times at 30 s on, 30 s off. Samples were then centrifuged at 13,300 RCF for 8 min. Protein concentration per sample was then determined using Bradford assay (Thermo Fisher Scientific, Paisley, UK). 25 µl of 200 mM DTT in NuPAGE™ LDS Sample Buffer (4X) (Themofisher Scientific)

Samples were stored at -20 ^oC until needed. Samples were heated at 70 ^oC for 10 min. Samples were centrifuged briefly before loading. 20 µl of sample was then loaded into each well of a NuPage 4-12% Bis-Tris Gel (Thermo Fisher Scientific). Gel ran in running buffer (380 ml of ddH_2O with 20 ml of 20x NuPage MES SDS Running buffer (Life Technologies)) for 1 h 15 min at 150 V. Proteins were transferred from gel to Polyvinylidene fluoride (PVDF) membrane (which has been activated in 100% methanol for 1 min before being washed in transfer buffer prior to usage). Transfer buffer was made up as follows; 350-375 ml ddH_2O, 50 ml 10x transfer buffer (2 M Glycine, 250 mM Tris base and 7 mM SDS) and 75-100 ml of methanol (amount of methanol varied depending on the size of the target protein). Proteins were Transfer was carried out for 2 h 50 min at 25 V. When transfer was

completed, membrane was blocked via incubated in 5% (m/v) milk solution (made in tris-buffered saline (TBS) with Tween 20 (TBS-T)) for 2 h at room temperature on a moving shaker. Membrane was rinsed 3 times in ddH_2O to remove milk solution and primary antibodies (1:1000 dilution (although dilution varied based on antibodies being used) in TBS-T with 5% bovine serum albumin (BSA) (Sigma Aldrich)) were added onto membrane. The membrane was incubated in antibodies at 4 ^oC on a moving shaker overnight. Primary antibodies were and returned to storage and the membrane was washed 3 times (5 min per wash) in TBS-T on a moving shaker at room temperature. Secondary antibodies (1:10000 dilution in 5% (m/v) milk solution was added to membrane and incubated at room temperature for one hour on a shaker. Antibodies were removed, and the membrane was washed 3 times (5 min per wash) in TBS-T. The membrane was incubated in Luminata western horse radish peroxidase (HRP) substrate (Merck Millipore) for 2 min before being developed on Fuji medical x-ray film (Tokyo, Japan). Strength of HRP substrate (Classico (weakest), Crescendo, Forte (strongest)) used depended on the target protein being tested.

2.2.5 Rescue assays

Trypsinised cells were plated into each well of a 24 –well plate. To each well, 500 µl of media was added. Cells were returned to incubator overnight to allow cells to adhere to the wells. In testing with Bafilomycin A1, after overnight incubation, media was removed and 1 ml of media containing either drug, drug containing 100 nM of bafilomycin A1 or DMSO was added to wells. In testing with methyl pyruvate, after overnight incubation, media was removed and 1 ml of media containing either drug, drug containing 8mM of methyl pyruvate or DMSO was added to wells. When testing with rapamycin, after overnight incubation, cells in selected wells were pre-treated for 1 h with 50 nM of rapamycin. After pre-treatment, media was removed and 1 ml of media containing either drug, drug with rapamycin or DMSO was added to designated wells. Cells were returned to incubator for designated time period (24 or 48 h). Flow Cytometry was carried out as previously mentioned. Western blotting for Phopho-RPS6 (for rapamycin rescue) Phospho-ACC, Phospho-AMPK, Sestrin 2 (for methyl pyruvate) and LC3 and p62 (for bafilomycin rescue) were carried out to show that rapamycin, methyl pyruvate and bafilomycin A1 were working as expected.

2.2.6 mRNA extraction and reverse transcription

1,000,000 *Tsc2*+/+ and 750,000 *Tsc2*-/- MEF cells were plated onto 60 mm^2 plates (TPP) and 5 ml of media was added to each plate. Plates were incubated overnight to allow cells to adhere. After incubation, media was removed and 5 ml of media containing drug or DMSO was added and plates returned to incubator for 6 h. After incubation, cells were washed in 500 µl of chilled PBS then lysed using 500 µl Qiagen RNAprotect Cell Reagent. Samples stored at -80 ^oC until needed. RNA was extracted using the RNeasy Plus mini kit and homogenized using Qiashredders during the procedure (Qiagen). The concentration of RNA was determined by measuring the absorbance of 1µl of sample at 260 nm and 280 nm in a Nanodrop spectrophotometer with the results given in ng/µl. Total RNA from each sample (1 µg) was transcribed into cDNA using Quantitect reverse transcription kit. An initial volume of 14 µl per sample used was calculated as follows:

1. 1,000 / ng/µl reading = amount of sample in µl
2. 12 µl – amount of sample µl = amount RNase-free water µl
3. 2 µl gDNA was added to all samples to make a total of 14 µl / tube

Samples were incubated at 42 °C for 2 min to remove gDNA in an Applied Biosystems GeneAmp 9700 PCR system (Thermo Fisher Scientific). 6 µl of reverse transcriptase master mix (1µl Primer mix, 1 µl Quantiscript reverse transcriptase and 4 µl Quantiscript RT buffer 5x per sample) were added to each sample to give a final volume of 20 µl. Samples were incubated at 42 °C for 15 min followed by 95 °C for 3 min. All reagents used for mRNA extraction and reverse transcription were purchased from Qiagen (West Sussex, U.K).

2.2.7 XBP-1 splicing

XBP1 primers [Forward: 5′-AAA CAG AGT AGC AGC TCA GAC TGC-3′; Reverse: 5′-TCC TTC TGG GTA GAC CTC TGG GA-3′] were synthesised through MWG Operon-Eurofin (Ebersberg, Germany). Mouse ACTB (β-actin) primers were purchased from Thermofisher Scientific. For XBP-1 splicing carried out in chapter 3, a master mix for XBP-1 (5 µl 10x buffer (200 mM Tris-HCl pH 8.4, 500 mM KCl), 1 µl 10 mM deoxyribonucleotide triphosphates (dNTPs), 2.5 µl forward XBP-1 primer (100 pmol/µl), 2.5 µl reverse XBP-1 primer (100 pmol/µl), 1.5 µl 50 mM Magnesium Chloride (MgCl), 36.3 µl ddH20 and 0.2 µl *Taq* DNA polymerase (5 U/µl) per sample) and β-actin ((5 µl 10x buffer, 1 µl dNTPs, 5 µl β actin primers, 1.5 µl MgCl, 36.3 µl

ddH20 and 0.2 µl *Taq* DNA polymerase (5 U/µl) per sample) was prepared. For splicing carried out in chapter 6, a master mix for XBP-1 (2.5 µl 10x buffer, 0.5 µl dNTPs, 0.25 µl forward XBP-1 primer (100 pmol/µl), 0.25 µl reverse XBP-1 primer (100 pmol/µl), 0.75 µl MgCl, 19.5 µl ddH20 and 0.25µl (5 U/µl) *Taq* DNA polymerase per sample) and β-actin ((2.5 µl 10 x buffer, 0.5 µl dNTPs, 5µl β actin primers, 0.75 µl MgCl, 19.5 µl ddH20 and 0.25 µl *Taq* DNA polymerase (5 U/µl) per sample) was prepared. Taq DNA polymerase, dNTPs and MgCl were purchased from Thermofisher Scientific.

49 µl of master mix was added to 1 µl of cDNA. Samples were mixed well and centrifuged to eliminate air bubbles from samples. PCR was performed in an Applied Biosystems GeneAmp 9700 PCR system. For splicing in Chapter 3, the following settings were used: initial denaturation step (94 °C, 3 min); 31 cycles of denaturation (94 °C, 45 s); annealing step (60 °C, 30 s); extension step (72 °C, 1 min): final extension step (72 ºC, 10 min). For splicing in Chapter 6, the following settings were used: initial denaturation step (95 °C, 5 min); 32 cycles of denaturation (95 °C, 30 s); annealing step (61 °C, 30 s); extension step (72 °C, 45 s): final extension step (72 ºC, 8 min). 3% (w/v) agarose (Appleton, Birmingham, UK) 1× Tris-acetate-EDTA (40 mM Tris-base (pH 8.0), 1.27 mM EDTA and 1.7 ml acetic acid in 1 L deionized water) was made with 0.005% (v/v) GelRed nucleic acid stain (Biotium, Fremont, CA, USA). DNA samples were loaded with Orange G loading buffer (15 ml 30% (v/v) glycerol, 100 mg Orange G powder, deionized water, total volume 50 ml) and resolved on the gel at 100 V. After 1 h, β-actin samples were analysed and recorded. After an additional 1-2 h (depending on degree on separation) XBP-1 splicing was analysed and recorded. PCR products of XBP1 were 480 base pairs (bp), unspliced, and 454 bp, spliced.

2.2.8 RNA sequencing

Total RNA quality and quantity was assessed using Agilent 2100 Bioanalyser and a RNA Nano 6000 kit (Agilent Technologies, Stockport, Cheshire, UK). 100-900 ng of Total RNA with a RIN value >8 was used as the input and the sequencing libraries were prepared using the Illumina® TruSeq® RNA sample preparation v2. (Illumina Inc., Fulbourn, Cambridge, UK). The steps included 2 rounds of purification of the polyA containing mRNA molecules using oligo-dT attached magnetic beads followed by RNA fragmentation, 1st strand cDNA synthesis, 2nd strand cDNA

synthesis, adenylation of 3' ends, adapter ligation, PCR amplification (15-cycles) and validation. The manufacturer's instructions were followed. The libraries were validated using the Agilent 2100 Bioanalyser and a high-sensitivity kit (Agilent Technologies) to ascertain the insert size, and the Qubit® (Life Technologies) was used to perform the fluorometric quantitation. Following validation, the libraries were normalized to 4 nM and pooled together. The pool was then sequenced using a 75-base paired-end (2x75 bp PE) dual index read format on the Illumina® HiSeq2500 in rapid mode according to the manufacturer's instructions. Quality control checks of the resultant reads were performed using FastQC before mapping to the UCSC mouse mm10 reference genome using Tophat and Bowtie. Differentially expressed transcripts were identified using a DeSeq2 analysis on normalised count data with the design formula setup to analyse all pairwise comparisons in the dataset using contrasts. The resultant p-values were corrected for multiple testing and false discovery issues using the FDR method. Genes involved in cell survival were selected based on GO:0008219 (cell death) from the complete list on AmiGo 2. Data analysis and heat map generation was carried out using Genview2. Data collected was then plotted as volcano plots using Microsoft Excel. RNA sequencing and initial bioinformatics was carried out by Wales Gene Park (Cardiff, Wales).

2.2.9 Rhodamine 123 assay

Rhodamine 123 is a cell-permeant, cationic, green-fluorescent dye that is readily sequestered by active mitochondria without cytotoxic effects. While it is classically used to measure mitochondrial integrity, it is also a substrate of P-glycoprotein (an ATP-binding cassette (ABC) membrane transporter acting as a drug efflux pump which exhibits multiple resistance to a wide variety of structurally-unrelated anticancer drugs). Rhodamine 123 has been shown to be useful for determining the inhibitory potential of drugs against P-glycoprotein activity as 14 known p-glycoprotein inhibitors (including verapamil, cyclosporin A, elacridar, zosuquidar) were found to increase rhodamine 123 accumulation in p-glycoprotein-overexpressing MCF7R cells, thus allowing the determination of their p-glycoprotein inhibitory potential. Inhibitory effects on p-glycoprotein activity are determined by measuring intracellular accumulation of rhodamine 123 in the absence or presence of drugs (Lee *et al.* 1994; Vee *et al.* 2015; Jouan *et al.* 2016).

12,500 *Tsc2*+/+ and 10,000 *Tsc2*-/- cells in 200 µl of media were plated into wells of a 96-well plate and incubated overnight. The outer wells of the plate were filled with media to prevent evaporation occurring in inner wells. The next day, 100 µl of media was removed and 100 µl of media containing 2x the target concentration of drug treatment (with 10.5 µM rhodamine 123) or DMSO (with 10.5 µM rhodamine 123) was then added to each well giving a total volume of 200 µl per well and a final 1x concentration of DMSO or drug (and 5.25 µM rhodamine 123) in each well. Cells were returned to the incubator and incubated for 30 min. After 30 min, all media was removed. Plate was washed three times with 200 µl of chilled 1x PBS. After washing, cells were lysed in 200 µl of warmed deionised water (37 ^{o}C) and was returned to incubator for 15 min. Fluorescence was read on Cytation 3 Imaging reader (Biotek, Swindon, UK) with the following measurements; excitation at 480 nm and emission at 520 nm.

2.2.10 Tumour formation assay

A 1.2% (w/v) Agar solution was made in 1x PBS using Difco Agar Noble (BD, Oxford, UK). The solution was boiled to dissolve Agar into PBS. Solution was then transferred to 50 ml tube and place in an incubator at 50 ^{o}C to prevent the solution from cooling. 2.5 ml of a 1:1 mixture of media and agar was made and added to wells in a 6 well plate and allowed to cool for 20 min. 100,000 (used in chapter 6) - 150,000 (used in chapter 3) *Tsc2*-/- MEFs were added to a 1:4 mixture agar/media mixture and 3 ml of mixture was added to wells and allowed to cool for 1 h. Plates incubated overnight. 2 ml of media contain drugs or DMSO was added the next day. After 48 h, plates were refreshed with new media containing drug or DMSO. Plates were then treated every 2-3 days with DSMO or drug for 14 days. Images were taken using an EVOS XL Core camera (Life Technologies). Tumour size (diameter) analysed using ImageJ. Software (developed at the National Institutes of Health (NIH)).

2.2.11 Tumour outgrowth assay

A 1.5% Agarose solution was made in PBS. Solution was boiled to dissolve agarose. While the solution was still hot, 70 µl of solution was added to each well of a 96 well plate and allowed to cool and harden. After hardening, 1000 *Tsc2*-/- MEFs in 140 µl of media were added to each well. Plate was then incubated overnight. Plate was

examined the next day and any wells which failed to form a single spheroid (e.g., have 2 or more spheroids or no spheroids) were discarded from future analysis. Plate was returned to incubator for another 48 h. Wells were imaged to give a 0 h time point. After imaging, 70 µl of media was removed and replace with 70 µl of fresh media containing 2x concentration of drug or DMSO to each well. Plate was incubated for 48 h. 70 µl of media was removed and fresh media contain 1x concentration drug or DMSO and 6 µM of DRAQ7 (to give a final concentration of 3 µM DRAQ7). Plate was incubated for another 48 h. Dual channel images were acquired using a Zeiss Axio Observer Z1 microscope (Carl Zeiss Microimaging, Gottingen, Germany) with a black box chamber (Solent Scientific Ltd, Segensworth, U.K.) at 0 and 96 h timepoints. Spheroid size (transmission mode) and DRAQ7 labelling (fluorescence excitation 488 nm/emission above 695 nm) were assessed using MetaMorph acquisition software. Following imaging, spheroids were transferred to a standard, tissue culture coated 24 well plate with 1 ml of fresh culture media (no drug treatments) and imaged using an EVOS XL Core camera (Life Technologies) after 0, 24, 48 and 72 h. Total outgrowth area from the spheroid was measured using ImageJ. software.

2.2.12 ROS production analysis

ROS Production was analysed using the DCFDA/H2DCFDA - Cellular Reactive Oxygen Species Detection Assay Kit from Abcam (Cambridge, U.K.). 25,000 *Tsc2*+/+ and 22,000 *Tsc2*-/- MEFs were plated into a black flat-bottom 96-well plate. Plate was placed in incubator overnight to allow cells to adhere to the wells. After overnight incubation, cells were washed in 100 µl per well of 1x Assay buffer (provided by kit and warmed to 37 ^{o}C prior to use). Cells were then stained in 100 µl of 25 µM of 2', 7' –dichlorofluorescin diacetate (DCFDA) for 45 min at 37 ^{o}C in the dark. After DCFDA incubation, cells were washed with 100 µl per well of 1x Assay buffer. Cells were then treated with the chosen drugs for 4 h in incubator at 37 ^{o}C. After incubation, cells were analysed in a Cytation 3 Imaging reader (Biotek, Swindon, UK) as plate was measured at excitation at 485 nm and emission at 535 nm in endpoint mode using Gen5 microplate reader and imager software (version 3.02, Biotek). Results were carried out in duplicate and the average was taken.

2.2.13 Protein synthesis assay

444,444 *Tsc2*+/+ and 333,333 *Tsc2*-/- cells were grown in were plated into 35 mm^2 plates (TTP, Switzerland). 2 ml of media was added to each plate. Plates incubated overnight to allow cells to settle. After incubation, media was removed and replaced with 2 ml of methionine-free media containing DMSO or drug. Plates were then incubated for 6 h. After incubation period, cells were labelled via pulse-chase with 12.5 mCi/ml 35S-methionine for 20 min prior to harvesting in extraction buffer. The protein concentrations in the extracts were then quantified using the Bradford assay. Aliquots (20 µl) of cell extract were applied to 161 cm squares of 3MM filter paper (Whatman) which were then washed three times for 1 min in boiling 5 % (w/v) trichloro-acetic acid containing a trace of cold L-methionine. Filters were rinsed once in ethanol and dried before radioactivity was determined by scintillation counting in Econofluor (Packard). Data were normalized to the protein content of each extract.

2.2.14 Statistical analysis

All experiments were carried out 3 times. Where applicable, results were written as mean +/- the standard deviation or if stated otherwise in the figure legend, as mean +/- the standard error of the mean (SEM) depending on the experiment type performed. Depending on the experiment type and the factors involved, either two-way ANOVA (with Bonferroni's multiple comparison post-test) or unless otherwise stated in the figure legend, one-way ANOVA (with Tukey's multiple comparison post-test) were used to determine statistical significance of results. Significance was reported as a p value <0.05 (*), <0.01 (**) or <0.001 (***).

Chapter 3: Mefloquine and nelfinavir combination caused selective cell death in mTORC1 hyperactive cells

3.1 Introduction:

3.1.1 Mefloquine

3.1.1.1 General Properties of mefloquine

Mefloquine is a highly lipophilic 4-quinolinemethanol antimalarial drug (Figure 3.1) that comes in a white/almost-white crystalline compound that is structurally similar to quinine. It is slightly water soluble but soluble in alcohols (such as methanol and ethanol), and in DMSO. It is a chiral drug with two dissimilar asymmetric centres that exist as two racemic forms, erythro and threo. The erythro forms of the drug have been in used in all clinical trials and treatments as a 50:50 racemic mixture of (-)-(R,S) mefloquine and (+)-(R,S) mefloquine (Alisky *et al.* 2006; Schlagenhauf *et al.* 2010; Xiao 2013).

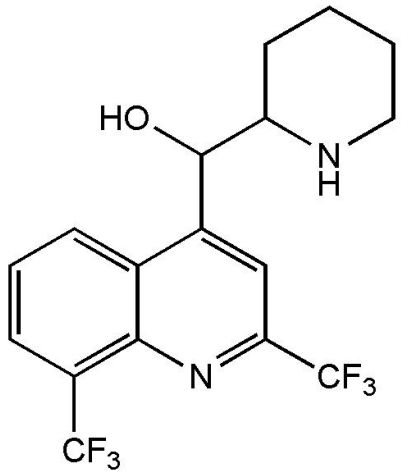

Figure 3.1: Structure of Mefloquine. Chemical structure of Mefloquine. Taken from *(*Osonwa *et al.* 2017)

3.1.1.2 Mefloquine and Malaria

Malaria is a mosquito-borne infectious disease that continues to be a major cause of illness and death worldwide. In 2015, the World Health Organisation (WHO) reported 214 million cases of the disease, which in turn, caused 438,000 deaths globally (Peixoto *et al.* 2016). The disease is caused by the parasite genus *Plasmodium* (Du Plessis *et al.* 2014), with the most severe form of the disease being caused by *Plasmodium falciparum* (Dwivedi *et al.* 2016). Chemotherapy using quinolines, such as chloroquine and primaquine were successfully used in the early days of malaria treatment (Graves 2003). However, resistance to these drugs developed with the first case of chloroquine-resistance reported in 1957 (Dwivedi *et al.* 2016).

Mefloquine was developed by the U.S. Army's Antimalarial Drug Program in 1968 over concerns of chloroquine resistance (Nevin 2012). Mefloquine was made available for malarial chemoprophylaxis in 1985 in Europe and in the U.S.in 1990 (Schlagenhauf *et al.* 2010). Mefloquine is currently sold under the trademark name Lariam by Hoffman La-Roche. Mefloquine is used as part of a combination therapy with artesunate in Africa (except Northern Cameroon), South America and South East Asia (except Northern Cambodia). Mefloquine is not used in northern Cameroon and Cambodia due to high levels of resistance to the drug being reported in these regions in the 1990s (Schlagenhauf *et al.* 2010; Veiga *et al.* 2010; Dwivedi *et al.* 2016). Mefloquine is the only antimalarial approved of chemoprophylaxis in Japan, although it is not widely accepted among Japanese travellers and Japanese travel health advisors, possibly due to concerns over adverse effects caused by the drug (discussed later) (Fujii *et al.* 2007). Mefloquine is used for the treatment of mild to moderate acute malaria caused by *Plasmodium falciparum*. While mefloquine's exact mode of action against malarial parasites is still unknown, research evidence suggests that mefloquine targets the 80S ribosome to inhibit protein synthesis of *Plasmodium falciparum* (Wong *et al.* 2017).

Mefloquine has been recommended for malaria treatment in children by major global authorities, such as WHO, CDC, DTG, UK, French and Canadian expert groups as they recognise mefloquine as a valuable chemoprophylaxis for small children weighing < 20 kg although dosage schedules should be based on weight of the child (Schlagenhauf *et al.* 2011). There is evidence showing that children have a similar predictable pharmacokinetic mefloquine profile compared to adults, although clearance is higher in older children (5-12 years) compared to

younger children (24 months – 6 years) (Singhasivanon *et al.* 1992; Singhasivanon *et al.* 1994).

Mefloquine treatment has been used in chloroquine-resistant regions as pregnant women are at an increased risk (especially in first or second pregnancies) and infection is also associated with adverse outcomes for both mother (severe anaemia) and infant (low birth weight, neonatal mortality). In these regions, patients treated with mefloquine were shown to have significantly lower risk of persistent or breakthrough malarial infection and significantly lower risk of having parasitaemia at delivery in the maternal peripheral blood, placental blood and infant umbilical cord blood compared to chloroquine-treated patients (Steketee *et al.* 1996; González *et al.* 2018). However, mefloquine usage for pregnant women has become a tale of conflicting reports. On the one hand, the WHO sanctioned the use of mefloquine in pregnant women in their second and third trimester. Mefloquine is also considered appropriate chemoprophylaxis for pregnant women of all gestational ages in high-risk malaria endemic regions by several organisations including U.S. Centre for Disease Control (CDC) and the French Reference Centre for Teratogenic Agents (CRAT). The use of mefloquine, in this way however, should be based on a risk/benefit analysis of adverse effects (such as dizziness and vomiting) (Schlagenhauf *et al.* 2010; González *et al.* 2014). On the other hand, Nevin *et*. *al*. (2012) reported an increased risk of miscarriages and stillbirths in women in the first trimester treated with mefloquine. Nevin *et*. *al*. presented the cause of this increased risk is due to mefloquine's ability to block gap junction protein alpha 1 (GJA1) gap junction intercellular communication (GJIC). This communication was thought to be crucial to successful embryonic implantation and early placental development. González *et al.* (2018) suggested that these conflicting reports were due to a lack of double-blind randomized controlled tests that were carried out as in the 18 articles they reviewed, they only found one article was double-blinded.

3.1.1.3 Mefloquine and other parasites

Although mefloquine has been primarily used as a treatment for malaria, research has also shown its uses against other parasitical infections. *Echinococcosus* is a genus of tapeworm which is responsible for two life-threatening conditions, alveolar echinococcosis which is caused by *E. multilocularis* (small fox tapeworm) and cystic echinococcosis which is caused by *E. granulosus* (small dog tapeworm). These

diseases are caused by the growth of “cyst-like” larvae on the liver, lungs and other organs (Hemphill *et al.* 2014). Mefloquine has shown evidence of being a suitable treatment for the disease as *in vitro* studies showed that treatment of 5-10 μg/ml of mefloquine (but no less than 1 μg/ml) caused *E. granulosus* larval death within 24 h after administration (Liu *et al*. 2015a). However, in terms of murine models, when Liu *et. al.* tried to administer mefloquine to mice orally (200 and 400 mg/kg twice weekly for two weeks), they observed no reduction in parasite weight. This would appear more to a problem with the method of delivery as opposed to drug efficacy as Küster *et al.* (2011) showed that intraperitoneal application of mefloquine (25 mg/kg twice a week) showed a reduction in parasite weight in infected mice.

Schistosomiasis is a widespread disease of the tropics and sub-tropics which caused by a parasitic flatworm called schistosomes that can result in liver damage, kidney failure, infertility and bladder cancer. In 2008, a Belgian group were the first to suggest that mefloquine could have antischitosomal activity as mice (infected with *Schistosoma mansoni*) treated with mefloquine had significantly less eggs (although there was no effect seen on parasite burden) (Van Nassauw *et al.* 2008). This data was also confirmed by Keiser *et al.* (2009), as they used 200 and 400 mg/kg of mefloquine (as opposed to 150 mg/kg used by Van Nassauw) and saw that mefloquine had a potent effect on both juvenile and adult schistosomes (indicating that lower doses work well at targeting eggs while higher concentrations of mefloquine are needed to target the actual parasites). Mefloquine has also been shown to have antischitosomal activity against other species of schistosomes (*S. haematobium* and *S. japonicum*) (Keiser *et al.* 2014).

Progressive multifocal leukoencephalopathy (PML) is a rare demyelinating disease of the central nervous system which is caused by the JC polyoma virus (JC virus). PML occurs in patients who are immunocompromised either due to HIV/AIDS (of which 85% of PML patients have a concurrent infection), autoimmune disease, organ transplant or haematological malignancies (in particular, the use of rituximab in the treatment of non-Hodgkin’s lymphoma). A screening of 2000 drugs showed that mefloquine was able to inhibit JC Virus infection via inhibiting viral replication (after cell entry) and its ability to transfer into the cerebral spinal fluid. Combining mefloquine with mirtazapine (a serotonin receptor blocker) for the treatment of PML have also shown positive results in clinical studies (Yoshida *et al.* 2014; Sano *et al.* 2015; Silverio and Patel 2015).

3.1.1.4 Mefloquine and Cancer

Mefloquine has shown plenty of potential to be used as an anti-cancer drug either as a single agent or in combination. P-glycoprotein plays an important role in multidrug resistance in several different tumour types and involves overexpression of the *MDR1* gene (the gene responsible for P-glycoprotein). As seen with malaria treatment, inhibition of P glycoprotein plays a role in the anticancer properties of mefloquine. A multi-drug resistant subline of human oral squamous carcinoma KB, KBV20C, when treated with mefloquine, caused cells to become extremely sensitive to several drugs including the microtubule targeting anticancer agents vinblastine, colchicine and halaven (a drug recently developed to overcome resistance to antimitotic drugs), all via the same mechanism of blocking P-glycoprotein activity (Choi *et al.* 2016; Kim *et al.* 2013; Cheon *et al.* 2016).

In gastric cancer cell lines mefloquine (whether as a single agent or in combination with paclitaxel) caused apoptosis in *in vitro* cell studies. In two independent gastric cancer xenograft mouse *in vivo* models, apoptosis occurred, via suppression of the PI3K-Akt-mTOR pathway. There was a decreased phosphorylation of PI3K, Akt and mTOR in cell lines where there was no constitutive overexpression of Akt. This mode of action was shown to be dependent on calyculin A, a protein phosphatase.

PC3 cells (the most commonly used prostate cancer cell line) are sensitive to mefloquine. A single 10 μM dose of mefloquine was able to achieve the IC_{50} at 24 h, although no further toxicity was detected either 48 or 72 h. Mefloquine at 40 μM was shown to cause 30% cell death at 60 min. Experimental observations showed that the cells were killed in a non-apoptotic manner, which was caused by a significant increase in reactive oxygen species (ROS) production (Yan *et al.* 2013).

Mefloquine has been shown to inhibit autophagy, trigger ER stress and induced cell death in both hormone receptor positive (T47D) and negative (MDA-MB-231) breast cancer cells. Mefloquine was observed to cause a mixture of caspase-dependent and independent cell death as a rescue assay with pan-caspase inhibitor (ZVAD-FMK) only caused partial rescue of treated cells. Mefloquine was shown to be more potent than chloroquine, where effective concentrations of mefloquine used fell between 2.5-15 μM compared to higher concentrations of 30 μM to over 100 μM with chloroquine (Sharma *et al.* 2012).

Mefloquine was shown to be more potent at killing glioblastoma cells regardless of TP53 (also known as p53) status compared to the more readily available chloroquine, and also had superior penetration of the blood-brain barrier compared to chloroquine (Geng *et al.* 2010). Cell death was apoptotic in nature which is the result of autophagy inhibition. These results were validated after a drug screen of quinolone-based antimalarial drugs was carried out on glioma cell lines (LN229, U251 and U87) (Schönthal *et al*. 2015). Mefloquine was shown to be the second most cytotoxic drug (just behind quinacrine, while chloroquine was observed to be the second least effective drug, just above quinine) in both drug-sensitive and drug-resistant (including to temozolomide) cell lines. Cell death observed in this research was similar to that seen by Geng *et al.* (2010) (apoptotic and caused by autophagy inhibition), although enhanced ER stress was also observed. In the cancer setting, mefloquine is currently in a phase I clinical factorial trial (NCT01430351) in combination with the DNA-damaging agent temozolomide for glioblastoma multiforme.

3.1.2 Hypothesis

Results from Johnson *et al. (*2014) showed that a combination of chloroquine (20 μM) and nelfinavir (20 μM) was able to selective kill *Tsc2*-/- MEFs over a 24 h period via entrapment of chloroquine to acidified lysosomal/endosomal compartments, causing cells to become sensitised to nelfinavir-induced death. While investigating the cytotoxic potential of this combination, a mefloquine (10 μM) and nelfinavir (20 μM) combination was also tested and was shown to not only to have selective cytotoxicity for *Tsc2*-/- MEFs but was more potent than chloroquine/nelfinavir combination over a 24 h period. The purpose of this chapter was to further investigate this finding by optimising and determining synergy of a mefloquine and nelfinavir combination. Once an optimised combination was determined, the focus of this chapter was to identify the mechanism of drug action, and to explore the potency of this drug combination against *Tsc2*-/- deficient cells and sporadic cancer cell lines that are known to have aberrant activation of the mTORC1 signalling pathway.

3.2 Results:

3.2.1 An optimized combination of mefloquine and nelfinavir synergises to selectively target mTORC1 hyperactive cells and causes caspase-independent cell death.

To determine a suitable combination of mefloquine and nelfinavir that can selectively kill *Tsc2*-/- cells, while being tolerated by *Tsc2*+/+ cells, various combinations of each drug were tested either as a single agent, or in combination (using a range of varying concentrations). Cells were incubated for 48 h as a median ground to observe both short and long-term effects of drugs on cells.

To determine the drugs effect on cell proliferation, a CyQUANT assay was carried out. Results were calculated as a % of total cell number that was normalised to 100% for DMSO treated cells. Results from the assay showed that mefloquine as a single agent and mefloquine/nelfinavir combinations over a range of various concentrations were able to selective inhibit cell proliferation of *Tsc2*-/- MEF cells compared to *Tsc2*+/+ MEFs (Figure 3.2A). Nelfinavir, on the other hand, only selectively inhibited *Tsc2*-/- MEFs when treated with concentrations over 10 µM. A combination of 2.5 µM mefloquine and 5 µM nelfinavir showed the greatest selectivity for inhibiting cell proliferation (47.13% +/- 7.88 SEM cell proliferation of *Tsc2*+/+ MEFs vs 21.84% +/- 4.62 SEM cell proliferation of *Tsc2*-/- MEFs compared to DMSO-treated cells). However, when this selected drug combination was tested for cell death using flow cytometry, the combination failed to cause cell death in *Tsc2*-/- MEFs (i.e., the combination of drugs at these concentrations was cytostatic not cytotoxic properties). Therefore, drug combinations were retested with flow cytometry using 10 µM nelfinavir as the minimum concentration for combinations.

To determine the effectiveness of combinations in terms of cell death, both *Tsc2*-/- and *Tsc2* +/+ MEFs were treated with several combinations of mefloquine and nelfinavir as well as single agents. Etoposide (a topoisomerase II inhibitor) was used as a positive control to induce cell death through the induction of DNA damage. Results were written as % cell death. As single agents, mefloquine and nelfinavir failed to cause significant cell death in either cell line with no single agent treatment causing more than 20% cell death. Results showed that combinations of 10 µM mefloquine and 10 µM nelfinavir, and 5 µM mefloquine and 20 µM nelfinavir showed the highest level of selective cell death (Figure 3.2B). While both combinations

showed somewhat similar results in *Tsc2*+/+ MEF cell death (37.62% +/- 11.79 SD in 10 µM mefloquine and 10 µM nelfinavir combination and 30.36% +/- 8.67 SD in 5 µM mefloquine and 20 µM nelfinavir combination respectively) the 10 µM mefloquine and 10 µM nelfinavir combination had a much higher level of cell death amongst *Tsc2*-/- MEFs (96.09% +/- 1.98 SD vs 79.95% +/- 12.13 SD) compared to the 5 µM mefloquine and 20 µM nelfinavir combination. Because of this, most of the characterisation experiments using this drug combination for the rest of this chapter used the 10 µM mefloquine and 10 µM nelfinavir combination.

To identify how synergistic the combined mefloquine/nelfinavir treatment was, a range of mefloquine and nelfinavir concentrations were tested via flow cytometry. Results were then processed in CompSyn to generate a Combination Index (CI) value where a score of less than 1 is considered synergistic, a score of 1 is additive and more than 1 is antagonistic. Results showed that the combined mefloquine and nelfinavir treatment was highly synergistic in *Tsc2*-/- MEFs (CI value = .03) while being antagonistic in *Tsc2*+/+ MEFs (CI value =1.10) (Figure 3.2C (iv)). The 100 µM mefloquine and 10 µM nelfinavir combination also appears to act synergistically to induce cell death in both cell lines (CI values = 0.20 and 0.69 in *Tsc2*+/+ and *Tsc2*-/- MEFs respectively), while in combinations containing less than 10 µM mefloquine, the CI values showed drug combinations to be extremely antagonistic (CI values = 20.36 and 11.40 in *Tsc2*+/+ and *Tsc2*-/- MEFs treated with 1 µM mefloquine combination and CI values = 37.66 and 15.76 in *Tsc2*+/+ and *Tsc2*-/- MEFs treated with 0.1 µM mefloquine combination (Figure 3.2C (iv)).

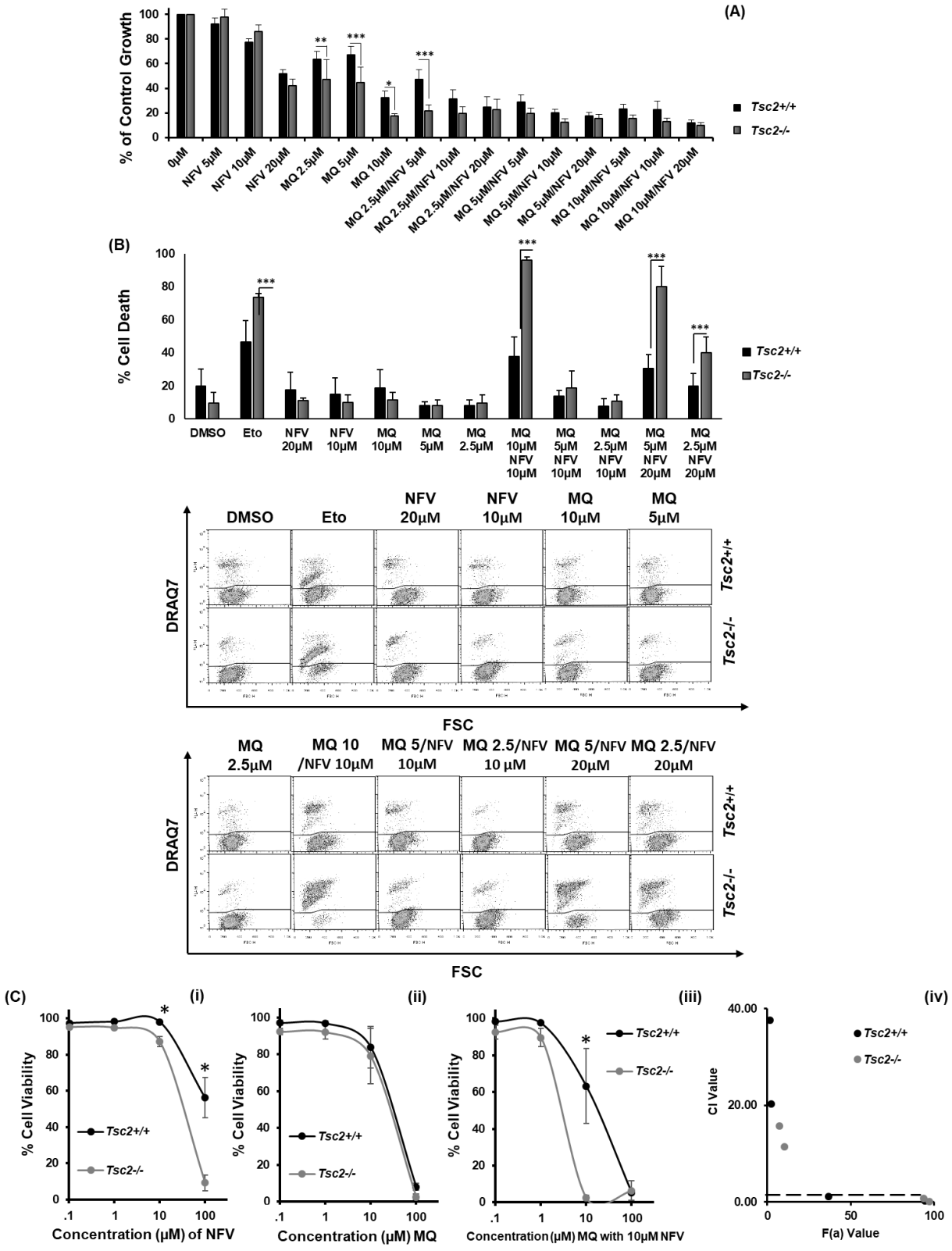

Figure 3.2: Optimization and synergy of mefloquine and nelfinavir. (A) CyQUANT Assay to determine the effects of mefloquine (MQ) and nelfinavir (NFV) on *Tsc2*+/+ and *Tsc2*-/- MEFs as single agents at various concentrations and in combination (MQ/NFV) using various concentrations of mefloquine and nelfinavir on cell proliferation after 48 h treatment. Fluorescence was read on a plate reader with excitation maximum at 480 nm and emission maximum at 520 nm. Statistical significance is shown between *Tsc2*+/+ MEFs and *Tsc2*-/- MEFs (n=3; mean +/- SEM). (B) Flow cytometry (with scatter blots) was performed to measure cell death in *Tsc2*+/+ and *Tsc2*-/- MEFs

treated with dimethyl sulfoxide (DMSO), etoposide (ETO), mefloquine (MQ) or nelfinavir (NFV) as single agents at various concentrations or in combination (MQ/NFV) at various concentrations after 48 h treatment (n=3; mean +/- SD). (C) Dose response curves were performed in *Tsc2*+/+ and *Tsc2*-/- MEFs using flow cytometry to measure cell death following treatment with (i) nelfinavir (NFV); (ii) mefloquine (MQ) and (iii) combined mefloquine with a fixed concentration of 10 µM nelfinavir (MQ/NFV). Synergy was then calculated using CompuSyn and graphed (iv) as F(a) value vs CI value. Statistical significance is shown with combination or single agent treated *Tsc2-/-* MEFs compared to their wild-type controls (n=3; mean +/- SD).

To confirm that *Tsc2* loss was responsible for the induction of cell death, the mefloquine/nelfinavir combination was tested using ELT3 cell lines (both null type (V3) and *Tsc2* re-expressed (T3)) via flow cytometry. Results showed a similar cell death pattern to results seen in MEFs, although cell death was lower in V3 cells compared to *Tsc2*-/- MEFs (76.27% +/- 6.26 SD vs 96.09% +/- 1.98 SD respectively). Mefloquine also appeared to be less tolerated by both cell lines compared to the MEFS (39.44% +/- 7.43 SD vs 51.07% +/- 15.17 SD in ELT3 cell lines compared to 18.91% +/- 10.87 SD vs 11.47% +/- 4.72 SD in MEF cell lines respectively) (Figure 3.3A).

To determine if the combination could be used to target sporadic cancers, the mefloquine/nelfinavir combination was tested against three different types of mTORC1 hyperactive cancer cell lines (breast, colorectal and lung). The cell lines used were previously shown to be mTORC1 hyperactive by previous work by the lab group; NCI-H460 was used by (Johnson *et al*. 2015) and HCT116 and MCF7 were used by (Johnson *et al.* 2018). Results from the flow cytometry showed that the combination caused high levels of cell death in all sporadic cancer lines tested (95.64% +/- 1.95 SD in HCT116 (colorectal), 88.05% +/- 2.74 SD in NCI-H460 (lung) and 65.98% +/- 8.30 SD in MCF7 (breast) cells). HCT116 and NCI-H460 cells also appeared to be sensitive to mefloquine as a single agent (81.39% +/- 5.50 SD and 65.21% +/- 3.97 SD cell death in HCT116 and NCI-H460 cells respectively) (Figure 3.3B).

To determine the manner of cell death, western blots were carried out to determine if cell death was intrinsically (characterized by permeabilization of the mitochondria and release of cytochrome c into the cytoplasm) or extrinsically (mediated by tumour necrosis factor (TNF) induction or Fas-Fas ligand mediation) apoptotic. *Tsc2*+/+ and *Tsc2*-/- MEFs were incubated in treatment for 48 h. Results

from western blots showed that no caspase cleavage occurred in either extrinsic (caspase 8) or intrinsic (caspase 9) pathways, in samples treated with the combination or single agents, i.e., the combination was killing cells in a caspase-independent manner.

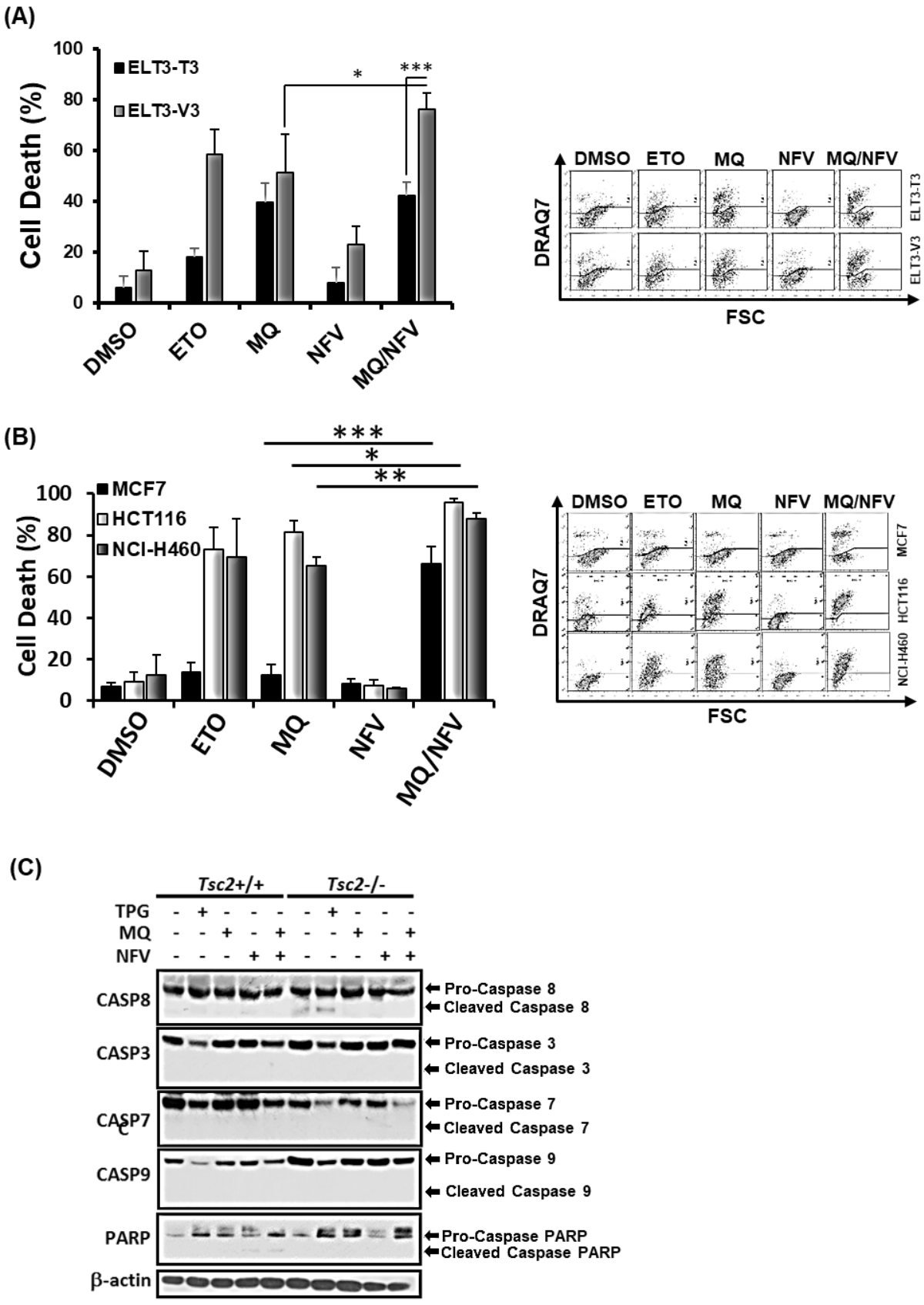

Figure 3.3: The combination of mefloquine and nelfinavir caused cytotoxicity in mTORC1 hyperactive tumour cells and cell death in MEFs is caspase-independent. (A) ELT3-T3 and ELT3-V3 (n=3; mean +/- SD); (B) MCF7, HCT116 and NCI-H460 were treated with either DMSO, 100 μM etoposide (ETO), 10 μM mefloquine (MQ), 10 μM nelfinavir (NFV) or combination (MQ/NFV) for 48 h. Cells were then tested by flow cytometry and cells were separated into viable and non-

viable cell populations via DRAQ7 staining (n=3; mean +/- SD). (C) *Tsc2*+/+ and *Tsc2*-/- MEFs were treated with DMSO, 1 μM thapsigargin (TPG) MQ, NFV or MQ/NFV for 48 h. Caspase cleavage activity was then measured via western blot. Blots are representative of n=3 runs. Statistical significance is shown with combination treated ELT3-V3 cells compared to their wild-type controls and (calculating by one-way ANOVA) comparing single drug treatment of mefloquine and combination with the ELT3-V3, MCF7, HCT116 and NCI-H460.

3.2.2 Mefloquine/nelfinavir combination prevented tumour colony formation and prevented tumour regrowth from treated spheroids.

To determine the effects of mefloquine/nelfinavir combination in a 3D environment, *Tsc2*-/- MEFs were either plated in either agar (for tumour colony formation assay) or agarose (for tumour outgrowth assay).

To determine if the drug combination could prevent the formation of tumour colonies, *Tsc2*-/- MEFs were treated with drugs for 14 days before being photographed and measured. Results for the colony assay showed that the mefloquine/nelfinavir combination significantly reduced the size of tumour colonies compared to single agents, or in the presence of DMSO (Figure 3.4A).

For the tumour outgrowth assay, *Tsc2*-/- MEFs were incubated for 72 h to form spheroids and were photographed before being treated with drugs for 96 h (the last 48 h including DRAQ7) before being photographed again and spheroid were placed in fresh non-drug media for 72 h (photographed every 24 h). Results show that there no change in size between any of the treatment conditions after 96 h of treatment. The morphologies of DMSO and nelfinavir treated cells remained the same, however, samples treated with either mefloquine or mefloquine/nelfinavir combination changed to a “fluffier” appearance, where the cells at the edge of the spheroid appeared less compacted. Both groups were also divided based on the amount of DRAQ7 fluorescence as combination and mefloquine have similar values (1423.71 +/- 404 SEM and 1215.70 +/- 328 SEM Mean Fluorescent units (MFU)) compared to nelfinavir and DMSO samples (767.62 +/- 214 SEM and 668.15 +/- 146 SEM MFU, respectively) (Figure 3.4B). Once placed back into clean media, spheroids incubated in drug combination failed to grow out into the media (indicating that there are no viable cells left in the spheroid) after 72 h. All other spheroids did eventually grow out into media (indicating the presence of viable cells left in the spheroid), although mefloquine grew at a much slower rate compared to DMSO and nelfinavir samples (Figure 3.4C).

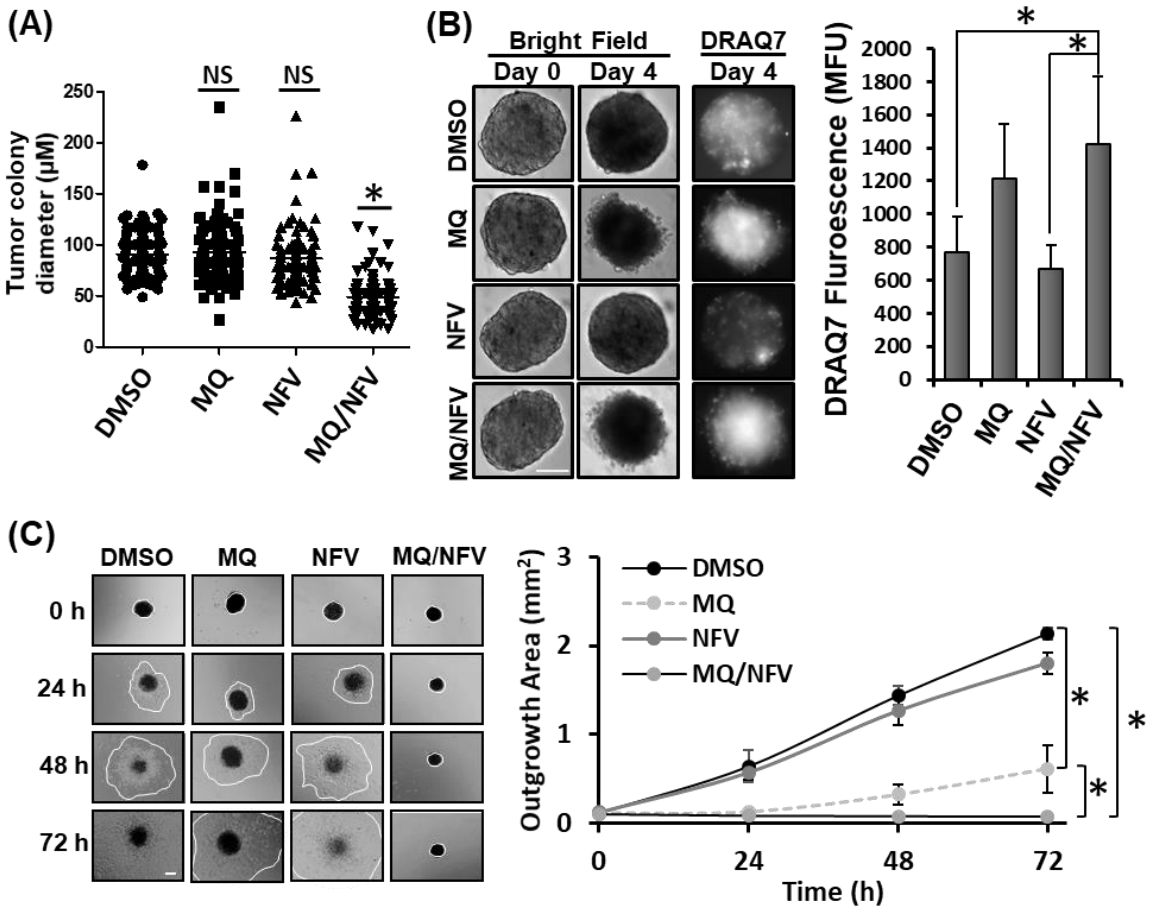

Figure 3.4: Mefloquine/nelfinavir combination prevented tumour formation and tumour spheroid growth. Colony formation was tested in *Tsc2-/-* MEFs seeded on soft agar that were treated for 14 days with Dimethyl Sulfoxide (DMSO), 10 μM mefloquine (MQ), 10 μM nelfinavir (NFV) or in combination MQ/NFV. Tumour diameters were measured using Image J. Significance was observed when comparing combined nelfinavir and mefloquine treatment to DMSO vehicle control (n=3: mean +/- SD). (B) *Tsc2*−/− MEF spheroids were grown for 72 h before being treated under the same conditions as (A) for 96 h. DRAQ7 was supplemented for the final 48 h to monitor cell death before images were taken and DRAQ7 fluorescence quantified (n=3; mean +/- SEM). (C) Spheroids treated in (B) were re-plated onto standard tissue culture plates and grown in drug-free media. Images were taken every 24 h and the area of outgrowth was calculated using Image J., scale bar represents 200 μm and outgrowth area was graphed. Statistical significance (calculated by one-way ANOVA) is shown with combination treated tumour colony size compared to their wild-type controls, comparing fluorescence emitted by combination treated spheroids to nelfinavir and DMSO treated spheroids and comparing outgrowth of combination treated spheroids to single agent and DMSO treated spheroids (n=3).

3.2.3 Mefloquine/nelfinavir combination targeted *Tsc2*-/- cells in a mTOR and autophagy/lysosomal-independent manner.

To determine if mTORC1-hyperactivity was important for the induction of cell death, flow cytometry was carried out on *Tsc2*-/- MEF, HCT116 and NCI-H460 and MCF7 cell lines treated with DMSO, drug combination, or drug combination with 50 nM rapamycin for 48 h. Results showed that the introduction of rapamycin failed to rescue cell death in *Tsc2*-/- MEF, HCT116 and NCI-H460 cell lines. In MCF7 cells, the introduction of rapamycin led to a slight nonsignificant increase in cell death (88.83% +/- 11.01 with rapamycin vs 75.44% +/- 4.63 without rapamycin). To confirm if rapamycin was inhibiting mTORC1 activity, western blots were carried on the previously mentioned cell lines treated in the same conditions as the flow cytometry. Results showed that samples treated with combination and rapamycin showed a complete or near complete inhibition of RPS6 phosphorylation, confirming rapamycin was successfully inhibiting the mTORC1 pathway (Figure 3.5A).

To determine if the autophagy flux was altered by the combination, western blots were carried out on *Tsc2*+/+ or *Tsc2*-/- MEFs treated for 3 h. A combination of 20 µM chloroquine with 20 µM nelfinavir was used as a positive control as this drug combination has previously been proven to prevent autophagy (Johnson *et al*. 2015). Results showed that the mefloquine/nelfinavir combination caused LC3-II accumulation but was less when compared to chloroquine/nelfinavir combination in *Tsc2*-/- MEFs. Furthermore, there was more pronounced LC3-II accumulation in *Tsc2*+/+ MEFs, which was also less than the samples treated with chloroquine/nelfinavir. SQTSM1/p62 was basally elevated in *Tsc2*-/- MEFs compared to *Tsc2*+/+ MEFs and did not appear to be significantly affected by combined treatments with either mefloquine or chloroquine (Figure 3.5B).

To determine if the drug combination affected lysosomal function, *Tsc2*+/+ and *Tsc2*-/- MEFs were treated for 24 h (to observe short term effects of combination) with either DMSO, drug combination or drug combination with 100 nM bafilomycin A1 (a v-ATPase inhibitor) before being analysed via flow cytometry. V-ATPases are ATP-driven proton pumps that function within both intracellular compartments and the plasma membrane in a wide array of normal physiological and pathophysiological processes. V-ATPase plays an important role in keeping low intralysosomal pH, which is essential for lysosomal hydrolase activity (Mauvezin *et al.* 2015). Bafilomycin A1 disrupts autophagic flux by inhibiting both V-ATPase-dependent acidification and Ca-P60A/SERCA-dependent autophagosome-

lysosome fusion (Mauvezin and Neufeld 2015). Members of the quinone family (chloroquine, hydrochloroquine and mefloquine) have all been shown to accumulate in the lysosome. Bafilomycin A1 has been shown to prevent the build-up of chloroquine and MEFAS (a synthetic salt derived from mefloquine and artesunate) in the lysosome (Glaumann *et al*. 1992; Kaufmann and Krise 2007; de Pilla Varotti *et al*. 2008; Harhaji-Trajkovic *et al*. 2012). Results showed that bafilomycin A1 failed to rescue cell death after nelfinavir and mefloquine, but instead caused an increase in the level of cell death (51.23% +/- 11.23 SD vs 63.80% +/- 3.79 SD in the presence of bafilomycin A1 compared to 43.53% +/- 10.58 SD vs 58.57% +/- 13.39 SD in just mefloquine/nelfinavir treatment). To confirm that the concentration of bafilomycin A1 was sufficient to block autophagy, western blots were carried out with both cell lines to determine LC3-II and p62 accumulation, treated for either 3 h or 24 h. Western blots showed that samples treated with bafilomycin A1 had an accumulation of LC3 and p62 at both 3 and 24 h timepoints compared to just mefloquine and nelfinavir or DMSO treatment indicating that bafilomycin A1 was blocking autophagy (Figure 3.5C).

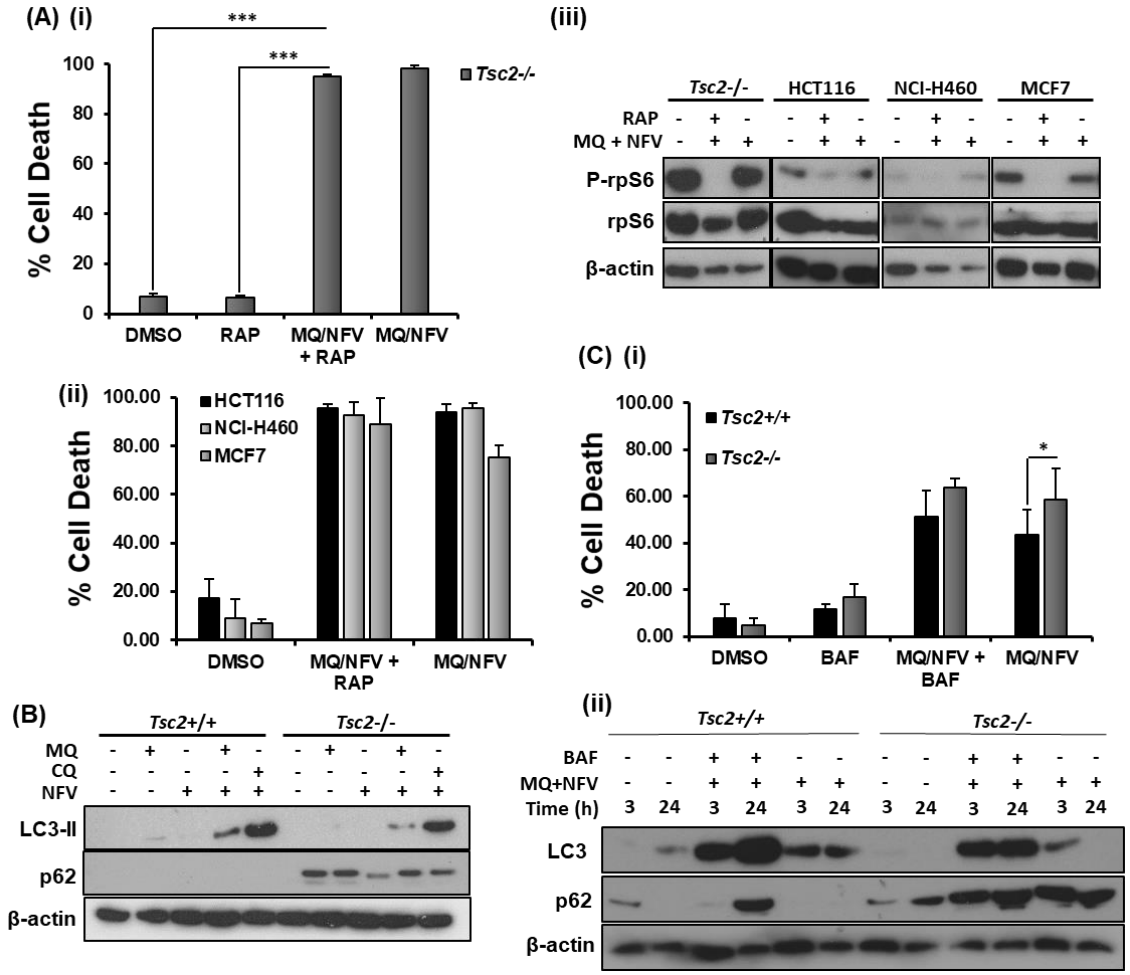

Figure 3.5: mTORC1 hyperactivity was not associated with Mefloquine/nelfinavir combination induced cell death and caused minimal inhibition of autophagy. (A(i)) *Tsc2-/-* MEFs, (A(ii)) NCI-H460, MCF7 and HCT116 cells were pre-treated with 50 nM rapamycin (RAP) for 1 h, where indicated, before being treated with either 10 μM nelfinavir (NFV) and 10 μM mefloquine (MQ) or MQ/NFV with RAP for 48 h. Cell death was determined using flow cytometry (n=3; mean +/- SD). Statistical significance (calculated by one-way ANOVA) is shown control cells, cells treated MQ/NFV and MQ/NFV treated cells and RAP treated cells. (A(iii)) To determine if RAP was functioning as expected, western blotting was carried out to determine rp-S6 phosphorylation at $Ser^{235/236}$ in the cells treated in (A) after 48 h of treatment. (B) *Tsc2*+/+ and *Tsc2-/-* cells were treated with DMSO, 10 μM mefloquine (MQ), 20 μM chloroquine (CQ), 10 μM mefloquine combined with 10 μM nelfinavir or 20 μM chloroquine combined with 20 μM nelfinavir for 3 h. Accumulation of lipidated LC3-II and p62 was analysed by western blot. (C(i)) *Tsc2*-−− and *Tsc2*+/+ MEFs were treated with 10 μM nelfinavir (NFV) and 10 μM mefloquine (MQ) or MQ/NFV with 100 nM bafilomycin A1 (BAF) for 24 h. Cell death was determined using flow cytometry (n=3; mean +/- SD). (C(ii)) To determine if BAF was functioning as expected, western blotting was carried out to determine the accumulation of lipidated LC3-II and p62 in the cells treated in (A) after 3 h and 24 h of treatment. Total protein levels of β-actin were used as a loading control. All Blots in figure 3.5 are representative of n=3 runs. Statistical significance is shown between combination treated *Tsc2*+/+ and *Tsc2-/-* MEFs.

3.2.4 Mefloquine and nelfinavir as single drug agents, as well as in combination, blocked P-glycoprotein activity in *Tsc2*+/+ and *Tsc2*-/- MEFS.

P-glycoprotein is a 170 kDa membrane glycoprotein which is associated with multidrug resistance in cancer cells as it acts as an ATP-dependent drug efflux protein. A substrate of P-glycoprotein is nelfinavir which causes increased expression of the P-glycoprotein and is a possible mechanism reducing drug exposure after multiple doses. Another substrate of P-glycoprotein is mefloquine which has been shown to inhibit the functional activity of P-glycoprotein (Riffkin *et al*. 1996; Faucette *et al*. 2004). To determine if mefloquine could inhibit P-glycoprotein activity and cause accumulation of nelfinavir in cells, contributing to cell death, both *Tsc2*+/+ and *Tsc2*-/- MEFs were treated with either mefloquine/nelfinavir combination or control, with all treatments containing 5.25 µM of rhodamine123 (which is a substrate of P-glycoprotein) for 30 min at 37 ^{o}C. Samples were then lysed in warmed deionised water and a fluorescence reading was taken. Results were recorded as a % of DMSO treated control (which was normalised to 100%). Results showed that mefloquine, as a single agent was able to increase rhodamine 123 uptake (i.e., inhibited P-glycoprotein activity) compared to DMSO in both *Tsc2*-/- and *Tsc2*+/+ MEFs (188.31% +/- 8.61 SEM in *Tsc2*+/+ MEFs and 198.55% +/- 3.22 SEM in *Tsc2*-/- MEFs compared to 100% in DMSO treated cells respectively). Nelfinavir, as a single agent caused partial inhibition of P-glycoprotein activity which was seen in a slight increase in rhodamine 123 uptake in *Tsc2*+/+ cells but caused a large inhibition of P-glycoprotein activity (in the form of a large uptake of rhodamine 123) in *Tsc2*-/- cells (120.11% +/- 13.82 SEM in *Tsc2*+/+ MEFs compared to 210.36% +/- 3.22 SEM in *Tsc2*-/- MEFs). The combination of mefloquine and nelfinavir failed to stop P-glycoprotein activity (evident by the slight increase in rhodamine 123 uptake) in *Tsc2*-/- MEFs but caused massive inhibition of p-glycoprotein activity (as seen in the large uptake of rhodamine 123) in *Tsc2*+/+ MEFs (223.04% +/- 8.49 SEM in *Tsc2*+/+ MEFs compared to 114.09% +/- 13.15 SEM in *Tsc2*-/- MEFs) (Figure 3.6).

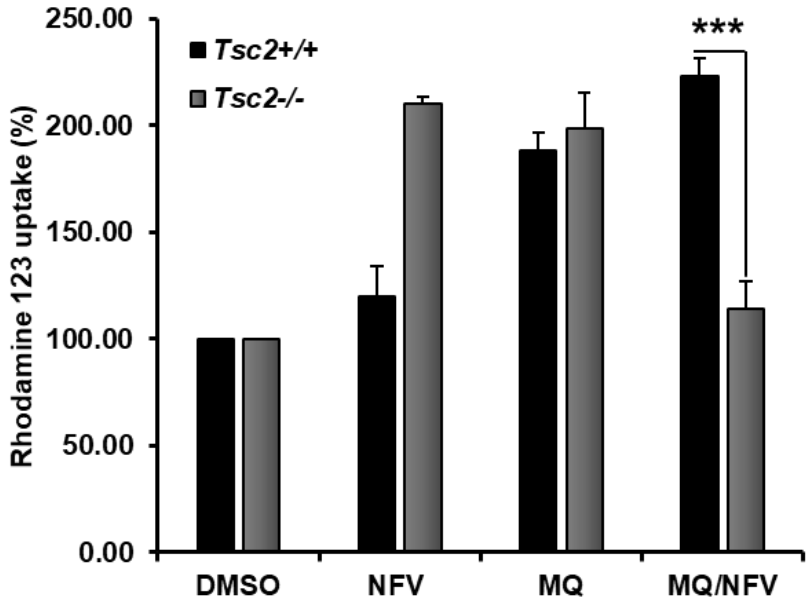

Figure 3.6: Mefloquine/nelfinavir combination affected rhodamine 123 uptake. Rhodamine 123 is a substrate of P-glycoprotein and can be used to observe if a drug can inhibit P-glycoprotein activity and to what extent. The inhibitory effects of target drug on P-glycoprotein is determined the amount of intracellular Rhodamine 123 accumulation (written as Rhodamine 123 uptake %). In this experiment, *Tsc2*+/+ and *Tsc2*-/- MEFs were treated with DMSO, 10 μM mefloquine, 10 μM nelfinavir or a combination of mefloquine and nelfinavir (all containing 5.25 μM rhodamine 123) for 30 min at 37 ^{o}C before being lysed in warmed deionised water. Fluorescence was analysed via plate reader at excitation maximum at 480 nm and emission maximum at 520 nm (n=3; mean +/- SEM). Statistical significance is shown between combination treated Tsc2+/+ and Tsc2-/- MEFs.

3.2.5 Mefloquine/nelfinavir combination induced enhanced and prolonged ER stress in *Tsc2*-/- cells via the PERK pathway.

Nelfinavir is a well-known ER stress enhancer. To determine the effects the combination would have on ER stress pathways in both *Tsc2*+/+ and *Tsc2*-/- MEFs, western blots were performed on *Tsc2*+/+ and *Tsc2*-/- MEFs treated for 6 h with drugs. Tharsigargin was used as a positive control drug that induced ER stress. Results showed that there was a large difference in expression of ER stress makers between *Tsc2*+/+ and *Tsc2*-/- MEFs. There was a higher basal level of IRE1α protein expression in the *Tsc2*-/- MEFs when compared to the *Tsc2*+/+ MEFs that was unchanged with drug treatment. In the *Tsc2*-/- MEFs, there was higher level of protein expression of several components of the PERK pathway after drug treatments, such as GADD34, CHOP and ATF4. The level of protein expression of these ER stress markers was higher in the presence of drug combination when compared to single mefloquine treatments. However, there is no significant

difference in expression levels between nelfinavir-treated *Tsc2*-/- MEFs and Tsc2-/- MEFs treated with the mefloquine/nelfinavir combination. Components of the mTORC1 pathway were also tested. Results showed a higher basal level of S6K1 phosphorylation in *Tsc2*-/- MEFs compared to *Tsc2*+/+ MEFs. Results also confirmed that *Tsc2*-/- MEFs had no TSC2 expression. The nelfinavir and mefloquine drug combination failed to cause any form of significant change in S6K1 phosphorylation when compared to single drug treatments (Figure 3.7A).

To determine how long ER stress persisted after treatment, western blots were carried out on *Tsc2*+/+ *and Tsc2*-/- MEF samples treated for either 6 h or 48 h. In *Tsc2*+/+ MEF samples treated with drug combination, data showed an increased expression of CHOP and ATF4 at 6h. However, at the 48 h time point, CHOP and ATF4 expression was no longer apparent, indicating that the *Tsc2*+/+ MEFs had recovered from the ER stress. Like the *Tsc2*+/+ MEFs, *Tsc2*-/- MEFs showed high protein expression levels of ATF4, CHOP and GADD34 at the 6 h time point (higher than seen in the *Tsc2*+/+ MEFs). However, unlike the *Tsc2*+/+ MEFs, a higher level of protein expression was still evident at the 48 h time point, indicating that these *Tsc2*-/- MEFS were unable to fully recover from the drug induced ER stress (Figure 3.7C).

To confirm that ER stress was occurring, XBP1 splicing was investigated (an event which only occurs in an ER stress-induced environment due to activation of IRE1α). MEFs were treated for 6 h with DMSO, mefloquine, nelfinavir or mefloquine/nelfinavir combination, using tharsigargin as a positive control. mRNA was extracted and then converted to cDNA. The cDNA was used as a template to analyse XBP1 splicing by PCR. PCR products were resolved on an agarose gel, where the unspliced XBP1 size was 480 base pairs and the spliced XBP1 product size was 454 base pairs. Results showed a higher degree of XBP1 splicing in the *Tsc2*-/- MEFs compared to *Tsc2*+/+ MEFs in both untreated and treated conditions. With *Tsc2*-/- cells, splicing occurred in samples treated with drug combination at a much higher rate when compared to single agents or DMSO (Figure 3.7B(i)). To confirm that the PCR products were XBP1, spliced and unspliced samples were subjected to *Pst*1 restriction digests (which cleaved DNA at the recognition sequence 5′-CTGCA/G-3′, which is found in unspliced but not spliced XBP1). Results showed digestion occurred in unspliced samples treated with XBP1 confirming XBP1 was being tested (Figure 3.7B(ii)).

To determine the transcriptional effects of nelfinavir and mefloquine drug treatments on the level of RNA expression, RNA sequencing was carried out on *Tsc2*+/+ and *Tsc2*-/- MEFs treated for 6 h in either DMSO, 20 µM nelfinavir or drug combination with nelfinavir and mefloquine. A Heat map was generated for a panel of ER stress associated genes. The Heat map represents RNA expression as low levels of expression (or no expression) were represented by blue (were the darkest blue represents lowest level of expression (a score of 0)). Increased RNA expression is represented by a colour shift from blue to white to red were the darkest red represents the highest RNA expression score (in this case, a score of 6767). A selection of genes was then further graphed and analysed. The overall RNA sequencing data was represented in a volcano plot where chosen ER stress genes were highlighted. Colours represent differences in expression levels which have at least a 1-fold difference in *Tsc*2+/+ MEFs (Blue) and *Tsc*2-/- MEFs (Red). Genes which are involved in cell survival such as CREBREF and IMPACT (negative regulators of ER stress) were shown to have a 2-3-fold increase in expression in *Tsc2*+/+ MEFs when compared to *Tsc2*-/- MEFS, especially in the presence of drug treatment. Conversely, pro-ER stress genes linked to cell death, such as DDIT4 (also known as CHOP), ERO1L, ATF3 and TRIB3 (which inhibits transcriptional activity of CHOP and is involved in CHOP-dependent cell death during ER stress) were expressed at a much higher level within the *Tsc2*-/- MEFs. FAM129A (which is responsible for Niban which regulates phosphorylation of several proteins involved in translation regulation) and DDIT4L (which translates REDD2 which inhibits cell growth by regulating the mTORC1 signalling pathway upstream of the TSC1-TSC2 complex and downstream of AKT) were almost exclusively expressed in *Tsc2*-/- MEFS compared to *Tsc2*+/+ MEFs. Results show that the introduction of the mefloquine/nelfinavir combination was able to significantly influence RNA expression of nearly all genes within *Tsc2*-/- MEFs compared to *Tsc2*-/- MEFs treated with DMSO (except CREBRF and DDIT4L). The mefloquine/nelfinavir combination was also able to significantly influence RNA expression of SESN2, IMPACT, DDIT4 and ERO1L within *Tsc2*+/+ MEFs compared to *Tsc2*+/+ MEFs treated with DMSO. Results also showed elevated expression levels of SESN2 gene (which translates the Sestrin 2 protein, involved in the communications between ER stress and energy stress) were basally enhanced (nearly 10-fold) in *Tsc2*-/- MEFS compared to *Tsc2*+/+ MEFS. When treated with nelfinavir and mefloquine, there

was nearly a two-fold change in expression of SESN2 mRNA in *Tsc2*-/- MEFS compared to control *Tsc2*-/-MEFs (Figure 3.7D-F).

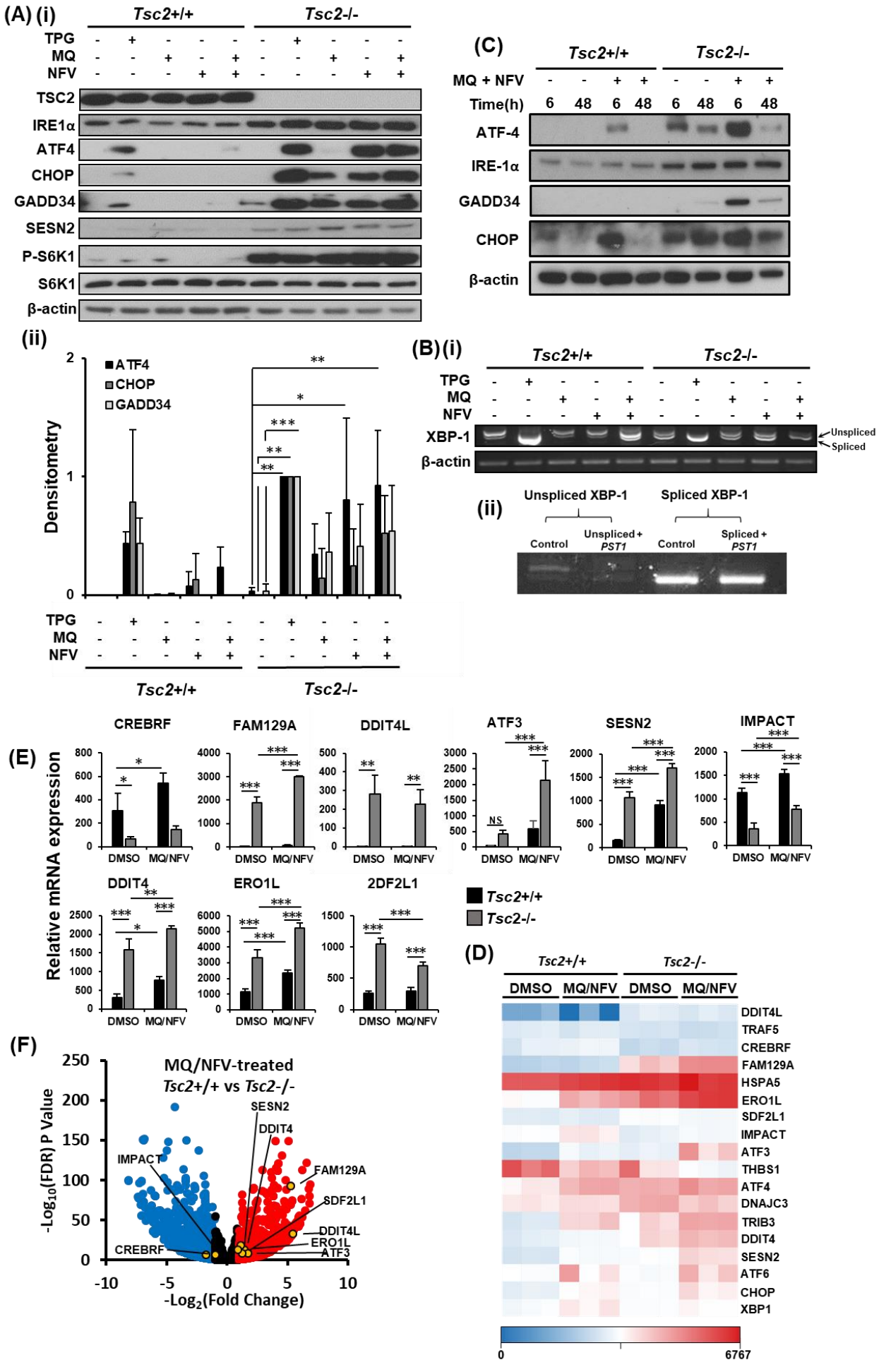
(A) (i)
Tsc2+/+
Tsc2-/-
TPG
MQ
NFV
TSC2
IRE1α
ATF4
CHOP
GADD34
SESN2
P-S6K1
S6K1
β-actin
(ii)
ATF4
CHOP
GADD34
Densitometry
(C)
MQ + NFV
Time(h)
6 48 6 48 6 48 6 48
ATF-4
IRE-1α
GADD34
CHOP
β-actin
(B) (i)
XBP-1
Unspliced
Spliced
(ii)
Unspliced XBP-1
Spliced XBP-1
Control
Unspliced + PST1
Spliced + PST1
(E)
Relative mRNA expression
CREBRF
FAM129A
DDIT4L
ATF3
SESN2
IMPACT
DDIT4
ERO1L
2DF2L1
DMSO
MQ/NFV
Tsc2+/+
Tsc2-/-
(D)
DDIT4L
TRAF5
CREBRF
FAM129A
HSPA5
ERO1L
SDF2L1
IMPACT
ATF3
THBS1
ATF4
DNAJC3
TRIB3
DDIT4
SESN2
ATF6
CHOP
XBP1
0
6767
(F)
MQ/NFV-treated
Tsc2+/+ vs Tsc2-/-
-Log10(FDR) P Value
-Log2(Fold Change)
SESN2
DDIT4
IMPACT
FAM129A
SDF2L1
DDIT4L
ERO1L
ATF3
CREBRF

Figure 3.7: The effects of mefloquine/nelfinavir combination on ER stress. (A) (i) *Tsc2*+/+ and *Tsc2*-/- MEFs were treated with either DMSO, 1 µM thapsigargin (TPG), 10 µM mefloquine (MQ), 10 µM nelfinavir (NFV), or mefloquine and nelfinavir combination (MQ/NFV) for 6 h, where indicated. Total protein levels of TSC2, IRE1α, ATF4, CHOP, GADD34, S6K1 and β-actin and S6K1 phosphorylated at Thr389 were detected by western blot. (A) (ii) Densitometry of western blots for ATF4, CHOP and GADD34 measured. Statistical significance is shown comparing DMSO treated *Tsc2*-/- MEFs to TPG treated *Tsc2*-/- MEFs (ATF4, CHOP, GADD34), comparing DMSO treated Tsc2-/- MEFs to NFV treated *Tsc2*-/- MEFs (ATF4) and comparing DMSO treated Tsc2-/- MEFs to MQ/NFV treated *Tsc2*-/- MEFs (ATF4). (B) (i) Xbp1 mRNA splicing was determined from the same treatments as described in (A) (ii) *Pst1* restriction digestion to confirmed XBP-1. PCR products were resolved on agarose gels (unspliced = 480 bp upper band, spliced = 454 bp lower band). (C) Tsc2+/+ and Tsc2-/- MEFs were treated with DMSO or mefloquine (MQ) and nelfinavir (NFV) combination for 6 h and 48 h. Total protein levels of ATF4, IRE-1α, GADD34, CHOP and β-actin were determined by western blot. All blots in figure 3.7 are representative of n=3 runs. (D–F) RNQ sequencing. *Tsc2*+/+ and *Tsc2*-/- MEFs were treated with either DMSO or mefloquine and nelfinavir combination (MQ/NFV) for 6 h. A heat map for a panel of ER stress-linked genes is shown (D). Heat map shows expression as dark blue for low levels of RNA expression while dark red (via going from blue to white to red) represents high levels of RNA expression. A selection of genes from the ER stress panel were then further graphed in (E) (n=3; mean +/- SD). (F) A volcano plot showing the entire RNA sequencing where genes shown in (E) are highlighted. Statistical significance is shown comparing combination treated *Tsc2*+/+ and *Tsc2*-/- MEFs and comparing DMSO treated *Tsc2*+/+ and *Tsc2*-/-, comparing *Tsc2*+/+ MEFs treated with either DMSO or MQ/NFV and *Tsc2*-/- MEFs treated with either DMSO or MQ/NFV.

To determine if mefloquine could be used with inhibitors of other components of the UPR, nelfinavir was replaced with 1 µM 17AAG (a HSP90 inhibitor). *Tsc2*+/+ and *Tsc2*-/- MEFs were treated for 48 h and tested via flow cytometry. Results showed that 17AAG as a single agent could selectively target *Tsc2*-/- MEFs while being well tolerated by *Tsc2*+/+ MEFs (69.23% +/- 10.23 vs 18.04% +/- 2.77, respectively). Results also showed that when used in combination with 10 µM mefloquine, cell death of *Tsc2*-/- MEFS rose to 86.39% +/- 3.51 compared to 20.79% +/- 12.25 in *Tsc2*+/+ MEFs (Figure 3.8A). To determine if this drug combination was synergistic, flow cytometry was carried on samples that were treated with either various concentrations of mefloquine, 17AAG or a drug combination that had a fixed ratio of 10 µM mefloquine: 1µM 17AAG. Results were analysed in CompuSyn. Results are presented in Table 3.1. Data showed that a concentration of 10 µM mefloquine and 1µM 17AAG failed to achieve the same level of cell death in *Tsc2*-/- MEFs as seen in figure 3.8A (57.79% +/- 1.95 vs 69.23% +/- 10.23) and was

shown to be antagonistic in both cell lines (CI value = 1.28 in *Tsc2*+/+ MEFs and CI value = 1.12 in *Tsc2*-/- MEFs.). However, MQ/17AAG combinations were shown to be synergistic at 20 μM Mefloquine/ 2 μM 17AAG (CI value = 0.79 in *Tsc2*+/+ MEFs and CI value = 0.79 in *Tsc2*-/- MEFs.) and synergistic in *Tsc2*+/+ MEFs only at 40 μM Mefloquine/ 4 μM 17AAG (CI value = 0.78 in *Tsc2*+/+ MEFs and CI value = 1.90 in *Tsc2*-/- MEFs.) (Figure 3.8B-E).

Table 3.1 Results of Mefloquine/17AAG synergy. Results for synergy assay for mefloquine and 17AAG combinations. Results written as % Cell Death. Results also in CI value for combinations tested.

	TSC2+/+			TSC2-/-		
Drug	**Average Cell Death (%)**	**SD**	**CI Value**	**Average Cell Death (%)**	**SD**	**CI Value**
DMSO	1.50	0.40		3.58	1.08	
Mefloquine 40 μM	97.07	1.54		97.50	0.84	
Mefloquine 20 μM	65.65	19.01		98.18	0.60	
Mefloquine 10 μM	11.43	5.91		8.00	5.33	
Mefloquine 5 μM	2.42	0.84		2.87	1.31	
Mefloquine 2.5 μM	1.75	0.31		2.49	0.95	
17AAG 4 μM	32.92	5.91		52.35	4.80	
17AAG 2 μM	41.33	13.13		51.81	2.82	
17AAG 1 μM	23.61	6.23		41.88	6.07	
17AAG 0.5 μM	10.57	3.33		19.51	8.18	
17AAG 0.25 μM	4.31	0.71		6.42	3.17	
Mefloquine 40 μM/ 17AAG 4 μM	97.18	0.91	0.78	90.93	4.94	1.90
Mefloquine 20 μM/ 17AAG 2 μM	84.51	5.74	0.79	94.34	0.38	0.79
Mefloquine 10 μM/ 17AAG 1 μM	33.53	4.56	1.28	57.79	1.95	1.12
Mefloquine 5 μM/ 17AAG 0.5 μM	17.85	9.12	1.09	32.48	6.95	1.00
Mefloquine 2.5 μM/ 17AAG 0.25 μM	5.52	2.10	1.50	15.91	8.77	0.93

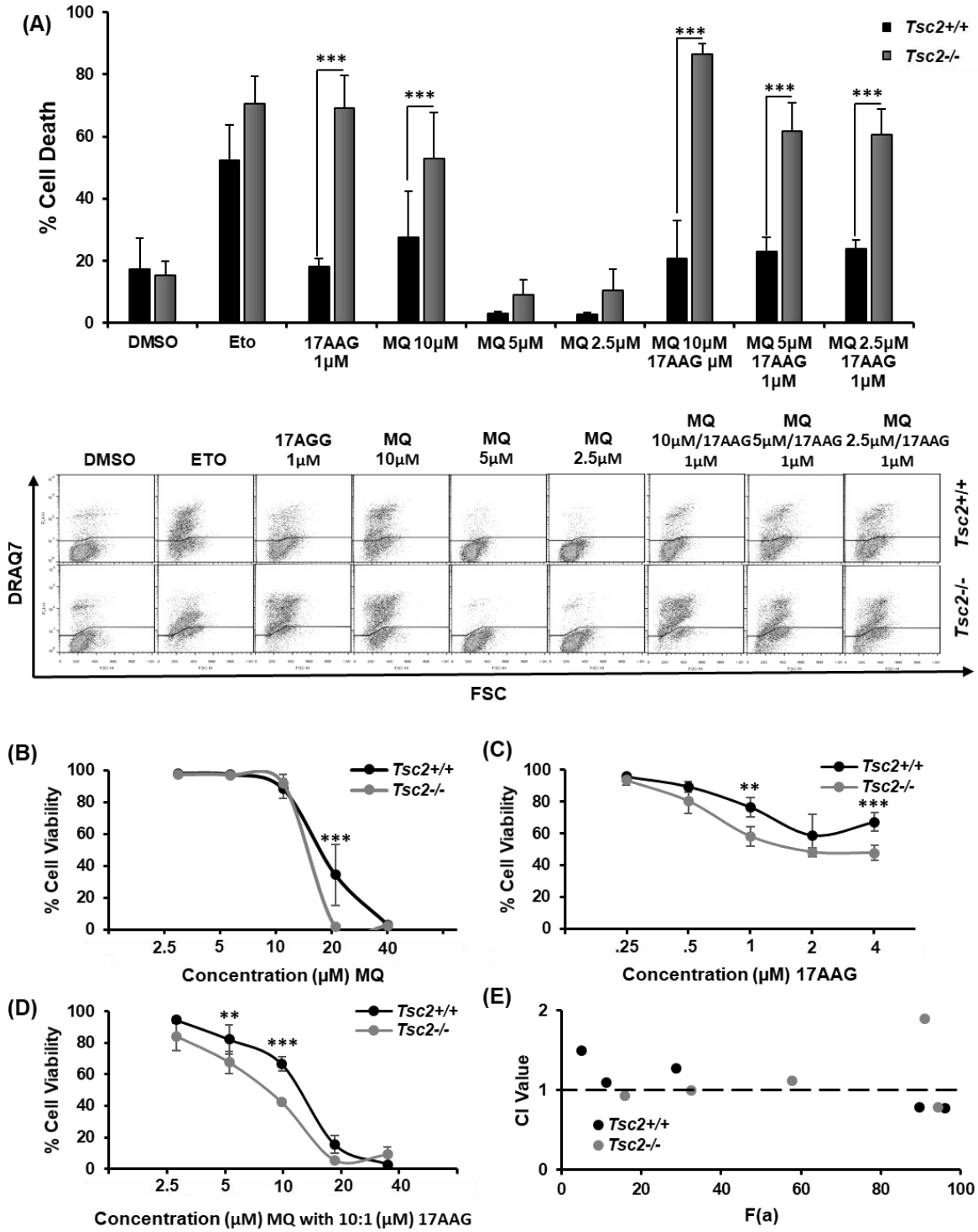

Figure 3.8: Combination of mefloquine and 17AAG caused selective cell death in *Tsc2*-/- MEFs but did not synergise. (A) Flow cytometry (with scatter blots) performed to measure cell death in *Tsc2*+/+ and *Tsc2*-/- MEFs treated with dimethyl sulfoxide (DMSO), etoposide (ETO), mefloquine (MQ) or 1 μM 17AAG (17AAG) as single agents at various concentrations or in combination (MQ/17AAG) at various concentrations after 48 h treatment (n=3 mean+/- SD). (B-D) Dose response curves were performed in *Tsc2*+/+ and *Tsc2*-/- MEFs using flow cytometry to measure cell death following treatment with (B) 17AAG (17AAG); (C) mefloquine (MQ) and (D) combined mefloquine with a fixed concentration of 10 μM nelfinavir (MQ/NFV): 1 μM 17AAG (n=3; mean +/- SD). Synergy was then calculated using CompuSyn and graphed (E) as F(a) value vs CI value. Statistical

significance is shown with combination or single agent treated *Tsc2-/-* MEFs compared to their wild-type controls.

3.2.6 Mefloquine/nelfinavir combination affects energy stress levels in *Tsc2-/-* cells.

To explore alternative mechanisms that might be the cause of cell death, a more in-depth analysis of the RNA sequencing data was carried to compare gene expression changes in the *Tsc2*+/+ and *Tsc2*-/- MEFs. A Heat map was generated for a panel of energy stress associated genes (Figure 3.9A). The Heat map represents RNA expression as low levels of expression (or no expression) were represented by blue (were the darkest blue represents lowest level of expression (a score of 0)). Increased RNA expression is represented by a colour shift from blue to white to red were the darkest red represents the highest RNA expression score (in this case, a score of 3445). A selection of genes was then further graphed and analysed (Figure 3.9C). The overall RNA sequencing data was represented in a volcano plot where chosen energy stress genes were highlighted (Figure 3.9B). Colours represent differences in expression levels which have at least a 1-fold difference in *Tsc*2+/+ MEFs (Blue) and *Tsc*2-/- MEFs (Red). Genes involved in the regulation of metabolism and energy homeostasis were shown to be up-regulated in the *Tsc2-/-* MEFs during combined treatment with nelfinavir and mefloquine. PPARGC1α (which is the gene for PGC1α (peroxisome proliferator-activated receptor gamma coactivator 1α), which is involved in mitochondrial biogenesis) was basally expressed at a higher level in *Tsc2-/-* MEFs when compared to the *Tsc2*+/+ MEFs. Genes regulated by PPARGC1α were observed to be more highly expressed in the *Tsc2-/-* MEFs when compared to *Tsc2*+/+ MEFs. These included genes involved in glucose and lipid metabolism, such as peroxisome proliferator-activated receptor delta (PPARδ) and gamma (PPARγ), where there is more than a 2-fold increase in PPARδ expression and a nearly 17-fold difference in PPARγ expression in the *Tsc2-/-* MEFs compared to the *Tsc2*+/+ MEFS. Expression of genes involved in glycolysis were also upregulated, indicating metabolic stress. This included pyruvate dehydrogenase kinase 1 (PDK1), pyruvate carboxylase (PCX), lactate dehydrogenase B (LDHB) and glycerol-3-phosphate dehydrogenase 1 (GPD1). AMP-dependent protein kinase (AMPK) is known to function upstream of PGC1α and is involved in the gene-expression of PGC1α as well as its transcriptional activity. AMPK-regulated genes involved in glucose metabolism/storage such as

acetyl-CoA carboxylase 2 (ACC2, encoded by the ACACB gene) and glycogen synthase 1 (GYS1) were expressed at a much higher level in *Tsc2*-/- MEFs and were further increased upon drug treatment with nelfinavir and mefloquine. HDAC5 (which is involved in the AMPK regulation of the glucose transporter GLUT4) was found to be more highly expressed in *Tsc2*+/+ MEFs when compared to *Tsc2*-/- MEFs. However, when looking at the differences in RNA expression between cells treated DMSO and the mefloquine/nelfinavir combination, the introduction of the mefloquine/nelfinavir combination only cause significant differences in PPARGC1α, HAS2, GYS1 and RORA (in *Tsc2*-/- MEFs) and HDAC5 and HAS2 (in *Tsc2*+/+ MEFs) The overall increase of mRNA expression of key genes involved in energy metabolism gives evidence that the *Tsc2*-/- MEFs were likely energy stressed.

To determine if the drug combination of nelfinavir and mefloquine influenced energy stress, flow cytometry was carried out in *Tsc2*-/- MEFs treated for 48 h with either DMSO or drug combination in the absence or presence of methyl pyruvate (a pyruvic ester, which can rescue cells from energy stress by freely crossing the inner membrane of the mitochondria and is cleaved by matrix esterases to generate intramitochondrial pyruvate. The additional pyruvate allows for the stimulation of ATP production (Gergely *et al.* 2009; Divakaruni *et al.* 2013). Methyl pyruvate was also shown to be more efficient than pyruvate in supporting the intramitochondrial conversion of pyruvate metabolites to amino acids (Jijakli *et al.* 1996)). Results showed that methyl pyruvate partially rescued cell death. To confirm that methyl pyruvate was restoring energy stress, western blots were carried on *Tsc2*-/- MEFs treated for 24 h in conditions identical to the flow cytometry experimentation. Results showed a reduction in the production of SESN2 and in the phosphorylation of both AMPK and ACC in *Tsc2*-/- MEFs treated with drug combination and methyl pyruvate compared to samples treated with just the drug combination.

To determine the duration of the effects of energy stress management, western blots were carried on *Tsc2*-/- and *Tsc2*+/+ MEFs treated for 6 and 24 h with mefloquine and nelfinavir combination, in the presence or absence of methyl pyruvate. The data indicated that in *Tsc2*-/- MEFs treated with mefloquine/nelfinavir combination and methyl pyruvate and *Tsc2*+/+ MEFs had high levels of ACC phosphorylation at 6 h before declining at the 24 h time point. On the other hand, the level of ACC phosphorylation did not peak until the 24 h time point in the *Tsc2*-/- MEFs treated with the drug combination only.

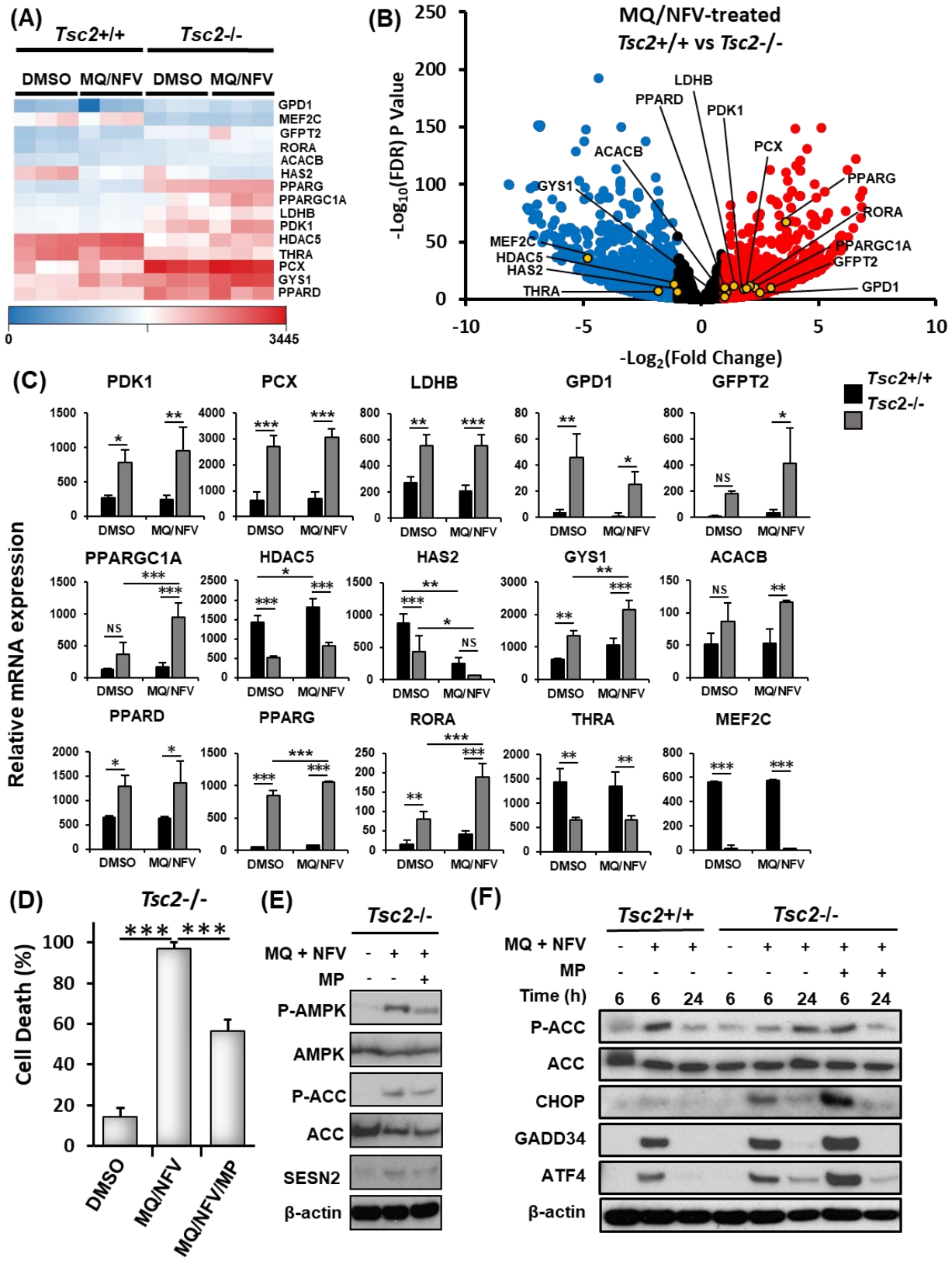

Figure 3.9: Mefloquine/nelfinavir combination affected energy metabolism and the introduction of methyl pyruvate rescued *Tsc2*-/- MEFs. (A) The RNA sequencing data used for Figure 3.7C−E was assessed for the expression of genes involved in energy homeostasis. A heat map for a panel of energy stress-linked genes was generated. Heat map shows expression as dark blue representing low levels of RNA expression while dark red (via going from blue to white to red)

represents high levels of RNA expression. A selection of genes from the Energy Stress panel were then further graphed in (C) (n=3; mean +/- SD). (B) A volcano plot showing the entire RNA sequencing where genes shown in (C) are highlighted. Statistical significance is shown comparing combination treated *Tsc2*+/+ and *Tsc2*-/- MEFs, comparing DMSO treated *Tsc2*+/+ and *Tsc2-/-* MEFs, comparing *Tsc2*+/+ MEFs treated with either DMSO or 10 μM mefloquine and 10 μM nelfinavir combination (MQ/NFV) and *Tsc2*-/- MEFs treated with either DMSO or MQ/NFV. (D) Tsc2-/- cells were treated with DMSO, MQ/NFV or mefloquine/nelfinavir combination with the addition of 8 mM methyl pyruvate (MQ/NFV/MP) for 48 h. Cells were then stained with DRAQ7 and % cell death determined by flow cytometry. Flow cytometry was carried out by Charlotte Johnson (McCann *et al.* 2018) (n=3; mean +/- SD). Statistical significance (calculated by one-way ANOVA) is shown comparing combination treated *Tsc2*-/- and combination plus methyl pyruvate treated *Tsc2*-/- MEFs. (E) *Tsc2*-/- were treated with either DMSO or 10 μM mefloquine and 10 μM nelfinavir combination in the presence or absence of 8 mM methyl pyruvate for 24 h and total and phosphorylated ACC and AMPK and total SESN2 was determined by western blot. (F) *Tsc2*+/+ and *Tsc2*-/- cells were treated with either DMSO or 10 μM mefloquine and 10 μM nelfinavir combination in the presence or absence of 8 mM methyl pyruvate for 6 and 24 h, where indicated. Total protein levels of ACC, CHOP GADD34 and ATF4 as well as phosphorylated ACC were detected by western blot. All Blots in figure 3.9 are representative of n=3 runs

3.2.7 Mefloquine/nelfinavir combination did not affect the production of reactive oxygen species (ROS).

To confirm if the combination was causing an effect on the production of reactive oxidative species (ROS), both *Tsc2*+/+ and *Tsc2*-/- MEFs were stained with DCFDA before being treated with several different treatments; DMSO, Tert-Butyl hydroperoxide (TBHP) (as a positive control), drug combination and drug combination with either methyl pyruvate or N-acetyl-L-cysteine (NAC) (both of which are known ROS scavengers so would act as negative controls). Results written as ROS Generation fluorescence (RGF). Results showed that the drug combination caused no major differences to ROS production compared to samples treated with just DMSO (Figure 3.10A). To determine if ROS production played a role in cell death, flow cytometry was carried out in *Tsc2*-/- MEFs treated for 24 h (as NAC is a short-lived inhibitor) with either DMSO, drug combination or drug combination with NAC. Results showed that the presence of NAC was able to partially rescue cells from death as cell death dropped just under 15% compared to death seen in cells treated with just mefloquine/nelfinavir combination (63.33% +/- 14.31 SD when treated with mefloquine/nelfinavir combination and NAC compared to 77.90% +/- 15.42 SD when treated with just the combination) (Figure 3.10B).

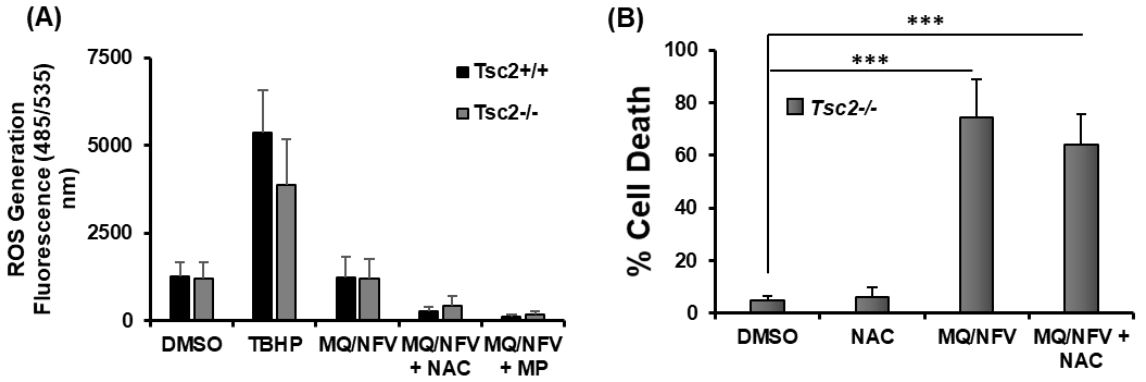

Figure 3.10: Mefloquine/nelfinavir combination caused minimal effect on ROS production. (A*) Tsc2*+/+ and *Tsc2*-/- MEFs were stained in 25 µM 2', 7' –dichlorofluorescin diacetate (DCFDA) for 45 min at 37ºC. Cells were washed and treated with DMSO, tert-butyl hydroperoxide (H_2O_2), mefloquine and nelfinavir combination (MQ/NFV), combination plus N-acetyl-L-cysteine (MQ/NFV + NAC) or combination plus methyl pyruvate (MQ/NFV + MP) for 4 h. Fluorescence was read on a plate reader (excitation at 485 nm and emission at 535 nm) (n=3; mean +/- SEM). (B) *Tsc2*-/- MEFs were treated with DMSO, mefloquine and nelfinavir combination (MQ/NFV) or combination plus N-acetyl-L-cysteine (MQ/NFV + NAC) for 24 h. Cell death was measured via flow cytometry using DRAQ7 staining. Statistical significance (calculated by one-way ANOVA) is shown between DMSO-treated cells and MQ/NFV treated cells and between NAC-treated and MQ/NFV treated cells (n=3; mean +/- SD).

3.3 Discussion:

The purpose of this chapter was to determine an optimised concentration of mefloquine and nelfinavir and determine the mechanism of action that the mefloquine/nelfinavir combination used against *Tsc2*-/- MEFs. Initial experiments were designed to determine the optimum concentration of mefloquine and nelfinavir for synergistic action. This chapter also examined possible mechanisms of drug action to determine how the nelfinavir and mefloquine drug combination was selectively triggering cell death in the *Tsc2*-/- MEFs, while the *Tsc2*+/+ MEFs were survived treatment.

Data from these experiments identified an optimal concentration of 10 µM mefloquine and 10 µM nelfinavir for inducing cell death. A second concentration of 5 µM mefloquine and 20 µM nelfinavir was also sufficient for inducing a cell death response in *Tsc2*-/- MEFs but was less effective compared to the 10 µM mefloquine and 10 µM nelfinavir. Manipulating either of these concentrations caused either decreased effectiveness in causing cell death or loss of selective cytotoxicity to the *Tsc2*-/- MEFs. The data from these experiments have shown that the combination

of nelfinavir and mefloquine has a very narrow drug concentration range at which they are selectively cytotoxic to the *Tsc2*-/- MEFs. The concentrations of both drugs used in this study are clinically viable. As 10 μM falls within the concentration range of mefloquine found in patient serum (Kollaritsch *et al.* 2000). Regarding nelfinavir, the 10 μM concentration used in this study is higher than the manufacturer recommended trough concentration (1−3 μM). However, nelfinavir serum concentrations have previously been reported in HIV patients at a similar concentration to the 10 μM used in this chapter, ranging from 4.96 μM (Zhang *et al.* 2001) up to 18 μM (Marzolini *et al.* 2001). In fact, it has been reported that nelfinavir is well tolerated in cancer patients at doses 2.5 times the FDA-approved dose for HIV management (Bernstein *et al*. 2015b).

Previous investigations by the research team were carried out on the cytotoxic drug activities of a combination of nelfinavir and chloroquine (Johnson *et al*. 2015). The chloroquine/nelfinavir combination was able to block autophagy; however, the introduction of bafilomycin A1 prevented the accumulation of chloroquine in the lysosome. Since chloroquine and mefloquine belong to the same drug family, it was initially postulated that they should have a similar mode of drug action. Testing the mefloquine/nelfinavir combination for autophagic flux, results showed that this combination caused noticeably less autophagic inhibition in terms of LC3 accumulation compared to chloroquine/nelfinavir combination. Levels of p62 in *Tsc2*-/- MEFs were also not altered by the mefloquine/nelfinavir combination, although chloroquine/nelfinavir also failed to cause any differences in protein levels of p62 in this project nor in published data (Johnson *et al*. 2015). There was also increased levels of cell death when bafilomycin A1 was introduced to the mefloquine/nelfinavir combination, contrasting with the results seen in chloroquine/nelfinavir treated cells (which rescued cell death). These contrasting findings may be explained by the use of mefloquine. Shin *et al.* (2012) showed that inhibiting autophagy (e.g., by introducing bafilomycin A1) increased the cytotoxicity of mefloquine in neuroblastoma cells. Overall, these results showed that the combination of mefloquine/nelfinavir was unlikely to induce a cytotoxic drug activity by blocking autophagy, unlike chloroquine/nelfinavir combination.

Instead, mefloquine and nelfinavir combination may trigger cell death via enhanced ER stress. After 6 h of mefloquine and nelfinavir treatment, *Tsc2*-/- MEFs showed robust activation of the PERK pathway (which was expected as nelfinavir is as a well-known ER stress enhancer (Gills *et al*. 2007). Results showed that the

mefloquine and nelfinavir combination induced higher expression levels of PERK pathway components compared to single agent treatments such as mefloquine. However, the mefloquine/nelfinavir combination only caused as a slight non-significant increase in protein expression compared to nelfinavir, suggesting that nelfinavir is solely responsible for ER stress associated with the combination. The duration of ER stress was also investigated by examining the protein expression of ER stress components. The data from this experiment showed that the *Tsc2*-/- MEFs were still expressing ER stress markers at an elevated level after 48 h, a time point when the majority of these cells had undergone cell death. This data indicates that these cells were trying to recover from ER stress. To determine if ER stress is playing a role in cell death, a viable option would be to test cells using an ATF4 inhibitor (since nelfinavir doesn't effect PERK activity as discussed in chapter 1) such as Ursolic acid and Tomatidine (Ebert *et al.* 2015) to determine if cells can be rescued from the mefloquine/nelfinavir treatment. While ER stress is unlikely to be the trigger of cell death, recovery from ER stress might contribute to the depletion of energy through *de novo* protein synthesis of chaperone and heat shock proteins as well as the actual protein unfolding and re-folding - processes that heavily consume ATP. A recent study showed that TSC2-knockdown leads to mitochondrial oxidative stress (Yang *et al.* 2018). This degree of energy stress is presumably why TSC2-deficent cells are vulnerable to conditions that induce energy starvation (Choo *et al.* 2010).

During the RNA sequencing, expression of the gene *PPARGC1A* (that encodes PGC1α) was greatly increased in *Tsc2*-/- cells, especially when treated with the mefloquine/nelfinavir combination. PGC1α acts as a master regulator of mitochondrial biogenesis and also plays a role in energy regulation as it interacts with PPARγ (Duncan 2011). PPARγ is involved with glucose metabolism and was also elevated in the RNA sequencing data carried out in this chapter. This study indicates that mitochondrial biogenesis is basally upregulated in *Tsc2*-/- MEFs compared to *Tsc2*+/+ MEFs, suggesting that these cells are more likely to experience energy deficiency when treated with nelfinavir and mefloquine. To confirm if energy deprivation was occurring in the treated *Tsc2*-/- MEFs, AMPK signalling was examined (which is activated when the ATP:AMP ratio in the cell favours higher levels of AMP (Hardie 2015)). Both the phosphorylation levels of AMPK and ACC (which regulates fatty acid biosynthesis) were increased in the presence of the nelfinavir and mefloquine drug combination supporting this

hypothesis. Supplementing methyl pyruvate to the media markedly reduced the level of AMPK and ACC phosphorylation and caused a significant recovery of cell death. To determine if this observed energy stress was connected to the increased ER stress, SESN2 levels were examined in the same manner as AMPK and ACC. SESN2 activates AMPK either via direct physical association or indirect transcriptional regulation (but only in the presence of ATF4 (Pasha *et al.* 2017)). Expression patterns for SESN2 matched those seen for both ACC and AMPK phosphorylation. As a result, it is possible that a combined spike in both ER and energy stress after mefloquine and nelfinavir treatment is responsible for cell death in *Tsc2*-/- MEFs. This may occur through caspase independent mechanisms triggered by PPARγ which has been shown above to be upregulated. A similar mechanism has been shown previously induced by Ciglitazone (a PPARγ agonist) (Kang *et al*. 2008).

An unusual observation was made during the investigation of energy stress, in terms of when energy stress was at its highest. The response of *Tsc2*-/- MEFs treated with mefloquine/nelfinavir combination and methyl pyruvate (and *Tsc2* +/+ MEFs), to increased energy stress were detected within 6 h of administration of mefloquine and nelfinavir combination to the cells (which coincides with the increase in ER stress markers at the 6 h time point), as seen in Figure 3.9F. The response appears to return to normal at 24 h that possibly coincides with ER stress cell recovery and survival in these cells. However, in *Tsc2*-/- MEFs treated with only the mefloquine and nelfinavir combination, energy stress response does not peak until after 24 h of treatment, showing that there is a delayed energy stress response compared to the other cells tested. It is possible that there is a signalling disconnect between mTORC1 and AMPK, which hampers effective energy sensing and causes energy starvation in the *Tsc2*-/- MEFs. The reason for this possible delay in energy sensing is unknown and out of the scope of this chapter due to time restraints. Further investigations into why this occurs and whether this possible delayed response also occurs in mTORC1 hyperactive sporadic cancer cell lines should be investigated in the future. This will help to determine if this delayed response is a general mechanism for the mefloquine/nelfinavir combination or if it is cell-line specific.

As ER stress and mitochondrial activity both generate ROS, the effects that the mefloquine and nelfinavir combination had on ROS production were tested. Experimental data showed that there was only a minor, non-significant increase in

ROS levels between control cells and *Tsc2*-/- MEFs treated with the mefloquine/nelfinavir combination. A minor, non-significant decrease in cell death was also observed in the rescue assay when NAC was introduced to the mefloquine and nelfinavir combination. Data from these two experiments showed evidence that ROS production may play a role (although a very minor role) in the cell death induced by mefloquine and nelfinavir treatment.

One of the most interesting aspects that arose from these results was how the effects of mefloquine changed between cell lines. In the *Tsc2*-/- MEFs, mefloquine failed to cause significant cytotoxicity at 10 µM. However, when the same concentration of mefloquine was used to treat either NCI-H460 or HCT116 cells, a large amount of cell death was observed. One possible reason is due to AKT signalling. As mentioned in this chapter's introduction, mefloquine was shown to be a suppressor of PI3K, AKT and mTOR via dephosphorylation of these proteins. In *Tsc2*-/- MEFs, signal transduction through AKT was decreased due to continuous activation of mTORC1, resulting in an increased activation of S6K1 and subsequent downregulation of IRS (Tavares *et al.* 2015). This lack of AKT activation prevents mefloquine working on these components in *Tsc2-/-* MEFs. In HCT116, NCI-H460 cells, and MCF7 cells, on the other hand, mTORC1 hyperactivity is not due to mutations in TSC proteins but, instead, mutations further upstream in the PI3K-AKT pathway (e.g., PTEN).

The original target population for treatment with the mefloquine and nelfinavir combination was TSC patients. However, complications could arise when considering this population for treatment. The main problem lies with mefloquine. Mefloquine was found to be neurotoxic in 2006 (McCarthy 2015). It was withdrawn from the U.S. market in 2009 by Hoffman La-Roche and has loss market shares in the U.K. and Australia (Remington L. Nevin 2012). Usage of mefloquine has been greatly curtailed by the U.S. Army in favour of doxycycline, and the British Defence Committee declared mefloquine to be a "drug of last resort" (Tickell-Painter *et al.* 2017; Remington L. Nevin 2012). Mefloquine, on rare occasions, is known to cause several neuropsychiatric adverse effects, including cognitive disturbances, anxiety, depression, psychosis, and violence (Mawson 2013) that may persist even after discontinuing administration of the drug. Side effects associated with the central nervous system occur in 1:10,000 people although the odds rise when factors such as history of psychiatric problems, female sex, low body mass index and first-time usage are taken into account. Side effects appear to be dose-dependent These

side effects may be due to mefloquine being able to potentiate dopamine, cause clinical anticholinergic syndrome, inhibit P-glycoprotein and interfere with calcium homeostasis and gap junction function in neurons (Alisky *et al.* 2006). Because of its ability to cross the blood-brain barrier, there is also a risk of mefloquine accumulation in the central nervous system which could worsen symptoms (Toovey 2009). Mefloquine is not recommended for treatment in patients with a history of epilepsy as it has been reported to cause seizures. These reports mean that only 20% of TSC patients could benefit from the use of the mefloquine/nelfinavir combination as most TSC patients suffer from some form of epilepsy and patients can develop TANDs (as discussed in Chapter 1) in later life.

There are still plenty of opportunities for the mefloquine and nelfinavir combination as a treatment for mTORC1 hyperactive sporadic tumours. Results from this chapter showed that the mefloquine and nelfinavir combination worked exceptionally well on sporadic cancer cell lines such as HCT116 and NCI-H460. These initial observations showed that a mefloquine/nelfinavir combination could be a viable treatment option for these tumour types (i.e., colorectal and lung cancers) in the future should the mefloquine/nelfinavir combination pass pre-clinical and clinical trials. The MCF7 cell line is derived from drug resistant breast carcinoma cells. In the presence of the mefloquine/nelfinavir combination, cell death occurred in over 60% of treated cells and cell death was non-significantly enhanced by introducing rapamycin to the mefloquine/nelfinavir combination. As a result, further investigations into the use of a mefloquine/nelfinavir combination (with and without rapamycin) as a treatment for breast cancer should be undertaken in the future.

The next logical step for this research would be to test the mefloquine/nelfinavir combination in *in vivo* cancer models. Murine models with xenographs of several different *Tsc2*-/- tumour types such as AML, LAM or SEGA would be suitable candidates. Murine models with patient-derived SEGA xenographs would also be extremely useful, allowing exploration of the previously mentioned risk of seizures and psychosis during mefloquine treatment.

In conclusion, the data from this chapter showed that an optimised concentration of mefloquine and nelfinavir selectively targets mTORC1 hyperactive cells in a TSC-based or sporadic tumour-based setting. Experimental evidence presented here shows that cytotoxicity caused by the mefloquine/nelfinavir combination is likely due to an increase in energy stress possibly in combination with an enhanced ER stress

burden. This energy stress cannot be optimally restored in cells without *Tsc2* and as a result, triggers cell death.

Chapter 4: A combination of Bortezomib and Nelfinavir caused selectively cell death in mTORC1 hyperactive cells

4.1 Introduction:

4.1.1 The proteasome

The proteasome is a highly conserved and essential protein complex necessary for degrading the majority (80-90 %) of intracellular proteins in eukaryotic cells (Papandreou and Logothetis 2004; Dou and Zonder 2014). Because of this, the proteasome can make up to 1 % of the cellular protein content of eukaryotic cells (Buac *et al.* 2013). Several proteins degraded by this pathway include cell cyclins (that regulate the progression of cells through the cycle), several transcription factors (such as c-myc and n-myc), NF-kB inhibitors (IkB), and enzymes (phosphatase cdc-25, tyrosine-amino transferase, topoisomerase I, topoisomerase IIα) (Roccaro *et al*. 2011).

The 26S proteasome was first described as a giant protease with multiple subunits with a combined molecular weight of 2400 kDa. The 26S proteasome is composed of a 700 kDa 20S core particle which consists of four subunits, two α- and two β-rings. The β-rings contain multiple enzymatic sites with chymotrypsin-like (β5), trypsin-like (β2), and post-glutamyl peptide hydrolase-like (caspase-like, β1) activities. The core particle is then flanked at each end by 19S regulatory complexes. These regulatory complexes contain a “lid” of nine or more non-ATPases which recognise polyubiquitinated proteins and a base of 6 ATPases and 4 non-ATPases. The base ATPases and non-ATPases are responsible for denaturing target proteins and deliver them to the proteolytic core (Buac *et al.* 2013; Dick & Fleming, 2010; Dou & Zonder, 2014; Papandreou & Logothetis, 2004; Roccaro *et al.* 2006).

Because of this essential role in the cell, the proteasome and protein degradation has been considered as a drug target for treating cancer cells. For instance, inhibition of the proteasome can overwhelm the response of tumour cells to effectively recover from a variety of stress conditions, such as lactic acidosis, chromosome instability, DNA damage, ROS and heat shock, which can trigger cell death (Bose *et al*. 2014). Proteasome inhibition in mTORC1 hyperactive tumour

cells was shown to cause selective toxicity (Babcock *et al*. 2013; Siroky *et al*. 2017). It is also been shown that inhibiting just the chymotrypsin-like activity of the 20S core particle was able to significantly block proteasomal protein degradation (Nussbaum *et al*. 1998).

4.1.2 Bortezomib

Bortezomib is a dipeptide boronic acid derivative containing pyrazinoic acid, phenylalanine and leucine with boronic acid in its structure and was originally synthesised by Myogenics in 1995 (Dou and Zonder 2014). It became the first proteasome inhibitor used in humans after being fast-track approved by the FDA in 2003 for the treatment of multiple myeloma (newly diagnosed and relapsed/refractory) and of relapsed/refractory mantle cell lymphoma. This was based on the results from a large phase II clinical trial and received full approval after the 2005 APEX (Assessment of Proteasome Inhibition for Extending Remission) phase III trial (1.3 mg/m^2 for eight 21-day cycles and then three 35-d cycles) (Chen *et al.* 2011; Kapoor *et al.* 2012). Bortezomib (1.3 mg/m^2) can be administered either intravenously or subcutaneously. In a phase III clinical trial in adults with refractory multiple myeloma, there was no significant difference observed between either method of administration (intravenously or subcutaneously) in terms of median time to first response, median progression-free survival median time to progression and 1-year overall survival. Subcutaneous administration , however, was shown to have a significant reduction in the incidences of peripheral neuropathy (Hoy 2013).

Bortezomib can reversibly bind to the 20S core particle of the proteasome. Bortezomib has the highest affinity for the β5 subunit and has lesser affinity for the β1 and β2 subunits as well (Wallington-Beddoe *et al.* 2018). Originally, Bortezomib was designated as a NF-κB inhibitor, as it is able to prevent the degradation of IκB (a NF-κB inhibitor) (Brüning and Jückstock 2015). Another anti-cancer property of Bortezomib is via upregulation of the expression of NOXA (a pro-apoptotic member of the Bcl-2 family). Upregulation of NOXA has been shown to cause apoptosis via two possible methods; selective interaction with anti-apoptotic proteins of the Bcl-2 family (Bcl-XL and Bcl-2) or by stimulating other pro-apoptotic factors (D. Chen *et al.* 2011). Bortezomib has also been shown to inhibit angiogenesis in a dose

dependent manner, to inhibit c-Jun and to downregulate growth factor expression (Roccaro *et al*. 2011).

4.1.3 Bortezomib and blood cancers

Bortezomib is primarily used for the treatment of blood cancers, having originally been approved for the treatment of multiple myeloma. *In vitro* studies showed that Bortezomib could inhibit proliferation in different myeloma cell lines including doxorubicin, mitoxantrone, and melphalan sensitive and resistant RPMI-8226 cell lines (Dou and Li 1999).

A large phase II clinical trial (SUMMIT – Study of Uncontrolled Multiple Myeloma Managed with Proteasome Inhibition Therapy) showed that there was a 35% overall (complete + partial + minimal) response rate with Bortezomib (1.3 mg/m^2 on days 1, 4, 8, and 11 of a 3-week cycle for up to eight cycles) in 202 patients with relapsed and refractory multiple myeloma (Richardson *et al.* 2003). Phase II clinical trials with Bortezomib have also shown promising results in the treatment of mantle-cell lymphoma and non-Hodgkin's lymphoma. In patients with mantle cell lymphoma, there was a 46.2% response rate with Bortezomib (1.3 mg/m^2 given on days 1, 4, 8 and 11 every 21 days) (Sehn *et al*. 2006). A 58% response rate to Bortezomib (1.5 mg/m^2 on days 1, 4, 8, and 11) was observed in patients with indolent non-Hodgkin's lymphoma and mantle cell lymphoma (Adams *et al*. 2004).

The previously mentioned APEX phase III trial, showed that there was a 6 month survival advantage in patients (who received at least one prior treatment) when compared to patients treated with dexamethasone (Richardson *et al.* 2007). In a clinical setting, Bortezomib has been shown to restore abnormal bone remodelling caused by myeloma by normalizing the level of bone turnover markers. In addition, a bone anabolic effect was described in responding myeloma patients treated with Bortezomib, as seen by the increase in osteoblast numbers (Aversa *et al*. 2015). Bortezomib was shown to cause induction of the lytic cycle of Epstein-Barr virus (EBV) and Kaposi sarcoma herpes virus (KSHV). Bortezomib has also been shown to be able to induce the lytic cycle in human Burkitt's lymphoma, EBV+ Akata cells and EBV-T lymphoma and natural killer cells at 0.5 μM (Kaluza *et al.* 2006; Iwata *et al.* 2011). Bortezomib was also shown to have promising activity in Waldenström's macroglobulinemia as a single agent (1.3 mg/m^2 intravenously days 1, 4, 8, and 11 on a 21-day cycle until two cycles past complete response (CR),

stable disease (SD) attained, progression (PD), or unacceptable toxicity) (Chen *et al.* 2007; Treon *et al.* 2007).

4.1.4 Bortezomib and solid cancers

Bortezomib has shown less clinical promise in solid cancers. For instance, Bortezomib failed to show efficiency compared to previously established treatments when tested against breast cancer, hormone-resistant prostate cancer, chemotherapy-naïve advanced stage non-small cell lung cancer, unresectable/metastatic gastric and gastroesophageal junction adenocarcinoma, metastatic neuroendocrine tumours, and advanced renal cell carcinoma (Dou and Zonder 2014). However, Bortezomib affected the growth of thyroid cancer ATC cell lines as a single agent or in combination with other drugs ranging from 4.5 nM up to 10 mM (Mitsiades *et al.* 2006).

4.1.5 Bortezomib combinations

Combining Bortezomib with other drugs has shown degrees of clinical success. When Bortezomib is combined with other chemotherapies or with corticosteroids, response rates go from approximately 30% to between 60% and 90% (Murray *et al.* 2014). In the VERTICAL phase II trial, a combination of Bortezomib (1.6 mg/m^2 on days 1, 8, 15, and 22, cycles one to five), Bendamustine and Rituximab showed an overall response rate of 88% (53% complete response) in patients with relapsed and refractory follicular lymphoma (Shi *et al*. 2011). Ruan *et al.* (2011) carried out a phase I/II trial using Bortezomib (0.7 mg/m^2, 1.0 mg/m^2, or 1.3 mg/m^2 on days 1 and 4 for six cycles), Cyclophosphamide, doxorubicin, Vincristine, Prednisone and Rituximab and showed this combination had an evaluable overall response rate of 100% with 86% complete response/unconfirmed complete response and 91% and 72%, respectively, in refractory/relapsed mantle cell lymphoma patients. Using Bortezomib with lenalidomide and dexamethasone in a phase I/II trial showed a 100% response rate in myeloma patients (75% showing a very good partial response or higher – although 25% of all patients did relapse after cessation of treatment (Dimopoulos *et al*. 2010)).

A combination of Bortezomib (1.2 mg/m^2 on days 1, 4, and 8) with paclitaxel (175 mg/m^2 on day 2) and carboplatin was tested for the treatment of solid tumours (Dakhil *et al*. 2010). However, this drug combination failed as a first-line therapy for

patients with metastatic oesophageal, gastric and gastroesophageal cancers. A combination of Bortezomib (1.3 mg/m^2 on days 1, 4, 8, and 11 of an every-21-day cycle) and pegylated liposomal doxorubicin (30 mg/m^2 on day 4) on patients with pre-treated metastatic breast cancer was shown to be well tolerated, however, it only had a minimal effect on the tumour (Irvin *et al.* 2010). A phase II clinical study of Bortezomib (1 mg/m^2) and gemcitabine (1,000 mg/m^2) in patients with metastatic pancreatic cancer showed that patients had a median survival time of 4.8 months, a 6-month survival rate of 41% and a 10% response rate (Alberts *gills* 2005). A positive and synergistic response was demonstrated when Bortezomib and irradiation (IR) were combined for the treatment of oral cancer cells (Wu *et al.* 2018). This Bortezomib (25 nM) and IR combination induced autophagic cell death via inhibition of IR-induced TRAF6 ubiquitination and TRAF6-mediated Akt activation. Bortezomib reduced TRAF6 protein expression through autophagy-mediated lysosomal degradation.

4.1.6 Bortezomib limitations

As with most chemotherapeutics, Bortezomib usage has been reported to have adverse effects on patients. The most common side effect of Bortezomib is peripheral neurotoxicity that occurs in 37-44% of patients. This neurotoxicity can be sensory, distal, symmetric and usually affects the feet more than the arms and the effects are usually reversible when treatment has ceased (Bose *et al.* 2014). Other common side effects include fatigue, nausea, diarrhoea, vomiting, low platelet and erythrocytes counts and a high rate of shingles. Less common side effects include headache, insomnia, joint pain, arthralgia, myalgias, oedema (of the face, hands, feet or legs), and low white blood cell count (Chen *et al.* 2011).

Another problem associated with Bortezomib usage is the risk of acquiring resistance to the drug. Bortezomib resistance can occur by several means. Mutations in the β5-subunit, especially substitution of Ala^{49}, can cause resistance with the most common substitute being threonine as seen in myelomonocyte THP1 cells, Jurkat cells and myeloma cell lines KMS-11 and OPM-2 (Lü *et al.* 2008; Oerlemans *et al.* 2008; Ri *et al.* 2010). Aberrant expression of the ubiquitin-proteasome pathway components such as β5, β1 and β2 was found in Bortezomib-resistant THP1 cells, although this was reversible after cells were placed in drug-free media (Oerlemans *et al.* 2008). Bortezomib usage can cause activation of the

aggresome-autophagy pathway to compensate for the loss in the activity of the proteasome, leading to resistance (Catley *et al.* 2006). Another mechanism of resistance is that inhibition of proteasomal protein degradation with Bortezomib could also lead to the induction of heat shock proteins, which has been shown to confer resistance (Mitsiades *et al.* 2002).

Interference to Bortezomib activity can also occur from external causes. The consumption of green tea can block the anticancer drug effects of Bortezomib. This occurs due to the presence of polyphenols especially (-)-epigallocatechin gallate (EGCG) that bind directly to boronic acid-based proteasome inhibitors, such as Bortezomib. Consequently, EGCG prevents the binding of Bortezomib to the proteasome, which was shown to prevent the triggering of ER stress and caspase-7 activation, meaning no induction of cell death (Golden *et al.* 2009).

4.1.7 Bortezomib and ER stress

ER stress is caused by the accumulation of unfolded/misfolded proteins. Bortezomib (5-25 nM) has been shown to induce ER stress, which eventually leads to mitochondrial-mediated Ca^{2+}-dependent apoptosis (Escalante *et al.* 2013). Decreased dephosphorylation of eIF2α has been shown to enhance cell death of Bortezomib, as cells with deregulated eIF2α have resistance to Bortezomib. When a non-toxic dose of salubrinal (an inhibitor of GADD34-PP1c complex) or a phosphorylated mimetic eIF2αS51D was used in combination with Bortezomib (4 nmol/L), both Bortezomib-sensitive and -resistant myeloma RPMI 8226 and U266B1 cells were nearly entirely eradicated. However, this appears to be the case only in blood cancers as results have been shown to be opposite in solid tumours (Schewe and Aguirre-Ghiso 2009). Bortezomib (10 nM) was tested against a panel of 10 pancreatic cancer cell lines and found that cell lines with defective induction of eIF2α phosphorylation had a higher level of drug sensitivity. Bortezomib-sensitive cell lines showed impaired translation attenuation which led to a toxic accumulation of protein aggregates and ROS. On the other hand, Bortezomib-resistant cell lines displayed increased levels of eIF2α phosphorylation, had decreased translation, few protein aggregates, and minimal ROS production (White *et al.* 2018).

Heat shock protein 90 (HSP90) is a chaperone protein that assists in the folding and function of proteins, stabilises proteins from heat stress and aids protein degradation. The use of HSP90 inhibitors and Bortezomib in combination have

shown varying degrees of success. A combination of 17AAG (150mg/m^2) with Bortezomib (0.7mg/m^2) in a clinical trial for patients with acute myeloid leukaemia, showed no clinical response but reported severe adverse effects (Walker *et al.* 2013). On the other hand, tanespimycin (another HSP90 inhibitor) had a better response when combined with Bortezomib. This tanespimycin (100-340 mg/m^2) and Bortezomib (0.7-1.3 mg/m^2 given on days 1, 4, 8 and 11 in each 21 day cycle combination) showed a 27 % objective response rate in refractory and relapsed multiple myeloma and was well tolerated (Richardson *et al.* 2011). However, this combination failed to have any effect on solid tumours (Schenk *et al.* 2013). Inhibiting Ca^{2+}-dependent enzyme, calpain has been shown to enhance cell death in myeloma cells via inhibiting autophagic survival response (which can cause Bortezomib resistance). A combination therapy with Bortezomib and Nelfinavir was shown to inhibit calpain, reversed Bortezomib resistance and induced near-complete tumour regressions in a SCID mouse xenograft model of myeloma (Escalante *et al.* 2013).

4.1.8 Bortezomib and nelfinavir

As mentioned in the last section, a Bortezomib and nelfinavir combination was able to cause a regression of tumour xenograft in myeloma mouse models. However, this is not the only time this combination has been tested. A combination of Bortezomib and Nelfinavir was shown to target cisplatin-resistant cervical cancer cell line (SiHa) via caspase-like proteasome activity which in turn triggered apoptosis. The Bortezomib (20 ng/ml)/nelfinavir (20 µg/ml) combination was able to enhance an apoptosis-inducing TRAIL receptor antibody against SiHa cells (Bruning *et al*. 2011). The Bortezomib (15 ng/mL) and nelfinavir (15 µg/ml) combination was also shown to inhibit mTOR activity via ATF4-mediated SESN2 upregulation in several cancer cell lines including breast (MDA-MB-453), ovarian (OVCAR3) and cervical adenocarcinoma (HeLa) (Brüning *et al.* 2013).

Combinations of nelfinavir and Bortezomib were shown to synergistically kill NSCLC (H157 and A549) and multiple myeloma (RPMI 8226 and L363) cell lines via the induction of ER stress markers and apoptosis (Kawabata *et al.* 2012). It was also found that nelfinavir (20 µM) augments proteasome inhibition by Bortezomib (20 nM) in myeloma cells (Kraus, Bader, Overkleeft, & Driessen 2013). Combined

nelfinavir and Bortezomib therapies have also been trialled in several clinical trials (ClinicalTrials.gov: NCT01164709, NCT02188537, NCT01555281).

4.1.9 Hypothesis

In non-cancerous cells, autophagy and the proteasome work together to breakdown old or damaged proteins to recycle amino acids back into protein synthesis. However, in mTORC1 hyperactive cancer cells, autophagy is suppressed due to persistent inhibitory phosphorylation of ULK1 by mTORC1. At the same time, mTORC1 activation mediates increased expression of proteasome genes through the induction of NRF1 (Zhang *et al* .2014). As a result of hyperactive mTORC1, protein degradation and recycling of amino acids solely relies on the proteasome, making targeting the proteasome a potential vulnerability. To determine if inhibiting the proteasome would cause selective cell death in *Tsc2*-/- MEFs, while being tolerated by *Tsc2*+/+ MEFs, a combination of Bortezomib and Nelfinavir (both ER stress inducers which inhibit the proteasome) were used on these cell lines. The results from this chapter were published in (Johnson *et al.* 2018).

4.2 Results:

4.2.1 A combination of Bortezomib and nelfinavir selectively targeted *Tsc2*-/- cells in a caspase-dependent manner.

To determine if a combination of Nelfinavir and Bortezomib selectively induced cell death in *Tsc2*-/- MEFs compared to *Tsc2*+/+ MEFs. Cell death was quantified by flow cytometry after 24 h treatment with DRAQ7 labelling using MG132 (another proteasome inhibitor), as a single agent and in combination with 20 μM Nelfinavir as a control. Both MG132 and Bortezomib as single agents caused selective cell death in the *Tsc2*-/- MEFs but not in *Tsc2*+/+ MEFs, indicating that *Tsc2*-/- MEFs are dependent on the proteasome for their survival (17.89% +/- 0.732 SD in *Tsc2*+/+ MEFs vs approximately 63.89% +/- 8.16 SD in *Tsc2*-/- MEFs when treated with MG132 and approximately 11.28% +/- 6.10 SD in *Tsc2*+/+ MEFs vs approximately 41.42% +/- 9.09 SD in *Tsc2*-/- MEFs when treated with Bortezomib). Treatment with Bortezomib/Nelfinavir combination enhanced cell death in the *Tsc2*-/- MEFs (83.2% +/- 9.2 SD cell death), with minimal toxicity observed in the *Tsc2*+/+ MEFs (17.5%

+/- 7.7 SD). The low level of cell death in the *Tsc2*+/+ MEFs was not significantly different to the DMSO vehicle control. A similar pattern was observed for the MG132/Nelfinavir combination (24.70% +/- 7.07 SD in *Tsc2*+/+ MEFs and 89.00% +/- 7.39 SD in Tsc2-/- MEFs) (Figure 4.1A).

To further examine cell death in *Tsc2*-/- MEFs, several apoptosis markers were analysed by western blot after both *Tsc2*+/+ and *Tsc2*-/- MEFs were treated in an identical manner as the flow cytometry. We observed cleavage of caspase 8, caspase 3 and PARP in *Tsc2*-/- MEFs upon treatment with Bortezomib alone or co-treatment with nelfinavir and proteasome inhibitors, whilst no cleavage was apparent in wild-type cells (Figure 4.1B).

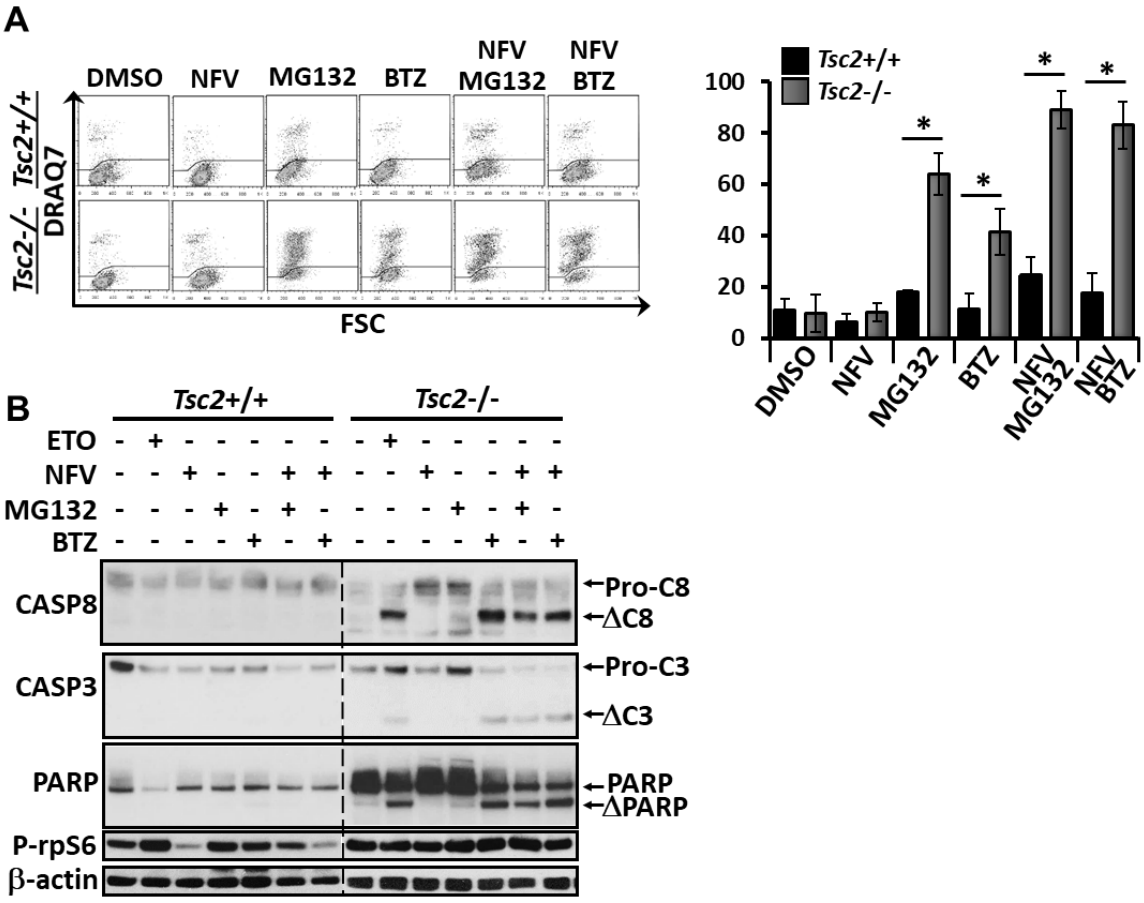

Figure 4.1: The combinations of Bortezomib/nelfinavir and MG132/nelfinavir selectively targeted *Tsc2*-/- MEFs in a caspase-dependent manner. (A) Flow cytometry carried out to determine cell death in *Tsc2*-/- and *Tsc2*+/+ MEFs treated with DMSO, 1 μM MG132, 50 nM Bortezomib (BTZ), 20 μM nelfinavir (NFV) or in combination for 24 h. Cell death was determined via DRAQ7 staining (n=3; mean +/- SD). (B) To determine if caspase activity was affected by combinations, *Tsc2*-/- and *Tsc2*+/+ MEFs were treated in an identical manner as seen in (A) (with the addition of 100 μM etoposide was also used as a control) for 24 h. Total protein levels of Caspase-

8 (CASP8), Caspase-3 (CASP3), PARP, phospho-rpS6 and β-actin were measured by western blot analysis. Flow cytometry was carried out by Dr. Charlotte Johnson and western blotting was carried out by Dr. Sara Seifan. All Blots in figure 4.1 are representative of n=3 runs

4.2.2 Bortezomib/nelfinavir combination killed tumour spheroids and prevented outgrowth.

To determine the effects of Bortezomib/nelfinavir on established tumours in a 3D environment, *Tsc2*-/- MEFs were incubated for 72 h on an agarose layer to form spheroids and photographed before being treated with drugs for 96 h (the last 48 h including DRAQ7) before being photographed again. Treated spheroids were then placed in fresh non-drug media for 72 h (photographed every 24 h) to determine the amount of outgrowth from spheroids (i.e., indicate whether tumours were still viable). Because of the prolonged exposure to the drug (as opposed to 2D models) the concentration of Bortezomib was reduced from 50 nM to 20 nM and 10 nM Rapamycin was used as a control. Results showed that there was no change in size between treatment conditions after 96 h of treatment, except rapamycin-treated samples as a size reduction was observed (as expected). Treated groups were also tested for the amount DRAQ7 fluorescence (as an indicator of the extent of cell death). Results showed that while there were no major differences between DMSO and rapamycin treated spheroids, there was a 2-fold increase in DRAQ7 staining in spheroids treated with Bortezomib/nelfinavir combination (Figure 4.2A). Once placed back into clean media, spheroids incubated in Bortezomib/nelfinavir combination failed to regrow after 72 h. All other spheroids did eventually grow back, although rapamycin treated spheroids grew at a much slower rate compared to DMSO treated spheroids (Figure 4.2B).

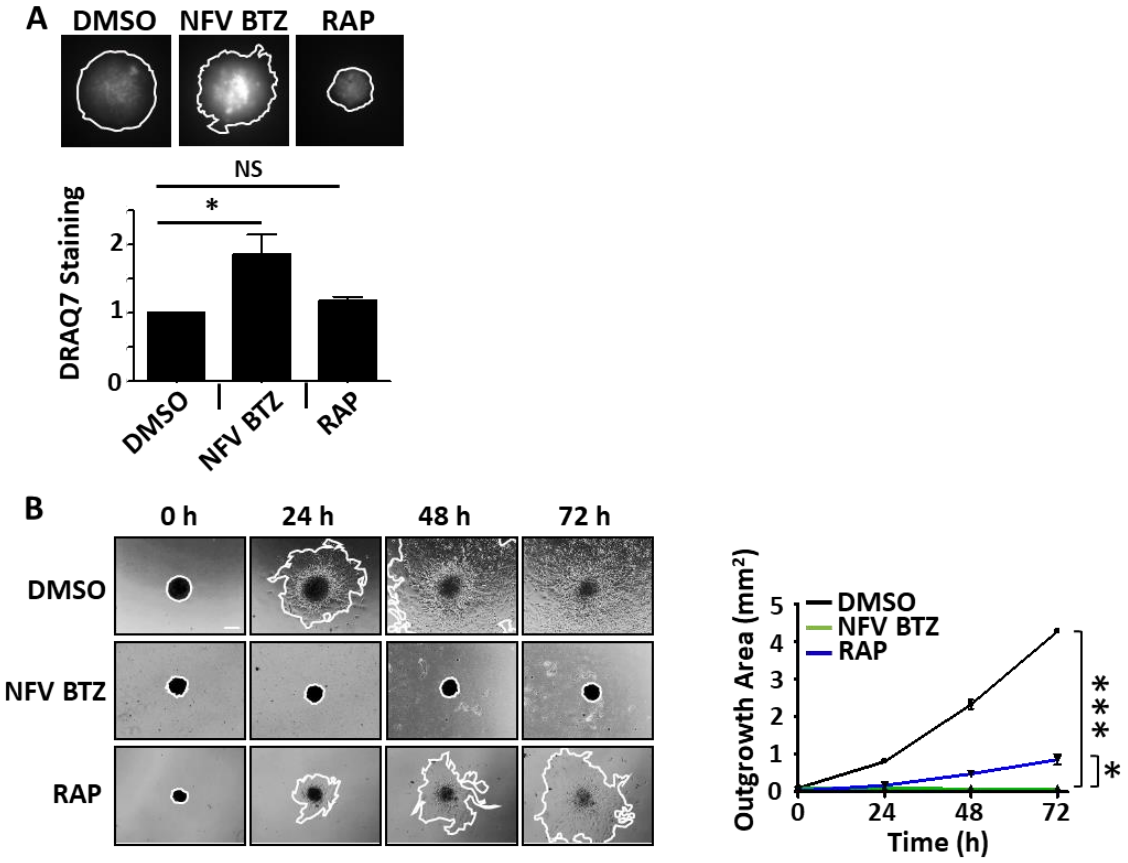

Figure 4.2: Bortezomib caused cell death in established tumour spheroids and prevented outgrowth. (A) *Tsc2*-/- MEF spheroids were treated with DMSO vehicle control, 20 μM nelfinavir combined with 20 nM Bortezomib (NFV BTZ), or 25 nM rapamycin (RAP), for 96 h. DRAQ7 was added for the final 48 h to monitor cell death before images were taken and quantified. Spheroid diameter was determined from phase contrast images after 96 h drug treatment and plotted against DRAQ7 staining intensity. Statistical significance (calculated by one-way ANOVA) shows significance between DMSO and BTZ/NFV treated spheroids in terms of fluorescence (n=3; mean +/- SEM). (B) Spheroids were re-plated onto standard tissue culture plates and grown under drug-free conditions. Images were taken every 24 h and the area of outgrowth calculated using Image J (n=3). Scale bar is 200 μm and outgrowth areas are graphed. Work done in this figure was in collaboration with Dr. Elaine Dunlop (generated graphs) and Dr. Sara Seifan (assisted in taking images for outgrowth assay). Henry McCann generated images for (A) and (B). Statistical significance (calculated by one-way ANOVA) shows significance in outgrowth rate between DMSO and BTZ/NFV treated spheroids and between DMSO and RAP treated spheroids.

4.2.3 Bortezomib/nelfinavir combination induced enhanced and prolonged ER stress in *Tsc2-/-* cells via the PERK pathway.

To determine the effects the combined Bortezomib/nelfinavir treatment would have on the ER stress pathway, western blots were performed on *Tsc2*+/+ and *Tsc2*-/- MEFs treated for 6 h with drug treatment. Thapsigargin was used as positive control.

In the *Tsc2*-/- samples, there were high levels of expression for several components of the PERK pathway such as GADD34, CHOP and ATF4 when cells where treated with single agents; nelfinavir, Bortezomib and MG132 and with thapsigargin. Expression levels were also shown to be higher in the presence of either Bortezomib/nelfinavir or MG132/nelfinavir combination when compared to single agents or control. Results showed that there was an increased expression of ATF4 in MG132/nelfinavir treated *Tsc2*+/+ MEFs compared to Bortezomib/nelfinavir treatment while Bortezomib/nelfinavir treated cells had higher expression of CHOP compared to MG132/nelfinavir treatment in both cell lines. Ubiquitin blots show accumulation of ubiquitin in any cells treated with Bortezomib, MG132 or their respective combination showing an inhibition of the proteasome. Blots show that accumulation of ubiquitin is higher in single agent treated cells compared to combination treated cells. Results also confirmed that *Tsc2*-/- MEFs had no TSC2 expression (Figure 4.3A).

To determine how long this enhanced ER stress persisted, western blots were carried out on *Tsc2*+/+ and *Tsc2*-/- MEFs treated for either 6, 16 or 24 h with Bortezomib/nelfinavir combination or DMSO. In *Tsc2*+/+ MEFs treated with the combination, there was an increased expression of CHOP and ATF4 at the 6 h time point, but this steadily decreased at 18 and 24 h (although there a tiny increase in CHOP at the 24 h time point). However, *Tsc2*-/- MEFs showed high expression levels of ATF4 and CHOP (higher than those observed in the wildtype samples) at the 6 h time point. At the 16 h time point, expression of both proteins plummeted before rebounding at the 24 h time point (compared to the *Tsc2*+/+ MEFs) (Figure 4.3B).

To confirm that ER stress was occurring, an investigation into XBP1 splicing (an event which only occurs in an ER stress environment due to activation of IRE1α) was carried out. Cells were treated for 6 h with drug, using thapsigargin as a positive control, before mRNA was extracted and converted to cDNA. Results were then processed by PCR and analysed on an agarose gel. Results showed that splicing occurs at a higher level in *Tsc2*-/- MEFs compared to *Tsc2*+/+ MEFs. With *Tsc2*-/- cells, splicing occurred in samples treated with the combined Bortezomib/nelfinavir treatment at a much higher rate compared to Bortezomib and DMSO although splicing levels were almost identical to those seen in thapsigargin and nelfinavir treated cells (Figure 4.3C).

To determine the effect of inhibiting the PERK pathway would have on the Bortezomib and nelfinavir treated cells, *Tsc2*-/- MEFs were pre-treated for 30 min with 2 μM GSK2606414 (a PERK inhibitor), before being treated with Bortezomib/nelfinavir for 24 h. Flow cytometry was then carried out on samples. Results showed that not only did GSK2606414 fail to rescue cells, but instead enhanced cell death, 55.43% +/- 4.30 SD when treated with just combination vs 82.4 3% +/- 6.00 SD when GSK2606414 was included (Figure 4.3E).

Elevation of protein synthesis by mTORC1 hyper-activation is likely to drive ER stress in TSC2 deficient cells but has not been examined to date. To determine the effects of the Bortezomib/nelfinavir combination on *de novo* protein synthesis, cells were treated in methionine-free media with treatment for 6 h before being labelled with 12.5 mCi/ml 35S-methionine for 20 min prior to harvesting in extraction buffer. Samples were then quantified using Bradford assay and results were reported in terms % positive control. Results showed the *Tsc2*-/- MEFs naturally have a much higher level of protein synthesis compared to *Tsc2*+/+ MEFs (346.2 % +/- 56.78 % vs 100 % +/- 0.0007 %). In terms of combination, there was a significant drop in protein synthesis in both cell lines with regards to their respective controls (24.7% +/- 14.74% in *Tsc2*+/+ MEFs vs 61.8% +/- 28.11% in *Tsc2*-/- MEFs) (Figure 4.3D).

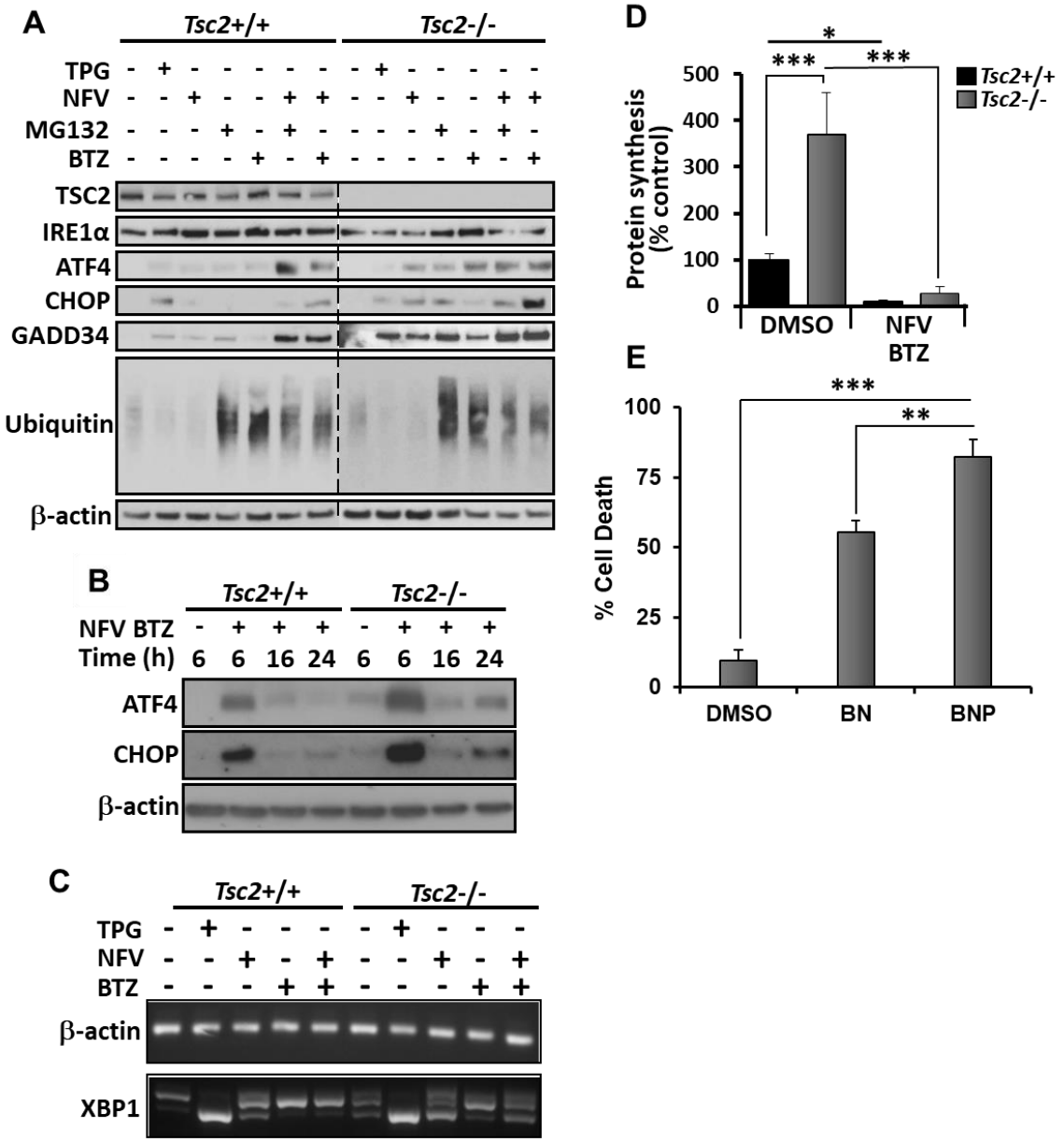

Figure 4.3: Bortezomib/nelfinavir combination affected ER stress and protein synthesis. (A) *Tsc2*+/+ and *Tsc2*-/- MEFs were treated with either DMSO, 1 μM thapsigargin (TPG), 50 nM Bortezomib (BTZ), 1 μM MG132, 20 μM nelfinavir (NFV), Bortezomib and nelfinavir combination (BTZ/NFV) or MG132 and nelfinavir combination (MG132/NFV) for 6 h, where indicated. Total protein levels of TSC2, IRE1α, ATF4, CHOP, GADD34, Ubiquitin and β-actin were detected by Western blot. Work was carried out by Dr. Charlotte Johnson. (B) *Tsc2*+/+ and *Tsc2*-/- MEFs were treated with DMSO or BTZ/NFV combination for 6 h, 16 h and 24 h. Total protein levels of ATF4, CHOP and β-actin were determined by Western blot (C) XBP1 mRNA splicing was determined from the same treatments as described in (A) (except for MG132 and MG132/NFV). PCR products were resolved on agarose gels (unspliced = 480 bp upper band, spliced = 454 bp lower band). Work was done with the assistance of Dr. Elaine Dunlop. (D) Levels of protein synthesis were determined for both DMSO control cells and BTZ/NFV treated cells after 6 h treatment using 12.5 mCi/ml 35S-methionine and quantified using Bradford assay. Work was done with the assistance of Dr. Andrew Tee (E) Effects of inhibiting ER stress while cells were treated with BTZ/NFV combination were determined by treating *Tsc2*-/- MEFs with DMSO, BTZ/NFV combination or BTZ/NFV combination with 2 μM

GSK2606414 (PERK inhibitor) (BNP) (n=3; mean +/- SD). Cell death determined by flow cytometry and DRAQ7 staining. Statistical significance (calculated one-way ANOVA) was shown between *Tsc2*+/+ and *Tsc2*-/- MEFs in terms of protein synthesis and between MEFs treated with DMSO and BTZ/NFV (n=3; mean +/- SD). Statistical significance was also shown (by one-way ANOVA) between Tsc2-/- MEFs treated with BTZ/NFV and BNP. All Blots in figure 4.3 are representative of n=3 runs

4.2.4 Bortezomib/nelfinavir combination did not affect energy stress levels

To determine if the Bortezomib/nelfinavir combination affected energy levels within treated cells, *Tsc2*-/- MEFs were treated with DMSO, combination or combination with methyl pyruvate for 24 h. Cells were then tested for cell death using flow cytometry and DRAQ7 staining. Results showed that the introduction of methyl pyruvate was not able to rescue the treated cells from death, but instead caused a slight increase in the amount of cell death (73.77% +/- 18.16 SD in combination treated MEFs vs 78.13% +/- 9.35 SD in combination plus methyl pyruvate treated MEFs). Western blot was carried out to show that methyl pyruvate was effectively restoring energy stress (e.g., was sufficient to reduce phosphorylation of AMPK and ACC). Blots confirmed that methyl pyruvate was functioning accordingly (Figure 4.4A).

4.2.5 Nelfinavir and Bortezomib/nelfinavir combination blocked P-glycoprotein activity in *Tsc2*+/+ and *Tsc2*-/- MEFS.

Bortezomib is a substrate of P-glycoprotein and it has been shown that P-glycoprotein expression causes resistance in cells treated with Bortezomib (O'Connor *et al.* 2013). To determine the effects that the Bortezomib/nelfinavir combination could have on P-glycoprotein activity, both *Tsc2*+/+ and *Tsc2*-/- MEFs were treated with either the Bortezomib/nelfinavir combination or control, with all treatments containing 5.25 µM of Rhodamine 123 (which is a substrate of P-glycoprotein) for 30 min at 37^{o}C. Samples were then lysed in warmed deionised water and fluorescence reading was taken. Results were recorded as a % of DMSO treated control. Data confirmed that Bortezomib failed to inhibit P-glycoprotein (as seen in the small increase in rhodamine 123 uptake) (115.19% +/- 2.82 SEM in *Tsc2*+/+ MEFs vs 105.59% +/- 7.61 SEM in Tsc2-/- MEFs). In *Tsc2-/-* MEFs treatment with nelfinavir, there was a slight increase in Rhodamine 123 uptake (127.47% +/- 7.42 SEM) indicating a minor decrease in p-glycoprotein activity (as a higher uptake of Rhodamine 123 indicates decreased p-glycoprotein function). In

Tsc2+/+ MEFs, on the other hand, nelfinavir caused a large inhibition of activity (i.e., a large uptake of rhodamine 123) in *Tsc2*+/+ MEFs (166.80% +/- 7.16 SEM) The combination of Bortezomib and nelfinavir surprisingly caused moderately high levels of activity inhibition (large increase in Rhodamine 123 uptake) in both cell lines (153.18% +/- 14.00 SEM in *Tsc2*+/+ MEFs compared to 148.71% +/- 3.74 SEM in *Tsc2*-/- MEFs) (Figure 4.4B).

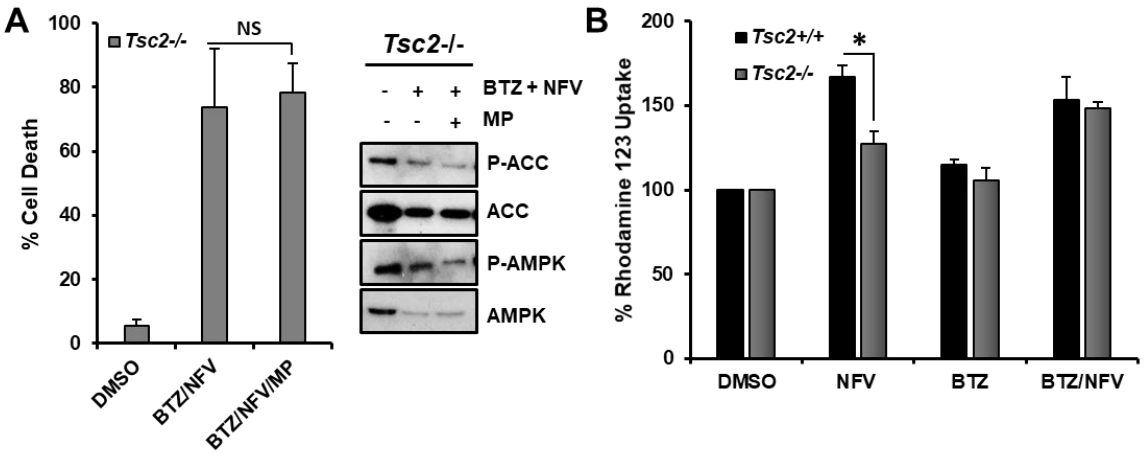

Figure 4.4: The effects of Bortezomib/nelfinavir combination of energy stress and P-glycoprotein inhibition. (A) *Tsc2−/−* cells were treated with DMSO, 50 nM Bortezomib and 20 μM nelfinavir combination (BTZ/NFV) or BTZ/NFV combination with the addition of 8 mM methyl pyruvate (BTZ/NFV/MP) for 24 h. Cells were then stained with DRAQ7 and % cell death determined by flow cytometry (n=3; mean +/- SD). Total protein levels and phosphorylation of ACC and AMPK was determined by western blot. (B) *Tsc2*+/+ and *Tsc2*-/- MEFs were treated with DMSO, 50 nM Bortezomib, 20 μM nelfinavir or a combination of BTZ/NFV (all containing 5.25 μM Rhodamine 123) for 30 min at 37ºC before being lysed in warmed deionised water. Fluorescence was analysed via plate reader at excitation at 480 nm and emission at 520 nm (n=3; mean +/- SEM). Statistical significance is shown between Nelfinavir treated *Tsc2*+/+ and *Tsc2*-/- MEFs. All Blots in figure 4.4 are representative of n=3 runs

4.3 Discussion:

The purpose of this chapter was to determine whether a combination of Bortezomib and nelfinavir could be used to selectively target *Tsc2*-deficient cells while being well tolerated by wildtype cells. Experimental data from flow cytometry showed that after just 24 h, the Bortezomib/nelfinavir combination caused selective cytotoxicity in *Tsc2*-/- MEFs. This contrasts with the control MEFs treated with the Bortezomib/nelfinavir combination that showed only a very minor increase in cell

death compared to cells treated with DMSO. A similar result was seen in cells treated with the MG132 and nelfinavir combination, however cell death was slightly higher in both cell lines after 24 h. As single agents, Bortezomib and MG132 were both able to cause selectivity in cell death in the *Tsc2*-deficent cells, although at a lower level compared to when both were combined with nelfinavir. This gives evidence that cells which are *Tsc2*-deficient cells are highly sensitive to inhibition of proteasome inhibition. The reason for this is likely due to hyperactivity of mTORC1, which suppresses autophagy and makes these cells more dependent on proteasomal activity (which mTORC1 hyperactivity enhances). The combinations of either Bortezomib or MG132 with nelfinavir were observed to trigger caspase and PARP cleavage, which is indicative that both Bortezomib/nelfinavir and MG132/nelfinavir combinations induced apoptosis. To confirm if caspase 8 cleavage is triggering cell death, further testing into caspase 8 activity should be done. An easy method of testing activity would be to treat cells with Z-IETD-FMK (a caspase 8 inhibitor) and investigate whether the introduction of Z-IETD-FMK is able to rescue cells treated with the bortezomib/nelfinavir combination.

During the tumour outgrowth experiment (i.e., 3D modelling), it was decided that Bortezomib should be reduced to 20 nM Bortezomib compared to the rest of this chapter. This was because when spheroids treated with 50 nM Bortezomib as a single agent failed to grow back after replating into fresh media (data not shown). This showed that established spheroids are incredible sensitive to Bortezomib as a single agent at 50 nM. It is worth mentioning that the reduction in the concentration of Bortezomib to 20 nM still killed the spheroids when combined with nelfinavir. This indicates that in the Bortezomib and nelfinavir combination, the concentration of Bortezomib used can be reduced without affecting the cytotoxic ability of the Bortezomib/nelfinavir combination. This evidence could be useful in future experiments as it could reduce the risk of adverse effects in in the clinic through using a reduced concentration of Bortezomib.

As seen with all the nelfinavir-based combinations used in this thesis, Bortezomib/nelfinavir and MG132/nelfinavir combinations showed high levels of expression of ER stress biomarkers such as ATF4, CHOP and GADD34 in the *Tsc2*-deficient cell lines. The time course experiments analysing ER stress components showed differences of ER stress induction and recovery between MEF cell lines. In the *Tsc2*+/+ MEFs, there was a high level of expression of ATF4 and CHOP at the expected 6 h time point after treatment with Bortezomib and nelfinavir before

steadily declining to normal levels at 16 and 24 h time points (although there was a tiny increase in CHOP expression at 24 h). On the other hand, in the treated *Tsc2*-/- MEFs, the expected expression levels of ATF4 and CHOP were observed at 6 h before declining at 16 h. However, expression levels rebound at 24 h, although at a lower level than at 6 h. The re-expression of ER stress markers, ATF4/CHOP, indicates that expression of these ER stress markers is biphasic, and that cell death in *Tsc2*-deficient cells can be influenced by the second spike of CHOP expression during the later time points. There appears to be no real difference in the level of XBP1 splicing between the *Tsc2*-/- MEFs treated with either nelfinavir or nelfinavir in combination with Bortezomib. This indicates that nelfinavir is solely responsible for inducing XBP-1 splicing.

In non-tumourgenic cells, down-regulated protein synthesis in an ER stressed environment is an efficient strategy that prevents the further build-up of unfolded protein within the ER. In *Tsc2*-deficient MEFS, there was elevated protein synthesis despite higher background levels of ER stress, with a 4-fold increase in protein synthesis in *Tsc2*-/- MEFs compared to wild-type controls. These elevated levels of protein synthesis would likely further promote ER stress within the *Tsc2*-deficient cells. As well as promoting translation, mTORC1 hyperactivation increased the activity of the proteasome while reducing autophagy. As discussed above, downregulation of autophagy means the proteasome becomes the principal mechanism to reduce ER stress via protein degradation in mTORC1-driven cells.

The introduction of the combined treatment of Bortezomib with nelfinavir to *Tsc2*+/+ and *Tsc2*-/- MEFs caused a dramatic reduction in the levels of protein synthesis. For instance, protein synthesis was nearly non-existent after 6 h of Bortezomib/nelfinavir treatment in both the *Tsc2*-/- and *Tsc2*+/+ MEFs. The introduction of the PERK inhibitor, GSK2606414 was shown to cause a large increase in cell death in the *Tsc2*-/- MEFs after 24 h of treatment with both nelfinavir and Bortezomib. This gives evidence that the induction of ER stress via PERK was required for cell survival during treatment with ER stress inducers. By blocking PERK pathway activation, it is possible that *Tsc2*-/- MEFs were unable to tolerate higher levels of ER stress. This piece of evidence could be useful for the development of future combinations for mTORC1 hyperactive cells.

The work in this chapter demonstrated for the first time that functional loss of TSC2 and subsequent mTORC1 hyperactivation sensitised cells to combined

proteasomal inhibition and ER stress induction. These findings have clinical relevance in stratified medicine, where cancers with a compromised signal transduction through the PI3K-AKT-mTORC1 pathway may be sensitised to nelfinavir and Bortezomib. This data implies that high ER stress burden along with hyperactive mTORC1 signalling could function as predictive biomarkers of drug efficacy when considering combined nelfinavir and Bortezomib treatment.

In conclusion, the combination of Bortezomib and nelfinavir was successfully able to selectively kill *Tsc2*-/- cells while being well tolerated by wildtype controls in an apoptotic manner caused by prolonged ER stress and proteasome inhibition.

Chapter 5: Drug screen identified a combination of cepharanthine and nelfinavir that selectively targeted Tsc2-/- cells.

5.1 Introduction:

5.1.1 Piperlongumine

Piperlongumine (also called piplartine) is an amide alkaloid which is a biologically and pharmacologically active constituent of the plant *Piper longum (*Long pepper) from South East Asia (Farooqi *et al.* 2018; Piska *et al.* 2018). Piperlongumine has become a compound of interest in the field of cancer research due to its ability to selectively kill a variety of cancer cell types via targeting the JAK-STAT, NF-κB and PI3K/AKT/mTOR pathways (Farooqi *et al.* 2018).

A combination of piperlongumine (5 mg/kg) and approved chemotherapeutic agent gemcitabine (25 mg/kg) was shown to cause cell death in pancreatic ductal adenocarcinoma (PDAC) cell lines, MIA PaCa-2 and PANC-1. Cell death was caused through a caspase-dependent mechanism via increased ROS levels and caused cell cycle arrest in the G0/G1 phase of the cell cycle (Mohammad *et al.* 2018). A similar result was demonstrated when piperlongumine (up to 8 μM) was combined with cotylenin A (a plant growth regulator – 15 μg/ml) although in this combination, elevated levels of ROS production caused cell death via ferroptosis (programmed cell death dependent on iron and characterized by the accumulation of lipid peroxides) (Yamaguchi *et al.* 2018).

Piperlongumine (up to 5 μM) has also been proven to cause cell death in several other cancer cell lines. For instance, piperlongumine was shown to be able to target the cancer stem cell population in oral cancer cell line models (SAS and CGHNC8) via gene-expression of stemness-related transcription factors, SRY-Box 2, POU class 5 homeobox 1, and Nanog homeobox (Chen *et al.* 2018). A combination of piperlongumine (10 μM), and the p53-reactivator, APR246 (25 μM), demonstrated selective induction of apoptosis and autophagic cell death in a head and neck squamous cell carcinoma (HNSCC) cell line (UMSCC10A) via ROS production and suppression of glutathione (GSH) S-transferase pi 1 (GSTP1, a GST

family member that catalyses the conjugation of GSH with electrophilic compounds to fulfil its detoxification function) (Li *et al*. 2018a).

Piperlongumine has also been shown to have antiproliferative properties in the lung cancer cell line A549 via increased ROS production, decreased expression of cyclin D1, CDK4, CDK6 and p-Rb (retinoblastoma), suppressed phosphorylation of AKT (but increased ERK1/2 phosphorylation) and significantly decreased nuclear translocation of NF-κB p65 in cells when treated with 40 μM of piperlongumine (Seok *et al.* 2018). It was observed that piperlongumine inhibited cell growth and induced apoptosis via ROS mediated mitochondrial disruption and interference of the JNK pathway in the melanoma cell line A375 (Xiong *et al*. 2018). Furthermore, a study showed that piperlongumine nanoparticles had anticancer activity *in vitro* against colorectal cancer cell lines, A549 and CT26 cells, and anti-metastatic activity in an *in vivo* CT26 cell pulmonary metastasis mouse model (Cha *et al*. 2018).

5.1.2 Chelerythrine Chloride

Chelerythrine is a natural benzo[c]phenanthridine alkaloid and is extracted from plant species, such as *Chelidonium majus, Macleaya cordata,* and *Sanguinaria Canadensis*. Chelerythrine was originally identified as an inhibitor of protein kinase C (PKC) 9 and the Bcl-2 family proteins (Wu *et al*. 2018a). However, it is now known that chelerythrine has multiple drug targets/mechanisms depending on the cancer cell line being used. In NSCLC cell lines, chelerythrine (up to 20 μM) was shown to cause a decrease in cell viability and colony formation, and induced apoptosis in a concentration-dependent manner in A549 and NCI-H1299 cells via increased ROS production (Tang *et al.* 2018). Chelerythrine was observed to induce distinctive autophagy in both cell lines (accompanied autophagy in the A549 cells and pro-death autophagy in the NCI-H1299 cells). Another study demonstrated that a combination of chelerythrine with Erlotinib (an EGFR tyrosine kinase inhibitor) in SK-MES-1, A549, HCC827, SK-MES-1 and A549 cells had additive effects (He *et al.* 2017).This combination of chelerythrine (5 μM) with Erlotinib (5 μM) was able to decrease cell viability, clonogenicity, migratory and invasive capabilities and induce apoptosis via effectively blocking EGFR signalling through decreased protein phosphorylation of downstream targets such as STAT3, ERK1/2, p38 MAPK and Bad.

More recently it was showed that chelerythrine (5 μM) selectively inhibited the growth of triple-negative breast cancer (TNBC) cell lines compared to non-TNBC cell lines and was able to induce apoptosis in these cell lines via inhibition of Protein Kinase N2 (PKN2 – a PKC subtype). It was also shown that chelerythrine synergistically targeted TNBC cell lines when combined with the chemotherapy reagent, taxol (Lin *et al.* 2017). In MCF7 cells, chelerythrine (10 μM) was found to down regulate the gene-expression of *VEGFA*, *BCL2* and *KRAS* (genes involved in evasion, angiogenesis and self-sufficiency of cancer cells) via binding to *in cellulo* quadruplex motifs found at the promoter regions of these oncogenes (Kundu *et al*. 2017).

Chelerythrine has also been able to target several other cancer cell lines. For instance, it was demonstrated that chelerythrine (up to 10 μM) suppressed the growth of renal cancer cell lines, HEK-293 and SW-839, in a time- and dose-dependent manner and was able to induce apoptosis in these cell lines via significantly decreasing phosphorylation of extracellular signal-regulated kinase (ERK) and AKT, upregulation of p53, B-cell lymphoma 2 (Bcl-2)-associated X protein (Bax), cleaved caspase-3 and cleaved poly (adenosine diphosphate-ribose) polymerase (PARP), and downregulation of Bcl-2, caspase-3 and PARP (Chen *et al.* 2016). A recent study described that chelerythrine could change the cell cytoskeletal structure of hepatocellular carcinoma cancer (HCC) cell line Hep3B, by reducing the expression of p-FAK (focal adhesion kinase), as well as inhibiting metastasis by downregulating the expression of MMP-2/9 (matrix metalloproteinase) mainly through the PI3K/AKT/mTOR signalling pathway (Zhu *et al*. 2017b). It was found in prostate cancer that chelerythrine (10 μM) caused an increased accumulation of ROS, leading to a rise in ER stress and apoptosis (Wu *et al*. 2018a). An unbiased drug screen in *TSC2*-null patient-derived cells that examined the loss of cell viability was carried out and identified chelerythrine (Medvetz *et al.* 2015). In this study, chelerythrine (2 μM) was found to induce ROS and to deplete GSH selectively in TSC2-null cells, resulting in selectively induced necroptosis.

5.1.3 BPTES

Bis-2-(5-phenylacetamido-1,3,4-thiadiazol-2-yl)ethyl sulphide (BPTES) is an allosteric glutaminase (GLS) inhibitor (Xiang *et al.* 2015) which binds to the loop

segment of the protein that regulates access of glutamine to the active site and to the dimer:dimer interface that participates in the phosphate-dependent oligomerization and activation of the enzyme (McDonald *et al*. 2014). BPTES has been used to target several cancer cell types. BPTES was able to induce cell cycle arrest by reducing glutamate leading to a significant reduction in ATP levels (although levels of ROS or GSH were not affected by the treatment) in NSCLC cell lines (Lee *et al.* 2016). It was also showed that when BPTES (10 μM) is combined with 5-fluorouracil (5-FU – a thymidylate synthase inhibitor) (5-10 μM), it caused synergistic cell death via cell cycle arrest in NSCLC cell lines. BPTES was also used by Ulanet *et al.* (2014) to identify NSCLC cell lines which are GLS dependent and had express markers characteristic of a mesenchymal phenotype (low E-cadherin and high vimentin expression). They are also showed that if lung cancer cells were induced (using TGF-β) to undergo epithelial to mesenchymal transition (EMT), it would cause cells to become more sensitive to BPTES and was associated with impaired mitochondrial respiratory capacity and increased sensitivity to oxidative stress.

Encapsulated BPTES in nanoparticles with dense poly (ethylene glycol) (PEG) surface coatings provided an effective method of delivering BPTES to pancreatic tumours while minimizing toxicity to cycling pancreatic cells (Zimmermann *et al*. 2016). However, this failed to target noncycling hypoxic pancreatic cells. To counter this, the encapsulated BPTES was combined with metformin. GLS inhibition in PDAC MiaPaCa2 cells induced by BPTES (500 nM) sensitized the cells to ß-lapachone (an NADPH:quinone oxidoreductase). This results in NADPH depletion via high levels of ROS production and caused nicotinamide adenine dinucleotide (NAD)+ depletion through PARP hyperactivation. This completely overwhelmed the ability of the DNA repair machinery to repair ß-lap-induced DNA lesions (Luo *et al*. 2015).

BPTES induced metabolism changes in the breast cancer cell lines MCF7 (an oestrogen receptor dependent cell line) and MDA-MB231 (a triple negative cell line) compared to non-cancerous MCF10A cells in glutamine metabolism, glycolysis, TCA cycle and amino acids pathways. The metabolic response, however, was distinctly different in both cancer cell types (Nagana Gowda *et al.* 2018). This is probably due to different genetic regulations such as preferences to estrogen receptor and dependence of glucose or glutamine for proliferation. A combination of BPTES with etoposide and cisplatin was tested on TNBC cell lines HCC1937 and

BT-549. Results showed that in HCC1937 cells, pre-treatment with BPTES (10 μM) caused an increase in the toxic effects of cisplatin and etoposide, as demonstrated by reduced proliferation, increased expression of apoptosis-related proteins (cleaved-PARP, cleaved-caspase 9, and cleaved-caspase 3) and a decreased ratio of Bcl-2/BAX. However, in BT-529 cells, enhanced cell death was only seen when cells were treated with a combination of BPTES and etoposide (Chen *et al.* 2016).

5.1.4 Paroxetine Hydrochloride Hemihydrate

Paroxetine (also known as Paxil and Seroxat) is an antidepressant that belongs to the selective serotonin reuptake inhibitor (SSRI) class. It is used to treat major depressive disorder, obsessive-compulsive disorder, social anxiety disorder, panic disorder, posttraumatic stress disorder, generalized anxiety disorder and premenstrual dysphoric disorder. It has been used in the treatment of menopausal hot flashes and night sweats. Paroxetine is also used for the treatment of depression and hot flashes in breast cancer patients and survivors (although it did not influence fatigue levels in patients/survivors) (Stearns *et al.* 2000; Pezzella *et al.* 2001; Morrow *et al.* 2003; Roscoe *et al.* 2005). It has also been shown to have cytotoxicity in several cancer cell lines.

Paroxetine (up to 50 μM) was able to induce apoptosis in oral cancer cell lines (OC2) in a Ca^{2+}-independent manner. Paroxetine was shown to induce an increase in cytosolic free Ca^{2+} concentrations by causing phospholipase C-independent Ca^{2+} release from the ER and Ca^{2+} influx via store operated Ca^{2+} channels in a manner regulated by protein kinase C and phospholipase A2 (Fang *et al.* 2011). In cultured human osteosarcoma cells (MG63), paroxetine was shown to reduce cell viability in a concentration- and time-dependent manner and was able to induce apoptosis via inducing p38 MAPK-associated caspase-3 activation (Chou *et al.* 2007). As seen by Fang *et al.* (2011), cell death was Ca^{2+}-independent but also induced an increase in cytosolic free Ca^{2+} concentrations via mobilization of intracellular Ca^{2+} stored in the ER and Ca^{2+} influx from an extracellular medium. Paroxetine also caused an increase in cytosolic free Ca^{2+} concentrations in treated PC3 human prostate cancer cells (Pan *et al.* 2009).

Paroxetine has been shown to reduce cell viability in colon carcinoma cells HT29 and has been shown to arrest HT29 and LS1034 cells at the G0/G1 stage of the cell cycle and stimulate DNA fragmentation in a dose-dependent manner. Cells

appear to die in an apoptotic manner as there is evidence of increased caspase-3 activation, increased c-Jun and decreased Bcl-2 expression (Arimochi and Morita 2006; Gil-Ad *et al.* 2008).

5.1.5 Trifluoperazine

Trifluoperazine (sold as Eskazinyl, Eskazine, and Jatroneura, etc.) is a calmodulin inhibitor and an antipsychotic drug used for the treatment of schizophrenia (Wang *et al.* 2018). Trifluoperazine has good bioavailability in brain and has shown an anticancer effect in several types of cancer (Feng *et al.* 2018). A library of 80 dopaminergic ligands were screened and it was demonstrated that trifluoperazine inhibited the growth and proliferation of glioblastoma cancer cells in a dose dependent manner (Pinheiro *et al.* 2018). Treatment with trifluoperazine (up to 10 μM) caused an increased accumulation of LC3B-II and p62, indicating a disruption of autophagy flux and impaired acidification of the lysosomes in glioblastoma cancer cells U251, U87 and P3 (Zhang *et al.* 2017). It was also shown that trifluoperazine had an additive effect when combined with radiation via down-regulation of cathepsin L. Trifluoperazine potently suppressed proliferation, motility, and invasion of glioblastoma cells *in vitro*, and tumour growth in *in vivo* xenograft mouse model (Kang *et al*. 2016). It was demonstrated that this was caused by massive and irreversible release of Ca^{2+} from intracellular stores by inositol 1,4,5-trisphosphate receptor (IP_3R) subtypes 1 and 2 by directly interacting at the TFP-binding site of a Ca^{2+}-binding protein, calmodulin subtype 2 (CaM2). However, it was also showed that trifluoperazine failed to improve the survival time in mice models of glioblastoma. However, analogs of trifluoperazine were able to reduce tumour size and increased the survival time in brain xenograft mouse model of glioblastoma via increased Ca^{2+} like trifluoperazine (Kang *et al.* 2018). In doxorubicin (DOX) resistant SHG44/DOX glioma cells, doxorubicin resistance was reduced by using trifluoperazine via inhibition of the nuclear exclusion of Forkhead box O1 (FOXO1) (a tumour suppressor) leading to a downregulation of MDR genes. This resulted in an increase in the intracellular concentration of doxorubicin which resulted in cytotoxicity, cell cycle arrest and early apoptosis (Chen *et al.* 2018).

Trifluoperazine caused an increase in the nuclear localization of FOXO1 in HCC lines SMMC-7721 and Bel-7402. Trifluoperazine was shown to inhibit the vitality of both cell lines and induce cell cycle arrest at G0/G1, while *in vivo* restricted

angiogenesis and tumour growth with a reduced expression of VEGF, Bcl-2, and PCNA (Cai *et al*. 2017). In TNBC cell lines, MDA-MB-468, MDA-MB-231, and 4T1, trifluoperazine (up to 20 μM) induced G0/G1 cell cycle arrest via decreasing the expression of both cyclin D1/CDK4 and cyclin E/CDK2, and stimulated mitochondria-mediated apoptosis. Trifluoperazine suppressed the growth of subcutaneous xenograft tumour and brain metastasis *in vivo* and prolonged the survival of mice bearing brain metastasis (Feng *et al.* 2018). A combination of trifluoperazine (TFP) with gemcitabine (GEM), and paclitaxel (PTX) was tested for the treatment of pancreatic cancer cells. The TFP-GEM-PTX combination was shown to be slightly synergistic and when each drug was used at it IC_{60}, it was shown to be optimal in inhibiting PDAC PANC-1 cells (Molins and Jusko 2018). Trifluoperazine was able to inhibit the formation of cancer stem cells (CSC) and down regulated the expression of CSC markers, CD44/CD133. It was also shown that trifluoperazine inhibited Wnt/β-catenin signalling in gefitinib-resistant lung cancer spheroids. When trifluoperazine (0.5-5 μM) and gefitinib (2.5-10 μM) were combined, they were able to overcome drug resistance in lung CSCs and enhanced the inhibitory activity of gefitinib in lung cancer metastatic and orthotopic CSC animal models (Yeh *et al.* 2012).

5.1.6 17-AAG

17-allylamino,17-demethoxygeldanamycin (17AAG) was the first inhibitor of heat shock protein 90 (Hsp90) to enter a phase I clinical trial in cancer. Colorectal (CRC) carcinoma cell lines HT29, HCT116, HCT15 and KM12 treated with 17AAG had depletion of c-raf-1 and AKT and inhibition of signal transduction and caused down regulation of hsp70, hsp90β, keratin 8, keratin 18 and caveolin-1 although expression of Hsp90 client protein genes was not affected (Workman *et al*. 2002). 17AAG was demonstrated to synergise well in a combination with either capecitabine and Irinotecan to cause cytotoxicity in HT29 cells. The combination of all three drugs was shown to down-regulate matrix metalloproteinase-9 (MMP-9) and vascular endothelial growth factor (VEGF) mRNA levels, have anti-metastatic properties, and caused elevated lipid peroxidation and reduced total antioxidant capacity in HT-29 cells (Zeynali-Moghaddam *et al*. 2019). A triple combination of 17AAG (IC_{50} = 62 nM in HT29 cells and 14.4 nM in HCT116 cells), capecitabine (IC_{50} = 3.27 μM in HT29 cells and 1.63 μM in HCT116 cells) and oxaliplatin (IC_{50} = 4.60 μM in HT29 cells and 1.74 μM in HCT116 cells) showed that while a double

combination of 17AAG with either capecitabine or oxaliplatin showed synergy in HT29 and HCT116 cells, but when all three drugs were used in combination, synergy only occurred in HCT116 cells (Mohammadian *et al.* 2017).

17AAG sensitizes NSCLC cells expressing high levels of p185 to paclitaxel-mediated growth arrest and apoptosis via depletion of p185. In cells with low levels of p185, the combination had only an additive effect (Nguyen *et al.* 1999). 17-AAG enhanced cytotoxicity and cell growth inhibition of etoposide in NSCLC cell lines H1703 and H520, which were associated with the downregulation of XPC expression and inactivation of AKT (Chen *et al.* 2018).

17AAG was shown to be able to inhibit the hypoxic induction of the HIF-1 target genes in malignant plasma cells (Kocemba-Pilarczyk *et al.* 2018). Using solid lipid nanoparticles to carry a combination of 17AAG and paclitaxel to target gastric cancer cells, the encapsulated combination was shown to reduce cell viability and colony formation in cell line MKN45 and induced apoptosis, inhibited growth of xenograft and influenced the protein levels of Hsp90, MnSOD, Cleaved caspase 3 and Cleaved PARP (Ma *et al.* 2018). In HNCC lines, HN30 and HN6, the expression of PTEN and p53 proteins were suppressed and AKT and Mdm2 expression was reduced by the presence of 17AAG (2 μmol/L) (Pontes *et al.* 2018).

5.1.7 Etoposide

Etoposide (VP-16–213, epipodophyllotoxin, 4′-demethyl-9-[4,6–0-ethylidene-D-glucopyranoside]) is a topoisomerase II inhibitor, which was approved by the FDA in 1983 after demonstrating antineoplastic activity in AML, Hodgkin's lymphoma, non-Hodgkin's lymphoma, lung cancer (both small cell and non-small cell), gastric cancer, breast cancer and ovarian cancer (Hande 1998). Kaufmann (1989) showed that exposing human HL-60 or KG1A leukaemia cells to 17 μM etoposide for 45 min was able to cause DNA degradation 4 h later. Etoposide (up to 3 μM) was also shown to be able to inhibit MYB – a transcription factor which plays key roles in hematopoietic cells and has been implicated in the development of leukemic HL60 cells, although it did require a 10x fold higher concentration to achieve this compared to teniposide usage (Yusenko *et al.* 2018). A combination of azacytidine, etoposide, and cytarabine was shown to generate an increased response and prolonged survival rates in patients with poorly prognosed AML (Onec *et al.* 2018). A combination of lomustine, cytarabine, cyclophosphamide and etoposide was

shown to be an effective and well-tolerated conditioning regimen prior to hematopoietic stem cell transplant (HSCT) in patients with primary refractory or relapsed lymphoma (Gokarn *et al*. 2018). A combination of bendamustine, etoposide, and dexamethasone was shown to be able to mobilize peripheral blood hematopoietic stem cells for autologous transplantation in non-Hodgkin lymphoma (Press *et al*. 2018).

Etoposide has become one of the most commonly used cancer drugs. Using 6 cycles of cisplatin combined with etoposide (60 mg/m^2 etoposide on days 1–3 and 50 mg/m^2 cisplatin on day 1 at 21-day intervals), a complete response was achieved in a patient with small cell neuroendocrine carcinoma at the primary lesion and at the cervical lymph node metastases (Wang *et al.* 2018). A patient with large cell neuroendocrine carcinoma was successfully treated with a cisplatin/etoposide combination (four cycles of cisplatin (80 mg/m^2, on day 1) and etoposide (100 mg/m^2, on days 1, 2, and 3)) as well (Hidaka *et al*. 2018).

Gestational trophoblastic neoplasia (GTN) is a highly chemosensitive and curable gynaecologic malignancy. Aminimoghaddam *et al.* (2018) used a combination regimen of etoposide, methotrexate, actinomycin-D/etoposide, and cisplatin (EMA/EP) to cause a complete remission in 88% of patients treated for high risk GTN. In low-risk GTN, Kanno *et al.* (2018) showed that primary remission rates and drug resistant rates of 5-day etoposide treatment (drip infusion) were significantly higher and significantly lower than those of 5-day intramuscular methotrexate treatment.

A complete response was achieved in a patient with metastatic oesophageal carcinosarcoma comprising of neuroendocrine carcinoma, squamous cell carcinoma, and sarcoma after 4 cycles of a etoposide/cisplatin combination (cisplatin at 60 mg/m^2 on day 1 and etoposide at 100 mg/m^2 on days 1–3) (Tsuchihashi *et al*. 2018). Unfortunately, in this case, the patient's tumour reoccurred 5.5 months after the final course of treatment. The addition of atezolizumab (a humanized monoclonal anti–programmed death ligand 1 (PD-L1) antibody) to a chemotherapeutic combination of carboplatin and etoposide as a first-line treatment for extensive-stage small-cell lung cancer was shown to induce significantly longer overall survival and progression-free survival than treatment with carboplatin/etoposide combination alone (Lin *et al*. 2018). An elderly patient with Langerhans's cell sarcoma was successfully treated using a combination of

etoposide, prednisone, vincristine, cyclophosphamide, and doxorubicin (Matsukawa *et al.* 2018).

5.1.8 Doxorubicin

Doxorubicin (also called Adriamycin) is a cytotoxic anthracycline antibiotic obtained from *Streptomyces peucetius var caesius* used for the treatment of several forms of cancer. It is believed to act as a topoisomerase I inhibitor and intercalates between adjacent base pairs of the double helix of DNA thus impairing the synthesis of DNA, RNA, and proteins. In fourteen randomised trials that used pegylated liposomal doxorubicin (PLD – a liposome-encapsulated formulation of doxorubicin) on ovarian cancer cell lines, it was shown that there were no overall survival rate differences between PLD-based treatment and other regimens. However, there was a significant progression free survival benefit of a PLD-based schedule observed, particularly in second-line and in platinum-sensitive subgroups (Staropoli *et al.* 2014). Similar results were observed when PLD was combined with carboplatin and compared to the combination of carboplatin and paclitaxel (La-Beck *et al*. 2013). However, both combinations have different side effect profiles as PLD/carboplatin had more gastrointestinal toxicity, anaemia, thrombocytopenia, cutaneous toxicity, and mucositis/stomatitis, but less neutropenia, neuropathy, and alopecia when the combination was compared to carboplatin and paclitaxel. A phase II trial which involved a combination of PLD (30 mg/m^2 on day 3) and irinotecan (80 mg/m^2 on days 1 and 15) for the treatment of recurrent ovarian cancer was carried out by Shoji *et al.* (2014). Results showed that the combination was a useful treatment method with a high response rate and manageable adverse reactions. The use of pegylated liposomal doxorubicin hydrochloride (PLDH), topotecan, paclitaxel, trabectedin and gemcitabine in the treatment of advanced recurrent or refractory ovarian cancer was reviewed (Edwards *et al.* 2015). It was shown that there were significant benefits for PLDH plus platinum in terms of overall survival (OS) compared to platinum monotherapy. PLDH plus platinum significantly prolonged progression-free survival (PFS) compared to paclitaxel plus platinum. In terms of non-platinum-based treatments, PLDH monotherapy and trabectedin plus PLDH were found to significantly increase OS, but not PFS, compared to topotecan monotherapy. With regards to platinum-resistant/-refractory (PRR) disease, there was no significant differences for any treatment compared with alternative regimens in OS and PFS.

Doxorubicin is one of the most effective agents for both early and advanced breast cancer. A meta-analysis of ten randomised controlled trials for the use of liposomal doxorubicin in advanced breast cancer found that liposomal doxorubicin had a significant reduction in the risk of cardiotoxicity and significant improvement in the overall response rate compared with conventional doxorubicin (Xing *et al.* 2015). No significant difference between the two forms of doxorubicin was reported in terms of overall survival. Resveratrol was shown to reduce hypoxia-induced resistance to doxorubicin in MCF7 breast cancer cells via decreased CBR1 expression by decreasing HIF-1α protein expression (Mitani *et al.* 2014). In MCF7 cells with multidrug resistance, using mesoporous silica nanoparticles to encapsulated doxorubicin, it was able to overcome drug resistance and improve doxorubicin cytotoxicity in these cells (Wang *et al.* 2014). Combining short-time focused ultrasound (FUS) hyperthermia with PLD was shown to be able to significantly enhance the PLD delivery into brain metastases of breast cancer and effectively inhibit tumour growth compared with mono-treatments of either PLD or short-time FUS hyperthermia (Wu *et al.* 2014).

Loading doxorubicin into composite (polyethylene glycol-polycaprolactone/Pluronic P105) micelles (an aggregate of surfactant molecules dispersed in a liquid colloid) was shown to significantly enhance cellular doxorubicin accumulation and inhibit doxorubicin release (Xu *et al.* 2012). It was also showed that the micelles were able to radiosensitise lung cancer A549 multicellular spheroids and cause significantly reduced survival of cells treated by radiation and composite micelles compared with those treated with radiation and free doxorubicin or radiation alone. Introduction of 1-guanyl-1,7-diaminoheptane (GC7) sensitizes bladder cancer (BIU-87, J82, and UM-UC-3) cells to doxorubicin (up to 1 μg/ml) by preventing epithelial–mesenchymal transition through inhibition of eukaryotic translation initiation factor 5A2 activation (Liu *et al*. 2015d). Human atherosclerotic plaque-specific peptide-1 (AP1) conjugated to liposomal doxorubicin was observed to cause selective cell death in IL-4Rα-overexpressing murine CRC CT26 cells. It was also showed that there was significant inhibition of tumour growth and decreased cardiotoxicity of doxorubicin in mouse models treated with the conjugate when it is administered intravenously (Yang *et al.* 2015).

5.1.9 Luteolin

Luteolin (3′,4′,5,7-tetrahydroxyflavone) is a flavonoid identified in a variety of vegetables, including broccoli, green peppers and celery and has been shown to have *in vitro* and *in vivo* anti-cancer activity against various cancer cells (Feng *et al.* 2018; Han *et al.* 2018). Luteolin was observed to be able to selectively target hepatocellular carcinoma cell (HCC) line SK-Hep-1 cells compared to normal cells. Cell death was apoptotic with activation of caspase 8, −9 and −3 and cleavage of PARP was caused by inhibiting AKT phosphorylation (and disrupting the PI3K/AKT/mTOR pathway) (Im *et al.* 2018). A combination of luteolin (10 μM) with sorafenib (3 μM) (a small-molecule multi-kinase inhibitor) synergistically killed HCC cell lines Hep3B and SMMC-7721 via JNK-mediated apoptosis (Feng *et al.* 2018).

ProFine is a combination of luteolin, quercetin, and kaempferol formed into a composition (Mamouni *et al.* 2018). This combination was shown to synergistically cause cell death in prostate cancer cell line C4-2 in an apoptotic manner and cause suppression of androgen receptor expression and inhibit transcription of androgen-regulated genes. Luteolin was shown to be able to suppress the stemness of prostate cancer cells by Wnt singling pathway inhibition via upregulation of FZD6 (frizzled class receptor 6 - a negative regulator of β-catenin transcriptional activity) (Zhou *et al*. 2018).

Luteolin was observed to be able to obstruct metastasis through both direct and indirect mechanisms (Cook 2018). Luteolin can suppress breast cancer invasion by inhibiting VEGF production and its receptor's activity and can decrease epithelial–mesenchymal transition markers and metastatic proclivity. Luteolin was observed to be antiproliferative via suppressing receptor tyrosine-kinase (RTK) activity. In CRC cells, luteolin (up to 80 μM) suppressed cell proliferation and cellular transformation of HCT116 and HT29 cells in a dose-dependent manner via epigenetic modifications of the *nrf2* gene with subsequent induction of its downstream antioxidative stress pathway (Zuo *et al.* 2018). Luteolin (up to 100 μM) showed proapoptotic activity in pancreatic cancer cell line SW1990 by targeting the BCL-2. Luteolin was shown to displace BAX from the hydrophobic cleft of BCL-2, allowing mitochondrial permeabilization (Li *et al*. 2018b).

5.1.10 Trequinsin

Trequinsin is a phosphodiesterase III inhibitor which is used as a strong antihypertensive agent. A combination of trequinsin with epigallocatechin-3-O-gallate (EGCG - green tea polyphenol which is a substrate of 67-kDa laminin receptor (67LR)) was shown to be able to suppress cancer stem cell properties in PDACs via suppression of the FOXO3 and CD44 axis. *In vivo*, this combination suppressed PDAC tumour growth and metastasis (Kumazoe *et al.* 2017).

5.1.11 FLLL31

FLLL31 is a small molecule derived from curcumin (Holmer *et al.* 2015). This compound was designed to bind selectively to Janus kinase 2 (JAK2) and to the Src homology-2 domain of Signal Transducer and Activator of Transcription 3 (STAT3) (which serve crucial roles in STAT3 dimerization and signal transduction). FLLL31 (up to 10 μM) was shown to be able to inhibit STAT3 phosphorylation, DNA-binding activity, and transactivation *in vitro* which could impede multiple oncogenic processes and induced apoptosis in pancreatic and breast cancer cell lines (PANC-1 and MDA-MB-231 respectively) (Lin *et al* .2010). It was also shown that FLLL31 inhibited colony formation in soft agar and cell invasion. It was also shown to synergise well with doxorubicin against breast cancer cells. A combination of FLLL31 (5 μM) with Tumour Necrosis Factor-Related Apoptosis Inducing Ligand (TRAIL) (20ng/ml) synergised to cause apoptosis in pancreatic cancer cell lines (S2013 and S2VP10) by preventing down-regulation of DR5 (Majumder *et al.* 2016).

5.1.12 Hypothesis

This lab group has seen several successful combinations containing nelfinavir such as mefloquine (McCann *et al.* 2018), chloroquine (Johnson *et al*. 2015), bortezomib (Johnson *et al.* 2018) and salinomycin (Dunlop *et al*. 2017), which can selectively target mTORC1 hyperactive cell lines. The purpose of this chapter was to identify any potential combination with nelfinavir from the above drugs which can selectively target mTORC1 hyperactive cell lines. To do this, the drugs in question were tested through several layers on screening in order and the combinations with the strongest selectivity for *Tsc2*-/- MEFs underwent further testing.

5.2 Results:

5.2.1 Drug combinations tested showed selective inhibition of Tsc2-/- cells.

To determine if the drugs chosen for the screen can inhibit cell growth, drugs were divided into two panels with drugs at varying concentrations in combination with 20 μM nelfinavir and cells and treated for 48 h. Concentrations for the chosen drugs were selected based on a literature search of concentrations used for the treatment of cancer cell lines. To determine inhibition of cell proliferation, a CyQUANT assay was carried out. Results were calculated as a % of cell number which was normalised to 100% for DMSO treated cells.

The first panel consisted of piperlongumine, chelerythrine chloride, BPTES, paroxetine hydrochloride hemihydrate, cepharanthine and trifluoperazine (Figure 5.1A). Results from the panel are summarised in Table 5.1.

Table 3.1: Results from CyQUANT panel screen 1. Results for the first CyQUANT Panel which featured rapamycin (RAP) as a control, chelerythrine chloride (CC), piperlongumine (Pip), BPTES, paroxetine hydrochloride hemihydrate (Paro), and cepharanthine (Cep) in combination with nelfinavir (NFV)

	% of Control Cell Number			
	Tsc2+/+		*Tsc2-/-*	
Drug	**Average**	**SEM**	**Average**	**SEM**
DMSO	100.00	0.00	100.00	0.00
Rap 100nM	64.95	5.52	63.57	5.86
NFV 20µM	50.32	3.22	51.78	4.20
Pip 5µM/NFV 20µM	43.21	1.77	37.79	3.54
Pip 10µM/NFV 20µM	35.20	8.05	25.09	6.71
Pip 20µM/NFV 20µM	38.45	8.25	23.08	5.40
CC 5µM/NFV 20µM	17.77	5.66	8.74	2.45
CC 7.5µM/NFV 20µM	9.31	2.93	6.66	2.53
CC 10µM/NFV 20µM	12.86	4.31	11.27	1.93
BPTES 5µM/NFV 20µM	44.73	4.50	49.96	1.76
BPTES 10µM/NFV 20µM	41.22	6.04	48.09	3.58
BPTES 20µM/NFV 20µM	39.85	3.76	26.50	6.04
Paro 1.25µM/NFV 20µM	48.57	1.16	38.85	6.85
Paro 2.5µM/NFV 20µM	44.41	6.72	31.69	6.66
Paro 5µM/NFV 20µM	38.49	5.63	24.99	5.49
Tri 1.25µM/NFV 20µM	49.89	1.55	37.05	8.55
Tri 2.5µM/NFV 20µM	43.67	2.22	34.93	7.53
Tri 5µM/NFV 20µM	44.33	1.87	26.54	6.22
Cep 1.25µM/NFV 20µM	40.46	5.86	25.68	4.90
Cep 2.5µM/NFV 20µM	40.02	5.24	25.70	4.79
Cep 5µM/NFV 20µM	39.86	6.04	24.87	4.17

The second drug panel was made up of 17-AAG, etoposide, doxorubicin hydrochloride, luteolin, trequinsin and FLLL31 (Figure 5.1B). Results from this second panel are summarised in Table 5.2.

Table 5.2: Results from CyQUANT panel screen 2. Results for the first CyQUANT Panel which featured rapamycin (RAP) as a control, etoposide (ETO), doxorubicin hydrochloride (Dox), 17AAG, luteolin (Lut), trequinsin (Tre), and FLLL31 in combination with nelfinavir (NFV)

	% of Control Cell Number			
	Tsc2+/+		*Tsc2-/-*	
Drug	**Average**	**SEM**	**Average**	**SEM**
DMSO	100.00	0.00	100.00	0.00
Rap 100nM	81.67	3.02	73.42	3.87
NFV 20µM	64.19	8.56	62.06	2.42
Eto 25µM/NFV 20µM	47.96	5.61	52.26	2.71
Eto 50µM/NFV 20µM	55.16	7.50	46.23	1.86
Eto 100µM/NFV 20µM	59.00	2.74	54.93	4.45
Dox 12.5nM/NFV 20µM	62.78	5.56	54.99	2.23
Dox 25nM/NFV 20µM	54.16	3.74	53.67	3.42
Dox 50nM/NFV 20µM	48.61	5.47	48.53	5.99
17-AAG .5µM/NFV 20µM	57.39	7.48	48.34	3.88
17-AAG 1µM/NFV 20µM	54.57	8.05	48.17	2.71
17-AAG 2µM/NFV 20µM	52.81	8.48	45.04	2.65
Lut 5µM/NFV 20µM	33.36	2.80	49.36	2.56
Lut 10µM/NFV 20µM	27.92	4.92	46.86	0.43
Lut 20µM/NFV 20µM	41.41	5.49	43.74	2.13
Tre 10uM/NFV 20µM	44.42	5.02	51.98	3.81
Tre 20uM/NFV 20µM	38.60	3.15	46.34	5.01
Tre 40uM/NFV 20µM	34.79	3.47	29.68	7.91
FLLL31 1.25µM/NFV 20µM	33.16	2.25	35.38	6.76
FLLL31 2.5µM/NFV 20µM	27.54	2.15	24.91	3.39
FLLL31 5µM/NFV 20µM	25.45	6.45	15.05	0.53

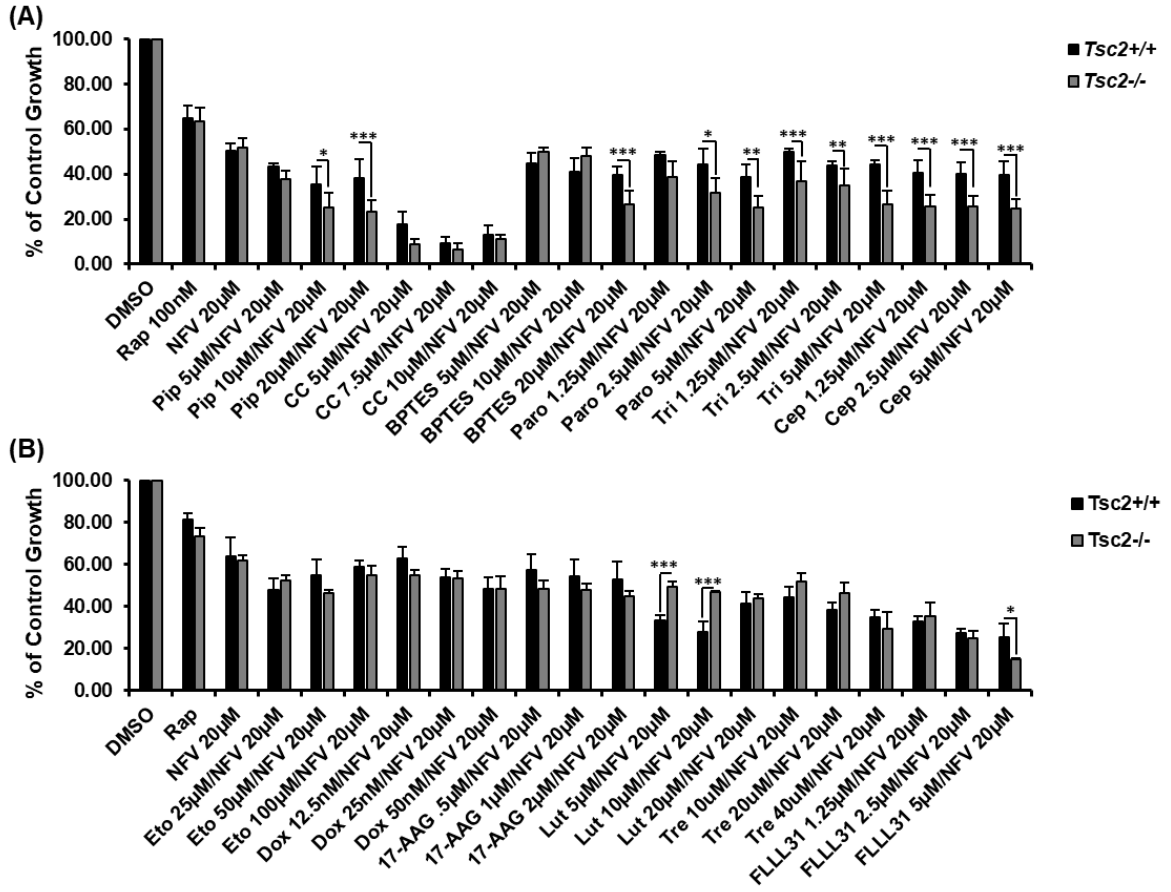

Figure 5.1: Drug screen to see the effects of drug combinations on cell proliferation. Tsc2+/+ and Tsc2-/- MEFs were treated with (A) 100 nM rapamycin (RAP), piperlongumine, chelerythrine chloride (CC), BPTES, paroxetine hydrochloride hemihydrate (Paro), cepharanthine (Cep) and trifluoperazine (Tri) (n=3; mean +/- SEM) (B) 17-AAG, etoposide (ETO), and doxorubicin hydrochloride (Dox), luteolin (Lut), trequinsin (Tre), and FLLL31 at various concentration combined with 20 μM nelfinavir (NFV) for 48 hours. Fluorescence was read on a plate reader with excitation at 480 nm and emission at 520 nm (n=3; mean +/- SEM). Results written as mean +/- SEM. Statistical significance is shown between treated *Tsc2*+/+ MEFs and *Tsc2*-/- MEFs.

5.2.2 A combination of cepharanthine and nelfinavir selectively killed Tsc2-/- cells.

To determine if the drug combinations tested have cytotoxicity capabilities, several drug combinations were selected from the CyQUANT screening carried out and tested at two concentrations representing the higher and lower ranges of therapeutic concentrations in combination with 20 μM nelfinavir (Figure 5.2). Reasons for the drugs and concentrations used will be discussed in the discussion section of this chapter.

Chelerythrine combinations showed slight cytotoxic selectivity for *Tsc2*-/- cells when compared to results seen in wildtype cells. However, at the higher concentration (5 µM) combination, both cell types suffered high toxicity; 74.36% +/- 16.08 SD vs 80.24% +/- 15.23 SD while at the 2.5 µM combination both cell types suffered minimal cell death compared to the control cells (8.07% +/- 0.81 SD in *Tsc2*+/+ MEFs vs 20.28% +/- 4.38 SD in *Tsc2*-/- MEFs) in combination treated cells compared to 4.94% +/- 2.02 (in *Tsc2*+/+ MEFs) vs 4.83% +/- 3.08 (in *Tsc2*-/- MEFs) in control cells.

Trifluoperazine combinations showed selective cytotoxicity for *Tsc2*-/- cells. However, the 10 µM trifluoperazine combination (representing the higher concentration range) wiped out both the *Tsc2*+/+ and *Tsc2*-/- MEFs (95.80% +/- 3.13 SD vs 96.92% +/- 2.31 SD). In the lower concentration range combination (2.5 µM trifluoperazine), selective cytotoxicity occurred in *Tsc2*-/- cells, however, cell death in both cell lines was quite poor (12.89% +/- 7.55 SD in *Tsc2*+/+ MEFs vs 20.37% +/- 7.07 SD in *Tsc2*-/- MEFs).

Combinations containing paroxetine showed higher cell death in *Tsc2*-/- cells compared to wildtype cells. The 5µM paroxetine combination showed much higher selective cell death compared to other high range concentrations used for other drugs tested; 21.70% +/- 1.85 SD in *Tsc2*+/+ MEFs vs 65.42% +/- 6.40 SD in *Tsc2*-/- MEFs. The 2.5 µM paroxetine combination showed similar results to other drug combinations used in a similar concentration and failed to show much cell death in either cell line; 13.43% +/- 1.77 SD in *Tsc2*+/+ MEFs vs 26.90% +/- 12.38 SD in *Tsc2*-/- MEFs.

Trequinsin-based combinations failed to show significant cell death at either range of concentrations used for this assay. The 10 µM trequinsin combination failed to cause high levels of cell death compared to the other drug combinations used at this range; 7.55% +/- 2.96 SD in *Tsc2*+/+ MEFs vs 19.20% +/- 5.08 SD in *Tsc2*-/- MEFs. The 2.5 µM combination showed similar results as seen with the lower range concentration of all previous drugs tested; 7.37% +/- 3.07 SD in *Tsc2*+/+ MEFs vs 15.78% +/- 3.56 SD in *Tsc2*-/- MEFs.

Cepharanthine containing combinations showed higher levels of selectivity compared to all other drug combinations tested for cytotoxicity. The higher range of 10 µM cepharanthine, showed similar levels of cell death as seen in the two cell lines; 84.28% +/- 2.28 SD in *Tsc2*+/+ MEFs vs 96.88% +/- 2.97 SD in *Tsc2*-/- MEFs.

However, in the 2.5 µM cepharanthine combination, results show the highest level of selectivity seen in this assay with 16.85% +/- 7.54 SD cell death reported in in *Tsc2*+/+ MEFs compared to 87.66% +/- 11.65 SD cell death seen in in *Tsc2*-/- MEFs.

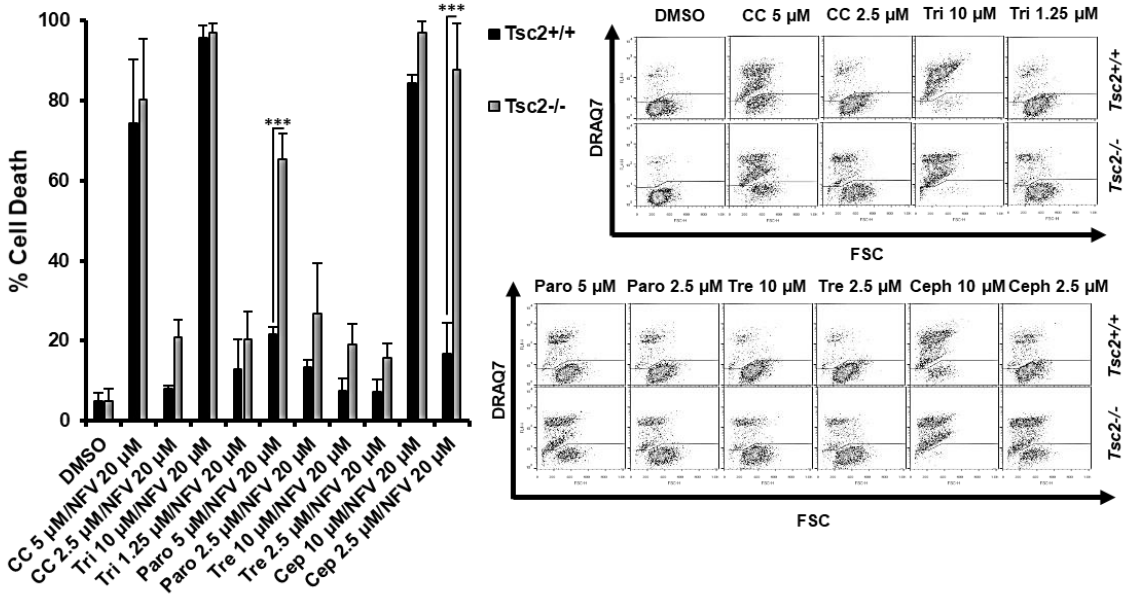

Figure 5.2: Drug screen to determine the effects of drug combinations on cell death. *Tsc2*+/+ and *Tsc2*-/- MEFs were treated with chelerythrine chloride (CC), paroxetine hydrochloride hemihydrate (Paro), cepharanthine (Cep) and trifluoperazine (Tri) and trequinsin at various concentration combined with 20 µM nelfinavir (NFV) for 48 h. % Cell death was measured via flow cytometry and DRAQ 7 Staining. Statistical significance is shown between treated *Tsc2*+/+ MEFs and *Tsc2*-/- MEFs (n=3; mean +/- SD).

5.3 Discussion:

The purpose of this chapter was to identify any potential nelfinavir-based combinations from a drug screen of the above chosen drugs. which could be further investigated. The drugs chosen for this screen were selected either for their selectivity for TSC2-deficient cells (chelerythrine, paroxetine, trifluoperazine – drug screen carried out by (Medvetz *et al.* 2015)) or for their potential role in the combination such as DNA damage (doxorubicin), oxidative stress (luteolin, piperlongumine, FLLL31 and cepharanthine) or ER stress (17AAG).

The range of concentrations, used in the CyQUANT assay, were selected based on literature searches of each drug in relation to treatments of cancer cell

lines and then decreased by 2-fold each time, to prevent non-specific cytotoxicity in *Tsc2*+/+ control MEFs due to synergy with nelfinavir. The fixed 20 μM nelfinavir was chosen as this standard nelfinavir concentration was used by the lab group in relation to combinations unless results showed different nelfinavir concentration improved optimisation (see (Johnson *et al.* 2014), (Johnson *et al.* 2018) and (McCann *et al.* 2018) for details). Data obtained from the CyQUANT assay showed that all combinations tested were able to inhibit cell proliferation although only four combinations demonstrated a significant difference in inhibition between the *Tsc2*+/+ and *Tsc2*-/- MEFs when tested at two different concentrations (paroxetine, trifluoperazine, piperlongumine and luteolin) and only one at three different concentrations (cepharanthine). Luteolin, trequinsin, BPTES were shown to favour *Tsc2*-/- MEFs proliferation compared to control MEFs (although significance was only seen in luteolin treated samples). As a result, these drugs were initially eliminated from further testing. However, seeing the problems of trying to convert results from the CyQUANT to data for cell death concentrations in Chapter 3, all the drugs were allowed to proceed to the cell death stage of drug screen.

For the first part of the cell death drug screen, all drug combinations tested in the CyQUANT stage were investigated via observation assay (observing both *Tsc2*+/+ and *Tsc2*-/- MEFs under light phase microscopy to check for cell coverage, changes in cell morphology and signs of cell death when compared to cells treated with DMSO after 48 h of treatment. The data for this observation assay was not included in this result chapter. After this assay, an initial flow cytometry was performed to confirm observed results (Data not shown) at two different concentrations, one representing high concentration and one representing a low concentration. It was from this initial flow cytometry that several drugs (Piperlongumine, BPTES and Luteolin) were eliminated due to either lack of selectivity or due to lack of cytotoxicity in the *Tsc2*-/- cells. For etoposide, doxorubicin, 17AAG and FLLL31, these drugs were eliminated for different reasons. FLLL31 was redirected towards projects which were purely focused on inhibiting the STAT3 pathway in *TSC2*-deficient cell models. 17AAG was eliminated as results from Chapter 3 (Figure 3.8) showed that 17AAG was more than capable of selectively targeting *Tsc2*-/- MEFs as a single agent. In terms of doxorubicin and etoposide, doxorubicin and nelfinavir combinations have previously been tested (Srinivas *et al.* 1998; Lucia *et al.* 2011) and both combinations are currently being

tested with nelfinavir in several clinical trials (NCT01555281 for doxorubicin; NCT00589056 and NCT01108666 for etoposide).

Within the drug screens, only two drugs showed promise as potential selective combinations: paroxetine and cepharanthine. Both drugs appeared to be well tolerated at lower concentrations by *Tsc2*+/+ MEFs and to target *Tsc2*-/- MEFs, selectively. Of the two drugs, cepharanthine showed the highest level of cytotoxicity compared to the paroxetine which had nearly 90 % cell death compared to approximately 65 %. As a result, it was decided that the primary focus was to further optimise the cepharanthine/nelfinavir combination to maximise cell death in mTORC1-hyperactivity cells, while being well tolerated by control cells and identifying the mode of action (see Chapter 6).

In conclusion, this drug screen identified that a combination of nelfinavir and cepharanthine was well-tolerated by *Tsc2*+/+ MEFs while causing maximum cell death in *Tsc2*-/- MEF.

Chapter 6: Cepharanthine and nelfinavir combination selectively targeted *Tsc2-/-* cells.

6.1 Introduction:

6.1.1 Cepharanthine

Cepharanthine is a cationic and amphipathic bisbenzylisoquinoline alkaloid derived from the plant *Stephania cepharantha Hayata* (a member of the *Menispermaceae* family, indigenous to Japan and China). It makes up 19.5 to 33.5 % of the extract from the plant (Furusawa & Wu, 2007; Paudel, Karki, & Kim, 2016). Cepharanthine has been used in Japan for over 40 years to treat a variety of diseases including snakebites, bronchial asthma, alopecia areata, leukopenia, allergies and HIV without any serious side effects reported (Edashige *et al*. 1991; Harada *et al*. 2001; Kawahara *et al*. 2005; Seubwai *et al*. 2010; Rogosnitzky and Danks 2011).

Cepharanthine has also been shown to cause perturbation of plasma membrane function, lipid peroxidation, inhibition of histamine release, anti-inflammatory effects such as TNFα-mediated NFκB activation, suppression of cytokines and inhibition of platelet aggregation (Ita *et al.* 2008; Kikukawa *et al.* 2008). Cepharanthine was also demonstrated to have an anti-atherosclerotic effect through attenuation of inflammation, lipid peroxidation and vascular smooth muscle cell migration and proliferation (Paudel *et al.* 2016). Cepharanthine has also been known for its antitumor properties seen over a variety of different cancer types.

6.1.2. Cepharanthine and blood cancers

Cepharanthine was shown to be able to inhibit the growth of primary effusion lymphoma (a rare form of non-Hodgkin's lymphoma) cell lines (BCBL-1, TY-1 and RM-P1) in both an *in-vitro* and *in-vivo* setting. It was shown that cepharanthine was able to cause apoptosis in these cells via inhibition of NF-κB that is hyperactivated in these cells (Takahashi-Makise *et al.* 2009). In human leukaemia cell lines, Jurkat and K562, cepharanthine was able to induce apoptosis via selective activation of mitogen-activated protein kinases (MAPKs) – cepharanthine activated extracellular signal-regulated kinases (ERKs) and p38 MAPK but did not activate JNKs (Wu *et al.* 2002). Cepharanthine was shown to halt the progression of thrombocytopenic

purpura with low doses (Tabata *et al.* 2012). Cepharanthine also demonstrated an anti-myeloma effect. Myeloma cells exposed to cepharanthine had an increased production of ROS and triggered capase-3 activation (Kikukawa *et al.* 2008).

6.1.3 Cepharanthine and solid cancers

Cepharanthine was shown to have a cytotoxic effect in several different cell lines; CRC cell lines HT29, LS174T and SW620 and HCC cell line HepG2 with an IC_{50} of between 2.4 and 5.3 μM (Bun *et al*. 2008). Cepharanthine stimulated AMPK-mTOR dependent induction of autophagy and autophagic cell death in a panel of apoptosis-resistant cells (Law *et al*. 2015).

Cepharanthine was shown to inhibit tumour growth and angiogenesis in oral squamous cell carcinoma cells (OSCC), both *in vitro* and *in vivo*. Growth and angiogenesis were prevented via inhibiting expression of pro-angiogenic interleukin 8 (IL8), vascular endothelial growth factor (VEGF) and NF-κB activity (Harada *et al.* 2009). Treatment of Cepharanthine on cholangiocarcinoma cell lines caused a significant inhibition of growth in a dose- and time-dependent manner. It was found that Cepharanthine caused NF-κB inactivation by inhibiting nuclear translocation, which led to caspase 3 and 9 activated apoptosis in these cell lines (Seubwai *et al.* 2010).

Cepharanthine was shown to be able to inhibit 12-0-tetradecanoyl phorbol-13-acetate (TPA) mediated tumour promotion in two stage mouse skin carcinogenesis initiated 7,12-dimethylbenz[α]anthracene (DMBA). Cepharanthine was able to inhibit the phosphorylation of HI histone by Ca^{2+}-phospholipid-dependent protein kinase (PKC) in a concentration dependent manner. Cepharanthine also inhibited the association of HI histone with phospholipid vesicles, but it did not inhibit autophosphorylation of PKC. Cepharanthine also inhibited TPA-stimulated phosphorylation of some cytoplasmic proteins of mouse skin epidermis (Edashige *et al.* 1991; Yasukawa *et al.* 1991).

The treatment of cepharanthine against human adenosquamous carcinoma cells caused G1 arrest via expression of $p21^{WAF1}$ that led to caspase 3 mediated apoptosis (Harada *et al.* 2001). Cepharanthine was found to inhibit angiogenesis and tumour growth *in vivo* in a cholesterol-dependent manner. Cepharanthine inhibited the endolysosomal trafficking of free-cholesterol and low-density lipoprotein in human umbilical vein endothelial cells (HUVEC) by binding to

Niemann-Pick disease, type C1 (NPC1) protein and increasing the lysosomal pH (Lyu *et al.* 2017).

Cepharanthine inhibited cell growth and tumourgenesis in nasopharyngeal carcinoma cell lines *in vitro* by modifying the regulation of genes involved in several roles including cell cycle, DNA repair, apoptosis and NF-κB pathway (Liu *et al*. 2015b). There was a direct antitumour effect in ICR mice exhibiting Ehlrich ascites tumour treated with cepharanthine (Asaumi *et al.* 1995).

6.1.4 Cepharanthine combinations

Cepharanthine has shown success in both blood and solid tumours when used in combination with other drugs. When combined with vincristine and Adriamycin, cepharanthine enhanced cytotoxicity in leukaemia cell lines L1210 and p388 (Kato and Suzumura 2017) and in HNCC cell lines HC-2, HC-3, HC-4, HC-7 and HC-9 (Komiyama *et al.* 1989). The combination of cepharanthine and Adriamycin was also shown to be further enhanced by the introduction of hyperthermia (Nagaoka *et al.* 1987). Combining vincristine, epirubicine and cepharanthine was shown to have a beneficial effect on bone metastasis which arise from renal cell carcinoma (Shichiri *et al.* 1994).

Combining cepharanthine to radiotherapy has been shown to improve treatment. In human cervical adenocarcinoma (HeLa) cell line, cepharanthine/radiotherapy combination therapy caused radiation sensitivity via inhibition of the STAT3 pathway and COX2 (Fang *et al*. 2013). Cepharanthine induced radio-sensitivity in OSCC cell lines (Tamatani *et al.* 2007). Cepharanthine was shown to be able to suppress γ-irradiation induced inflammatory response (NF-κB activity and the production of IL-6 and IL-8) while at the same time enhancing PARP cleavage. In OSCC cells, the combination was also able to inhibit double stranded DNA repair after exposure to radiation (Harada *et al.* 2012). A combination of cepharanthine with an oral antineoplastic agent, S-1 was also shown to have a very good effect on human OSCC xenografts and significantly induced apoptosis (Harada *et al.* 2009).

The introduction of cepharanthine to interferon-β/-γ was shown to have a synergistic effect in terms of anti-proliferative properties in a dose-dependent manner on several cancer cell lines including: CRC (RPMI 4788), human lung carcinoma (PC 10), human uterine cervical cancer (HeLa) and human breast cancer

(ZR-75-1). A combination of cepharanthine and interferon-γ was shown to suppress metastatic development (Ono *et al.* 1994). A combination of cepharanthine and dacomitinib was able to enhance dacomitinib's anti-cancer properties in NSCLC cell lines as cepharanthine was able to inhibit autophagic survival response which is induced due to dacomitinib usage (Tang *et al.* 2018).

A combination of cepharanthine and nimustine hydrochloride was seen to enhance cell death in malignant glioma cell lines: U87MG, U251MG and T98G via apoptosis in both *p53* wildtype cells and *p53* mutant cells (Kono *et al.* 2002). In NSCLC A549 cells that are resistant to gemcitabine, cepharanthine was able to inhibit multidrug resistance protein 7 (MRP7) and reverse gemcitabine resistance. A combination of cepharanthine with onconase (a ribonuclease from oocytes or early embryos of Northern Leopard frog) was able to completely abolish cell growth in several cancer cell lines including human promyelocytic leukaemia (HL-60), histiomonocytic lymphoma (U937), multiple myeloma (RPMI-8228), prostate carcinoma (DU145) and prostate adenocarcinoma (LNCaP) (Ita *et al.* 2008). Cepharanthine was shown to enhance the toxicity of conjugates of epidermal growth factor with *Pseudomonas* exotoxin when used against HeLa cells (Shiraishi *et al*. 1988). In terms of lung metastasis induced by Lewis lung carcinoma, metastasis was greatly inhibited by a combination of cepharanthine and 5-fluorouracil (5-FU) (Ito *et al*. 2008).

6.1.5 Hypothesis

In the drug screen within Chapter 5, cepharanthine was demonstrated to selectively induce cell death in *Tsc2*-/- MEFs and was well tolerated by wildtype control cells when combined with the HIV inhibitor, nelfinavir. The purpose of this chapter was to expand on this initial finding, to further optimise this drug combination and to explore whether both drugs were synergistic. Once an optimised drug combination was determined, this chapter investigated the mechanism(s) of drug action that induced selective cytotoxicity in the *Tsc2*-/- MEFs.

6.2 Results:

6.2.1 An optimized combination of cepharanthine and nelfinavir synergised to selectively target mTORC1 hyperactive cells.

Having determined that a combination of cepharanthine and nelfinavir was a suitable candidate for selective cytotoxicity of *Tsc2*-/- cells (see Chapter 5), the next step was to determine an optimised combination of both drugs. To optimise this cepharanthine and nelfinavir drug combination, each drug was tested either as a single agent or in a combination of varying concentrations. Cells were incubated for 48 h and results from flow cytometry were written as % cell death (Figure 6.1A). Results are summarised in Table 6.1.

Table 6.1 Results from cell death flow cytometry. Results of flow cytometry to determine how cytotoxic cepharanthine (Ceph) and nelfinavir (NFV) are to *Tsc2*+/+ and *Tsc2*-/- MEFs as single agents or in combination over a range of concentrations

	% Cell Death			
	***Tsc2*+/+**		***Tsc2*-/-**	
Drug	**Average**	**SD**	**Average**	**SD**
DMSO	2.43	0.33	3.31	0.56
NFV 20 µM	9.31	7.30	15.80	1.77
NFV 10 µM	4.72	6.92	9.54	2.01
Ceph 5 µM	5.20	1.80	5.25	1.33
Ceph 2.5 µM	1.44	0.34	4.84	2.69
Ceph 1.25 µM	1.35	0.21	4.23	1.06
Ceph 5/NFV 20 µM	19.83	6.65	93.90	1.92
Ceph 2.5/NFV 20 µM	8.93	6.21	92.60	2.69
Ceph 1.25/NFV 20 µM	4.49	1.28	85.73	4.88
Ceph 5/NFV 10 µM	4.73	1.97	19.53	1.67
Ceph 2.5/NFV 10 µM	2.83	0.04	12.44	6.73
Ceph 1.25/NFV 10 µM	2.86	0.36	11.56	5.42

To figure out how synergistic this drug combination was, various concentration of cepharanthine, nelfinavir and several combinations of cepharanthine and nelfinavir using 20 µM nelfinavir as a base were tested via flow cytometry. Results were then processed in CompuSyn and a CI value was

generated. Results showed that combinations containing ≥ 2.5 µM cepharanthine showed high levels of synergy in wildtype cells while all combinations tested showed good synergy in *Tsc2*-/- MEFs (CI value = 0.05 in *Tsc2*+/+ MEFs vs 0.11 in *Tsc2*-/- MEFs when treated with 10 µM cepharanthine/20µM nelfinavir, 0.15 vs 0.13 with 5 µM cepharanthine/20µM nelfinavir, and 0.52 vs 0.16 with 2.5 µM cepharanthine/20µM nelfinavir respectively). In combinations where the cepharanthine was less than 2.5 µM, results in wildtype MEFs were only minorly synergistic when compared to *Tsc2*-/- MEFs treated with identical treatments (CI value = 0.90 in *Tsc2*+/+ MEFs vs 0.31 in *Tsc2*-/- MEFs with 1.25 µM cepharanthine/20µM nelfinavir and 0.91 vs 0.61 with 0.625 µM cepharanthine/20µM nelfinavir) (Figure 6.1B (i-iv)).

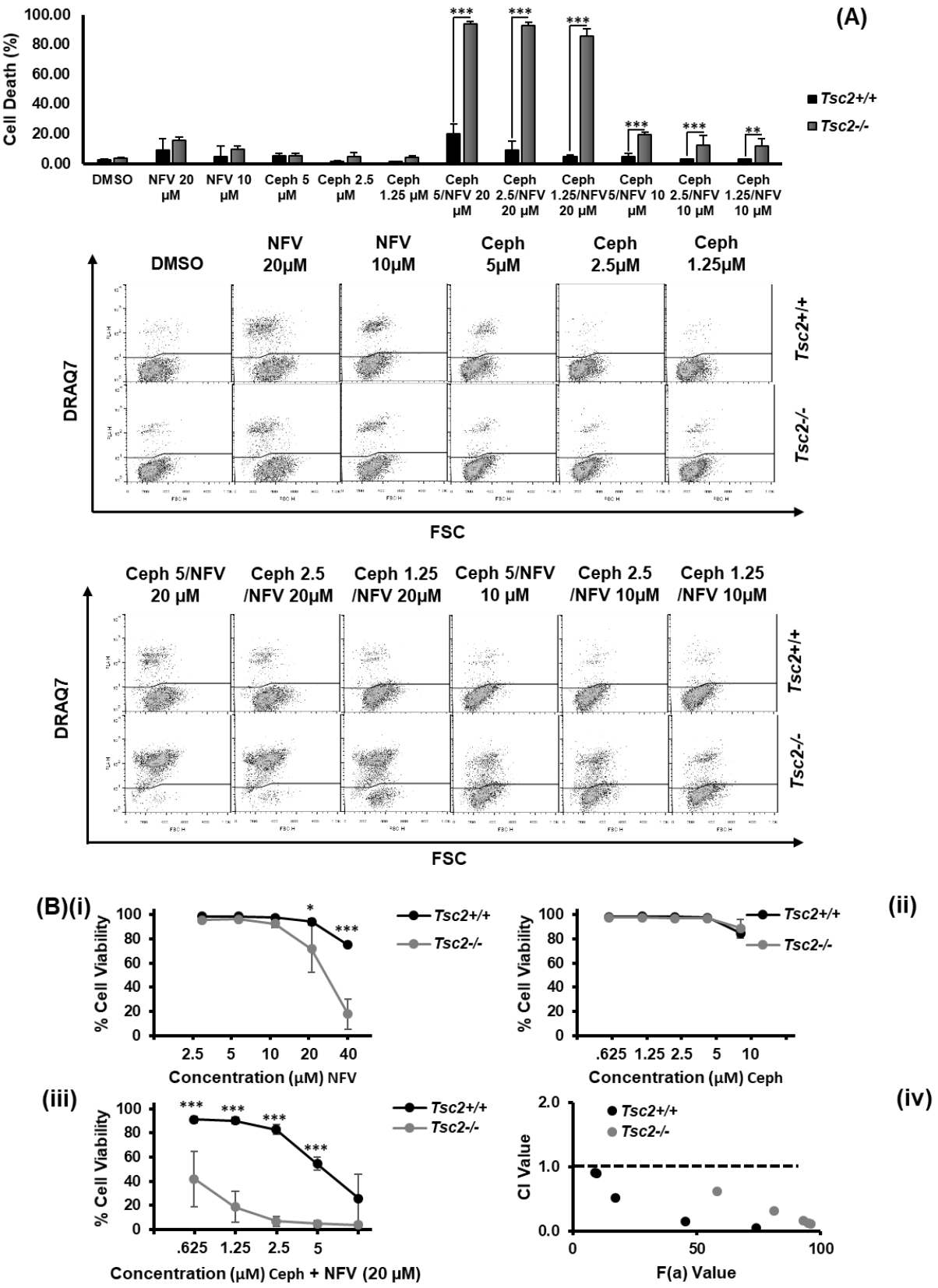

Figure 6.1: Optimization and synergy of cepharanthine and nelfinavir. (A) Flow cytometry (with scatter blots) performed to measure cell death in *Tsc2*+/+ and *Tsc2*-/- MEFs treated with dimethyl sulfoxide (DMSO), cepharanthine (Ceph) or nelfinavir (NFV) as single agents at various concentrations or in combination (Ceph/NFV) at various concentrations after 48 h treatment (n=3; mean +/- SD). (B) Dose response curves were performed in *Tsc2*+/+ and *Tsc2*-/- MEFs using flow

cytometry to measure cell death following treatment with (i) nelfinavir (NFV); (ii) cepharanthine (Ceph) and (iii) combined cepharanthine with a fixed concentration of 20 μM nelfinavir (Ceph/NFV) (n=3; mean +/- SD). Synergy was then calculated using CompuSyn and graphed (iv) as F(a) value vs CI value. Statistical significance is shown with combination or single agent treated *Tsc2*-/- MEFs compared to their wild-type controls.

To confirm that *Tsc2* loss was responsible for the induction of cell death, the concentration was tested using ELT3 cell lines (both null type (V3) and *Tsc2* re-expressed (T3)) via flow cytometry. Results were recorded as % cell death and etoposide was used as a positive control. Results showed that in both cell lines, the combination of cepharanthine and nelfinavir were extremely cytotoxic (80.93% +/- 20.37 SD in ELT-T3 cells vs 92.55% +/- 8.99 SD in ELT-V3 cells). Both cepharanthine and nelfinavir used as single agents were also shown to be more cytotoxic in ELT3 cell lines when compared to MEFs (9.3 % +/- 7.30 SD in *Tsc2*+/+ MEFs vs 15.80% +/- 1.77 SD in *Tsc2*-/- MEFs compared to 14.09% +/- 5.39 SD in ELT-T3s vs 34.90% +/- 9.38 SD in ELT-V3s when treated with nelfinavir and 5.20% +/- 1.80 SD in *Tsc2*+/+ MEFs vs 5.25% +/- 1.33 SD in *Tsc2*-/- MEFs compared to 25.83% +/- 8.13 SD in ELT-T3s vs 55.70% +/- 5.98 SD in ELT3-V3s when treated with cepharanthine) (Figure 6.2A).

To determine if the combination could be used to target sporadic cancers, the combination was tested against three different types of mTORC1 hyperactive cancer cell lines (breast, colorectal and lung). Results were recorded as % cell death and etoposide was used as a positive control. Results from the flow cytometry showed that the combination caused high levels of cell death in all sporadic cancer lines tested (96.95% +/- 1.86 SD in HCT116, 90.13% +/- 7.48 SD in NCI-H460 and 66.13% +/- 14.91 SD in MCF7 cells). HCT116 cells appeared to be sensitive to 20 μM nelfinavir as a single agent as results showed a high level of cell death (67.53% +/- 4.65 SD) (Figure 6.2B).

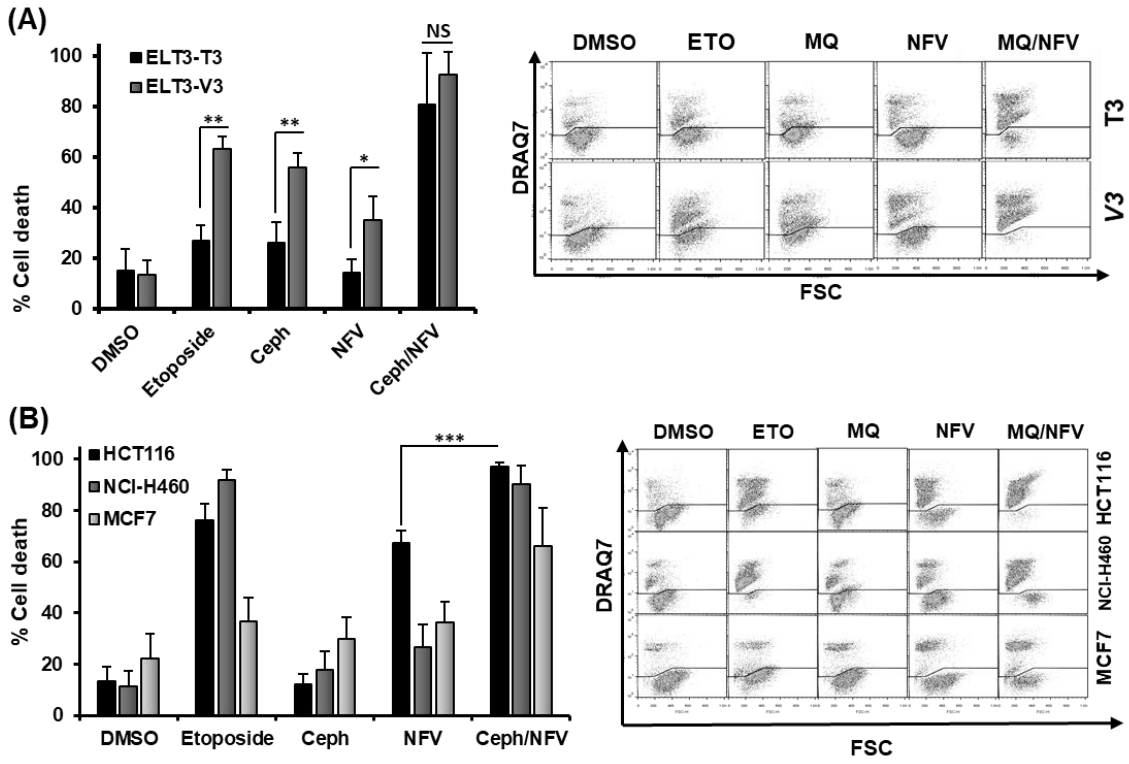

Figure 6.2: Combination of cepharanthine and nelfinavir caused cytotoxicity in mTORC1 hyperactive tumour cells. (A) ELT3-T3 and ELT3-V3; (B) MCF7, HCT116 and NCI-H460 were treated with either DMSO, 100 μM etoposide (ETO), 5 μM cepharanthine (Ceph), 20 μM nelfinavir (NFV) or cepharanthine and nelfinavir combination (Ceph/NFV) for 48 h. Cells were then tested by flow cytometry and cells were separated into viable and non-viable cell populations via DRAQ7 staining(n=3; mean +/- SD). Statistical significance is shown with combination treated ELT3-V3 cells to their wild-type controls and comparing single drug treatment of nelfinavir and combination in HCT116.

6.2.2 Cepharanthine/nelfinavir combination prevented tumour colony formation and prevented tumour regrowth from treated spheroids.

To determine the effects of cepharanthine/nelfinavir in a 3D environment, *Tsc2*-/- MEFs were either plated in either agar (for tumour colony formation assay) or agarose (for tumour outgrowth assay).

To determine if the combined cepharanthine/nelfinavir treatment could prevent the formation of tumours, *Tsc2*-/- MEFs were treated with drugs for 14 days before being photographed, using rapamycin as a positive control. Results for the colony assay showed that the cepharanthine/nelfinavir combination significantly reduced the size of tumour colonies compared to single agents or in the presence of DMSO. Colonies treated with 5 μM Cepharanthine/ 20 μM Nelfinavir showed a similar size when compared to colonies treated with rapamycin (62.24 μm +/- 20.88

SD in combination treated colonies vs 63.39 µm +/- 19.58 SD in rapamycin treated colonies). Colonies treated with cepharanthine and nelfinavir as single agents also showed a reduction in colony size compared to the DMSO-treated spheroids (231.99 µm +/- 90.98 SD in DMSO-treated colonies compared to 126.29 µm +/- 53.27 SD in cepharanthine treated colonies and 108.26 µm +/- 32.20 SD in nelfinavir treated colonies) (Figure 6.3A).

To determine the effects of the combination on established tumour spheroids, *Tsc2*-/- MEFs were incubated for 72 h to form spheroids on agarose and photographed before being treated and after being treated with drugs for 96 h (the last 48 h including DRAQ7). Spheroids were then place in fresh non-drug media for 72 h (photographed every 24 h). Results showed that there was no change in size between any of the treatment conditions after 96 h of treatment. The morphologies of DMSO cepharanthine and nelfinavir treated cells remained the same, however, samples treated with the cepharanthine/nelfinavir combination changed to an increased “fluffy” appearance (Figure 6.3B). Once placed back into clean drug-free media, spheroids previously incubated in the combined cepharanthine/nelfinavir treatment failed to regrow after 72 h. All other spheroids did eventually grow back, although while cepharanthine and nelfinavir treated spheroids grew at similar rates, these were slower compared to DMSO treated spheroids (Figure 6.3C).

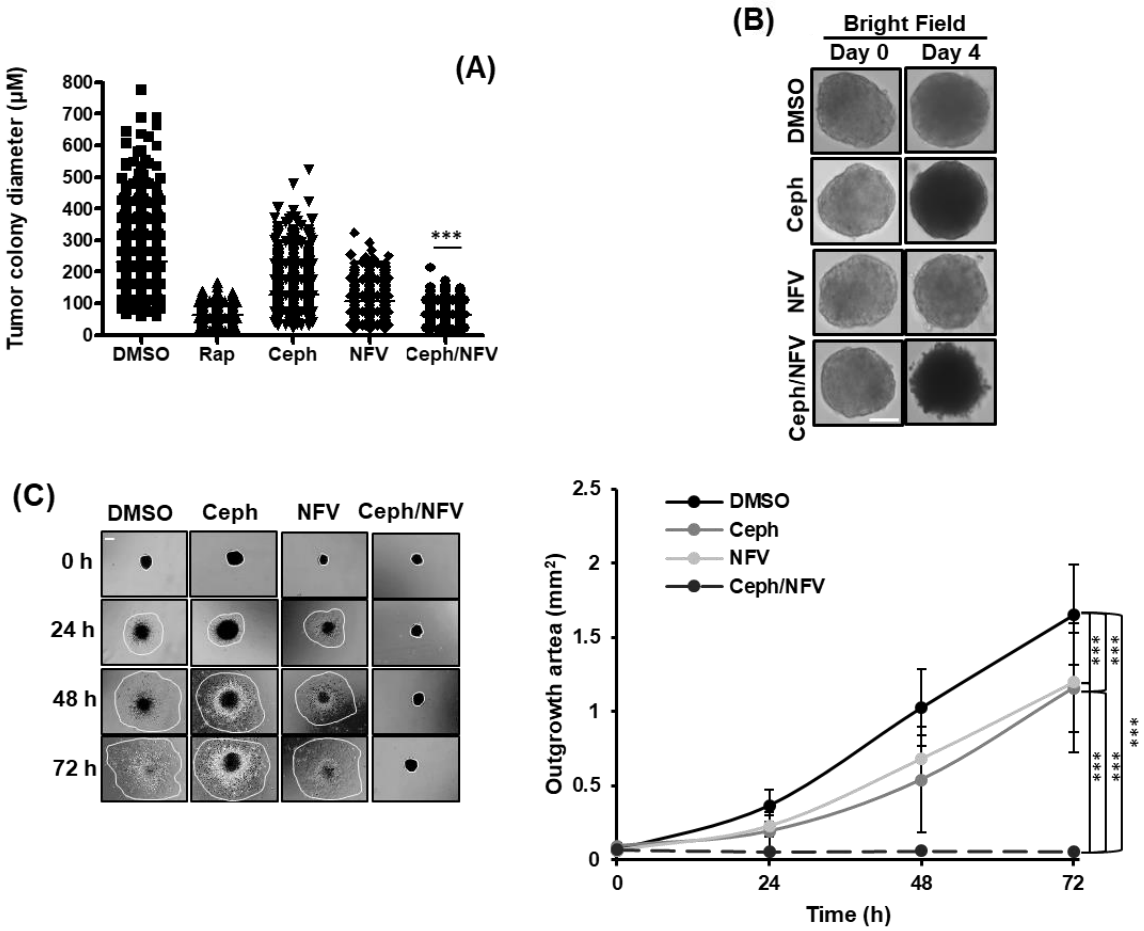

Figure 6.3: Mefloquine/nelfinavir combination prevented tumour formation and tumour spheroid growth. Colony formation was tested in *Tsc2*-/- MEFs seeded on soft agar that were treated for 14 days with Dimethyl Sulfoxide (DMSO), 5 µM cepharanthine (Ceph), 20 µM nelfinavir (NFV) or in combination Ceph/NFV (n=3; mean +/- SD). Tumour diameters were measured using Image J. Significance was observed when comparing combined nelfinavir and cepharanthine treatment to DMSO vehicle control. Work done was assisted by Lauren McEneaney (B) *Tsc2*-/- MEF spheroids were grown for 72 h before being treated under the same conditions as (A) for 96 h. DRAQ7 was supplemented for the final 48 h to monitor cell death before images were taken. (C) Spheroids treated in (B) were re-plated onto standard tissue culture plates and grown in drug-free media. Images were taken every 24 h and the area of outgrowth was calculated using Image J, scale bar is 200 µm and outgrowth area is graphed. Statistical significance is shown with combination treated tumour colony size compared to their wild-type controls and comparing outgrowth of combination treated spheroids to single agent and DMSO treated spheroids (n=3; mean +/- SD).

6.2.3 Cepharanthine/nelfinavir combination targeted *Tsc2*-/- cells in an mTOR and autophagy/lysosomal-independent manner.

To determine if the autophagy flux was altered by the combination, western blots were carried out on *Tsc2*+/+ or *Tsc2*-/- MEFs treated for 3 h with bafilomycin A1 as a positive control. Results showed that cepharanthine was able to cause accumulation of LC3-II in both cell lines. The combination was also able to cause LC3-II accumulation in both cell lines. Accumulation levels were slightly higher in *Tsc2*+/+ MEFs compared to *Tsc2*-/- MEFs. p62 was basally elevated in *Tsc2*-/- MEFs compared to *Tsc2*+/+ MEFs and did not appear to be greatly affected by the treatment of bafilomycin A1, single agents or combination (Figure 6.4A).

Cepharanthine has been shown to accumulate in the lysosome and cause inhibition of lysosomal cathepsin B and cathepsin D maturation (Shiraishi *et al*. 1988b; Tang *et al*. 2018). To determine how the cepharanthine/nelfinavir combination would affect the lysosome, *Tsc2*-/- MEFs were treated for 48 h with either DMSO, cepharanthine/nelfinavir combination, cepharanthine/nelfinavir combination with 100 nM bafilomycin A1 (a v-ATPase inhibitor), or bafilomycin A1 before being analysed via flow cytometry. Results showed that bafilomycin A1 as a single agent was able to cause a considerable amount of cell death in *Tsc2*-/- MEFs (76.93% +/- 8.12 SD). Results also showed that bafilomycin A1 failed to rescue cells from death in *Tsc2*-/- MEFs treated with the cepharanthine/nelfinavir combination (86.63% +/- 9.05 SD in cells treated with just cepharanthine/nelfinavir vs 87.87% +/- 5.35 SD in cells treated with cepharanthine and bafilomycin A1). To confirm that bafilomycin A1 was working correctly, western blots were carried out with both *Tsc2*+/+ and *Tsc2*-/- MEFs, treated for either 3 h or 24 h in combination or combination with bafilomycin A1. Western blots showed that in combination plus bafilomycin A1 treated samples showed the accumulation of LC3-II in both cell lines increasing from 3 h to 24 h. Accumulation of p62 (also referred to as SQSTM1) was seen in both cell lines as well (at 24 h in *Tsc2*+/+ MEFs and at both 3 h and 24 h in *Tsc2*-/- MEFs). In *Tsc2*-/- MEFs treated with just combination, results showed that while accumulation of both LC3-II and p62 was observed at the 3 h time point, cells appeared to recover as no accumulation was detected at the 24 h time point (Figure 6.4B (i-ii)).

To determine if mTORC1-hyperactivity was important for the induction of cell death, flow cytometry was carried out on *Tsc2*-/- MEFs treated with DMSO, rapamycin, cepharanthine/nelfinavir, with rapamycin (along with a 1 h rapamycin

pre-treatment) for 48 h. Results showed that the introduction of rapamycin failed to rescue cell death in *Tsc2*-/- MEFs (86.63% +/- 9.05 SD in combination-treated cells vs 88.93% +/- 4.01 SD in combination plus rapamycin treated cells). Rapamycin also showed very little cell death when used as a single agent (6.36% +/- 3.55 SD). To confirm if rapamycin was inhibiting mTORC1 activity, western blots were carried on the previously mentioned cell lines treated in the same conditions as the flow cytometry. Results showed that samples treated with combination and rapamycin showed a complete or near complete inhibition of RSP6 phosphorylation, confirming rapamycin was successfully inhibiting the mTORC1 pathway (Figure 6.4C (i-ii)).

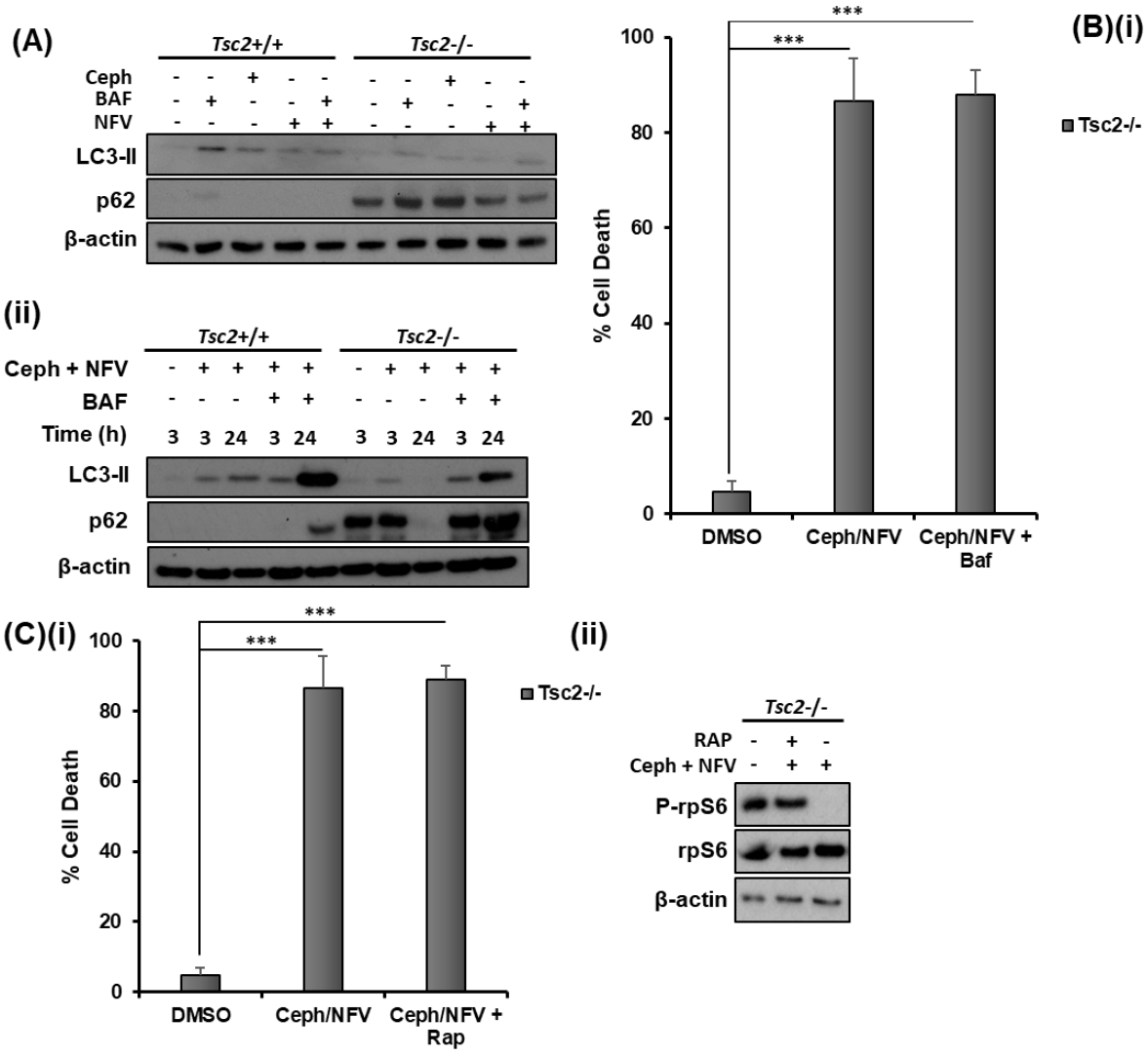

Figure 6.4: Inhibition of mTORC1 was not associated with combination-induced cell death and the combination caused minimal inhibition of autophagy which was not associated with cell death. (A) *Tsc2*-/- and *Tsc2*+/+ MEFs were treated with 20 μM nelfinavir (NFV) and 5 μM cepharanthine (Ceph), 100 nM bafilomycin A1 or cepharanthine and nelfinavir (Ceph/NFV) for 3 h. Accumulation of lipidated LC3-II and p62 were analysed by western blot. (B(i)) *Tsc2-/-* were treated

with 20 μM nelfinavir (NFV) and 5 μM cepharanthine (Ceph) or Ceph/NFV with 100 nM Bafilomycin A1 (BAF) for 48 h. Cell death was determined using flow cytometry (n=3; mean +/- SD). Statistical significance (calculated by one-way ANOVA) shown between DMSO-treated and Ceph/NFV treated cells and between DMSO-treated cells and Ceph/NFV/BAF treated cells. (B(ii)) To determine if BAF was functioning as expected, western blotting was carried out to determine the accumulation of lipidated LC3-II and p62 in the cells treated in (B(i)) after 3 h and 24 h of treatment. Total protein levels of β-actin were used as a loading control. (C(i)) *Tsc2*-/- MEFs were pre-treated with 50 nM rapamycin (RAP) for 1 h, where indicated, before being treated with either 20 μM nelfinavir (NFV) and 5 μM cepharanthine (Ceph) or MQ/NFV with RAP for 48 h. Cell death was determined using flow cytometry (n=3; mean +/- SD). (C(ii)) To determine if RAP was functioning as expected, western blotting was carried out to determine rp-S6 phosphorylation at Ser235/236 in the cells treated in (A) after 48 h of treatment. Statistical significance (calculated by one-way ANOVA) shown between DMSO-treated and Ceph/NFV treated cells and between DMSO-treated cells and Ceph/NFV/RAP treated cells. All Blots in figure 6.4 are representative of n=2 runs

6.2.4 Cepharanthine/nelfinavir combination did not affect the production of reactive oxygen species (ROS).

To confirm if the combination was causing an effect on the production of ROS, both *Tsc2*+/+ and *Tsc2*-/- MEFs were stained with DCFDA before being treated with several different treatments; DMSO, TBHP (positive controls), cepharanthine/nelfinavir and cepharanthine/nelfinavir with either methyl pyruvate or NAC (negative controls). Results written as ROS Generation fluorescence (RGF). Results showed that the cepharanthine/nelfinavir combination caused a decrease in ROS production compared to cells treated with just DMSO (862.54 RGF +/- 481.48 SEM in *Tsc2*+/+ MEFs vs 993.04 RGF +/- 492.61 SEM in *Tsc2*-/- MEFs). The introduction of the ROS scavengers also caused a reduction in ROS production (304.04 RGF +/- 201.78 SEM in *Tsc2*+/+ MEFs vs 447.91 RGF +/- 244.06 SEM in *Tsc2*-/- MEFs in the presence of NAC and 121.54 RGF +/- 45.26 SEM in *Tsc2*+/+ MEFs vs 208.92 RGF +/- 79.57 SEM in *Tsc2*-/- MEFs in the presence of methyl pyruvate) (Figure 6.5A).

To determine if ROS production played a role in cell death, flow cytometry was carried out in *Tsc2*-/- MEFs treated with either DMSO, drug combination or drug combination with NAC for 24 h (as NAC is a short-lived inhibitor). Results showed that the presence of NAC failed to rescue cells from death (41.20% +/- 6.90 SD when treated with mefloquine/nelfinavir combination and NAC compared to 44.82% +/- 3.60 SD when treated with just the combination) (Figure 6.5B).

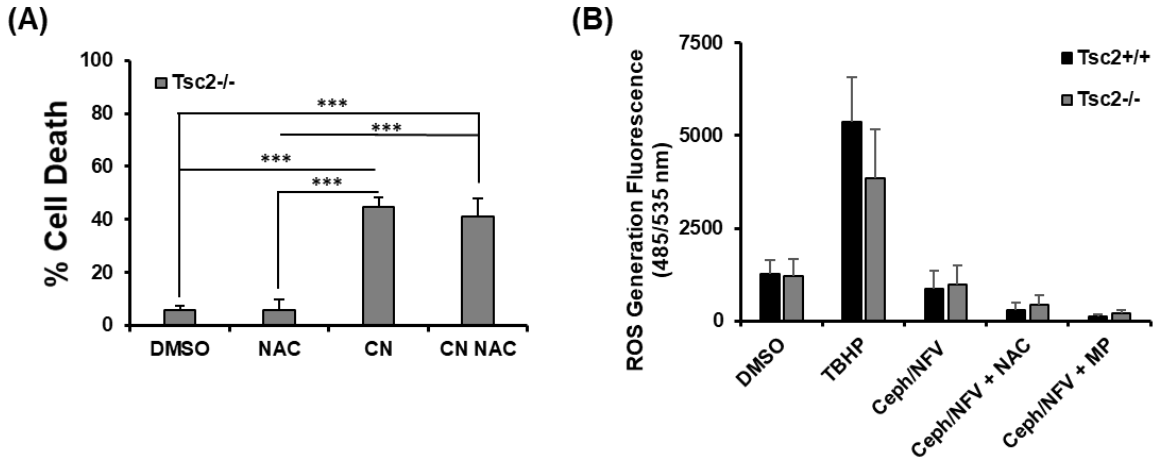

Figure 6.5: Cepharanthine/nelfinavir combination caused minimal effect on ROS production. (A) *Tsc2*+/+ and *Tsc2*-/- MEFs were stained in 25 µM 2', 7' –dichlorofluorescin diacetate (DCFDA) for 45 min at 37ºC. Cells were washed and treated with DMSO, Tert-Butyl Hydroperoxide (TBHP), cepharanthine and nelfinavir combination (Ceph/NFV), combination plus N-acetyl-L-cysteine (Ceph/NFV + NAC) or combination plus methyl pyruvate (Ceph/NFV + MP) for 4 h. Fluorescence was read on plate reader at excitation at 485 nm and emission at 535 nm (n=3; mean +/- SEM). (B) *Tsc2*-/- MEFs treated with DMSO, cepharanthine and nelfinavir combination (CN) or combination plus N-acetyl-L-cysteine (CN + NAC) for 24 h. Cell death was measured via flow cytometry using DRAQ7 staining (n=3; mean +/- SD). Statistical significance (calculated by one-way ANOVA) shown between DMSO-treated and Ceph/NFV treated cells, between NAC-treated cells and Ceph/NFV cells, between DMSO-treated cells and Ceph/NFV/NAC treated cell and between NAC-treated cells and Ceph/NFV/NAC treated cells.

6.2.5 Cepharanthine and nelfinavir as single agents, as well as in combination blocked P-glycoprotein activity in *Tsc2*+/+ and *Tsc2*-/- MEFS.

Cepharanthine has been shown to be a substrate of P-glycoprotein and binding causes inhibition of activity and transport of cytotoxic drugs out of cells (Mizobata *et al*. 2002). To determine if cepharanthine/nelfinavir combination could inhibit P-glycoprotein activity, both *Tsc2*+/+ and *Tsc2*-/- MEFs were treated with either combined cepharanthine/nelfinavir treatment or control, with all treatments containing 5.25 µM of Rhodamine123 (which is a substrate of P-glycoprotein) for 30 min at 37ºC. Samples were then lysed in warmed deionised water and a fluorescence reading was taken. Results were recorded as a % of DMSO treated control. Results confirmed that cepharanthine inhibited P-glycoprotein activity (as seen in the increased Rhodamine 123 uptake compared to DMSO) in *Tsc2*-/- but not in *Tsc2*+/+ MEFs (103.70% +/- 10.70 SEM in *Tsc2*+/+ MEFs and 147.16% +/- 15.56 SEM in *Tsc2*-/- MEFs compared to 100 % in DMSO treated cells respectively).

Nelfinavir (as seen in Chapter 4) also caused P-glycoprotein inhibition (large observable increase in rhodamine 123 uptake) in *Tsc2*+/+ cells but caused minor inhibition (slight observable uptake) in *Tsc2*-/- cells (166.80% +/- 7.16 SEM in *Tsc2*+/+ MEFs compared to 127.47% +/- 7.42 SEM in *Tsc2*-/- MEFs). The combination of cepharanthine and nelfinavir showed poor activity inhibition (as seen in a slight increase in rhodamine 123 uptake) in *Tsc2*-/- MEFs. It did however cause a greater level of inhibition (a larger uptake) in *Tsc2*+/+ MEFs (135.07% +/- 19.15 SEM in *Tsc2*+/+ MEFs compared to 117.25% +/- 8.62 SEM in *Tsc2*-/- MEFs) (Figure 6.6).

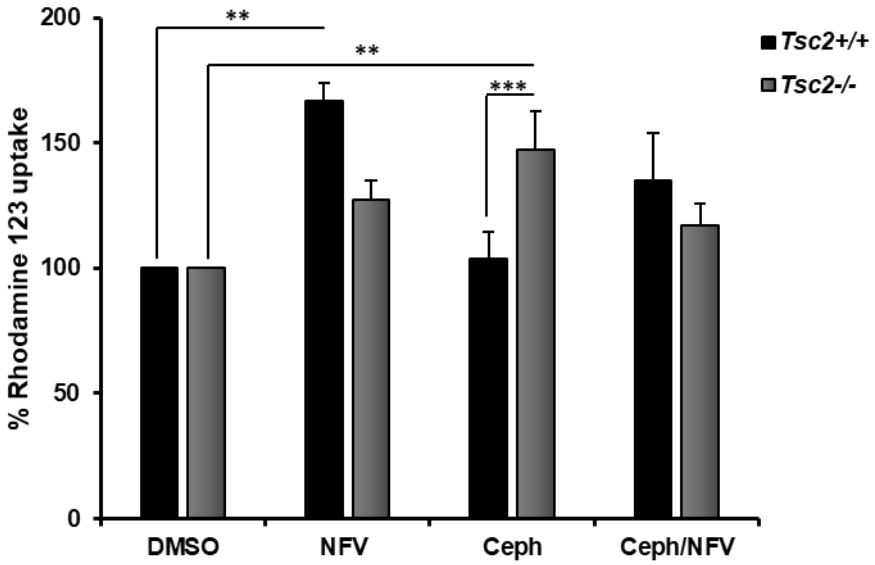

Figure 6.6: Mefloquine/nelfinavir combination affected rhodamine 123 uptake. *Tsc2*+/+ and *Tsc2*-/- MEFs were treated with DMSO, 5 µM cepharanthine, 20 µM nelfinavir or a combination of cepharanthine and nelfinavir (all containing 5.25 µM rhodamine 123) for 30 min at 37 ^{o}C before being lysed in warmed deionised water. Fluorescence was analysed via plate reader at excitation at 480 nm and emission at 520 nm (n=3; mean +/- SEM). Statistical significance is shown between combination treated *Tsc2*+/+ and *Tsc2*-/- MEFs

.

6.2.6 Cepharanthine/nelfinavir combination induced enhanced and prolonged ER stress in *Tsc2*-/- cells via the PERK pathway.

To determine the effects the combination would have on ER stress pathways in both *Tsc2*+/+ and *Tsc2*-/- MEFs, western blots were performed on *Tsc2*+/+ and *Tsc2*-/- MEFs treated for 6 h with drugs using tharsigargin was a positive control. Results showed that there was a large difference in expression of ER stress makers between *Tsc2*+/+ and *Tsc2*-/- MEFs as can be seen in IRE1α (although expression

levels showed a decrease in expression of the protein in *Tsc2*-/- MEFs and an increase in expression in *Tsc2*+/+ MEFS when both cell types are treated with the combination) and in SESN2 (in which expression appeared to be too greatly affect the presence of drugs, either control, single agent or combination). In the *Tsc2*-/- MEFs, there were high levels of expression for several components of the PERK pathway such as GADD34, CHOP and ATF4 when cells where treated with drugs, and levels were higher in the presence of the cepharanthine/nelfinavir combination when compared to single agents especially in CHOP although differences in GADD34 and ATF4 were less pronounced. At the same time point, components of the mTOR pathway were also tested to determine the effects on the pathway. Results showed a higher basal level of phosphorylation of S6K in *Tsc2*-/- MEFs compared to *Tsc2*+/+ MEFs although expression levels did decline in cells treated with single agent or combination. In terms of RPS6 phosphorylation, the presence of either nelfinavir or the combination caused a decreased phosphorylation in *Tsc2*+/+ MEFs compared to *Tsc2*-/- MEFs. Results also confirmed that *Tsc2*-/- MEFs had no *Tsc2* expression. (Figure 6.7A).

To confirm that ER stress was occurring, an investigation into XBP1 splicing was carried out. Both *Tsc2*+/+ and *Tsc2*-/- MEFs were treated for 6 h with treatments used in Figure 6.7A, using tharsigargin as a positive control, before mRNA was extracted and converted to cDNA. Results were then processed by PCR and analysed on an agarose gel. Results showed that splicing occurs at a higher level in *Tsc2*-/- MEFs compared to *Tsc2*+/+ MEFs. With *Tsc2*-/- cells, splicing occurred in samples treated with the cepharanthine/nelfinavir combination at a much higher rate compared to single agents or DMSO (Figure 6.7B).

6.2.7 Cepharanthine/nelfinavir combination affected energy stress levels in *Tsc2*-/- cells.

To determine if the combined cepharanthine/nelfinavir treatment influenced energy stress, flow cytometry was carried out in *Tsc2*-/- MEFs treated for 48 h with either DMSO, cepharanthine/nelfinavir combination or combination with methyl pyruvate. Results showed that the presence of methyl pyruvate was able to rescue *Tsc2*-/- cells from death (86.63% +/- 9.05 SD when treated with just cepharanthine/nelfinavir compared to 38.95% +/- 6.91 SD when cells were treated with both cepharanthine/nelfinavir and methyl pyruvate) (Figure 6.7C).

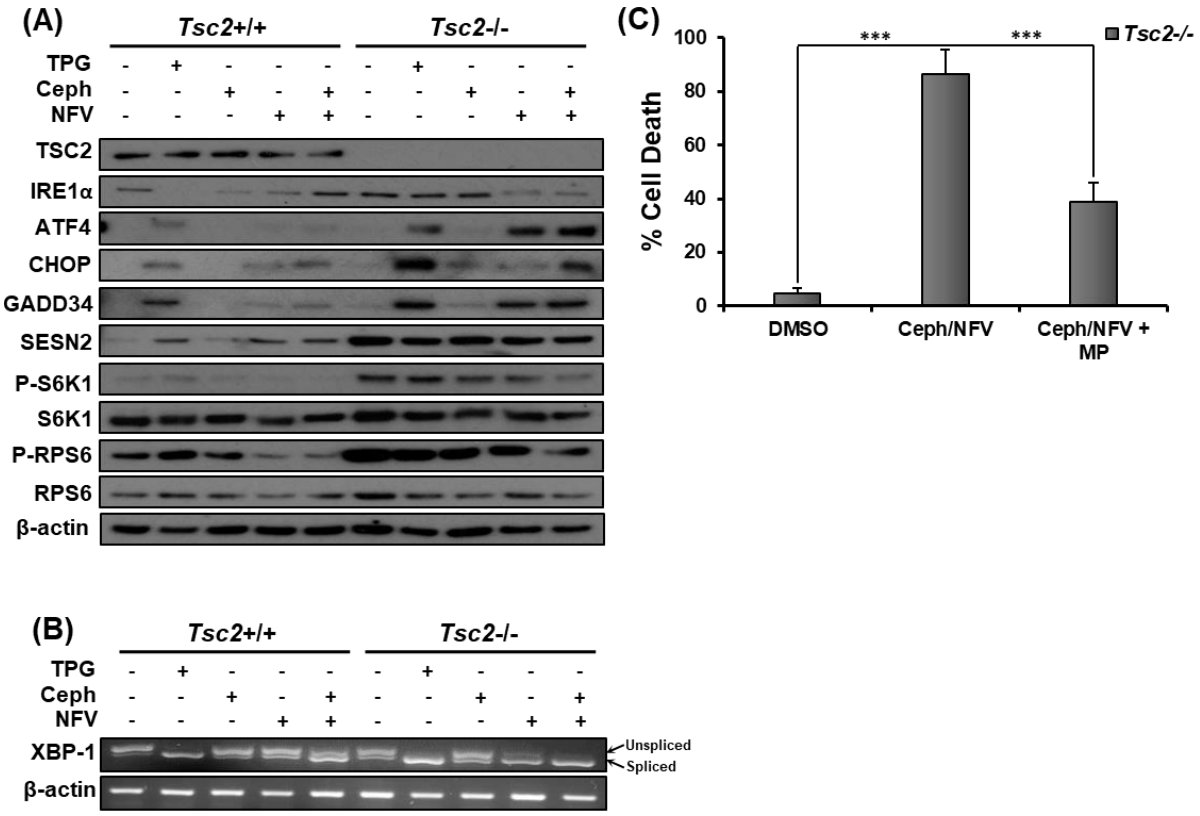

Figure 6.7: The effects of cepharanthine/nelfinavir combination on ER stress and energy stress. (A) *Tsc2*+/+ and *Tsc2*-/- MEFs were treated with either DMSO, 1 μM thapsigargin (TPG), 5 μM cepharanthine (Ceph), 20 μM nelfinavir (NFV), or cepharanthine and nelfinavir combination (Ceph/NFV) for 6 h, where indicated. Total protein levels of TSC2, IRE1α, ATF4, CHOP, GADD34, S6K1, SESN2 and β-actin and S6K1 phosphorylated at Thr389 and RPS6 phosphorylated at $Ser_{235/236}$ were detected by Western blot. (B) Xbp1 mRNA splicing was determined from the same treatments as described in (A). PCR products were resolved on agarose gels (unspliced = 480 bp upper band, spliced = 454 bp lower band). (C) *Tsc2*-/- cells were treated with DMSO, 5 μM cepharanthine and 20 μM nelfinavir combination (Ceph/NFV) or cepharanthine/nelfinavir combination with the addition of 8 mM methyl pyruvate (MQ/NFV/MP) for 48 h. Cells were then stained with DRAQ7 and % cell death determined by flow cytometry (n=3; mean +/- SD). Statistical significance is shown comparing combination treated *Tsc2*-/- and combination plus methyl pyruvate treated *Tsc2*-/- MEFs and DMSO. All Blots in figure 6.7 are representative of n=2 runs

6.3 Discussion:

In Chapter 5, a combination of cepharanthine and nelfinavir was shown to be highly selective for targeting *Tsc2*-/- MEFs while being well tolerated by wildtype controls. The purpose of this chapter was to further investigate this novel combination, to optimise it and identify potential modes of action against not only mutant MEFs, but against other sporadic mTORC1 hyperactive cells. To date, it appears that this is the first time that a combination of cepharanthine and nelfinavir has been used for the treatment of mTORC1 hyperactive tumour cells.

In terms of the concentration of cepharanthine used in this chapter, the 5 μM used falls in the same range as several other cancer cell lines including HeLa cells, cepharanthine (IC_{50} of 8.9 μM), multiple myeloma cells (IC_{50} between 2 and 8 μM and CRC cell lines (IC_{50} of between 2.4 μM and 5.3 μM) (Bun *et al*. 2008; Kikukawa *et al*. 2008; Law *et al*. 2015). Cepharanthine can also be used at a much higher concentration which can affect the mechanisms of action which will be discussed later in this section. With regards to nelfinavir, the concentration used was above the range discussed in chapter 3 (4.96 μM (Zhang *et al.* 2001) to 18 μM (Marzolini *et al.* 2001)). However, several combinations developed by the lab group have used this nelfinavir concentration and showed positive results (Johnson *et al*. 2015; Dunlop *et al*. 2017a; Johnson *et al*. 2018).

Cepharanthine combined with nelfinavir was able to cause high levels of cytotoxicity in *Tsc2*-/- MEFs when 20 μM of nelfinavir was used as the base. It is interesting to note that at this concentration of nelfinavir, all concentrations (1.25-5 μM) of cepharanthine used showed high levels of cell death in *Tsc2*-/- MEFs while being well tolerated in *Tsc2*+/+ MEFs (although the level of cell death did increase in a dose-dependent manner). On the other hand, using 10 μM Nelfinavir based combinations showed a dramatic decrease in cell death at all cepharanthine concentrations used (although there was still significant difference in cell death observed between both cell types). Initially a combination consisting of 2.5 μM cepharanthine and 20 μM nelfinavir was chosen as the optimised concentration for future testing as it had the same level of cell death as the 5 μM cepharanthine and 20 μM nelfinavir but had less cell death in the control cells. However, during experimentations in this chapter, it was observed that this combination started to fail in inducing cell death in *Tsc2*-/- MEFs as the cells became older and the cells reached passage numbers higher than p35. Because of this reduction in

performance, it was decided that a combination of 5 μM cepharanthine and 20 μM nelfinavir would be used for all future testing.

When testing against mTORC1 hyperactive sporadic cancer cell lines, two unusual results were observed. ELT3 cell lines were used to show that *Tsc2*-deficiency plays a role in selectivity in a cell line which is considered “hardier” than *Tsc2*-/- MEFs. ELT3 cells with the re-expression of TSC2 (ELT-T3) were used as a control to represent *Tsc2*+/+ MEFs. In the normal scenario, as seen in (Johnson *et al.* 2015; Johnson *et al.* 2018; McCann *et al.* 2018), the results from ELT3 cell lines are expected to be similar to those found in MEFs. In the case of cepharanthine/nelfinavir combination however, both ELT3 cell lines tested showed high cytotoxicity levels. High levels of toxicity were expected in wildtype ELT3 cells as seen in *Tsc2*-/- MEFs. However, in the ELT3-T3 cells, this level of cytotoxicity was not expected and significantly higher than compared to *Tsc2*+/+ MEFs. One reason for these high levels of cytotoxicity is possibly due to ELT3 cells having more mutations compared to MEFs (which only have mutations in *p53* and *Tsc2* as previously mentioned in Chapter 2). Getting a full detailed list of all the mutations in ELT3 cell lines used may allow for further investigations into possible modes of action based on the mutations present in the cells. Combining these results with the results of the rapamycin rescue assay carried out almost certainly confirms that lack of TSC2 or any activity of the mTOR pathway does not play a role in mechanism in which the cepharanthine/nelfinavir combination kills cells. Cepharanthine as a single agent also showed high levels of selectivity for wildtype ELT3 cells but at a lower rate compared to the cepharanthine/nelfinavir combination.

In HCT116 cells tested, the presence of 20 μM nelfinavir seemed to cause high levels of cell death. This is an unusual result as in Chapter 3, the presence of 10 μM nelfinavir caused minimal cell death to HCT116. It is an interesting observation that doubling the nelfinavir can cause such an increase in cell death as it could mean that using higher concentrations (such as 20 μM) of nelfinavir could be used as a monotherapy for this cell type of colorectal cancer. There are still plenty of opportunities for this combination with regards to sporadic tumours. Results from this chapter showed that against sporadic cell lines such as HCT116 and NCI-H460, the cepharanthine/nelfinavir combination worked exceptionally well against these tumour types and could be a viable treatment option in the future should the combination pass pre-clinical and clinical trials. Results also showed that the presence of the combination was able to cause high levels of cell death in the drug-

resistant cell line MCF7 compared to when these cells were treated with single agents or even the etoposide control. Because of this, further investigations into combination therapy as a treatment for forms of drug resistant breast cancer may be a viable option to undertake in the future. This is especially true with regards to identifying the mechanism of triggering cell death in this cell line which may be useful for treating other drug-resistant cell lines.

As described in this chapter's introduction, cepharanthine can be used as an autophagy inhibitor (Tang *et al.* 2018). Results showed that the combination was able to halt autophagy in both MEF cell lines after 3 h of treatment. However as seen in the autophagy time course, the evidence points to MEFs (both wildtype and mutant) being able to restore autophagic activity by the 24 h time point, indicating that while the combination disrupted autophagic activity, the effects were only short lived and more than likely does not play a role in cell death. The results of the bafilomycin A1 rescue assay, which was carried out to determine if bafilomycin A1 could prevent cell death, in a manner similar to that seen in chloroquine/nelfinavir combination (lysosomal accumulation of drug combination) (Johnson *et al*. 2015) also showed that lysosomal accumulation of cepharanthine/nelfinavir did not play a role in cell death.

Cepharanthine/nelfinavir combination was shown to cause a reduction in ROS production. This result is different from results seen in other treatments against other cancer cells. In both NSCLC cell lines H1299 and A549 and choroidal melanoma cells, the presence of cepharanthine caused an increase in ROS production which lead to cell death (Hua *et al*. 2015; Zhu *et al*. 2017a). However, one important fact to note is that the concentrations of cepharanthine used to cause cytotoxicity in the targeted cell lines were multiple fold higher compared to the 5 μM cepharanthine used in this chapter as Hua *et al.* (2015) used up to 120 μM and Zhu *et al.* (2017) used as high as 60 μM and even 80 μM in several experiments. In TK6 lymphoblastoid cells, a similar range of cepharanthine concentrations as to those in this chapter (up to 8.3 μM) were tested and similar results to the results in this chapter was observed in the form of ROS scavenging and protection of DNA (Sierra *et al*. 2015). The results of this chapter combined with the results observed in literature showed that cepharanthine can act as either a ROS scavenger or a ROS producer in a concentration-dependent. This knowledge could be useful for future cepharanthine-based combinations as it means the role of the cepharanthine can be changed based on the concentrations used if it does not induce high levels of

cytotoxicity in wild type normal cells. The NAC rescue assay also showed that ROS production did not play a role in cell death as the addition of NAC failed to rescue *Tsc2*-/- MEFs after 24 h treatment.

As with all combinations tested in this thesis, one of first ideas to what may be triggering cell death, was elevated levels of ER stress. When cells were treated with cepharanthine/nelfinavir combination, there were elevated expressions of the main components of the PERK pathway. Data from the XBP-1 splicing assay showed that the cepharanthine and nelfinavir combination was able to trigger near complete splicing of XBP-1. High levels of splicing were seen in cells treated with nelfinavir as a single agent although this was most likely due to the concentration of nelfinavir used (20 μM).

The cepharanthine/nelfinavir combination was tested in combination with methyl pyruvate to determine if energy stress was one of the principle causes of cell death. Results showed that the combination of cepharanthine and nelfinavir was causing cell death via energy stress death.

An unusual observation about cepharanthine is that there have been no major reports of significant safety issues or adverse effects (Masuda *et al.* 1993; Kakehi *et al.* 1994; Morita *et al.* 2002). As previously stated in Chapter 3, the original target population of this thesis were patients with TSC-associated tumours. Because of the many complications associated with TSC which were discussed in Chapter 1, it would be important to use drugs which would not worsen the effects associated with this disease. As a result, cepharanthine due to its low risk of adverse effects, would be a suitable candidate for future development of treatments and combinations for use in TSC patients and associated tumours.

In conclusion, the data showed that an optimised concentration of cepharanthine and nelfinavir synergised to selectively target mTORC1 hyperactive cells in a TSC-based or sporadic tumour-based setting. The data presented showed that cytotoxicity of the combined cepharanthine/nelfinavir treatment was likely due to an increase in energy stress, that was not optimally restored in cells without TSC2 and as a result, triggers cell death.

Chapter 7: General Discussion

7.1 Discussion introduction

The purpose of this thesis was to identify novel nelfinavir-based drug combinations that could be used to selectively kill mTORC1 hyperactive cells while being tolerated by wildtype cells. In this thesis, three nelfinavir-based combinations identified: mefloquine, Bortezomib and cepharanthine. The mefloquine/nelfinavir, Bortezomib/nelfinavir and cepharanthine/nelfinavir combinations were also investigated in depth to determine the mode of drug action to induce cytotoxicity in mTORC1 hyperactive cells. The data obtained from experimental work suggests that mefloquine/nelfinavir and cepharanthine/nelfinavir combinations caused cell death by induced energy stress possibly in combination with prolonged ER stress, while the Bortezomib/nelfinavir combination caused cytotoxicity via enhanced ER stress and proteasomal inhibition.

7.2 Optimisation and Synergy

7.2.1 Optimisation

A challenge associated with testing the cytotoxicity of drugs was choosing a suitable method to optimise the range of drug concentrations. Cell viability dyes such as resazurin and 3-(4,5-Dimethylthiazol-2-yl)-2,5-diphenyltetrazolium bromide (MTT) could be used, as they are suitable when screening cells in a 96 well plate format and would allow for a much wider spectrum of concentrations to be tested compared to using flow cytometry from cells grown on a 24-well plate. However, the main problem with these dyes is that they function via cell metabolism (converted from substrate to product via metabolic action of the tested cell). While this may be suitable in wildtype cells, *Tsc2*-/- MEFs are metabolically dysfunctional due to higher level of mTORC1 activation (as confirmed in the RNA sequencing in Chapter 3) meaning that there is a higher risk of false positives being generated.

The initial idea was to use the CyQUANT assay as it binds to DNA and not involved in metabolism and as a result avoids the above-mentioned concerns of false positivity. The CyQUANT is also a quick assay. Cells treated with the drugs can also be frozen (allowing for a flexible schedule of analysis) and was able to be

used in a 96-well plate format. However, the main problem with using the CyQUANT assay was that the assay was designed to show effects on cell number, which is dependent on both cell proliferation and loss of cell viability. As we see in Chapter 3 and Chapter 5, all drug combinations tested were able to affect cell number. This is likely due to reduced cell proliferation, to varying degrees. However, when the same conditions were tested via flow cytometry, there was no detectable cell death. Therefore, the CyQUANT experimental procedure was not sufficient to determine loss of cell viability due to the effects of the drugs. While the CyQUANT could show selectivity for reducing cell number between *Tsc2*+/+ and *Tsc2*-/- MEFs to a degree, it could not determine if inhibition of *Tsc2*+/+ cell numbers was due to cell death or simply the drug's effect to inhibit proliferation. For future projects, it is strongly recommended that CyQUANT assays should not be used exclusively as a technique to determine cell death. Rather, flow cytometry (using DRAQ7 or other cell death specific dye like propidium iodide) should be used as the principle measure of cell death for metabolically active *Tsc2*-/- MEFs.

There was a noticeable difference between the optimisation of mefloquine/nelfinavir and cepharanthine/nelfinavir. Mefloquine/nelfinavir optimisation was seen at only two sets of drug concentrations (as previously mentioned in Chapter 3); 5 μM mefloquine and 20 μM nelfinavir and 10 μM mefloquine and 10 μM nelfinavir. There was a narrow range of drug concentration where selectivity to cell death was observed in the *Tsc2*-/- MEFs. While the optimisation range for mefloquine/nelfinavir was incredible narrow, optimisation between cepharanthine and nelfinavir occurred over a wider range of cepharanthine concentration (when nelfinavir was set at 20 μM). At least three concentrations of cepharanthine showed high selectively for *Tsc2*-/- MEFs and were well tolerated by wildtype cells (which improved as cepharanthine concentration was reduced). However, a 10 μM nelfinavir base caused cepharanthine/nelfinavir combinations to become ineffective. It was also worth noting that the age of cells did not affect the cytotoxicity of the mefloquine/nelfinavir combination but did affect the cepharanthine/nelfinavir combination (initially a 2.5 μM cepharanthine/ 20 μM nelfinavir combination was chosen for further testing however, as discussed in Chapter 6; this concentration failed to kill *Tsc2*-/- MEFs after a passage number greater than 30). No optimisation was carried out on the Bortezomib/nelfinavir combination during this thesis as the chosen concentration of both drugs were determined previously (Johnson *et al.* 2018).

The drug concentrations used in chapter appear to fall into acceptable levels of testing. As discussed in chapter 3, the concentrations used for the mefloquine/nelfinavir combination (10 μM mefloquine and 10 μM nelfinavir) been shown to be viable in patients (nelfinavir 4.96-18 μM and mefloquine 2.1-23 μM (Marzolini *et al.* 2001; Zhang *et al.* 2001; Dow *et al.* 2005)). While the 20 μM nelfinavir used in the cepharanthine and bortezomib combinations falls slightly beyond the 18 μM range seen in Marzolini *et al. (*2001), nelfinavir at 20 μM has been used in several combinations for *in vitro* testing such as salinomycin and chloroquine (Johnson et al. 2015; Dunlop et al. 2017) and was lower than the nelfinavir concentration used with bortezomib in the treatment of cervical cancer cell lines (ranging from 26-35 μM (Bruning *et al.* 2011; Brüning *et al.* 2013)). The bortezomib concentration used in chapter 4 was similar to bortezomib/nelfinavir combinations against cervical cancer cell lines (39-50 nM).The 5 μM cepharanthine used in chapter 6 falls well with the concentration range used by *in vitro* studies; HeLa cells (IC_{50} of 8.9 μM), multiple myeloma cells (IC_{50} between 2 and 8 μM) and CRC cell lines (IC_{50} of between 2.4 μM and 5.3 μM) (Bun *et al*. 2008; Kikukawa *et al*. 2008; Law *et al*. 2015) while Hua *et al.* (2015) used up to 120 μM cepharanthine and Zhu *et al.* (2017) used as high as 60 μM and even 80 μM in several experiments.

7.2.2 Synergy

Both mefloquine/nelfinavir and cepharanthine/nelfinavir combinations had varying degrees on synergy. For the mefloquine/nelfinavir combinations, synergy for drug cytotoxicity was achieved only at 10 μM mefloquine and 10 μM nelfinavir and at 100 μM mefloquine and 10 μM nelfinavir in *Tsc2*-/- MEFs while in cepharanthine/nelfinavir combinations, all combinations tested in *Tsc2*-/- MEFs where shown to be synergistic (ranging from extremely synergistic to mildly synergistic). As shown in Chapter 3, mefloquine/nelfinavir combinations containing less than 10 μM mefloquine were extremely antagonistic compared to low concentration of cepharanthine/nelfinavir combinations (which were shown to be synergistic).

In *Tsc2*+/+ MEFs, mefloquine/nelfinavir was only synergistic at high concentrations (100 μM mefloquine/10 μM nelfinavir). At 10 μM mefloquine or lower, all the combinations were antagonistic (as seen and discussed in Chapter 3). Mefloquine/nelfinavir was well tolerated in the wildtype cells until the introduction of

higher concentration of mefloquine (>10 μM) which was shown to be cytotoxic. All cepharanthine/nelfinavir combinations were shown to be synergistic in the *Tsc2*-/- MEFs with combinations only showing reduced synergy (almost becoming additive) when the cepharanthine concentration in these combinations was reduced.

Synergy analysis was not carried out in this thesis for the nelfinavir and Bortezomib. However, synergy was undertaken by Johnson *et al.* (2018). They showed that like cepharanthine/nelfinavir combinations, combinations of Bortezomib and nelfinavir across a wide range of concentrations was synergistic in the *Tsc2*-/- MEFs. In *Tsc2*+/+ MEFs, the lowest concentration of Bortezomib/nelfinavir combination tested was shown to be antagonistic, while all other Bortezomib/nelfinavir combinations were shown to be synergistic.

7.3 Other cell lines

In this thesis, having shown that the mefloquine/nelfinavir and cepharanthine/nelfinavir combinations were able to selectively target mutated cells in a TSC-associated environment (i.e., *Tsc2*-/- MEFs), the next logical step was to determine cytotoxicity of these drug combinations on other TSC-associated (ELT3 cell lines) and sporadic cancer cell lines.

In ELT3 cell lines (which are *Tsc2*-null), results differed greatly when comparing the mefloquine/nelfinavir combination to the cepharanthine/nelfinavir combination. When treated with mefloquine/nelfinavir, both ELT3 cell lines (ELT3-V3 and the control ELT3-T3) showed similar results compared to those seen in the MEFs. On the other hand, the cepharanthine/nelfinavir combination was shown to cause non-selective cell death in both cell lines. The reason for this discrepancy between the two different drug combinations was already suggested in Chapter 6, as it may be possible that other mutations found in the ELT3 cells (they are cancer cells) may be sensitive to the cepharanthine/nelfinavir combination but not to mefloquine/nelfinavir combination. As mentioned in Chapter 6, an in-depth look at the mutations in the ELT3 cells may give clues into new possible targets to exploit.

As single drug agents, both cepharanthine and mefloquine were able to cause roughly the same amount of cell death in ELT3-V3 cells. In ELT3-T3 cells, mefloquine caused more cell death when compared to cepharanthine, however the introduction of nelfinavir did not affect the level of cell death caused by mefloquine,

while nelfinavir greatly enhanced cell death in these cells caused by cepharanthine. With regards, to nelfinavir, cell death in both cell lines were relatively similar when either 10 μM or 20 μM nelfinavir were used.

In this thesis, three mTORC1 hyperactive sporadic cancer cell lines representing three different cancer types were used; NCI-H460 (lung), HCT116 (CRC) and MCF7 (breast). When these three cancer types were treated with either mefloquine/nelfinavir combination or cepharanthine/nelfinavir combination, near complete eradication was seen in the NCI-H460 and HCT116 cells.

In MCF7 cells, both mefloquine/nelfinavir and cepharanthine/nelfinavir drug combinations were shown to induce a respectable level of cell death with over 60% cell death occurring in both treatments. Because of this result, a second breast cancer line (MBA-M40, which is tamoxifen resistant) was treated with both drug combinations. The observations made from the experiments with this cell line were positive as both combinations (as well as 10 μM mefloquine as a single agent) caused near-complete eradication of the cells. However, results from this analysis were limited as the high levels of cell death observed in the control cells (nearly 40 %). As a result, the data from MBA-M40 cells were not included in this thesis.

As a single drug agent, mefloquine could cause moderate levels of cell death in NCI-H460 and HCT116 cells when compared to cepharanthine-treated cells, although neither drug was able to kill the MCF7 cells without the addition of nelfinavir. As expected 20 μM nelfinavir caused a higher level of cell death compared to 10 μM nelfinavir in the NCI-H460 and HCT116 cells. An unusual observation was made when 20 μM nelfinavir was added to the HCT116 cells. It was found that 20 μM nelfinavir by itself caused over 60% cell death in the HCT116 cells. This high level of cell death in the HCT116 cells was not observed by Johnson *et al.* (2018) who found that nelfinavir only induced 20% cell death. The reason for this sizeable variance of cell death has not been determined but might be due to differences in passage number or the density of cells upon addition of nelfinavir.

While no work in this thesis was done with nelfinavir and Bortezomib in sporadic cell lines, Johnson *et al.* (2018) showed that this drug combination was able to cause significant cell death in HCT116 and NCI-H460 cell lines after just 24 h (at nearly 60%). Longer duration of treatment would be worthwhile for future studies, which might raise the percentage of cell death and drug effectiveness in MCF-7 cells.

7.4 Tumour spheroids

In a 2D tissue culture environment, mefloquine/nelfinavir, Bortezomib/nelfinavir and cepharanthine/nelfinavir combinations caused selective cytotoxicity to *Tsc2*-null and sporadic cancer cells. To progress our understanding of the combinations, the next step was to see whether they would also be effective in 3D tumour models, such as tumour spheroids. Tumours spheroids are thought to be the most suitable *in vitro* model for drug testing in oncology (Costa *et al.* 2016). This is due to their ability to reproduce common features found in solid tumours *in vivo.* These features include cellular heterogeneity (as spheroids could be generated from cancer cells cultured with other cell types (Costa *et al.* 2014)), cell-cell signalling, internal structure (different layers of cells which are affected by factors such as nutrients, oxygen, proliferation and pH (Koppenol *et al.* 2011)), cell-cell physical interactions (which can affect a drug's ability to penetrate a tumour spheroid (Ricci *et al.* 2013)), growth kinetics, gene expression and drug resistance.

The tumour colony formation assay is a tumourgenic assay that was originally used to identify and to help define tumour suppressor genes (Karuppusamy Rathinam *et al*. 2014). Tumour colony formation assays can also be used to determine if drugs (or drug combinations) have anti-tumourgenic properties (i.e., could be used as a preventative treatment as well as a curative treatment). Both mefloquine/nelfinavir and cepharanthine/nelfinavir combinations were shown to prevent the growth of soft agar-embedded tumour colonies over a 14-day period. As single agents, both mefloquine and 10 μM nelfinavir failed to inhibit the formation of tumour colonies while on the other hand, cepharanthine and 20 μM nelfinavir caused a moderate reduction in tumour colony formation. Bortezomib, as a single drug agent, was able to cause a 36% reduction to the formation of tumour colonies, while the combination of Bortezomib and nelfinavir was able to completely inhibit tumour colony formation similar to the results seen with both mefloquine and cepharanthine combinatory treatments with nelfinavir (Johnson *et al.* 2018).

While these results showed that all three nelfinavir drug combinations showed promise as preventative treatments for TSC patients who are prone to tumour development, it would be strongly recommended not to use the mefloquine/nelfinavir or the bortezomib/nelfinavir combinations for this purpose. This is due to the known side effects and weaknesses of both mefloquine and bortezomib (as discussed previously in Chapters 3 and 4). There is an argument to be made that rapamycin and (especially) everolimus could be used as a

preventative treatment, as supported by the results from the EXIST-1 trial. However, usage of rapalogs also carry complications of long-term usage such as pneumonitis (Atkins *et al.* 2004), immunosuppression (resulting in localized and systemic infections, including potentially life-threatening pneumonia and infections from bacteria, invasive fungi viral infections such as hepatitis B virus reactivation (Trelinska *et al.* 2015; Sadowski *et al.* 2016) and metabolic disorders (hyperglycaemia and diabetes (Vergès and Cariou 2015). Of all the drug combinations tested, the most promising for use as a preventative therapy would likely be cepharanthine/nelfinavir combination due to the lack of severe side effects associated with cepharanthine (although there are no studies into long-term usage of cepharanthine reported).

The tumour outgrowth carried out in this thesis was designed to examine the long-term effects of the drug combinations on established tumour spheroids and to investigate their penetration ability (i.e., whether the drug combination completely kill the bulk of tumour spheroids or only cause partial killing of the spheroid, allowing recovery of cells to grow back when the spheroid was replated into drug-free media). All three drug combinations were shown to cause complete penetration of tumour spheroid and could kill the spheroid, as shown by the failure of combination treated tumour spheroids to grow back once the spheroids were replated in fresh drug-free media. When the tumour spheroids were treated with any of the three drug combinations, all spheroids developed the same “fluffy” appearance (which may be due to cells on the outer rim dying and detaching from the spheroid). To determine if the drug combinations were effectively penetrating the spheroids, the spheroids were incubated with DRAQ7 (as a marker of cell death) for the last 48 h of drug treatment. Both mefloquine/nelfinavir and Bortezomib/nelfinavir treated tumour spheroids had incredibly high levels of DRAQ7 fluorescence when compared to the DMSO controls. This indicates that both drug combinations had the ability to fully penetrate tumour spheroids and cause cytotoxicity to all layers of the tumour spheroid.

Unusually, as discussed in Chapter 3, mefloquine (as a single drug agent)-treated spheroid also developed this “fluffy” appearance after 4 days of treatment and showed similar DRAQ7 fluorescence when compared to either mefloquine/nelfinavir or Bortezomib/nelfinavir combinations. However, this change in appearance and level of DRAQ7 fluorescence appeared to be superficial as mefloquine-treated spheroids grew out once replated in drug-free media. This

indicates that only the outer layers (and possibly not the core) of the spheroids were killed by mefloquine and that some cells survived this mono-drug therapy.

In DMSO solvent only, nelfinavir (at 20 μM and 10 μM) and cepharanthine (as a single agent) treated tumour spheroids: all treated tumour spheroids shared similar morphological appearance as round spheroids with low DRAQ7 fluorescence (indicating a higher proportion of cell survival) and grew back once they were re-plated in drug-free media (at varying rates). Cepharanthine-treated tumour spheroids rebounded a lot quicker compared to mefloquine-treated spheroids while 20 μM nelfinavir-treated spheroids were slower to grow out in comparison to the 10 μM nelfinavir-treated spheroids.

7.5 mTOR pathway

As the main aim of this thesis was to develop treatments which are selective for mTORC1 hyperactive cells, it was important to determine the potential effects of each drug combination on the mTORC1 pathway. In this thesis, the effects of mefloquine/nelfinavir and cepharanthine/nelfinavir combinations were examined. From data obtained from 6 h western blots both cepharanthine/nelfinavir and mefloquine/nelfinavir combination caused dephosphorylation of S6K1 and dephosphorylation of RSP6 (cepharanthine/nelfinavir treatment only) in the wildtype *Tsc2*+/+ MEFs. In *Tsc2*-/- MEFs, the cepharanthine/nelfinavir combination caused dephosphorylation of both S6K1 and RPS6, while treatment with mefloquine/nelfinavir caused no change in phosphorylation of S6K1 when compared to the DMSO control. To determine if mTORC1 signal transduction played a role in cell death, rapamycin was introduced to both nelfinavir drug combinations (to inhibit mTORC1 activity). Neither mefloquine/nelfinavir nor cepharanthine/nelfinavir treated *Tsc2*-/- MEFs were able to be rescued from cell death when rapamycin was introduced. This data shows that the state of mTORC1 activity in treated *Tsc2*-/- MEFs did not affect the mechanism of cytotoxicity triggered by either mefloquine/nelfinavir or cepharanthine/nelfinavir drug treatments. The state of mTORC1 activity also appeared not to play a role in the cytotoxicity of sporadic cancer cell lines (at least when treated with mefloquine/nelfinavir with or without rapamycin). This data strongly indicated that mefloquine/nelfinavir causes mTORC1-independent cell death in a variety of cell types. This could also be said

for the cepharanthine/nelfinavir combination, however, further testing in sporadic cancer cell lines would be required to validate this.

7.6 Autophagy and lysosomal activity

Mefloquine belongs to the quinine family (which contains known autophagy inhibitor chloroquine) and cepharanthine is also a known autophagy inhibitor (Johnson *et al*. 2015; Tang *et al*. 2018). Therefore, it was important to determine if either cepharanthine/nelfinavir or mefloquine/nelfinavir combination could affect autophagy and autophagy flux. It is possible that cytotoxicity of these drugs could be because of autophagy inhibition. After 3 h of treatment, both mefloquine/nelfinavir and cepharanthine/nelfinavir combinations were able to cause accumulation of LC3-II in both *Tsc2*+/+ and *Tsc2*-/- MEFs. The amount of LC3-II accumulation differed between the two drug combinations, as cepharanthine/nelfinavir was able to cause roughly the same amount of accumulation in both MEF lines (although the LC3-II accumulation in both cell lines were quite weak). On the other hand, accumulation of LC3-II was greater in the *Tsc2*+/+ MEFs than compared to the *Tsc2*-/- MEFs when cells were treated with the mefloquine/nelfinavir drug combination. Neither combination was able to cause much variation in the levels of p62 accumulation in either cell line.

As described in both Chapter 3 and Chapter 6, both mefloquine and cepharanthine are known to accumulate in the lysosome (Glaumann *et al.* 1992; Tang *et al.* 2018). Bafilomycin A1 was used to prevent H^+ build-up in lysosomes through the inhibition of v-ATPase leading to alkylation of the lysosomes. Consequently, Bafilomycin A1 prevented mefloquine drug accumulation within lysosomes (as quinine drugs become entrapped in acidic membrane compartments). Bafilomycin A1 was unsuccessful in rescuing *Tsc2-/-* MEFs from cell death with treatments with mefloquine, which suggested that the cytotoxic drug action of mefloquine is unlikely through the effects of mefloquine at lysosomes. Other acid membrane compartments where mefloquine could accumulate could possibly include mitochondria and the Golgi apparatus.

7.7 ROS production

From the observed data from Chapter 3 and Chapter 6, it is unlikely that the low level of ROS produced by either mefloquine/nelfinavir or cepharanthine/nelfinavir combinations influenced cell death in the *Tsc2*-/- MEFs. The low levels of ROS production was an unusual result for mefloquine/nelfinavir treatments, as mefloquine has previously been shown to enhance ROS production in prostate cancer cells (Yan *et al.* 2013), while nelfinavir has been shown to induce ROS production in breast cancer cells (Soprano *et al.* 2016). The low level of ROS production as a result of cepharanthine/nelfinavir treatment was expected, as the function of cepharanthine as a ROS producer or scavenger is determined by the concentration used (as discussed in detail in Chapter 6, where the concentrations used of cepharanthine in this thesis were unlikely to induce ROS) (Hua *et al*. 2015; Sierra *et al*. 2015; Zhu *et al*. 2017a). Interestingly, in mefloquine/nelfinavir-treated *Tsc2*-/- MEFs, NAC (non-significantly) caused a minor rescue in treated cells. However, no such rescue was achieved when NAC was introduced to cepharanthine/nelfinavir treated cells.

Loss of *TSC1* and *TSC2* and subsequent activation of mTORC1 is likely to increase the level of mitochondrial ROS and contribute to tumour formation through metabolic transformation. In MEFs and rat renal proximal tubular epithelial *Tsc2*-deficient cells, loss of *Tsc2* was shown to cause an increased expression of NADPH oxidase (Nox)1, Nox2, and Nox4 (Nox isoforms), which in turn, caused increased generation of ROS (Habib and Abboud 2016). Oxidative stress in cells can lead to increased expression of catalase and superoxide dismutase (SOD), which converts superoxides into water and restores oxidative stress (Wan *et al.* 2014). Glutathione synthetase (GSH) when inhibited by L-buthionine sulfoximine (BSO) was found to trigger cell death in *Tsc2*-/- MEFs (Li *et al.* 2016), and other antioxidant pathways (Lam *et al.* 2018). In *Tsc2*-/- MEFs, p62 accumulation levels remained roughly even, regardless of what treatment was used (as seen in Chapter 3 and Chapter 6). p62 in *Tsc2*-/- MEFs was found to protect the mitochondria from ROS production-associated damage by maintaining the levels of glutathione (an essential antioxidant) and possibly by promoting mitophagy (Lam *et al*. 2017b).

7.8 ER stress

The central hypothesis of this thesis was to exploit the homeostatic vulnerabilities within TSC2-deficient cells. mTORC1 hyperactivity enhances the volume of unfolded protein within the ER, as a result of heightened levels of *de novo* protein translation and a reduced efficiency of autophagy to remove the unfolded protein. Consequently, cell lines lacking *TSC2* become more sensitive to drug treatments that induce ER stress. Nelfinavir is a well-known ER stress enhancer and has been used as the basis for at least two other combination created by this research group (Johnson *et al*. 2015; Dunlop *et al*. 2017b). As a result, one of the initial ideas for the cytotoxic mechanism of the mefloquine, cepharanthine and/or Bortezomib combinations was prolonged ER stress.

All three combinations were able to induce the expression of components of the PERK pathway (ATF4, CHOP and GADD34). All three combinations were also shown to have little to no effect on the expression of IRE1α. As expected using 20 μM nelfinavir as a single agent increased expression of stress markers compared to 10 μM nelfinavir (used as a single agent).

The induction of ER stress was examined in detail in both Chapter 3 (mefloquine/nelfinavir) and Chapter 4 (Bortezomib/nelfinavir), with each giving an interesting insight into the induction of ER stress over time. At 6 h, both mefloquine and Bortezomib combinations resulted in the high expression of ATF4 and CHOP in both *Tsc2*+/+ and *Tsc2*-/- MEFs. After 16 h of treatment with Bortezomib/nelfinavir, ER stress recovery was observed in the *Tsc2*+/+ MEFs and unexpectedly in the *Tsc2*-/- MEFs. However, after 24 h of Bortezomib/nelfinavir treatment, expression of ER stress markers returned to similar levels seen in samples which were treated with mefloquine/nelfinavir combinations at 24 h and 48 h. To determine if this unexpected dip in expression levels was unique to the Bortezomib/nelfinavir treatment, it would be recommended post-thesis to carry out a short-term time course (6, 16, 24 h) using the mefloquine/nelfinavir and cepharanthine/nelfinavir treatments. All three combinations were able to cause near complete/ total splicing of XBP-1 with Bortezomib/nelfinavir showing the lowest amount of splicing. Interestingly, 20 μM nelfinavir (as a single agent) is nearly able to cause the same amount of splicing as Bortezomib/nelfinavir treatment (as seen in Chapter 4). Cepharanthine/nelfinavir, on the other hand caused near complete splicing. This indicates that while Bortezomib did not affect splicing levels when

combined with 20 μM nelfinavir, cepharanthine caused enhanced splicing when combined with the same concentration of nelfinavir.

While reviewing data from RNA sequencing, mefloquine/nelfinavir and Bortezomib/nelfinavir combinations, as carried out by (Johnson *et al.* 2018) were both shown to enhance expression of ER stress associated genes such *ATF4, CHOP (DDIT3), DDIT4* and *HSPA5* (HSP70) and *ERO1L* (which is involved in the formation of disulphide bonds in the ER lumen) in *Tsc2*+/+ and *Tsc2*-/- MEFs. Both drug combinations have also been shown to influence genes involved in pro-survival such as *IMPACT* and *TRAF5* as well as genes involved in pro-death such as ATF3.

7.9 Energy stress

In TSC2-deficient cells, ATP-heavy cellular activities such as lipogenesis and protein cause cells to become hypersensitive to glucose deprivation and highly dependent on glutamate dehydrogenase-dependent glutamine metabolism via the TCA cycle for survival (as discussed in Chapter 1). In order to counter this high energy demand, TSC-deficient cells enhance ATP generation by increasing mitochondrial biogenesis. Evidence of enhanced mitochondrial biogenesis was observed in the RNA sequencing carried out in Chapter 3 as *Tsc2*-/- MEFs naturally have a higher expression of genes involved in this process such as PPARGC1α, PPARδ, and PPARγ when compared to *Tsc2*+/+ MEFs. As previously mentioned in Chapter 3, this evidence showed that Tsc2-/- MEFs are sensitive to energy stress and could be a viable target for treatment.

Results from Chapters 3 and 6 showed that cell death in *Tsc2*-/- MEFs was rescued by the introduction of methyl pyruvate. Methyl pyruvate is a substrate of the TCA cycle which is preferentially metabolised in the mitochondria and is involved in stimulating ATP production and in supporting the conversion of pyruvate metabolites into amino acids (Jijakli *et al*. 2002). As methyl pyruvate rescued cell death from cepharanthine/nelfinavir and mefloquine/nelfinavir-based treatments, this gives evidence that both these drug combinations cause cell death via energy stress.

How methyl pyruvate could rescue these cells could one of several reasons: 1.) Methyl pyruvate replenishes the much-needed ATP for the Tsc2-/- MEFs, and as result, prevents energy deficiency; 2.) Methyl pyruvate is an alkalising agent (Jijakli *et al*. 2002) which could more indirectly prevent the cellular distribution of the

drugs to specific areas (such as mitochondria and/or lysosomes); 3.) methyl pyruvate is a ROS scavenger and could help in reducing the amount of ROS being produced by cells treated with the drug treatments (although from the data obtained from the ROS production assay in chapters 3 and 6 shows that ROS is unlikely to be involved in cytotoxicity).

What causes this increased energy stress in cells treated with mefloquine and cepharanthine combination may also be due to ER stress. While ER stress is unlikely the main trigger of cell death, recovery from ER stress might contribute to energy depletion through *de novo* protein synthesis of chaperone and heat shock proteins that are required for the unfolding and refolding of protein aggregates in the ER, processes that heavily consume ATP. As observed in both Chapter 3 and Chapter 4, ER stress can last up to 24 h, and even 48 h (in the case of mefloquine/nelfinavir) (Figure 7.1).

SESN2 (which acts as a link between ER stress and energy stress) was shown to be naturally elevated in *Tsc2*-/- MEFs compared to *Tsc2*+/+ MEFs. Neither mefloquine/nelfinavir or cepharanthine/nelfinavir combinations could affect expression levels of SESN2 at 6 h in *Tsc2*-/- MEFs. However, at 24 h, there was a noticeable difference in SESN2 expression in mefloquine/nelfinavir treated *Tsc2*-/- MEFs compared to DMSO and mefloquine/nelfinavir/methyl pyruvate-treated *Tsc2*-/- MEFs. This indicates the activation of energy stress in *Tsc2*-/- MEFs when treated with mefloquine/nelfinavir only occurred after prolonged exposure to drug therapy (which is corroborated by the energy stress time course carried out in Chapter 3).

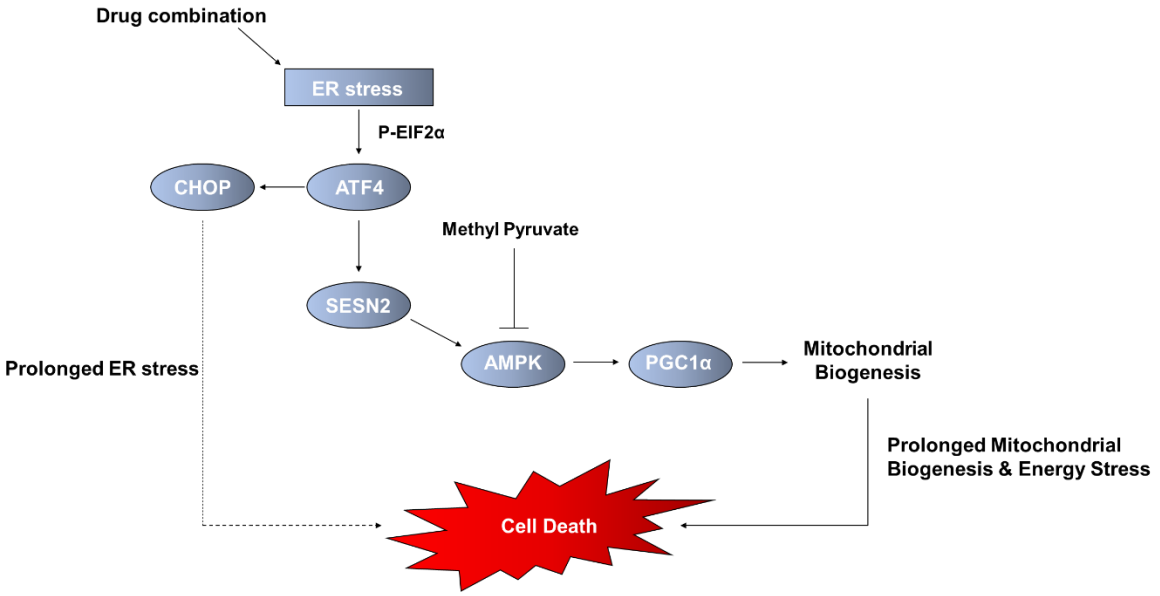

Figure 7.1: ER stress and energy stress. The introduction of drug combination caused ER stress via the PERK pathway. Production of ATF4 (combined with low ATP levels) caused activation of SESN2 which triggered the AMPK/PGC1α pathway resulting in mitochondrial biogenesis. Energy stress, which may be assisted by prolonged ER stress, triggered cell death in cells treated with drug combination.

The Bortezomib/nelfinavir combination was also tested using methyl pyruvate, however, the results from this assay showed that Bortezomib/nelfinavir did not cause energy stress. In fact, the introduction of methyl pyruvate caused a slight (non-significant) increase in cell death (after 24 h).

While this work explores drug treatments that were cytotoxic, there were differences in how the cells died depending on the treatment, i.e., whether cell death was controlled (apoptosis) or was uncontrolled (necrotic). Apoptosis is an ATP-dependent mechanism (Eguchi *et al.* 1997). As seen in Chapter 4, Bortezomib/nelfinavir treatment induced apoptosis via caspase 8 cleavage. Combined with the result of the methyl pyruvate assay from Chapter 4, this data showed that cell death by Bortezomib/nelfinavir combination is apoptotic in nature. On the other hand, evidence from Chapter 3 with regards to caspase cleavage and methyl pyruvate rescue could be seen as strong evidence that cell death caused by the mefloquine/nelfinavir combination is more likely to be uncontrolled. Whether or not this cell death is due to oncotic (impairment of ionic pumps, cell swelling, clearing of the cytosol, dilation of the ER and Golgi, mitochondrial condensation, chromatin clumping, and cytoplasmic bleb formation) or necrotic (the loss of cell membrane

integrity and an uncontrolled release of products of cell death into the extracellular space) in nature will require further examination post-thesis.

7.10 P-glycoprotein

Permeability glycoprotein (p-glycoprotein, also known as either multidrug resistance protein 1 (MDR1) or ATP-binding cassette sub-family B member 1 (ABCB1) or cluster of differentiation 243 (CD243)) is a 170 kDa membrane-associated glycoprotein and affiliated with the ABC superfamily. MDR1 is a product of the *MDR1* gene and functions an ATP-dependent efflux pump with broad substrate specificity which is responsible for pumping foreign substances (such as drugs) out of cells (Riffkin *et al.* 1996; Shao *et al.* 1997; Zhou *et al.* 2017). MDR1 is responsible for the development of multidrug resistance in several cancer types including breast, ovarian, bladder and oesophageal (Hanada *et al*. 2005; Zahedi *et al*. 2011; Rijpma *et al*. 2014; Zhou *et al*. 2017).

Through literature research, it became apparent that mefloquine, nelfinavir and cepharanthine are substrates of p-glycoprotein and shared the ability to inhibit p-glycoprotein activity. Cepharanthine-induced p-glycoprotein inhibition was shown to sensitize erythroleukemia cells (HEL) and gastric cancer cells (KATO-II) to tamoxifen (Mizobata *et al*. 2002), multidrug resistance (to vincristine, actinomycin D, daunomycin) in a KB epidermoid carcinoma cell subline (Shiraishi *et al.* 1987), oesophageal squamous cell carcinoma cells to cisplatin (Zhou *et al.* 2017) and ovarian cancer cell to docetaxel (Zahedi *et al.* 2011). The effects of mefloquine-induced p-glycoprotein inhibition was shown to affect a multi-drug resistant subline of the human oral squamous carcinoma cell lines KB and was described in detail in Chapter 3.

Nelfinavir is also a substrate of p-glycoprotein and has been shown to inhibit p-glycoprotein (Washington *et al.* 1998; Liu *et al.* 2018). However, as previously mentioned in Chapter 3, prolonged exposure to nelfinavir can cause an increase of P-glycoprotein expression that potentially could lead to reduced drug exposure after multiple doses (Faucette *et al*. 2004; Lucia *et al*. 2011). Choo *et al.* (2000) showed that inhibition of p-glycoprotein enhanced the distribution of nelfinavir, particularly to the brain and testes in male patients.

Mefloquine and cepharanthine are p-glycoprotein inhibitors and were shown to inhibit p-glycoprotein in both *Tsc2*+/+ and *Tsc2*-/- MEFs (both with mefloquine, and only the *Tsc2*-/- MEFs with cepharanthine) via rhodamine 123 uptake assay. It was hypothesised that the combination of cepharanthine/nelfinavir and mefloquine/nelfinavir would cause enhanced p-glycoprotein inhibition and be a cause of cell death via drug accumulation. However, results for both mefloquine/nelfinavir and cepharanthine/nelfinavir combinations showed stronger p-glycoprotein inhibition in *Tsc2*+/+ MEFs compared to *Tsc2-/-* MEFs.

One possible reason for low level of p-glycoprotein inhibition in *Tsc2*-/- MEFs may due to the type of experiment used. Rhodamine 123 is a substrate of p-glycoprotein (which is pumped out of the cell) and is often used to determine if a chemical alters p-glycoprotein function (higher uptake = less p-glycoprotein activity). While Rhodamine 123 is suitable for testing a single agent's effect on p-glycoprotein (as observed when mefloquine and cepharanthine were tested), using a combination of two chemicals, both of which are substrates of p-glycoprotein may have caused disruptions to the analysis possibly due to varying levels of selectivity of p-glycoprotein for each chemical. As a result, it is recommended that an alternative assay (possibly using labelled drugs, either radioactive or fluorescent) be used to determine if the results of Rhodamine 123 assay are correct or to give a better understanding of the relationship between the combinations and p-glycoprotein.

Bortezomib was also tested, as Bortezomib is a substrate of P-glycoprotein and P-glycoprotein expression causes Bortezomib-resistance in cancer cells treated with the drug (O'Connor *et al.* 2013). As expected Bortezomib failed to cause any inhibition of p-glycoprotein but the combination induced inhibition in both control and *Tsc2*-null cells and was most likely due to the presence of nelfinavir.

7.11 Comparing side effects

Nearly all the drugs used in this thesis have been shown to have some characteristic side effect associated with them. Bortezomib has its peripheral neurotoxicity (Bose *et al.* 2014) and potential for the target tumour cells to develop resistance after prolonged use (Lü *et al.* 2008; Oerlemans *et al.* 2008; Ri *et al.* 2010), which were discussed in detail in Chapter 4. The neurotoxic effect of mefloquine, such as seizures and neuropsychiatric adverse effects are discussed in Chapter 3.

Consequently, the side-effects of mefloquine has led to its replacement as a malaria treatment (Tickell-Painter *et al.* 2017; Remington L. Nevin 2012). However, of the three drug tested in combination with nelfinavir, cepharanthine is the only drug that that has mild side effects (Masuda *et al.* 1993; Kakehi *et al.* 1994; Morita *et al.* 2002). As the main target population of this thesis are TSC patients, it is vital that all complications associated with the disease be accounted for when developing treatments for TSC-associated tumours. Because of the low risk of adverse effects associated with cepharanthine, it would appear that cepharanthine would be the most suitable of the three drug combinations with nelfinavir for future work with regards to TSC-associated tumours.

7.12 Clinical relevance

To date, there have no reports of using either mefloquine/nelfinavir or cepharanthine/nelfinavir combinations being used as treatment for either TSC-associated tumours and/or sporadic cancers. Bortezomib/nelfinavir combination has been used several times before for the treatment of sporadic cancers such as cervical, ovarian, prostate and others as described in the introduction of Chapter 4. However, as mentioned in Chapter 4, this is the first time that Bortezomib and nelfinavir have been used in combination to target TSC-associated (or to be more precise, the first time that mTORC1 hyperactive cells have been shown to be sensitive to combined proteasomal inhibition and ER stress induction).

As discussed in their respective chapters, both mefloquine and cepharanthine (while not clinically approved for treatment at present) have been shown to have potent anticancer properties over a wide range of tumour types. As a result, combinations with nelfinavir could theoretically be used over a wide range of tumours (as many tumour types are also mTOR hyperactive as discussed in chapter 1).

These treatments also have clinical relevance as all drugs used in this thesis are clinically approved either as established anticancer treatments (as is the case of Bortezomib), or other medical treatment (malaria for mefloquine, HIV for nelfinavir and several different functions for cepharanthine in Japan as discussed in Chapter 6). Because of this, it is accepted that these drugs are safe to use in human patients and have established guidelines for usage and how to handle adverse effects. As a

result, this could allow all three combination therapies to be fast-tracked to clinical trials for both TSC-associated and sporadic cancers.

7.13 Future work

For the first step into future work, testing all three combinations in heterozygous *Tsc2*+/- MEFs would be the most logical. As mentioned in chapter 1, all TSC patients are *TSC1* or *TSC2* heterozygous (+/-). It is possible that these drug concentrations would have a higher basal level of toxicity in TSC patients. Furthermore, exosomes from *TSC1*-null cells have been shown to cause cells with preserved TSC1 function to behave like TSC1-/- cells (Patel *et al*. 2015), so these drugs might be cytotoxic to normal cells within the environment of the tumour site. Considering how potently cytotoxic the three combinations were against *Tsc2*-null MEFs, it is imperative that heterozygous cells that could mimic the 'normal' TSC patients' cells should also be tested. The main question involving heterozygous cells would be how well they would tolerate any of the three combinations (would these cells respond like the *Tsc2* wildtype with good tolerance or a worse response because of the heterozygosity of *Tsc2.* How the drug combinations' optimisation could be affected would also need to be answered as combinations may require lower concentrations of drugs to stabilise tolerance. While this may not be a problem for cepharanthine (as it works remarkably over a wide range of concentrations) and Bortezomib (as results were positive when cells were treated with either 50 nM or 20 nM Bortezomib/nelfinavir combinations). The problem arises in the case with mefloquine. As observed in Chapter 3 and discussed earlier in this chapter, mefloquine has an incredible narrow maximised therapeutic range and having to modify the concentration of either mefloquine or nelfinavir or both for *Tsc2*+/- MEFs could be disastrous for the combination effectiveness against *Tsc2-/-* MEFs and (in the worst-case scenario) render the combination useless for the treatment of TSC-associated tumours.

Should mefloquine/nelfinavir and/or cepharanthine/nelfinavir combinations show low cytotoxicity in *Tsc2*+/- MEFs, the next step would be to start testing in pre-clinical models. Bortezomib/nelfinavir has already been tested in mice bearing *Tsc2*-null ELT3 xenograft tumours (as seen in (Johnson *et al.* 2018)). Results showed combined nelfinavir and Bortezomib decreased tumour growth by approximately 70% compared with vehicle-treated mice. While Driessen *et al.* (2016) showed that

a Bortezomib/nelfinavir combination could be tolerated by human patients, the particular Bortezomib/nelfinavir combination used in this thesis and by Johnson *et al.* (2018) killed nearly 80 % of mice treated when compared to only approximately 14 % of mice in the vehicle treated group. Mefloquine/nelfinavir combinations (compared to cepharanthine/nelfinavir combinations) have better options with regards to types of tumours that can be tested. Mefloquine can pass the blood-brain barrier which means that mice models with SENs, SEGAs and cortical tubers can be used. It could also be important to use TSC mice models with epilepsy such as those developed by Zeng *et al.* (2011) to determine if the risk of mefloquine-associated seizures could worsen the frequency and severity of TSC-associated seizures. With cepharanthine/nelfinavir combinations, it would be interesting to see what side effects are observed in animals treated compared to cepharanthine as a single drug agent (which has been observed in human patients to have no adverse effects).

While earlier in the chapter (section 7.2.1), it was discussed how cepharanthine (when combined with 20 μM nelfinavir) can be used over a wider range of concentrations (5 μM – 1.25 μM tested) compared to mefloquine (which was only viable at 10 μM mefloquine and 10 μM nelfinavir and 5 μM mefloquine and 20 μM respectively). However, when compared to other drug treatments currently available for the treatment of TSC-associated and sporadic tumours, both drug combinations could be considered having very narrow windows of usage. As the work done in the thesis is purely *in vitro*, the use of animal models could be useful in investigating the maximised therapeutic range of these combinations. The main aim for using animal models in this manner would be to determine if the maximised therapeutic range could be made flexible in an *in vivo* environment, allow for a wider range of drug concentrations in each combination (provide that chosen concentrations maintain the high levels of selective cytotoxicity while producing minimal side effects).

From data obtained from the drug screen performed in Chapter 5, another drug combination that might be viable for the treatment of *Tsc2*-null tumours would be paroxetine and nelfinavir. Results from the drug screen showed that a combination of 5 μM paroxetine and 20 μM nelfinavir was well tolerated by control cells and caused considerable cytotoxicity to *Tsc2*-/- MEFs (over 60 %). The only reason further investigations into this combination were not pursued in this thesis was due to the comparatively better results obtained from the

cepharanthine/nelfinavir combination. From the initial data obtained in Chapter 5, like mefloquine/nelfinavir, paroxetine has a very narrow range as (when combined with 20 μM nelfinavir) a fold increase was shown to cause complete cell death in wildtype and mutant cells (data not shown), while a fold decrease caused a dramatic reduction in cytotoxicity. Further optimisation of drug (potentially by reducing the nelfinavir concentration allowing for wider range of paroxetine to be used) may be a potentially useful avenue to investigate in the future and could potentially lead to another successful nelfinavir-based therapeutic for the treatment of mTOR hyperactive tumours. It may also be important to determine if this concentration is biologically viable as well as patient who use paroxetine use it at a dose of 0.06 to 0.18 μM (Tomita *et al.* 2014).

7.14 Summary of thesis

The aim of this thesis was to identify novel drug combinations that selectively target TSC2-deficient cells. Through this work, the following significant findings have been discovered:

- The combination of mefloquine and nelfinavir caused selective cell death in mTORC1 hyperactive cells through energy stress.
- The combination of Bortezomib and nelfinavir caused selective cell death in mTORC1 hyperactive cells via prolonged ER stress and proteasome inhibition.
- After drug screening, a combination of cepharanthine and nelfinavir was able to cause cytotoxicity in mTORC1 hyperactive cells as a result of energy stress.
- Energy stress was shown to be a suitable vulnerability which could be exploited in terms of mTORC1 hyperactive cells.
- To date, none of the above combinations have been used in a TSC-based environment. Therefore, they could be of potential therapeutic use.

7.15 Conclusion

In conclusion, three novel nelfinavir-based treatments were presented in this thesis which selectively caused cell death in mTORC1 hyperactive cells while being tolerated by wildtype cells. Two of these combinations (mefloquine and cepharanthine) caused cytotoxicity via induced energy stress and potentially prolonged ER stress while the third (Bortezomib) caused cell death via inhibition of the proteasome and prolonged ER stress.

References:

Abbott, M. et al. 2016. AMPK Phosphorylates Desnutrin/ATGL and Hormone-Sensitive Lipase To Regulate Lipolysis and Fatty Acid Oxidation within Adipose Tissue. *Molecular and Cellular Biology* 36(14), pp. 1961–1976.

Adams, J. et al. 2004. Phase II Clinical Experience With the Novel Proteasome Inhibitor Bortezomib in Patients With Indolent Non-Hodgkin's Lymphoma and Mantle Cell Lymphoma. *Journal of Clinical Oncology* 23(4), pp. 676–684.

Adriaensen, M.E.A.P.M. et al. 2011. Radiological evidence of lymphangioleiomyomatosis in female and male patients with tuberous sclerosis complex. In: *Clinical Radiology*., pp. 625–628.

Ahmadian, M. et al. 2011. Desnutrin/ATGL is regulated by AMPK and is required for a brown adipose phenotype. *Cell Metabolism* 13(6), pp. 739–748.

Aizawa, Y. et al. 2016. The tuberous sclerosis complex model Eker (TSC2+/-) rat exhibits hyperglycemia and hyperketonemia due to decreased glycolysis in the liver. *Archives of Biochemistry and Biophysics* 590, pp. 48–55.

Al-Assar, O. et al. 2016. The radiosensitizing effects of Nelfinavir on pancreatic cancer with and without pancreatic stellate cells. *Radiotherapy and Oncology* 119(2), pp. 300–305.

Algra, A. et al. 2007. Overlapping neurologic and cognitive phenotypes in patients with TSC1 or TSC2 mutations. *Neurology* 70(12), pp. 908–915.

Alisky, J.M. et al. 2006. Drug interactions and pharmacogenetic reactions are the basis for chloroquine and mefloquine-induced psychosis. *Medical Hypotheses* 67(5), pp. 1090–1094.

Aminimoghaddam, S. et al. 2018. Outcome of treatment with EMA/EP (etoposide methotrexate and actinomycin-D/ etoposide and cisplatin) regimen in gestational trophoblastic neoplasia. *Medical Journal of The Islamic Republic of Iran* 32(1), pp. 210–213.

Appalla, D. et al. 2016. Mammalian Target of Rapamycin Inhibitor Induced Complete Remission of a Recurrent Subependymal Giant Cell Astrocytoma in a Patient Without Features of Tuberous Sclerosis Complex. *Pediatric Blood and Cancer*

63(7), pp. 1276–1278.

Arimochi, H. and Morita, K. 2006. Characterization of cytotoxic actions of tricyclic antidepressants on human HT29 colon carcinoma cells. *European Journal of Pharmacology* 541(1–2), pp. 17–23.

Asara, J.M. et al. 2012. TBC1D7 Is a Third Subunit of the TSC1-TSC2 Complex Upstream of mTORC1. *Molecular Cell* 47(4), pp. 535–546.

Asaumi, J.I. et al. 1995. Direct antitumor effect of cepharanthin and combined effect with adriamycin against Ehrlich ascites tumor in mice. *Anticancer Research* 15(1), pp. 67–70.

Atkins, M.B. et al. 2004. Randomized phase II study of multiple dose levels of CCI-779, a novel mammalian target of rapamycin kinase inhibitor, in patients with advanced refractory renal cell carcinoma. *Journal of Clinical Oncology* 22(5), pp. 909–918.

Aversa, F. et al. 2015. Mechanism of Action of Bortezomib and the New Proteasome Inhibitors on Myeloma Cells and the Bone Microenvironment: Impact on Myeloma-Induced Alterations of Bone Remodeling. *BioMed Research International* 2015, pp. 1–13.

Aylett, C.H.S. et al. 2016. Architecture of human mTOR complex 1. *Science* 351(6268), pp. 48–52.

Babcock, J.T. et al. 2013. Mammalian Target of Rapamycin Complex 1 (mTORC1) enhances bortezomib-induced death in Tuberous Sclerosis Complex (TSC)-null cells by a c-MYC-dependent induction of the unfolded protein response. *Journal of Biological Chemistry* 288(22), pp. 15687–15698.

Badawi, R.A. and Geddes, D.M. 2003. Exertional haemoptysis: LAM and TSC [1]. *Thorax*.

Baldassari, S. et al. 2016. GATOR1 complex: The common genetic actor in focal epilepsies. *Journal of Medical Genetics* 53(8), pp. 503–510.

Beaumont, T.L. et al. 2012. Advances in the management of subependymal giant cell astrocytoma. *Child's Nervous System* 28(7), pp. 963–968.

Ben-Sahra, I. et al. 2013. Stimulation of de novo pyrimidine synthesis by growth signaling through mTOR and S6K1. *Science* 339(6125), pp. 1323–1328.

Blanche, S. et al. 2016. In-utero exposure to nelfinavir-ethyl methyl sulfone. *Aids* 30(17), pp. 2729–2730.

Blumenthal, G.M. et al. 2014. A phase I trial of the HIV protease inhibitor nelfinavir in adults with solid tumors. *Oncotarget* 5(18).

Boettiger, D.C. et al. 2016. Is nelfinavir exposure associated with cancer incidence in HIV-positive individuals? *Aids* 30(10), pp. 1629–1637.

Bogorad, A.M. et al. 2017. Novel mechanisms of eIF2B action and regulation by eIF2 phosphorylation. *Nucleic Acids Research* 45(20), pp. 11962–11979.

Bose, P. et al. 2014. Bortezomib for the treatment of non-Hodgkin's lymphoma. *Expert Opinion on Pharmacotherapy* 15(16), pp. 2443–2459.

Both, P. et al. 2018. Tuberous sclerosis complex: Concerns and needs of patients and parents from the transitional period to adulthood. *Epilepsy and Behavior* 83, pp. 13–21.

Bouguéon, G. et al. 2015. Traitement des angiofibromes de la sclérose tubéreuse de Bourneville par des préparations topiques à base de sirolimus : état des lieux de la préparation en France et revue de la littérature. *Annales de Dermatologie et de Vénéréologie* 142(12), pp. S668–S669.

Bouguéon, G. et al. 2016. Formulation and characterization of a 0.1% rapamycin cream for the treatment of Tuberous Sclerosis Complex-related angiofibromas. *International Journal of Pharmaceutics* 509(1–2), pp. 279–284.

Bruning, A. et al. 2011. Bortezomib Targets the Caspase-Like Proteasome Activity in Cervical Cancer Cells, Triggering Apoptosis That Can be Enhanced by Nelfinavir. *Current cancer drug targets* 11(7), pp. 799–809.

Brüning, A. 2011. Analysis of nelfinavir-induced endoplasmic reticulum stress. *Methods in Enzymology* 491, pp. 127–142.

Brüning, A. et al. 2013. Nelfinavir and bortezomib inhibit mTOR activity via ATF4-mediated sestrin-2 regulation. *Molecular Oncology* 7(6), pp. 1012–1018.

Brüning, A. and Jückstock, J. 2015. Misfolded Proteins: From Little Villains to Little Helpers in the Fight Against Cancer. *Frontiers in Oncology* 5.

Budde, K. et al. 2015. Pharmacokinetics and pharmacodynamics of everolimus in patients with renal angiomyolipoma and tuberous sclerosis complex or

lymphangioleiomyomatosis. *British Journal of Clinical Pharmacology* 81(5), pp. 958–970.

Buijsen, J. et al. 2013. Phase i trial of the combination of the Akt inhibitor nelfinavir and chemoradiation for locally advanced rectal cancer. *Radiotherapy and Oncology* 107(2), pp. 184–188.

Bun, S.-S. et al. 2008. Cytotoxic activity of alkaloids isolated from Stephania rotunda in vitro cytotoxic activity of cepharanthine . *Phytotherapy Research* 23(4), pp. 587–590.

Cai, H. et al. 2017. Trifluoperazine Activates FOXO1-Related Signals to Inhibit Tumor Growth in Hepatocellular Carcinoma. *DNA and Cell Biology* 36(10), pp. 813–821.

Cai, Y. et al. 2018. Assessing the outcomes of everolimus on renal angiomyolipoma associated with tuberous sclerosis complex in China: A two years trial. *Orphanet Journal of Rare Diseases* 13(1), pp. 1–9.

Calkins, K.L. et al. 2018. Early dietary restriction in rats alters skeletal muscle tuberous sclerosis complex, ribosomal s6 and mitogen-activated protein kinase. *Nutrition Research* 54, pp. 93–104.

Campos, T. et al. 2016. Rapamycin requires AMPK activity and p27 expression for promoting autophagy-dependent Tsc2-null cell survival. *Biochimica et Biophysica Acta - Molecular Cell Research* 1863(6), pp. 1200–1207.

Cardamone, M. et al. 2014. Mammalian target of rapamycin inhibitors for intractable epilepsy and subependymal giant cell astrocytomas in tuberous sclerosis complex. *Journal of Pediatrics* 164(5), pp. 1195–1200.

Caron, A. et al. 2015. The Roles of mTOR Complexes in Lipid Metabolism. *Annual Review of Nutrition* 35(1), pp. 321–348.

Carsillo, T. et al. 2002. Mutations in the tuberous sclerosis complex gene TSC2 are a cause of sporadic pulmonary lymphangioleiomyomatosis. *Proceedings of the National Academy of Sciences* 97(11), pp. 6085–6090.

Castro, M. et al. 1995. Pulmonary tuberous sclerosis. *Chest*

Catley, L. et al. 2006. Aggresome induction by proteasome inhibitor bortezomib and α-tubulin hyperacetylation by tubulin deacetylase (TDAC) inhibitor LBH589 are

synergistic in myeloma cells. *Blood* 108(10), pp. 3441–3449.

Çelenk, P. et al. 2005. Fibrolipomatous hamartoma in a patient with tuberous sclerosis: Report of a case. *Oral Surgery, Oral Medicine, Oral Pathology, Oral Radiology and Endodontology* 99(2), pp. 202–206.

Cha, B. et al. 2018. Redox- and pH-Responsive Nanoparticles Release Piperlongumine in a Stimuli-Sensitive Manner to Inhibit Pulmonary Metastasis of Colorectal Carcinoma Cells. *Journal of Pharmaceutical Sciences* 107(10), pp. 2702–2712.

Champagnac, J. et al. 2016. Microaneurysms in renal angiomyolipomas: Can clinical and computed tomography features predict their presence and size? *Diagnostic and Interventional Imaging* 97(3), pp. 321–326.

Chang, L. et al. 2002. A central role for JNK in obesity and insulin resistance. *Nature* 420(6913), pp. 333–336.

Chang, W.Y.C. et al. 2014. A 2-year randomised placebo-controlled trial of doxycycline for lymphangioleiomyomatosis. In: *European Respiratory Journal*., pp. 1114–1123.

Chavez, A. et al. 2017. Post-transcriptional Regulation of De Novo Lipogenesis by mTORC1-S6K1-SRPK2 Signaling. *Cell* 171(7), pp. 1545-1558.e18.

Cheadle, J.P. et al. 2000. Molecular genetic advances in tuberous sclerosis. *Human Genetics* 107(2), pp. 97–114.

Chen, C.I. et al. 2007. Bortezomib is active in patients with untreated or relapsed Waldenström's macroglobulinemia: A phase II study of the National Cancer Institute of Canada Clinical Trials Group. *Journal of Clinical Oncology* 25(12), pp. 1570–1575.

Chen, D. et al. 2011. Bortezomib as the First Proteasome Inhibitor Anticancer Drug: Current Status and Future Perspectives. *Current Cancer Drug Targets* 11(3), pp. 239–253.

Chen, L. et al. 2016a. Glutamine deprivation plus BPTES alters etoposide- and cisplatin-induced apoptosis in triple negative breast cancer cells. *Oncotarget* 7(34), pp. 54691–54701.

Chen, X. et al. 2018. Trifluoperazine prevents FOXO1 nuclear excretion and

reverses doxorubicin-resistance in the SHG44/DOX drug-resistant glioma cell line. *International Journal of Molecular Medicine* 42(6), pp. 3300–3308.

Chen, X.M. et al. 2016b. Chelerythrine chloride induces apoptosis in renal cancer HEK-293 and SW-839 cell lines. *Oncology Letters* 11(6), pp. 3917–3924.

CHEON, J.H. et al. 2016. Highly Halaven-resistant KBV20C Cancer Cells Can Be Sensitized by Co-treatment with Fluphenazine. *Anticancer Research* 36(11), pp. 5867–5874.

Chiarini, F. et al. 2015. Current treatment strategies for inhibiting mTOR in cancer. *Trends in Pharmacological Sciences* 36(2), pp. 124–135.

Cho, C.H. 2011. Frontier of epilepsy research - mtor signaling pathway. *Experimental and Molecular Medicine* 43(5), pp. 231–274.

Choi, A.R. et al. 2016a. Attenuation of colchicine toxicity in drug-resistant cancer cells by co-treatment with anti-malarial drugs. *Anticancer Research* 36(11), pp. 5859–5866.

Choi, Y. et al. 2016b. An Insight into Drug Repositioning for the Development of Novel Anti-Cancer Drugs. *Current Topics in Medicinal Chemistry* 16(19), pp. 2156–2168.

Chong, Z. 2015. mTOR: A Novel Therapeutic Target for Diseases of Multiple Systems. *Current Drug Targets* 16(10), pp. 1107–1132.

Choo, A.Y. et al. 2010. Glucose Addiction of TSC Null Cells Is Caused by Failed mTORC1-Dependent Balancing of Metabolic Demand with Supply. *Molecular Cell* 38(4), pp. 487–499.

Choo, E.F. et al. 2000. Pharmacological inhibition of P-glycoprotein transport enhances the distribution of HIV-1 protease inhibitors into brain and testes. *Drug metabolism and disposition: the biological fate of chemicals* 28(6), pp. 655–60.

Chou, C.T. et al. 2007. Paroxetine-induced apoptosis in human osteosarcoma cells: Activation of p38 MAP kinase and caspase-3 pathways without involvement of [Ca2+]i elevation. *Toxicology and Applied Pharmacology* 218(3), pp. 265–273.

Chrast, J. et al. 2014. TBC1D7 Mutations are Associated with Intellectual Disability, Macrocrania, Patellar Dislocation, and Celiac Disease . *Human Mutation* 35(4), pp. 447–451..

Chu-Shore, C.J. et al. 2009. Cyst-like tubers are associated with TSC2 and epilepsy in tuberous sclerosis complex. *Neurology* 72(13), pp. 1165–1169.

Chu, S.C. et al. 1999. Comprehensive evaluation of 35 patients with lymphangioleiomyomatosis. *Chest* 115(4), pp. 1041–1052.

Clemens, M.J. 2013. Initiation Factor eIF2α Phosphorylation in Stress Responses and Apoptosis., pp. 57–89.

Cook, M.T. 2018. Mechanism of metastasis suppression by luteolin in breast cancer. *Breast Cancer: Targets and Therapy* 10, pp. 89–100.

Costa, E.C. et al. 2014. Optimization of liquid overlay technique to formulate heterogenic 3D co-cultures models. *Biotechnology and Bioengineering* 111(8), pp. 1672–1685.

Costa, E.C. et al. 2016. 3D tumor spheroids: an overview on the tools and techniques used for their analysis. *Biotechnology Advances* 34(8), pp. 1427–1441.

Costello, L.C. et al. 2000. High frequency of pulmonary lymphangioleiomyomatosis in women with tuberous sclerosis complex. *Mayo Clinic Proceedings* 75(6), pp. 591–594.

Courtwright, A.M. et al. 2017. The effect of mTOR inhibitors on respiratory infections in lymphangioleiomyomatosis. *European Respiratory Review* 26(143), pp. 0–6.

Crino, P.B. 2013. Evolving neurobiology of tuberous sclerosis complex. *Acta Neuropathologica* 125(3), pp. 317–332.

Cuccia, V. et al. 2003. Subependymal giant cell astrocytoma in children with tuberous sclerosis. *Child's nervous system : ChNS : official journal of the International Society for Pediatric Neurosurgery* 19(4), pp. 232–43.

Curatolo, P. et al. 2001. Vigabatrin for tuberous sclerosis complex. In: *Brain and Development*., pp. 649–653.

Curatolo, P. et al. 2016. The Role of mTOR Inhibitors in the Treatment of Patients with Tuberous Sclerosis Complex: Evidence-based and Expert Opinions. *Drugs* 76(5), pp. 551–565.

Dabora, S.L. et al. 2011. Multicenter phase 2 trial of sirolimus for tuberous sclerosis: kidney angiomyolipomas and other tumors regress and VEGF- D levels decrease. Zoccali, C. ed. *PloS one* 6(9), p. e23379.

Dadey, D.Y.A. et al. 2016. Laser interstitial thermal therapy for subependymal giant cell astrocytoma: technical case report. *Neurosurgical Focus* , p. E9.

Dakhil, S.R. et al. 2010. Bortezomib, Paclitaxel, and Carboplatin as a First-Line Regimen for Patients with Metastatic Esophageal, Gastric, and Gastroesophageal Cancer: Phase II Results from the North Central Cancer Treatment Group (N044B). *Journal of Thoracic Oncology* 3(5), pp. 516–520.

Dibble, C.C. and Cantley, L.C. 2015. Regulation of mTORC1 by PI3K signaling. *Trends in Cell Biology* 25(9), pp. 545–555.

Dick, L.R. and Fleming, P.E. 2010. Building on bortezomib: second-generation proteasome inhibitors as anti-cancer therapy. *Drug Discovery Today* 15(5–6), pp. 243–249.

Dimopoulos, M. et al. 2010. The efficacy and safety of lenalidomide plus dexamethasone in relapsed and/or refractory multiple myeloma patients with impaired renal function. *Cancer* 116(16), pp. 3807–14.

Divakaruni, A.S. et al. 2013. Thiazolidinediones are acute, specific inhibitors of the mitochondrial pyruvate carrier. *Proceedings of the National Academy of Sciences* 110(14), pp. 5422–5427.

Dodd, K.M. et al. 2015. mTORC1 drives HIF-1α and VEGF-A signalling via multiple mechanisms involving 4E-BP1, S6K1 and STAT3. *Oncogene* 34(17), pp. 2239–2250.

Dodd, K.M. and Dunlop, E.A. 2016. Tuberous sclerosis-A model for tumour growth. *Seminars in Cell and Developmental Biology* 52, pp. 3–11.

Domanska-Pakiela, D. et al. 2002. Mutational Analysis in a Cohort of 224 Tuberous Sclerosis Patients Indicates Increased Severity of TSC2, Compared with TSC1, Disease in Multiple Organs. *The American Journal of Human Genetics* 68(1), pp. 64–80.

Dou, Q. and Zonder, J. 2014. Overview of Proteasome Inhibitor-Based Anti-cancer Therapies: Perspective on Bortezomib and Second Generation Proteasome Inhibitors versus Future Generation Inhibitors of Ubiquitin-Proteasome System. *Current Cancer Drug Targets* 14(6), pp. 517–536.

Dou, Q.P. et al. 2013. From Bortezomib to other Inhibitors of the Proteasome and Beyond. *Current Pharmaceutical Design* 19(22), pp. 4025–4038.

Dou, Q.P. and Li, B. 1999. Proteasome inhibitors as potential novel anticancer agents. *Drug Resistance Updates* 2(4), pp. 215–223.

Dow, G.S. et al. 2005. Transcriptional profiling of mefloquine-induced disruption of calcium homeostasis in neurons in vitro. *Genomics* 86(5), pp. 539–550.

Driessen, C. et al. 2016. Treatment with the HIV protease inhibitor nelfinavir triggers the unfolded protein response and may overcome proteasome inhibitor resistance of multiple myeloma in combination with bortezomib: A phase I trial (SAKK 65/08). *Haematologica* 101(3), pp. 346–355.

Du, J. et al. 2017. Presurgical Administration of mTOR Inhibitors in Patients with Large Subependymal Giant Cell Astrocytoma Associated with Tuberous Sclerosis Complex. *World Neurosurgery* 107, pp. 1053.e1-1053.e6.

Duncan, J.G. 2011. Peroxisome Proliferator Activated Receptor-Alpha (PPARα) and PPAR gamma coactivator-1alpha (PGC-1α) regulation of cardiac metabolism in diabetes. In: *Pediatric Cardiology*., pp. 323–328.

Dunlop, E.A. et al. 2017. Targeting protein homeostasis with nelfinavir/salinomycin dual therapy effectively induces death of mTORC1 hyperactive cells. *Oncotarget* 8(30). Available at: http://www.oncotarget.com/fulltext/16232.

Dunlop, E.A. and Tee, A.R. 2013. The kinase triad, AMPK, mTORC1 and ULK1, maintains energy and nutrient homoeostasis. *Biochemical Society Transactions* 41(4), pp. 939–943.

Dunlop, E.A. and Tee, A.R. 2014. mTOR and autophagy: A dynamic relationship governed by nutrients and energy. *Seminars in Cell & Developmental Biology* 36(October), pp. 121–129.

Dwivedi, A. et al. 2016. Plasmodium falciparum parasite population structure and gene flow associated to anti-malarial drugs resistance in Cambodia. *Malaria Journal* 15(1), pp. 1–12.

Dwyer, J.M. et al. 1971. Pulmonary tuberous sclerosis. Report of three patients and a review of the literature. *The Quarterly journal of medicine* 40(157), pp. 115–25.

Ebert, S.M. et al. 2015. Identification and small molecule inhibition of an activating transcription factor 4 (ATF4)-dependent pathway to age-related skeletal muscle weakness and atrophy. *Journal of Biological Chemistry* 290(42), pp. 25497–25511.

Edashige, K. et al. 1991. Inhibition of 12-O-tetradecanoyl phorbol-13-acetate promoted tumorigenesis by cepharanthine, a biscoclaurine alkaloid, in relation to the inhibitory effect on protein kinase C. *Biochemical Pharmacology* 41(1), pp. 71–78.

Edwards, S.J. et al. 2015. Topotecan, pegylated liposomal doxorubicin hydrochloride, paclitaxel, trabectedin and gemcitabine for advanced recurrent or refractory ovarian cancer: A systematic review and economic evaluation. *Health Technology Assessment* 19(7), pp. 1–524.

Efeyan, A. and Sabatini, D.M. 2010. MTOR and cancer: Many loops in one pathway. *Current Opinion in Cell Biology* 22(2), pp. 169–176.

Eguchi, Y. et al. 1997. Intracellular ATP levels determine cell death fate by apoptosis or necrosis. *Cancer Research* .

Ehninger, D. and Silva, A.J. 2011. Rapamycin for treating Tuberous sclerosis and Autism spectrum disorders. *Trends in Molecular Medicine* 17(2), pp. 78–87.

El-Hashemite, N. et al. 2003. Loss of Tsc1 or Tsc2 induces vascular endothelial growth factor production through mammalian target of rapamycin. *Cancer Research* 63(17), pp. 5173–5177.

Escalante, A.M. et al. 2013. Preventing the autophagic survival response by inhibition of calpain enhances the cytotoxic activity of bortezomib in vitro and in vivo. *Cancer Chemotherapy and Pharmacology* 71(6), pp. 1567–1576.

Evans, L.T. et al. 2012. Epilepsy surgery in tuberous sclerosis: a review. *Neurosurgical Focus* 32(3), p. E5.

Fang, Y.C. et al. 2011. Paroxetine-induced Ca2+movement and death in OC2 human oral cancer cells. *Chinese Journal of Physiology* 54(5), pp. 310–317.

Fang, Z.H. et al. 2013. Inhibition of signal transducer and activator of transcription 3 and cyclooxygenase-2 is involved in radiosensitization of cepharanthine in HeLa cells. *International Journal of Gynecological Cancer* 23(4), pp. 608–614.

Farooqi, A.A. et al. 2018. Piperlongumine as anticancer agent: The story so far about killing many birds with one stone. *Cellular and Molecular Biology* 64(11), p. 102.

Faucette, S.R. et al. 2004. Regulation of CYP2B6 in primary human hepatocytes by

prototypical inducers. *Drug Metabolism and Disposition* 32(3), pp. 348–358.

Feng, X.Q. et al. 2018a. Luteolin and sorafenib combination kills human hepatocellular carcinoma cells through apoptosis potentiation and JNK activation. *Oncology Letters* 16(1), pp. 648–653.

Feng, Z. et al. 2018b. The antipsychotic agent trifluoperazine hydrochloride suppresses triple-negative breast cancer tumor growth and brain metastasis by inducing G0/G1 arrest and apoptosis. *Cell Death and Disease* 9(10), p. 1006.

Franz, D.N. et al. 2013. Efficacy and safety of everolimus for subependymal giant cell astrocytomas associated with tuberous sclerosis complex (EXIST-1): A multicentre, randomised, placebo-controlled phase 3 trial. *The Lancet* 381(9861), pp. 125–132.

Franz, D.N. et al. 2016. Long-term use of everolimus in patients with tuberous sclerosis complex: Final results from the EXIST-1 study. *PLoS ONE* 11(6), pp. 1–13.

Franz, D.N. et al. 2013. Mutational and Radiographic Analysis of Pulmonary Disease Consistent with Lymphangioleiomyomatosis and Micronodular Pneumocyte Hyperplasia in Women with Tuberous Sclerosis. *American Journal of Respiratory and Critical Care Medicine* 164(4), pp. 661–668. doi: 10.1164/ajrccm.164.4.2011025.

French, J.A. et al. 2016. Adjunctive everolimus therapy for treatment-resistant focal-onset seizures associated with tuberous sclerosis (EXIST-3): a phase 3, randomised, double-blind, placebo-controlled study. *The Lancet* 388(10056), pp. 2153–2163.

Friedlander, R. et al. 2000. A regulatory link between ER-associated protein degradation and the unfolded-protein response. *Nature Cell Biology* 2(7), pp. 379–384.

Fujii, T. et al. 2007. Malaria and mefloquine prophylaxis use among Japan ground self-defense force personnel deployed in East Timor. *Journal of Travel Medicine* 14(4), pp. 226–232.

Furusawa, S. and Wu, J. 2007. The effects of biscoclaurine alkaloid cepharanthine on mammalian cells: Implications for cancer, shock, and inflammatory diseases. *Life Sciences* 80(12), pp. 1073–1079.

Gallagher, L. et al. 2016. Advances in Autophagy Regulatory Mechanisms. *Cells* 5(2), p. 24.

Galvin, J.R. et al. 2007. Lymphangioleiomyomatosis: Radiologic-Pathologic Correlation. *RadioGraphics* 25(3), pp. 803–828.

Ganley, I.G. et al. 2011. Distinct Autophagosomal-Lysosomal Fusion Mechanism Revealed by Thapsigargin-Induced Autophagy Arrest. *Molecular Cell* 42(6), pp. 731–743.

Gao, L. et al. 2014. In pulmonary lymphangioleiomyomatosis expression of progesterone receptor is frequently higher than that of estrogen receptor. *Virchows Archiv* 464(4), pp. 495–503.

Garcia, D. and Shaw, R.J. 2017. AMPK: Mechanisms of Cellular Energy Sensing and Restoration of Metabolic Balance. *Molecular Cell* 66(6), pp. 789–800.

De Gassart, A. and Martinon, F. 2017. Translating the anticancer properties of eEF2K. *Cell Cycle* 16(4), pp. 299–300.

Geng, Y. et al. 2010. Chloroquine-induced autophagic vacuole accumulation and cell death in glioma cells is p53 independent. *Neuro-Oncology* 12(5), pp. 473–481.

Gergely, P. et al. 2009. Dual role of poly(ADP-ribose) glycohydrolase in the regulation of cell death in oxidatively stressed A549 cells. *The FASEB Journal* 23(10), pp. 3553–3563.

Gil-Ad, I. et al. 2008. Evaluation of the potential anti-cancer activity of the antidepressant sertraline in human colon cancer cell lines and in colorectal cancer-xenografted mice. *International Journal of Oncology* 33(2), pp. 277–286.

Gill, S. et al. 2005. PS-341 and gemcitabine in patients with metastatic pancreatic adenocarcinoma: a North Central Cancer Treatment Group (NCCTG) randomized phase II study. *Annals of Oncology* 16(10), pp. 1654–1661.

Gills, J.J. et al. 2007a. Nelfinavir, A Lead HIV Protease Inhibitor, Is a Broad-Spectrum, Anticancer Agent that Induces Endoplasmic Reticulum Stress, Autophagy, and Apoptosis In vitro and In vivo. *Clinical Cancer Research* 13(17), pp. 5183–5194.

Gipson, T.T. and Johnston, M. V. 2017. New insights into the pathogenesis and prevention of tuberous sclerosis-associated neuropsychiatric disorders (TAND).

F1000Research 6(0), p. 859.

Glace, L. et al. 2009. Estrogen-induced stromal cell-derived factor-1 (SDF-1/Cxcl12) expression is repressed by progesterone and by Selective Estrogen Receptor Modulators via estrogen receptor α in rat uterine cells and tissues. *Steroids* 74(13–14), pp. 1015–1024.

Glaumann, H. et al. 1992. Intracellular distribution and effect of the antimalarial drug mefloquine on lysosomes of rat liver. *Liver* 12(4), pp. 183–190.

Gocke, E. et al. 2009. Literature review on the genotoxicity, reproductive toxicity, and carcinogenicity of ethyl methanesulfonate. *Toxicology Letters* 190(3), pp. 254–265.

Goedbloed, M. et al. 2006. Unusually mild tuberous sclerosis phenotype is associated with TSC2 R905Q mutation . *Annals of Neurology* 60(5), pp. 528–539.

Gokarn, A. et al. 2018. Lomustine, cytarabine, cyclophosphamide, etoposide – An effective conditioning regimen in autologous hematopoietic stem cell transplant for primary refractory or relapsed lymphoma: Analysis of toxicity, long-term outcome, and prognostic factors. *Journal of Cancer Research and Therapeutics* 14(5), p. 926.

Golden, E.B. et al. 2009. Green tea polyphenols block the anticancer effects of bortezomib and other boronic acid-based proteasome inhibitors. *Blood* 113(23), pp. 5927–5937.

Gómez, M.R. 1995. History of the tuberous sclerosis complex. *Brain and Development* 17(SUPPL. 1), pp. 55–57.

González, R. et al. 2014. Mefloquine safety and tolerability in pregnancy: A systematic literature review. *Malaria Journal* 13(1), p. 75.

González, R. et al. 2018. Mefloquine for preventing malaria in pregnant women. *Cochrane Database of Systematic Reviews* 2018(3), p. CD011444.

Graves, P.R. 2003. Discovery of Novel Targets of Quinoline Drugs in the Human Purine Binding Proteome. *Molecular Pharmacology* 62(6), pp. 1364–1372.

Groenewoud, M.J. and Zwartkruis, F.J.T. 2013. Rheb and Rags come together at the lysosome to activate mTORC1: Figure 1. *Biochemical Society Transactions* 41(4), pp. 951–955.

Guan, M. et al. 2015. Nelfinavir and nelfinavir analogs block site-2 protease

cleavage to inhibit castration-resistant prostate cancer. *Scientific Reports* 5(1), p. 9698.

Guba, M. et al. 2002. Rapamycin inhibits primary and metastatic tumor growth by antiangiogenesis: Involvement of vascular endothelial growth factor. *Nature Medicine* 8(2), pp. 128–135.

Habib, S.L. and Abboud, H.E. 2016. Tuberin regulates reactive oxygen species in renal proximal cells, kidney from rodents, and kidney from patients with tuberous sclerosis complex. *Cancer Science* 107(8), pp. 1092–1100.

Hahn-windgassen, A. et al. 2005. Akt activates mTOR by regulating cellular ATP level and AMPK activity. *Journal of Biological Chemistry* 280(4).

Hanada, T. et al. 2005. Reversal of P-Glycoprotein-mediated Paclitaxel Resistance by New Synthetic Isoprenoids in Human Bladder Cancer Cell Line. *Japanese Journal of Cancer Research* 93(9), pp. 1037–1046.

Hanahan, D. and Weinberg, R.A. 2011. Hallmarks of cancer: The next generation. *Cell* 144(5), pp. 646–674.

Hande, K.R. 1998. Etoposide: Four decades of development of a topoisomerase II inhibitor. *European Journal of Cancer* 34(10), pp. 1514–1521.

Harada, K. et al. 2001. Characteristics of antitumour activity of cepharanthin against a human adenosquamous cell carcinoma cell line. *Oral Oncology* 37(8), pp. 643–651.

Harada, K. et al. 2009a. Cepharanthine inhibits angiogenesis and tumorigenicity of human oral squamous cell carcinoma cells by suppressing expression of vascular endothelial growth factor and interleukin-8. *International Journal of Oncology* 35(5), pp. 1025–1035.

Harada, K. et al. 2009b. Effects of cepharanthine alone and in combination with fluoropyrimidine anticancer agent, S-1, on tumor growth of human oral squamous cell carcinoma xenografts in nude mice. *Anticancer Research* 29(4), pp. 1263–1270.

Harada, T. et al. 2012. The enhancement of tumor radioresponse by combined treatment with cepharanthine is accompanied by the inhibition of DNA damage repair and the induction of apoptosis in oral squamous cell carcinoma. *International Journal of Oncology* 41(2), pp. 565–572.

Hardie, D.G. 2013. AMPK: A Target for Drugs and Natural Products With Effects on Both Diabetes and Cancer. *Diabetes* 62(7), pp. 2164–2172.

Hardie, D.G. 2015. AMPK: Positive and negative regulation, and its role in whole-body energy homeostasis. *Current Opinion in Cell Biology* 33, pp. 1–7.

Harding, H.P. et al. 1999. Protein translation and folding are coupled by an endoplasmic- reticulum-resident kinase. *Nature* 397(6716), pp. 271–274.

Harhaji-Trajkovic, L. et al. 2012. Chloroquine-mediated lysosomal dysfunction enhances the anticancer effect of nutrient deprivation. *Pharmaceutical Research* 29(8), pp. 2249–2263.

Hatch, S.D. et al. 2002. Viracept (Nelfinavir Mesylate, AG1343): A Potent, Orally Bioavailable Inhibitor of HIV-1 Protease. *Journal of Medicinal Chemistry* 40(24), pp. 3979–3985.

Hawley, S. a et al. 2003. Complexes between the LKB1 tumor suppressor, STRAD alpha/beta and MO25 alpha/beta are upstream kinases in the AMP-activated protein kinase cascade. *J Biol* 2(4), p. 28.

He, M. et al. 2017. Additive effects of cherlerythrine chloride combination with erlotinib in human nonsmall cell lung cancer cells. *PLoS ONE* 12(4).

Hess, E.J. et al. 2016. Cannabidiol as a new treatment for drug-resistant epilepsy in tuberous sclerosis complex. *Epilepsia* 57(10), pp. 1617–1624.

Hidaka, T. et al. 2018. Large Cell Neuroendocrine Carcinoma of the Mediastinum Successfully Treated with Systemic Chemotherapy after Palliative Radiotherapy. *Internal Medicine* 58(4), pp. 563–568.

Hill, E.J. et al. 2016. Clinical trial of oral nelfinavir before and during radiation therapy for advanced rectal cancer. *Clinical Cancer Research* 22(8), pp. 1922–1931.

Hinnebusch, A.G. 2000. *Mechanism and Regulation of Initiator Methionyl-tRNA Binding to Ribosomes*.

Hoelz, H. et al. 2018. Childhood-Onset Epileptic Encephalopathy Associated With Isolated Focal Cortical Dysplasia and a Novel TSC1 Germline Mutation. *Clinical EEG and Neuroscience* 49(3), pp. 187–191.

Holmer, R. et al. 2015. Interleukin-6 trans-signaling increases the expression of carcinoembryonic antigen-related cell adhesion molecules 5 and 6 in colorectal

cancer cells. *BMC cancer* 15, p. 975.

Hoover, A.C. et al. 2015. Efficacy of nelfinavir as monotherapy in refractory adenoid cystic carcinoma: Results of a phase II clinical trial. *Head and Neck* 37(5), pp. 722–726.

Hotamisligil, G.S. 2005. Role of endoplasmic reticulum stress and c-Jun NH2-terminal kinase pathways in inflammation and origin of obesity and diabetes. *Diabetes* 54(SUPPL. 2).

Hoy, S.M. 2013. Subcutaneous Bortezomib. *Drugs* 73(1), pp. 45–54.

Høyer-Hansen, M. and Jäättelä, M. 2007. Connecting endoplasmic reticulum stress to autophagy by unfolded protein response and calcium. *Cell Death and Differentiation* 14(9), pp. 1576–1582.

Hu, S. et al. 2016. Tuberous sclerosis complex: Imaging characteristics in 11 cases and review of the literature. *Journal of Huazhong University of Science and Technology [Medical Sciences]* 36(4), pp. 601–606.

Hua, P. et al. 2015. Cepharanthine induces apoptosis through reactive oxygen species and mitochondrial dysfunction in human non-small-cell lung cancer cells. *Biochemical and Biophysical Research Communications* 460(2), pp. 136–142.

Huang, J. et al. 2008. The TSC1-TSC2 Complex Is Required for Proper Activation of mTOR Complex 2. *Molecular and Cellular Biology* 28(12), pp. 4104–4115.

Huffman, T.A. et al. 2002. Insulin-stimulated phosphorylation of lipin mediated by the mammalian target of rapamycin. *Proceedings of the National Academy of Sciences* 99(2), pp. 1047–1052.

Hulbert, J. et al. 2015. Rates of interventional procedures in patients with tuberous sclerosis complex-related renal angiomyolipoma. *Current Medical Research and Opinion* 31(8), pp. 1501–1507.

Hung, Y.P. et al. 2017. Akt regulation of glycolysis mediates bioenergetic stability in epithelial cells. *eLife* 6.

Ikarashi, D. et al. 2017. Efficacy of Everolimus for Treating Renal Angiomyolipoma with Inferior Vena Cava Thrombus Associated with Tuberous Sclerosis: A Case Report. *Urology Case Reports* 11, pp. 11–13.

Im, E. et al. 2018. Luteolin induces caspase-dependent apoptosis via inhibiting the

AKT/osteopontin pathway in human hepatocellular carcinoma SK-Hep-1 cells. *Life Sciences* 209, pp. 259–266.

Irvin, W.J. et al. 2010. Phase II study of bortezomib and pegylated liposomal doxorubicin in the treatment of metastatic breast cancer. *Clinical Breast Cancer* 10(6), pp. 465–470.

Ita, M. et al. 2008. Remarkable enhancement of cytotoxicity of onconase and cepharanthine when used in combination on various tumor cell lines. *Cancer Biology and Therapy* 7(7), pp. 1104–1108.

Ito, H. et al. 2008. Inhibitory Effect of a Biscoclaurine Alkaloid, Cepharanthin, on Lung Metastasis of Lewis Lung Carcinoma. *The Japanese Journal of Pharmacology* 56(2), pp. 195–202.

Iwata, S. et al. 2011. Bortezomib induces apoptosis in T lymphoma cells and natural killer lymphoma cells independent of Epstein-Barr virus infection. *International Journal of Cancer* 129(9), pp. 2263–2273.

Jensen, K. et al. 2017. Nelfinavir inhibits proliferation and induces DNA damage in thyroid cancer cells. *Endocrine-Related Cancer* 24(3), pp. 147–156.

Jeong, A. et al. 2017. Predictors of Drug-Resistant Epilepsy in Tuberous Sclerosis Complex. *Journal of Child Neurology* 32(14), pp. 1092–1098.

Jiang, H.-Y. et al. 2004. Activating transcription factor 3 is integral to the eukaryotic initiation factor 2 kinase stress response. *Molecular and cellular biology* 24(3), pp. 1365–77.

Jiang, W. et al. 2007. HIV protease inhibitor nelfinavir inhibits growth of human melanoma cells by induction of cell cycle arrest. *Cancer Research* 67(3), pp. 1221–1227.

Jiang, X. et al. 2011. Glucose deprivation in tuberous sclerosis complex-related tumors. *Cell & Bioscience* 1(1), p. 34.

Jijakli, H. et al. 1996. Insulinotropic action of methyl pyruvate: Enzymatic and metabolic aspects. *Archives of Biochemistry and Biophysics* 335(2), pp. 245–257.

Jijakli, H. et al. 2002. Insulinotropic Action of Methyl Pyruvate: Enzymatic and Metabolic Aspects. *Archives of Biochemistry and Biophysics* 335(2), pp. 245–257.

Johnson, C.E. et al. 2015. Endoplasmic reticulum stress and cell death in mTORC1-

overactive cells is induced by nelfinavir and enhanced by chloroquine. *Molecular Oncology* 9(3), pp. 675–688.

Johnson, C.E. et al. 2018. Loss of tuberous sclerosis complex 2 sensitizes tumors to nelfinavir−bortezomib therapy to intensify endoplasmic reticulum stress-induced cell death. *Oncogene* 37(45), pp. 5913–5925.

Johnson, S.R. et al. 2010. European Respiratory Society guidelines for the diagnosis and management of lymphangioleiomyomatosis. *European Respiratory Journal* 35(1), pp. 14–26.

Johnson, S.R. and Tattersfield, A.E. 1999. Decline in lung function in lymphangioleiomyomatosis: Relation to menopause and progesterone treatment. *American Journal of Respiratory and Critical Care Medicine* 160(2), pp. 628–633.

Jouan, E. et al. 2016. Evaluation of P-glycoprotein inhibitory potential using a rhodamine 123 accumulation assay. *Pharmaceutics* 8(2).

Jóźwiak, S. et al. 2016. Safety of Everolimus in Patients Younger than 3 Years of Age: Results from EXIST-1, a Randomized, Controlled Clinical Trial. *The Journal of pediatrics* 172, pp. 151-155.e1.

K, H.K. et al. 2015. a Case Report of Tuberous Sclerosis. *Journal of Evidence Based Medicine and Healthcare* 2(1), pp. 56–59.

Kakehi, Y. et al. 1994. Intraarterial chemotherapy for metastatic renal cell carcinomas: Combination with MDR-overcoming agents. *Acta Urologica Japonica* 40(10), pp. 925–929.

Kaluza, V. et al. 2006. Bortezomib is a novel inducer of latent Epstein Barr Virus (EBV) in EBV+ lymphoma cell lines. *Blood (ASH Annual Meeting Abstracts)* 108(11), p. 2511.

Kaneda, M. 2017. Tuberous sclerosis complex. *Japanese Journal of Plastic Surgery* 60(8), pp. 912–920.

Kang, D.W. et al. 2008. Ciglitazone induces caspase-independent apoptosis through down-regulation of XIAP and survivin in human glioma cells. *Neurochemical Research* 33(3), pp. 551–561.

Kang, S. et al. 2018. Repositioning of the antipsychotic trifluoperazine: Synthesis, biological evaluation and in silico study of trifluoperazine analogs as anti-

glioblastoma agents. *European Journal of Medicinal Chemistry* 151, pp. 186–198.

Kang, S.S. et al. 2016. Trifluoperazine, a Well-Known Antipsychotic, Inhibits Glioblastoma Invasion by Binding to Calmodulin and Disinhibiting Calcium Release Channel IP 3 R . *Molecular Cancer Therapeutics* 16(1), pp. 217–227.

Kanno, T. et al. 2018. Treatment results of the second-line chemotherapy regimen for patients with low-risk gestational trophoblastic neoplasia treated with 5-day methotrexate and 5-day etoposide. *Journal of Gynecologic Oncology* 29(6), pp. 6–13.

Kapoor, P. et al. 2012. Bortezomib Combination Therapy in Multiple Myeloma. *Seminars in Hematology* 49(3), pp. 228–242.

Karbowniczek, M. et al. 2003. Recurrent Lymphangiomyomatosis after Transplantation. *American Journal of Respiratory and Critical Care Medicine* 167(7), pp. 976–982.

Karuppusamy Rathinam, M.K. et al. 2014. The Soft Agar Colony Formation Assay. *Journal of Visualized Experiments* (92), p. e51998.

Kato, T. and Suzumura, Y. 2017. Potentiation of Antitumor Activity of Vincristine by the Biscoclaurine Alkaloid Cepharanthine. *JNCI: Journal of the National Cancer Institute* 79(3), pp. 527–532.

Kattel, K. et al. 2015. Impact of CYP2C19 polymorphism on the pharmacokinetics of nelfinavir in patients with pancreatic cancer. *British Journal of Clinical Pharmacology* 80(2), pp. 267–275.

Katz, J.S. et al. 2017. Unique findings of subependymal giant cell astrocytoma within cortical tubers in patients with tuberous sclerosis complex: a histopathological evaluation. *Child's Nervous System* 33(4), pp. 601–607.

Kaufmann, A.M. and Krise, J.P. 2007. Lysosomal sequestration of amine-containing drugs: Analysis and therapeutic implications. *Journal of Pharmaceutical Sciences* 96(4), pp. 729–746.

Kaufmann, S.H. 1989. Induction of Endonucleolytic DNA Cleavage in Human Acute Myelogenous Leukemia Cells by Etoposide, Camptothecin, and Other Cytotoxic Anticancer Drugs: A Cautionary Note. *Cancer Research* 49(21), pp. 5870–5878.

Kawabata, S. et al. 2012. Synergistic effects of nelfinavir and bortezomib on

proteotoxic death of NSCLC and multiple myeloma cells. *Cell Death & Disease* 3(7), pp. e353–e353.

Kawahara, K. et al. 2005. Cepharanthine triggers apoptosis in a human hepatocellular carcinoma cell line (HuH-7) through the activation of JNK1/2 and the downregulation of Akt. *FEBS Letters* 580(2), pp. 703–710.

Keiser, J. et al. 2009. Mefloquine - An aminoalcohol with promising antischistosomal properties in mice. Williams, D. L. ed. *PLoS Neglected Tropical Diseases* 3(1), p. e350.

Keiser, J. et al. 2014. In vitro and in vivo antischistosomal activity of ferroquine derivatives. *Parasites and Vectors* 7(1), pp. 1–7.

Kikukawa, Y. et al. 2008. Induction of cell cycle arrest and apoptosis in myeloma cells by cepharanthine, a biscoclaurine alkaloid. *International Journal of Oncology* 33(4), pp. 807–814.

Kim, E. et al. 2008. Regulation of TORC1 by Rag GTPases in nutrient response. *Nature Cell Biology* 10(8), pp. 935–945.

Kim, J.H. et al. 2013. Co-treatment with the anti-malarial drugs mefloquine and primaquine highly sensitizes drug-resistant cancer cells by increasing P-gp inhibition. *Biochemical and Biophysical Research Communications* 441(3), pp. 655–660.

Kim, Y.C. and Guan, K.L. 2015. MTOR: A pharmacologic target for autophagy regulation. *Journal of Clinical Investigation* 125(1), pp. 25–32.

Kocemba-Pilarczyk, K.A. et al. 2018. Targeting the hypoxia pathway in malignant plasma cells by using 17-allylamino-17-demethoxygeldanamycin. *Acta Biochimica Polonica* 65(1), pp. 101–109.

Koenig, M.K. et al. 2012. Topical rapamycin therapy to alleviate the cutaneous manifestations of tuberous sclerosis complex: A double-blind, randomized, controlled trial to evaluate the safety and efficacy of topically applied rapamycin. *Drugs in R and D*.

Kohno, K. 2010. Stress-sensing mechanisms in the unfolded protein response: Similarities and differences between yeast and mammals. *Journal of Biochemistry* 147(1), pp. 27–33.

Kojima, E. et al. 2003. The function of GADD34 is a recovery from a shutoff of protein synthesis induced by ER stress: elucidation by GADD34-deficient mice. *The FASEB journal : official publication of the Federation of American Societies for Experimental Biology* 17(11), pp. 1573–1575.

Kollaritsch, H. et al. 2000. Mefloquine concentration profiles during prophylactic dose regimens. *Wiener klinische Wochenschrift* 112(10), pp. 441–7.

Komiyama, S. et al. 1989. Establishment of tumor cell lines from a patient with head and neck cancer and their different sensitivities to anti-cancer agents. *Cancer* 63(4), pp. 675–681.

Kono, K. et al. 2002. Effects of combination chemotherapy with biscoclaurine-derived alkaloid (Cepharanthine) and nimustine hydrochloride on malignant glioma cell lines. *Journal of Neuro-Oncology* 56(2), pp. 101–108.

Koppenol, W.H. et al. 2011. Otto Warburg's contributions to current concepts of cancer metabolism. *Nature Reviews Cancer* 11(5), pp. 325–337.

Koromilas, A.E. et al. 2018. mRNAs containing extensive secondary structure in their 5′ non-coding region translate efficiently in cells overexpressing initiation factor eIF-4E. *The EMBO Journal* 11(11), pp. 4153–4158.

Kothare, S. V. et al. 2014. Severity of manifestations in tuberous sclerosis complex in relation to genotype. *Epilepsia* 55(7), pp. 1025–1029.

Kraus, M. et al. 2013. Nelfinavir augments proteasome inhibition by bortezomib in myeloma cells and overcomes bortezomib and carfilzomib resistance. *Blood Cancer Journal* 3(3), pp. e103-9.

Kraus, M. et al. 2014. Ritonavir, nelfinavir, saquinavir and lopinavir induce proteotoxic stress in acute myeloid leukemia cells and sensitize them for proteasome inhibitor treatment at low micromolar drug concentrations. *Leukemia Research* 38(3), pp. 383–392.

Krueger, D.A. et al. 2013. Tuberous Sclerosis Complex Surveillance and Management: Recommendations of the 2012 International Tuberous Sclerosis Complex Consensus Conference. *Pediatric Neurology* 49(4), pp. 255–265.

Krymskaya, V.P. et al. 2002. Tuberin Regulates p70 S6 Kinase Activation and Ribosomal Protein S6 Phosphorylation. *Journal of Biological Chemistry* 277(34), pp. 30958–30967.

Kumasaka, T. et al. 2005. Lymphangiogenesis-mediated sheddinq of LAM cell clusters as a mechanism for dissemination in lymphangioleiomyomatosis. *American Journal of Surgical Pathology* 29(10), pp. 1356–1366.

Kumazoe, M. et al. 2017. PDE3 inhibitor and EGCG combination treatment suppress cancer stem cell properties in pancreatic ductal adenocarcinoma. *Scientific Reports* 7(1), p. 1917. Available at: http://www.nature.com/articles/s41598-017-02162-9.

Kundu, P. et al. 2017. Chelerythrine down regulates expression of VEGFA, BCL2 and KRAS by arresting G-Quadruplex structures at their promoter regions. *Scientific Reports* 7(1), p. 40706.

Kuo, C. et al. 2017. Piperlongumine inhibits cancer stem cell properties and regulates multiple malignant phenotypes in oral cancer. *Oncology Letters* 15(2), pp. 1789–1798.

Kushchayeva, Y. et al. 2014. The HIV protease inhibitor nelfinavir down-regulates RET signaling and induces apoptosis in medullary thyroid cancer cells. *Journal of Clinical Endocrinology and Metabolism* 99(5), pp. E734–E745.

Küster, T. et al. 2011. In vitro and in vivo efficacies of mefloquine-based treatment against alveolar echinococcosis. *Antimicrobial Agents and Chemotherapy* 55(2), pp. 713–721.

Kwiatkowski, D.J. et al. 2010. *Tuberous Sclerosis Complex: Genes, Clinical Features and Therapeutics*.

Kwiatkowski, D.J. et al. 2015. Response to everolimus is seen in TSC-associated SEGAs and angiomyolipomas independent of mutation type and site in TSC1 and TSC2. *European Journal of Human Genetics* 23(12), pp. 1665–1672.

La-Beck, N.M. et al. 2013. The Role of Pegylated Liposomal Doxorubicin in Ovarian Cancer: A Meta-Analysis of Randomized Clinical Trials. *The Oncologist* 18(9), pp. 1022–1031.

Lam, H.C. et al. 2017a. New developments in the genetics and pathogenesis of tumours in tuberous sclerosis complex. *Journal of Pathology* 241(2), pp. 219–225.

Lam, H.C. et al. 2017b. P62/SQSTM1 cooperates with hyperactive mTORC1 to regulate glutathione production, maintain mitochondrial integrity, and promote tumorigenesis. *Cancer Research* 77(12), pp. 3255–3267.

Lam, H.C. et al. 2018. Renal disease in tuberous sclerosis complex: pathogenesis and therapy. *Nature Reviews Nephrology* 14(11), pp. 704–716.

Laplante, M. and Sabatini, D.M. 2009a. An Emerging Role of mTOR in Lipid Biosynthesis. *Current Biology* 19(22), pp. R1046–R1052.

Laplante, M. and Sabatini, D.M. 2009b. mTOR signaling at a glance. *Journal of Cell Science* 122(20), pp. 3589–3594.

Lasanianos, N.G. et al. 2010. Intramedullary nailing as a 'second hit' phenomenon in experimental research: Lessons learned and future directions. *Clinical Orthopaedics and Related Research* 468(9), pp. 2514–2529.

Law, B.Y.K. et al. 2015. Natural small-molecule enhancers of autophagy induce autophagic cell death in apoptosis-defective cells. *Scientific Reports* 4(1), p. 5510.

Lee, C.H. et al. 2007. Constitutive mTOR activation in TSC mutants sensitizes cells to energy starvation and genomic damage via p53. *EMBO Journal* 26(23), pp. 4812–4823.

Lee, J.-S. et al. 2016. Dual targeting of glutaminase 1 and thymidylate synthase elicits death synergistically in NSCLC. *Cell Death & Disease* 7(12), pp. e2511–e2511.

Lee, J.S. et al. 1994. Rhodamine efflux patterns predict P-glycoprotein substrates in the National Cancer Institute drug screen. *Molecular pharmacology*

Lesma, E. et al. 2005. Isolation and Growth of Smooth Muscle-Like Cells Derived from Tuberous Sclerosis Complex-2 Human Renal Angiomyolipoma. *The American Journal of Pathology* 167(4), pp. 1093–1103.

Li, C. et al. 2013. Faslodex Inhibits Estradiol-Induced Extracellular Matrix Dynamics and Lung Metastasis in a Model of Lymphangioleiomyomatosis. *American Journal of Respiratory Cell and Molecular Biology* 49(1), pp. 135–142.

Li, C. et al. 2014a. Estradiol and mTORC2 cooperate to enhance prostaglandin biosynthesis and tumorigenesis in TSC2-deficient LAM cells. *The Journal of experimental medicine* 211(1), pp. 15–28.

Li, H. et al. 2011. mTORC2 Is Required for Proliferation and Survival of TSC2-Null Cells. *Molecular and Cellular Biology* 31(12), pp. 2484–2498.

Li, J. et al. 2014b. Rapamycin: One drug, many effects. *Cell Metabolism* 19(3), pp.

373–379.

Li, J. et al. 2016. MTORC1-driven tumor cells are highly sensitive to therapeutic targeting by antagonists of oxidative stress. *Cancer Research*.

Li, Y.-L. et al. 2018a. Piperlongumine and p53-reactivator APR-246 selectively induce cell death in HNSCC by targeting GSTP1. *Oncogene* 37(25), pp. 3384–3398.

Li, Y. et al. 2014c. New insights into the roles of CHOP-induced apoptosis in ER stress Structure and Properties of C / EBP Homologous Protein Roles of CHOP in ER Stress-Mediated Apoptosis. *Acta Biochim Biophys Sin* 46(8), pp. 629–640.

Li, Z. et al. 2018b. The dietary compound luteolin inhibits pancreatic cancer growth by targeting BCL-2. *Food and Function* 9(5), pp. 3018–3027.

Liang, N. et al. 2014. Regulation of YAP by mTOR and autophagy reveals a therapeutic target of tuberous sclerosis complex. *The Journal of Experimental Medicine* 211(11), pp. 2249–2263.

Lim, C.-S. et al. 2016. Everolimus improves neuropsychiatric symptoms in a patient with tuberous sclerosis carrying a novel TSC2 mutation. *Molecular Brain* 9(1).

Lim, Y.S. et al. 2017. Tuberous sclerosis and its rare association with macrodactyly and fibrous hamartomas. *Skeletal Radiology* 46(9), pp. 1293–1296.

Lin, L. et al. 2010. Novel STAT3 Phosphorylation Inhibitors Exhibit Potent Growth-Suppressive Activity in Pancreatic and Breast Cancer Cells. *Cancer Research* 70(6), pp. 2445–2454.

Lin, W. et al. 2017. Protein kinase C inhibitor chelerythrine selectively inhibits proliferation of triple-negative breast cancer cells. *Scientific Reports.*

Lin, W. et al. 2018. First-Line Atezolizumab plus Chemotherapy in Extensive-Stage Small-Cell Lung Cancer. *New England Journal of Medicine* 379(23), pp. 2220–2229.

Liu, C. et al. 2015a. In vivo and in vitro efficacies of mebendazole, mefloquine and nitazoxanide against cyst echinococcosis. *Parasitology Research* 114(6), pp. 2213–2222.

Liu, G. et al. 2015b. Mechanisms and in vitro effects of cepharanthine hydrochloride: Classification analysis of the drug-induced differentiallyexpressed genes of human nasopharyngeal carcinoma cells. *Oncology Reports* 34(4), pp. 2002–2010.

Liu, P. et al. 2013. Sin1 phosphorylation impairs mTORC2 complex integrity and inhibits downstream Akt signalling to suppress tumorigenesis. *Nature cell biology* 15(11), pp. 1340–50.

Liu, P. et al. 2015c. Ptdins(3,4,5) P3 -dependent activation of the mTORC2 kinase complex. *Cancer Discovery* 5(11), pp. 1194–11209.

Liu, W. et al. 2018. Targeting P-Glycoprotein: Nelfinavir Reverses Adriamycin Resistance in K562/ADR Cells. *Cellular Physiology and Biochemistry* 116044, pp. 1616–1631.

Liu, Y. et al. 2015d. N1-guanyl-1,7-diaminoheptane sensitizes estrogen receptor negative breast cancer cells to doxorubicin by preventing epithelial-mesenchymal transition through inhibition of eukaryotic translation initiation factor 5A2 activation. *Cellular Physiology and Biochemistry* 36(6), pp. 2494–2503.

Lü, S. et al. 2008. Point mutation of the proteasome beta5 subunit gene is an important mechanism of bortezomib resistance in bortezomib-selected variants of Jurkat T cell lymphoblastic lymphoma/leukemia line. *The Journal of pharmacology and experimental therapeutics* 326(2), pp. 423–431.

Lucia, M.B. et al. 2011. Exposure to HIV-protease inhibitors selects for increased expression of P-glycoprotein (ABCB1) in Kaposi's sarcoma cells. *British Journal of Cancer* 105(4), pp. 513–522.

Luo, X. et al. 2015. Targeting glutamine metabolism sensitizes pancreatic cancer to PARP-driven metabolic catastrophe induced by ß-lapachone. *Cancer & Metabolism* 3(1).

Lyu, J. et al. 2017. Pharmacological blockade of cholesterol trafficking by cepharanthine in endothelial cells suppresses angiogenesis and tumor growth. *Cancer Letters* 409, pp. 91–103.

Ma, L. et al. 2005. Phosphorylation and functional inactivation of TSC2 by Erk: Implications for tuberous sclerosis and cancer pathogenesis. *Cell* 121(2), pp. 179–193.

Ma, L. et al. 2018. Co-delivery of paclitaxel and tanespimycin in lipid nanoparticles enhanced anti-gastric-tumor effect in vitro and in vivo. *Artificial Cells, Nanomedicine, and Biotechnology* 14, pp. 1–8.

Ma, Y. et al. 2002. Two distinct stress signaling pathways converge upon the CHOP

promoter during the mammalian unfolded protein response. *Journal of Molecular Biology* 318(5), pp. 1351–1365.

Madke, B. 2013. Topical rapamycin (sirolimus) for facial angiofibromas. *Indian Dermatology Online Journal* 4(1), p. 54.

Majumder, K. et al. 2016. 1025 Curcumin Derivative FLLL-31 Sensitizes Pancreatic Cancer Cells to TRAIL Induced Cell Death Through Death Receptor Up-Regulation. *Gastroenterology* 150(4), p. S1200.

Malinowska, I.A. et al. 2013. Similar trends in serum VEGF-D levels and kidney angiomyolipoma responses with longer duration sirolimus treatment in adults with tuberous sclerosis. *PloS one* 8(2), p. e56199.

Mamouni, K. et al. 2018. A Novel Flavonoid Composition Targets Androgen Receptor Signaling and Inhibits Prostate Cancer Growth in Preclinical Models. *Neoplasia (United States)* 20(8), pp. 789–799.

Martínez, I.M. and Chrispeels, M.J. 2003. Genomic analysis of the unfolded protein response in Arabidopsis shows its connection to important cellular processes. *The Plant cell* 15(2), pp. 561–76.

Martinon, F. et al. 2015. An inhibitor of HIV-1 protease modulates constitutive eIF2α dephosphorylation to trigger a specific integrated stress response. *Proceedings of the National Academy of Sciences* 113(2), pp. E117–E126.

Marzolini, C. et al. 2001. Nelfinavir plasma levels under twice-daily and three-times-daily regimens: High interpatient and low intrapatient variability. *Therapeutic Drug Monitoring* 23(4), pp. 394–398.

Masuda, M. et al. 1993. [Clinical assessment of complement activation and leukocyte kinetics during cardiopulmonary bypass: the effect of cepharanthine]. *Kyobu Geka* 46(10), pp. 845–849.

Matsui, K. et al. 2000. Downregulation of estrogen and progesterone receptors in the abnormal smooth muscle cells in pulmonary lymphangioleiomyomatosis following therapy: An immunohistochemical study. *American Journal of Respiratory and Critical Care Medicine* 161(3 I), pp. 1002–1009.

Matsukawa, T. et al. 2018. Successful treatment of an elderly Langerhans cell sarcoma patient by EPOCH (etoposide, prednisone, vincristine, cyclophosphamide, and doxorubicin) chemotherapy. *Journal of Clinical and Experimental*

Hematopathology 58(4), pp. 4–7.

Mauvezin, C. et al. 2015. Autophagosome-lysosome fusion is independent of V-ATPase-mediated acidification. *Nature communications* 6, p. 7007.

Mauvezin, C. and Neufeld, T.P. 2015. Bafilomycin A1 disrupts autophagic flux by inhibiting both V-ATPase-dependent acidification and Ca-P60A/SERCA-dependent autophagosome-lysosome fusion. *Autophagy* 11(8), pp. 1437–1438.

Mawson, A. 2013. Mefloquine use, psychosis, and violence: A retinoid toxicity hypothesis. *Medical Science Monitor* 19, pp. 579–583.

McCann, H. et al. 2018. Energy Stress-Mediated Cytotoxicity in Tuberous Sclerosis Complex 2-Deficient Cells with Nelfinavir and Mefloquine Treatment. *Cancers* 10(10), p. 375.

McCarthy, S. 2015. Malaria Prevention, Mefloquine Neurotoxicity, Neuropsychiatric Illness, and Risk-Benefit Analysis in the Australian Defence Force. *Journal of Parasitology Research* 2015, pp. 1–23.

McCormack, F.X. et al. 2011. Efficacy and Safety of Sirolimus in Lymphangioleiomyomatosis. *New England Journal of Medicine* 364(17), pp. 1595–1606.

McCormack, F.X. et al. 2016. Official American thoracic society/Japanese respiratory society clinical practice guidelines: Lymphangioleiomyomatosis diagnosis and management. *American Journal of Respiratory and Critical Care Medicine* 194(6), pp. 748–761.

McDonald, C.J. et al. 2014. Effect of lysine to alanine mutations on the phosphate activation and BPTES inhibition of glutaminase. *Neurochemistry International* 88, pp. 10–14.

Medvetz, D. et al. 2015. High-Throughput Drug Screen Identifies Chelerythrine as a Selective Inducer of Death in a TSC2-null Setting. *Molecular Cancer Research* . doi: 10.1158/1541-7786.MCR-14-0440.

Mitani, T. et al. 2014. Resveratrol Reduces the Hypoxia-Induced Resistance to Doxorubicin in Breast Cancer Cells. *Journal of Nutritional Science and Vitaminology* 60(2), pp. 122–128.

Mitsiades, C.S. et al. 2006. Antitumor effects of the proteasome inhibitor bortezomib

in medullary and anaplastic thyroid carcinoma cells in vitro. *Journal of Clinical Endocrinology and Metabolism* 91(10), pp. 4013–4021.

Mitsiades, N. et al. 2002. Molecular sequelae of proteasome inhibition in human multiple myeloma cells. *Proceedings of the National Academy of Sciences* 99(22), pp. 14374–14379.

Mizobata, S. et al. 2002. Synergistic effects of tamoxifen and cepharanthine for circumventing the multidrug resistance. *Cancer Letters* 107(1), pp. 117–123.

Mohammad, J. et al. 2018. Piperlongumine potentiates the effects of gemcitabine in in vitro and in vivo human pancreatic cancer models. *Oncotarget* 9(12), pp. 10457–10469.

Mohammadian, M. et al. 2017. Cytotoxic effects of the newly-developed chemotherapeutic agents 17-AAG in combination with oxaliplatin and capecitabine in colorectal cancer cell lines. *Research in Pharmaceutical Sciences* 12(6), pp. 517–525.

Moir, L.M. 2016. Lymphangioleiomyomatosis: Current understanding and potential treatments. *Pharmacology & Therapeutics* 158, pp. 114–124.

Molins, E.A.G. and Jusko, W.J. 2018. Assessment of Three-Drug Combination Pharmacodynamic Interactions in Pancreatic Cancer Cells. *The AAPS Journal* 20(5), p. 80.

MOOLTEN, S.E. 2011. Hamartial Nature of the Tuberous Sclerosis Complex and Its Bearing on the Tumor Problem. *Archives of Internal Medicine* 69(4), p. 589.

Morita, K. et al. 2002. Seventeen Cases of Alopecia Areata: Combination of SADBE Topical Immunotherapy with Other Therapies. *The Journal of Dermatology* 29(10), pp. 661–664.

Morita, M. et al. 2013. mTORC1 Controls Mitochondrial Activity and Biogenesis through 4E-BP-Dependent Translational Regulation. *Cell Metabolism* 18(5), pp. 698–711.

Morita, M. et al. 2015. MTOR coordinates protein synthesis, mitochondrial activity. *Cell Cycle* 14(4), pp. 473–480.

Morrow, G.R. et al. 2003. Differential Effects of Paroxetine on Fatigue and Depression: A Randomized, Double-Blind Trial From the University of Rochester

Cancer Center Community Clinical Oncology Program. *Journal of Clinical Oncology* 21(24), pp. 4635–4641.

Mortaji, P. et al. 2017. Pancreatic neuroendocrine tumor in a patient with a TSC1 variant: case report and review of the literature. *Familial Cancer* 17(2), pp. 275–280.

MOSS, J. et al. 2001. Prevalence and Clinical Characteristics of Lymphangioleiomyomatosis (LAM) in Patients with Tuberous Sclerosis Complex. *American Journal of Respiratory and Critical Care Medicine* 164(4), pp. 669–671.

Mühlebner, A. et al. 2016. Specific pattern of maturation and differentiation in the formation of cortical tubers in tuberous sclerosis complex (TSC): Evidence from layer-specific marker expression. *Journal of Neurodevelopmental Disorders* 8(1), pp. 1–14.

Murray, M.Y. et al. 2014. Overcoming bortezomib resistance in multiple myeloma. *Biochemical Society Transactions* 42(4), pp. 804–808. doi: 10.1042/bst20140126.

Nagana Gowda, G.A. et al. 2018. A Metabolomics Study of BPTES Altered Metabolism in Human Breast Cancer Cell Lines. *Frontiers in Molecular Biosciences* 5.

Nagaoka, S. et al. 1987. Modification of cellular efflux and cytotoxicity of adriamycin by biscoclaulin alkaloid in vitro. *European Journal of Cancer and Clinical Oncology* 23(9), pp. 1297–1302.

Nandagopal, N. and Roux, P.P. 2014. Regulation of global and specific mRNA translation by the mTOR signaling pathway. *Translation* 3(1), p. e983402.

Van Nassauw, L. et al. 2008. Schistosomicidal activity of the antimalarial drug, mefloquine, in Schistosoma mansoni-infected mice. *Travel Medicine and Infectious Disease* 6(5), pp. 253–258.

Nasuti, P. et al. 2016. The economic burden of tuberous sclerosis complex in UK patients with renal manifestations: a retrospective cohort study in the clinical practice research datalink (CPRD). *Journal of Medical Economics* 19(12), pp. 1116–1126.

Nathan, N. et al. 2015. Improvement of tuberous sclerosis complex (TSC) skin tumors during long-term treatment with oral sirolimus. *Journal of the American Academy of Dermatology* 73(5), pp. 802–808.

Nathan, N. et al. 2016. The adult phenotype of tuberous sclerosis complex. *Acta Dermato-Venereologica* .

Nazio, F. et al. 2013. MTOR inhibits autophagy by controlling ULK1 ubiquitylation, self-association and function through AMBRA1 and TRAF6. *Nature Cell Biology* 15(4), pp. 406–416.

Neri, I. et al. 2014. Analysis of current data on the use of topical rapamycin in the treatment of facial angiofibromas in Tuberous Sclerosis Complex. *Journal of the European Academy of Dermatology and Venereology* 29(1), pp. 14–20.

Nevin, R.L. 2012. Mefloquine gap junction blockade and risk of pregnancy loss. *Biology of reproduction* 87(3), p. 65.

Nguyen, D.M. et al. 1999. Sequence-dependent enhancement of paclitaxel toxicity in non-small cell lung cancer by 17-allylamino 17-demethoxygeldanamycin. *Journal of Thoracic and Cardiovascular Surgery* 118(5), pp. 908–915.

Northrup, H. and Krueger, D.A. 2013. Tuberous Sclerosis Complex Diagnostic Criteria Update: Recommendations of the 2012 International Tuberous Sclerosis Complex Consensus Conference. *Pediatric Neurology* 49(4), pp. 243–254.

Nussbaum, A.K. et al. 1998. Cleavage motifs of the yeast 20S proteasome subunits deduced from digests of enolase 1. *Proceedings of the National Academy of Sciences* 95(21), pp. 12504–12509.

O'Callaghan, F.J. et al. 2004. An epidemiological study of renal pathology in tuberous sclerosis complex. *BJU International* 94(6), pp. 853–857.

O'Connor, R. et al. 2013. The interaction of bortezomib with multidrug transporters: Implications for therapeutic applications in advanced multiple myeloma and other neoplasias. *Cancer Chemotherapy and Pharmacology* 71(5), pp. 1357–1368.

Oerlemans, R. et al. 2008. Molecular basis of bortezomib resistance: proteasome subunit beta5 (PSMB5) gene mutation and overexpression of PSMB5 protein. *Blood* 112(6), pp. 2489–99.

Onec, B. et al. 2018. Combination therapy with azacitidine, etoposide, and cytarabine in the treatment of elderly acute myeloid leukemia patients: A single center experience. *Journal of Cancer Research and Therapeutics* 14(5), pp. 1105–1111.

Ono, M. et al. 1994. Positive interactions between human interferon and cepharanthin against human cancer cells in vitro and in vivo. *Cancer Chemother.Pharmacol* 35(0344-5704 (Print)), pp. 10–16.

Oprescu, N. et al. 2013. Clinical predictors of mortality and cause of death in lymphangioleiomyomatosis: A population-based registry. *Lung* 191(1), pp. 35–42.

Osonwa, U.E. et al. 2017. Enhancement of Antimalaria Effect of Mefloquine by Chlorpheniramine. *American Journal of Medicine and Medical Sciences* 7(6), pp. 248–264.

Ozcan, U. et al. 2008. Loss of the Tuberous Sclerosis Complex Tumor Suppressors Triggers the Unfolded Protein Response to Regulate Insulin Signaling and Apoptosis. *Molecular Cell* 29(5), pp. 541–551.

Pakula, T.M. et al. 2003. The Effects of Drugs Inhibiting Protein Secretion in the Filamentous Fungus Trichoderma reesei . *Journal of Biological Chemistry* 278(45), pp. 45011–45020.

Pan, C.C. et al. 2009. Effect of the antidepressant paroxetine on Ca 2+ movement in PC3 human prostate cancer cells. *Drug Development Research*.

Pan, J. et al. 2012. Phase i study of nelfinavir in liposarcoma. *Cancer Chemotherapy and Pharmacology* . doi: 10.1007/s00280-012-1961-4.

Papandreou, C.N. and Logothetis, C.J. 2004. Bortezomib as a potential treatment for prostate cancer. *Cancer Res* 64(15), pp. 5036–5043.

Park, S.-H. et al. 2002. Tuberous sclerosis in a 20-week gestation fetus: immunohistochemical study. *Acta Neuropathologica* 94(2), pp. 180–186.

Parkhitko, A. et al. 2011. Tumorigenesis in tuberous sclerosis complex is autophagy and p62/sequestosome 1 (SQSTM1)-dependent. *Proceedings of the National Academy of Sciences of the United States of America* 108(30), pp. 12455–60.

Parmar, V.M. and Schröder, M. 2012. Sensing endoplasmic reticulum stress. *Advances in Experimental Medicine and Biology* 738, pp. 153–168.

Pasha, M. et al. 2017. Sestrin2 as a Novel Biomarker and Therapeutic Target for Various Diseases. *Oxidative medicine and cellular longevity* 2017, p. 3296294.

Patel, B. et al. 2015. Exosomes mediate the acquisition of the disease phenotypes by cells with normal genome in tuberous sclerosis complex. *Oncogene* (April), pp.

1–10.

Patil, C. and Walter, P. 2001. Intracellular signaling from the endoplasmic reticulum to the nucleus: The unfolded protein response in yeast and mammals. *Current Opinion in Cell Biology* 13(3), pp. 349–355.

Paudel, K.R. et al. 2016. Cepharanthine inhibits in vitro VSMC proliferation and migration and vascular inflammatory responses mediated by RAW264.7. *Toxicology in Vitro* 34, pp. 16–25.

Peixoto, H.M. et al. 2016. Efficacy and safety of artesunate-mefloquine therapy for treating uncomplicated *Plasmodium falciparum* malaria: systematic review and meta-analysis. *Transactions of The Royal Society of Tropical Medicine and Hygiene* (December 2016), pp. 626–636.

Perluigi, M. et al. 2015. mTOR signaling in aging and neurodegeneration: At the crossroad between metabolism dysfunction and impairment of autophagy. *Neurobiology of Disease* 84, pp. 39–49.

Peron, A. et al. 2016. Do patients with tuberous sclerosis complex have an increased risk for malignancies? *American Journal of Medical Genetics, Part A* 170(6), pp. 1538–1544.

Peterson, T.R. et al. 2011. mTOR Complex 1 Regulates Lipin 1 Localization to Control the SREBP Pathway. *Cell* 146(3), pp. 408–420.

Pezzella, G. et al. 2001. Treatment of depression in patients with breast cancer: A comparison between paroxetine and amitriptyline. *Breast Cancer Research and Treatment* 70(1), pp. 1–10.

de Pilla Varotti, F. et al. 2008. Synthesis, Antimalarial Activity, and Intracellular Targets of MEFAS, a New Hybrid Compound Derived from Mefloquine and Artesunate. *Antimicrobial Agents and Chemotherapy* 52(11), pp. 3868–3874.

Pinheiro, T. et al. 2018. Reprint of: A chemical screen identifies trifluoperazine as an inhibitor of glioblastoma growth. *Biochemical and Biophysical Research Communications* 499(2), pp. 136–142.

Piska, K. et al. 2018. Piperlongumine (piplartine) as a lead compound for anticancer agents – Synthesis and properties of analogues: A mini-review. *European Journal of Medicinal Chemistry* 156, pp. 13–20.

Du Plessis, L.H. et al. 2014. Formulation and evaluation of Pheroid vesicles containing mefloquine for the treatment of malaria. *Journal of Pharmacy and Pharmacology* 66(1), pp. 14–22.

Pontes, F.S.C. et al. 2018. Effect of 17-allylamino-17-demethoxygeldanamycin (17-AAG) on Akt protein expression is more effective in head and neck cancer cell lineages that retain PTEN protein expression. *Journal of Oral Pathology and Medicine* 47(3), pp. 253–259.

Press, O.W. et al. 2018. Bendamustine, etoposide, and dexamethasone to mobilize peripheral blood hematopoietic stem cells for autologous transplantation in non-Hodgkin lymphoma. *Blood Research* 53(3), p. 223.

Priolo, C. et al. 2015. Tuberous Sclerosis Complex 2 Loss Increases Lysophosphatidylcholine Synthesis in Lymphangioleiomyomatosis. *American Journal of Respiratory Cell and Molecular Biology* 53(1), pp. 33–41.

Prizant, H. and Hammes, S.R. 2016. Minireview: Lymphangioleiomyomatosis (LAM): The 'other' steroid-sensitive cancer. *Endocrinology* 157(9), pp. 3374–3383.

Pyrko, P. et al. 2007. HIV-1 protease inhibitors nelfinavir and atazanavir induce malignant glioma death by triggering endoplasmic reticulum stress. *Cancer Research* 67(22), pp. 10920–10928.

Qin, X. et al. 2016. 4E-BP1, a multifactor regulated multifunctional protein. *Cell Cycle* 15(6), pp. 781–786.

Rabenou, R.A. and Charles, H.W. 2015. Differentiation of Sporadic Versus Tuberous Sclerosis Complex–Associated Angiomyolipoma. *American Journal of Roentgenology* 205(2), pp. 292–301.

Rabito, M.J. and Kaye, A.D. 2014. Tuberous sclerosis complex: perioperative considerations. *The Ochsner journal* 14(2), pp. 229–39.

Radzikowska, E. et al. 2015a. Everolimus for renal angiomyolipoma in patients with tuberous sclerosis complex or sporadic lymphangioleiomyomatosis: extension of a randomized controlled trial. *Nephrology Dialysis Transplantation* 31(1), pp. 111–119.

Radzikowska, E. 2015. Lymphangioleiomyomatosis: New Treatment Perspectives. *Lung* 193(4), pp. 467–75.

von Ranke, F.M. et al. 2015. Tuberous Sclerosis Complex: State-of-the-Art Review with a Focus on Pulmonary Involvement. *Lung* , pp. 619–627.

Ri, M. et al. 2010. Bortezomib-resistant myeloma cell lines: a role for mutated PSMB5 in preventing the accumulation of unfolded proteins and fatal ER stress. *Leukemia* 24(8), pp. 1506–1512.

Ricci, C. et al. 2013. Cancer tissue engineering - new perspectives in understanding the biology of solid tumours - a critical review. *OA Tissue Engineering* 1(1).

Richardson, P.G. et al. 2003. A Phase 2 Study of Bortezomib in Relapsed, Refractory Myeloma. *New England Journal of Medicine* 348(26), pp. 2609–2617.

Richardson, P.G. et al. 2007. Extended follow-up of a phase 3 trial in relapsed multiple myeloma: final time-to-event results of the APEX trial. *Blood* 110(10), pp. 3557–3560.

Richardson, P.G. et al. 2011. Tanespimycin and bortezomib combination treatment in patients with relapsed or relapsed and refractory multiple myeloma: Results of a phase 1/2 study. *British Journal of Haematology* 153(6), pp. 729–740.

Riffkin, C.D. et al. 1996. Modulation of the Function of Human MDRl P-Glycoprotein by the Antimalarial Drug Mefloquine. *Science* 52(96), pp. 1545–1552.

Rijpma, S.R. et al. 2014. Atovaquone and quinine anti-malarials inhibit ATP binding cassette transporter activity. *Malaria Journal* 13(1), pp. 1–8.

Roach, E.S. et al. 1998. Tuberous sclerosis complex consensus conference: Revised clinical diagnostic criteria. *Journal of Child Neurology* 13(12), pp. 624–628.

Roccaro, A.M. et al. 2011. Bortezomib in the Treatment of Cancer. In: *Frontiers in Anti-Cancer Drug Discovery*. BENTHAM SCIENCE PUBLISHERS, pp. 273–283.

Rodrigues, D.A. et al. 2012. Esclerose tuberosa. *Anais Brasileiros de Dermatologia* 87(2), pp. 184–196.

Rogosnitzky, M. and Danks, R. 2011. Therapeutic potential of the biscoclaurine alkaloid, cepharanthine, for a range of clinical conditions. *Pharmacological Reports* 63(2), pp. 337–347.

Rojas, M. et al. 2015. An eIF2α-binding motif in protein phosphatase 1 subunit GADD34 and its viral orthologs is required to promote dephosphorylation of eIF2α. *Proceedings of the National Academy of Sciences* 112(27), pp. E3466–E3475.

Roscoe, J.A. et al. 2005. Effect of paroxetine hydrochloride (Paxil®) on fatigue and depression in breast cancer patients receiving chemotherapy. *Breast Cancer Research and Treatment* 89(3), pp. 243–249.

Rosset, C. et al. 2017. TSC1 and TSC2 gene mutations and their implications for treatment in tuberous sclerosis complex: A review. *Genetics and Molecular Biology* 40(1), pp. 69–79.

Roszkowski, M. et al. 1995. Surgical treatment of intraventricular tumors associated with tuberous sclerosis. *Child's Nervous System* 11(6), pp. 335–339.

Ruan, J. et al. 2011. Bortezomib Plus CHOP-Rituximab for Previously Untreated Diffuse Large B-Cell Lymphoma and Mantle Cell Lymphoma. *Journal of Clinical Oncology* 29(6), pp. 690–697.

Ryu, J.H. et al. 2006. The NHLBI Lymphangioleiomyomatosis Registry. *American Journal of Respiratory and Critical Care Medicine* 173(1), pp. 105–111.

Ryu, J.H. et al. 2012. Frequency of undiagnosed cystic lung disease in patients with sporadic renal angiomyolipomas. *Chest* 141(1), pp. 163–168.

Sadowski, K. et al. 2016. Management of side effects of mTOR inhibitors in tuberous sclerosis patients. *Pharmacological Reports* 68(3), pp. 536–542.

Sahin, M. 2012. Targeted treatment trials for tuberous sclerosis and autism: No longer a dream. *Current Opinion in Neurobiology* 22(5), pp. 895–901.

Sahin, M. et al. 2016. Advances and future directions for tuberous sclerosis complex research: Recommendations from the 2015 strategic planning conference. *Pediatric Neurology* 60(April), pp. 1–12.

Salido-Vallejo, R. et al. 2014. Current options for the treatment of facial angiofibromas. *Actas Dermo-Sifiliograficas* .

Samueli, S. et al. 2015. Tuberous Sclerosis Complex: new criteria for diagnostic work-up and management. *Wiener klinische Wochenschrift* .

Sancak, O. et al. 2005. Mutational analysis of the TSC1 and TSC2 genes in a diagnostic setting: genotype – phenotype correlations and comparison of diagnostic DNA techniques in Tuberous Sclerosis Complex. *European Journal of Human Genetics* 13(6), pp. 731–741.

Sancak, O. 2005. *Tuberous Sclerosis Complex: Mutations, Functions and*

Phenotypes.

Sancak, Y. et al. 2008. The Rag GTPases Bind Raptor and Mediate Amino Acid Signaling to mTORC1. *Science* 320(5882), pp. 1496–1501.

Sano, Y. et al. 2015. Rituximab-associated Progressive Multifocal Leukoencephalopathy Derived from Non-Hodgkin Lymphoma: Neuropathological Findings and Results of Mefloquine Treatment. *Internal Medicine* 54(8), pp. 965–970.

Sarbassov, D.D. et al. 2005a. Growing roles for the mTOR pathway. *Current Opinion in Cell Biology* 17(6), pp. 596–603.

Sarbassov, D.D. et al. 2005b. Phosphorylation and regulation of Akt/PKB by the rictor-mTOR complex. *Science* 307(5712), pp. 1098–1101.

Sarbassov, D.D. et al. 2006. Prolonged Rapamycin Treatment Inhibits mTORC2 Assembly and Akt/PKB. *Molecular Cell* 22(2), pp. 159–168.

Sasongko, T.H. et al. 2015. Rapamycin and its analogues (rapalogs) for Tuberous Sclerosis Complex-associated tumors: a systematic review on non-randomized studies using meta-analysis. *Orphanet journal of rare diseases* 10(1), p. 95.

Saxton, R.A. and Sabatini, D.M. 2017. mTOR Signaling in Growth, Metabolism, and Disease. *Cell* 168(6), pp. 960–976.

Schenk, E. et al. 2013. Phase I study of tanespimycin in combination with bortezomib in patients with advanced solid malignancies. *Investigational New Drugs* 31(5), pp. 1251–1256.

Schewe, D.M. and Aguirre-Ghiso, J.A. 2009. Inhibition of eIF2α Dephosphorylation maximizes bortezomib efficiency and eliminates quiescent multiple myeloma cells surviving proteasome inhibitor therapy. *Cancer Research* 69(4), pp. 1545–1552.

Schlagenhauf, P. et al. 2010. The position of mefloquine as a 21st century malaria chemoprophylaxis. *Malaria Journal* 9(1), p. 357.

Schlagenhauf, P. et al. 2011. Use of mefloquine in children - A review of dosage, pharmacokinetics and tolerability data. *Malaria Journal* 10, pp. 1–11.

Schönthal, A.H. 2012. Endoplasmic Reticulum Stress: Its Role in Disease and Novel Prospects for Therapy. *Scientifica* 2012, pp. 1–26.

Schönthal, A.H. et al. 2015. Quinoline-based antimalarial drugs: a novel class of autophagy inhibitors. *Neurosurgical Focus* 38(3), p. E12.

Schreiber, K.H. et al. 2015. Rapamycin-mediated mTORC2 inhibition is determined by the relative expression of FK506-binding proteins. *Aging Cell* 14(2), pp. 265–273.

Schröder, M. and Kaufman, R.J. 2005. ER stress and the unfolded protein response. *Mutation Research* 569(1–2), pp. 29–63.

Scott, C.L. et al. 2010. Control of HIF-1{alpha} and vascular signaling in fetal lung involves cross talk between mTORC1 and the FGF-10/FGFR2b/Spry2 airway branching periodicity clock. *American journal of physiology. Lung cellular and molecular physiology* 299(4), pp. L455–L471.

Sehn, L. et al. 2006. A phase II study of bortezomib in mantle cell lymphoma: the National Cancer Institute of Canada Clinical Trials Group trial IND.150. *Annals of Oncology* 18(1), pp. 116–121.

Seok, J.S. et al. 2018. Piperlongumine decreases cell proliferation and the expression of cell cycle-associated proteins by inhibiting Akt pathway in human lung cancer cells. *Food and Chemical Toxicology* 111, pp. 9–18.

Seubwai, W. et al. 2010. Cepharanthine exerts antitumor activity on cholangiocarcinoma by inhibiting NF-κB. *Cancer Science* 101(7), pp. 1590–1595.

Seyama, K. et al. 2016. Isolation of individual cellular components from lung tissues of patients with lymphangioleiomyomatosis. *American Journal of Physiology-Lung Cellular and Molecular Physiology* 310(10), pp. L899–L908.

Shao, Y.M. et al. 1997. Mutually co-operative interactions between modulators of p-glycoprotein. *Biochimica et Biophysica Acta - Molecular Basis of Disease* 1360(1), pp. 30–38.

Sharma, N. et al. 2012. Inhibition of autophagy and induction of breast cancer cell death by mefloquine, an antimalarial agent. *Cancer Letters* 326(2), pp. 143–154.

Shaw, R.J. et al. 2004. The tumor suppressor LKB1 kinase directly activates AMP-activated kinase and regulates apoptosis in response to energy stress. *Proceedings of the National Academy of Sciences* 101(10), pp. 3329–3335.

SHEPHERD, C.W. et al. 1991. Causes of Death in Patients With Tuberous Sclerosis. *Mayo Clinic Proceedings* 66(8), pp. 792–796.

Sheth, R.A. et al. 2016. Angiographic and volumetric effects of mammalian target of rapamycin inhibitors on angiomyolipomas in tuberous sclerosis. *World Journal of Radiology* 8(3), p. 308.

Shi, H. et al. 2011. Bortezomib, Bendamustine, and Rituximab in Patients With Relapsed or Refractory Follicular Lymphoma: The Phase II VERTICAL Study. In: *Journal of Clinical Oncology*., pp. 3389–3395.

Shichiri, Y. et al. 1994. INTRA-ARTERIAL INFUSION CHEMOTHERAPY IN COMBINATION WITH A BISCOCLAURINE ALKALOID, CEPHARANTHIN", TO TREAT BONE METASTASIS ARISING FROM RENAL CELL CARCINOMA. *International Journal of Urology* (1), pp. 349–351.

Shim, J.S. et al. 2012. Selective inhibition of HER2-positive breast cancer cells by the HIV protease inhibitor nelfinavir. *Journal of the National Cancer Institute* 104(20), pp. 1576–1590.

Shimobayashi, M. and Hall, M.N. 2016. Multiple amino acid sensing inputs to mTORC1. *Cell research* 26(1), pp. 7–20.

Shin, J.H. et al. 2012. Suppression of autophagy exacerbates Mefloquine-mediated cell death. *Neuroscience Letters* 515(2), pp. 162–167.

Shiraishi, N. et al. 1987. Effect of Bisbenzylisoquinoline (Biscoclaurine) Alkaloids on Multidrug Resistance in KB Human Cancer Cells Effect of Bisbenzylisoquinoline (Biscoclaurine) Alkaloids on Multidrug Resistance in KB Human Cancer Cells1., pp. 2413–2416.

Shiraishi, N. et al. 1988a. Potentiation by a Biscoclaurine Alkaloid, Cepharanthine, of the Toxicity of Conjugates of Epidermal Growth Factor with Pseudomonas Exotoxin in HeLa Cells. *Cancer Research*

Shiraishi, N. et al. 1988b. Potentiation by a Biscoclaurine Alkaloid, Cepharanthine, of the Toxicity of Conjugates of Epidermal Growth Factor with Pseudomonas Exotoxin in HeLa Cells. *Cancer Research* 48(5), pp. 1307–1311.

Shoji, T. et al. 2014. A phase II study of irinotecan and pegylated liposomal doxorubicin in platinum-resistant recurrent ovarian cancer (Tohoku Gynecologic Cancer Unit 104 study). *Cancer Chemotherapy and Pharmacology* 73(5), pp. 895–901.

Sierra, H. et al. 2015. Confocal imaging-guided laser ablation of basal cell

carcinomas: An ex vivo study. *Journal of Investigative Dermatology* 135(2), pp. 612–615.

Silverio, K.A. and Patel, S.A. 2015. Progressive Multifocal Leukoencephalopathy with Negative JC Virus PCR following Treatment of Follicular Lymphoma: Implications for Biologics in the Era of Targeted Cancer Therapy. *Case Reports in Oncological Medicine* 2015, pp. 1–6.

Singh, R. et al. 2009. Autophagy regulates lipid metabolism. *Nature* 458(7242), pp. 1131–1135.

Singhasivanon, V. et al. 1992. Pharmacokinetics of mefloquine in children aged 6 to 24 months. *European journal of drug metabolism and pharmacokinetics* 17(4), pp. 275–9.

Singhasivanon, V. et al. 1994. Pharmacokinetic study of mefloquine in Thai children aged 5-12 years suffering from uncomplicated falciparum malaria treated with MSP or MSP plus primaquine. *European Journal of Drug Metabolism and Pharmacokinetics* 19(1), pp. 27–32.

Siroky, B.J. et al. 2017. Improvement in Renal Cystic Disease of Tuberous Sclerosis Complex After Treatment with Mammalian Target of Rapamycin Inhibitor. *Journal of Pediatrics* 187, pp. 318-322.e2.

Smith, M.P. et al. 2016. Inhibiting Drivers of Non-mutational Drug Tolerance Is a Salvage Strategy for Targeted Melanoma Therapy. *Cancer Cell* 29(3), pp. 270–284.

Soprano, M. et al. 2016. Oxidative Stress Mediates the Antiproliferative Effects of Nelfinavir in Breast Cancer Cells. Wang, Y.-J. ed. *PLOS ONE* 11(6), p. e0155970.

Speer, T. et al. 2012. Novel Insights Into the Critical Role of Bradykinin and the Kinin B2 Receptor for Vascular Recruitment of Circulating Endothelial Repair–Promoting Mononuclear Cell Subsets. *Circulation* 127(5), pp. 594–603.

Spiliotis, M. et al. 2014. Treatment of echinococcosis: albendazole and mebendazole – what else? *Parasite* 21, p. 70.

Srinivas, R. V et al. 1998. Human immunodeficiency virus protease inhibitors serve as substrates for multidrug transporter proteins MDR1 and MRP1 but retain antiviral efficacy in cell lines expressing these transporters. *Antimicrobial agents and chemotherapy* 42(12), pp. 3157–62.

Staropoli, N. et al. 2014. Pegylated liposomal doxorubicin in the management of ovarian cancer: A systematic review and metaanalysis of randomized trials. *Cancer Biology and Therapy* 15(6), pp. 707–720.

Stearns, V. et al. 2000. A pilot trial assessing the efficacy of paroxetine hydrochloride (Paxil®) in controlling hot flashes in breast cancer survivors. *Annals of Oncology* 11(1), pp. 17–22.

Steketee, R.W. et al. 1996. Malaria parasite infection during pregnancy and at delivery in mother, placenta, and newborn: efficacy of chloroquine and mefloquine in rural Malawi. *The American journal of tropical medicine and hygiene* 55(1 Suppl), pp. 24–32.

Sulaimanov, N. et al. 2017. Understanding the mTOR signaling pathway via mathematical modeling. *Wiley Interdisciplinary Reviews: Systems Biology and Medicine* 9(4), p. e1379.

Sun, P. et al. 2012. Outcomes of resecting subependymal giant cell astrocytoma (SEGA) among patients with SEGA-related tuberous sclerosis complex: a national claims database analysis. *Current Medical Research and Opinion* 28(4), pp. 657–663.

Sun, Y. et al. 2014. Progesterone and Estradiol Synergistically Promote the Lung Metastasis of Tuberin-Deficient Cells in a Preclinical Model of Lymphangioleiomyomatosis. *Hormones and Cancer* 5(5), pp. 284–298.

Tabata, R. et al. 2012. Low dose cepharanthine ameliorates immune thrombocytopenic purpura associated with multiple myeloma. *International Immunopharmacology* 13(3), pp. 242–244.

Takahashi-Makise, N. et al. 2009. Biscoclaurine alkaloid cepharanthine inhibits the growth of primary effusion lymphoma in vitro and in vivo and induces apoptosis via suppression of the NF-κB pathway. *International Journal of Cancer* 125(6), pp. 1464–1472.

Tamatani, T. et al. 2007. Cepharanthin-enhanced radiosensitivity through the inhibition of radiation-induced nuclear factor-kappaB activity in human oral squamous cell carcinoma cells. *International journal of oncology* 31(4), pp. 761–768.

Tang, Z.H. of a novel autophagic inhibitor cepharanthine to enhance the anti-cancer

property of dacomitinib in non-small cell lung cancer et al. 2018. Identification of a novel autophagic inhibitor cepharanthine to enhance the anti-cancer property of dacomitinib in non-small cell lung cancer. *Cancer Letters* 412, pp. 1–9.

Tavares, M.R. et al. 2015. The S6K protein family in health and disease. *Life Sciences* 131, pp. 1–10.

Taveira-DaSilva, A.M. et al. 2004. Decline in lung function in patients with lymphangioleiomyomatosis treated with or without progesterone. *Chest* 126(6), pp. 1867–74.

Taveira-DaSilva, A.M. and Moss, J. 2015. Clinical features, epidemiology, and therapy of lymphangioleiomyomatosis. *Clinical epidemiology* 7, pp. 249–57.

Tee, A.R. et al. 2005. Analysis of mTOR signaling by the small G-proteins, Rheb and RhebL1. *FEBS Letters* 579(21), pp. 4763–4768.

Tee, A.R. et al. 2016. The role of mTOR signalling in neurogenesis, insights from tuberous sclerosis complex. *Seminars in Cell and Developmental Biology* 52, pp. 12–20.

Tian, X. et al. 2011. Modulation of CCAAT/enhancer binding protein homologous protein (CHOP)-dependent DR5 expression by nelfinavir sensitizes glioblastoma multiforme cells to tumor necrosis factor-related apoptosis-inducing ligand (TRAIL). *Journal of Biological Chemistry* 286(33), pp. 29408–29416.

Ting-Chao Chou 2010. Drug Combination Studies and Their Synergy Quantification Using the Chou-Talalay Method. *Cancer research* 17(7), pp. 635–54.

Tomita, T. et al. 2014. Therapeutic reference range for plasma concentrations of paroxetine in patients with major depressive disorders. *Therapeutic Drug Monitoring* 36(4), pp. 480–485.

Toovey, S. 2009. Mefloquine neurotoxicity: A literature review. *Travel Medicine and Infectious Disease* 7(1), pp. 2–6.

Travers, K.J. et al. 2000. Functional and Genomic Analyses Reveal an Essential Coordination between the Unfolded Protein Response and ER-Associated Degradation. *Cell* 101(3), pp. 249–258.

Trelinska, J. et al. 2015. Complications of mammalian target of rapamycin inhibitor anticancer treatment among patients with tuberous sclerosis complex are common

and occasionally life-threatening. *Anti-Cancer Drugs* 26(4), pp. 437–442.

Trelinska, J. et al. 2017. Maintenance therapy with everolimus for subependymal giant cell astrocytoma in patients with tuberous sclerosis (the EMINENTS study). *Pediatric Blood & Cancer* 64(6), p. e26347.

Treon, S.P. et al. 2007. Multicenter clinical trial of bortezomib in relapsed/refractory Waldenstrom's macroglobulinemia: Results of WMCTG trial 03-248. *Clinical Cancer Research* 13(11), pp. 3320–3325.

Tsai, J.D. et al. 2017. Effects of everolimus on tuberous sclerosis complex-associated renal angiomyolipoma: A preliminary report. *Nephrology* 22(12), pp. 1017–1022.

Tsuchihashi, K. et al. 2018. Metastatic esophageal carcinosarcoma comprising neuroendocrine carcinoma, squamous cell carcinoma, and sarcoma. *Medicine* 97(41), pp. 1–5.

Tsuru, A. et al. 2016. Novel mechanism of enhancing IRE1α-XBP1 signalling via the PERK-ATF4 pathway. *Scientific Reports* 6, pp. 1–8.

Tyburczy, M.E. et al. 2014. Sun exposure causes somatic second-hit mutations and angiofibroma development in tuberous sclerosis complex. *Human Molecular Genetics* 23(8), pp. 2023–2029.

Tyburczy, M.E. et al. 2015. Mosaic and Intronic Mutations in TSC1/TSC2 Explain the Majority of TSC Patients with No Mutation Identified by Conventional Testing. Korf, B. R. ed. *PLOS Genetics* 11(11), p. e1005637.

Ulanet, D.B. et al. 2014. Mesenchymal Phenotype Predisposes Lung Cancer Cells to Impaired Proliferation and Redox Stress in Response to Glutaminase Inhibition. Petronini, P. G. ed. *PLoS ONE* 9(12), p. e115144.

Urban, T. et al. 1999. Pulmonary lymphangioleiomyomatosis: A study of 69 patients. *Medicine* 78(5), pp. 321–337.

Valvezan, A.J. et al. 2017. Lysosomal regulation of cholesterol homeostasis in tuberous sclerosis complex is mediated *via* NPC1 and LDL-R. *Oncotarget* 8(24), pp. 38099–38112.

Vee, M. Le et al. 2015. Regulation of human hepatic drug transporter activity and expression by diesel exhaust particle extract. *PLoS ONE* 10(3).

Veiga, M.I. et al. 2010. Antimalarial Exposure Delays Plasmodium falciparum Intra-Erythrocytic Cycle and Drives Drug Transporter Genes Expression. Snounou, G. ed. *PLoS ONE* 5(8), p. e12408.

Vergès, B. and Cariou, B. 2015. mTOR inhibitors and diabetes. *Diabetes Research and Clinical Practice* , pp. 1–8.

Verma, S. and Radhakrishnan, R. 2011. Clinically Relevant Imaging in Tuberous Sclerosis. *Journal of Clinical Imaging Science* 1(1), p. 39.

de Vries, P. et al. 2015. Tuberous Sclerosis Associated Neuropsychiatric Disorders (TAND) and the TAND Checklist. *Pediatric Neurology* 52(1), pp. 25–35.

Walker, A.R. et al. 2013. Pharmacokinetics and dose escalation of the heat shock protein inhibitor 17-allyamino-17-demethoxygeldanamycin in combination with bortezomib in relapsed or refractory acute myeloid leukemia. *Leukemia and Lymphoma* 54(9), pp. 1996–2002.

Walker, C.L. et al. 2003. Transdominant suppression of estrogen receptor signaling by progesterone receptor ligands in uterine leiomyoma cells. *Molecular and Cellular Endocrinology* 196(1–2), pp. 11–20.

Wallington-Beddoe, C.T. et al. 2018. Resistance to proteasome inhibitors and other targeted therapies in myeloma. *British Journal of Haematology* 182(1), pp. 11–28.

Walter, P. and Johnson, A.E. 1994. Signal Sequence Recognition and Protein Targeting to the Endoplasmic Reticulum Membrane. *Annual Review of Cell Biology* 10, pp. 87–119.

Wan, Y. et al. 2014. Constitutive mTORC1 activation upregulates catalase and SODs in melanoma cells. *FASEB Journal* 28(1).

Wang, B. et al. 2018a. Trifluoperazine induces apoptosis through the upregulation of Bax/Bcl-2 and downregulated phosphorylation of AKT in mesangial cells and improves renal function in lupus nephritis mice. *International Journal of Molecular Medicine* 41(6), pp. 3278–3286.

Wang, X. et al. 2014. Increasing the cytotoxicity of doxorubicin in breast cancer MCF-7 cells with multidrug resistance using a mesoporous silica nanoparticle drug delivery system. *International journal of clinical and experimental pathology* 7(4), pp. 1337–47.

Wang, X. et al. 2018b. Successful cisplatin-etoposide chemotherapy-based treatment of a primary small cell neuroendocrine carcinoma of the tonsil with multiple metastases: A case report. *OncoTargets and Therapy* 11, pp. 5391–5395.

Wang, Y.Y. et al. 2017. Epilepsy may be the major risk factor of mental retardation in children with tuberous sclerosis: A retrospective cohort study. *Epilepsy and Behavior*.

Warncke, J.C. et al. 2017. Pediatric Renal Angiomyolipomas in Tuberous Sclerosis Complex. *Journal of Urology* 197(2), pp. 500–506.

Washington, C.B. et al. 1998. Interaction of anti-HIV protease inhibitors with the multidrug transporter P-glycoprotein (P-gp) in human cultured cells. *Journal of Acquired Immune Deficiency Syndromes and Human Retrovirology* 19(3), pp. 203–209.

Wataya-Kaneda, M. 2015. Mammalian target of rapamycin and tuberous sclerosis complex. *Journal of Dermatological Science* 79(2), pp. 93–100.

Wei, C.-C. et al. 2018. Trend of seizure remission in patients with tuberous sclerosis complex: A retrospective medical review. *Journal of the Chinese Medical Association* 81(8), pp. 724–728.

Weidman, D.R. et al. 2015. Dose-level response rates of mtor inhibition in tuberous sclerosis complex (TSC) related subependymal giant cell astrocytoma (SEGA). *Pediatric Blood and Cancer* 62(10), pp. 1754–1760.

White, M.C. et al. 2018. HRI-mediated translational repression reduces proteotoxicity and sensitivity to bortezomib in human pancreatic cancer cells. *Oncogene* 37(32), pp. 4413–4427.

Williams, A.T. et al. 2007. Genotype/phenotype correlation in 325 individuals referred for a diagnosis of tuberous sclerosis complex in the United States. *Genetics in Medicine* 9(2), pp. 88–100.

Williams, M.E. et al. 2017. Utility of the Autism Observation Scale for Infants in Early Identification of Autism in Tuberous Sclerosis Complex. *Pediatric Neurology* 75, pp. 80–86.

Wilson, J.M. et al. 2016. ARCII: A phase II trial of the HIV protease inhibitor Nelfinavir in combination with chemoradiation for locally advanced inoperable pancreatic cancer. *Radiotherapy and Oncology* 119(2), pp. 306–311.

Wong, P.-M. et al. 2015. Regulation of autophagy by coordinated action of mTORC1 and protein phosphatase 2A. *Nature communications* 6(1), p. 8048.

Wong, W. et al. 2017. Mefloquine targets the Plasmodium falciparum 80S ribosome to inhibit protein synthesis. *Nature Microbiology* 2(March), p. 17031.

Woods, A. et al. 2003. LKB1 Is the Upstream Kinase in the AMP-Activated Protein Kinase Cascade. *Current Biology* 13(22), pp. 2004–2008.

Workman, P. et al. 2002. Gene expression profiling of human colon cancer cells following inhibition of signal transduction by 17-allylamino-17-demethoxygeldanamycin, an inhibitor of the hsp90 molecular chaperone. *Oncogene* 19(36), pp. 4125–4133.

Wu, J. et al. 2002. Modes of activation of mitogen-activated protein kinases and their roles in cepharanthine-induced apoptosis in human leukemia cells. *Cellular Signalling* 14(6), pp. 509–515.

Wu, N. et al. 2013. AMPK-Dependent Degradation of TXNIP upon Energy Stress Leads to Enhanced Glucose Uptake via GLUT1. *Molecular Cell* 49(6), pp. 1167–1175.

Wu, S.-K. et al. 2014. Short-time focused ultrasound hyperthermia enhances liposomal doxorubicin delivery and antitumor efficacy for brain metastasis of breast cancer. *International journal of nanomedicine* 9, pp. 4485–94.

Wu, S. et al. 2018a. Chelerythrine induced cell death through ROS-dependent ER stress in human prostate cancer cells. *OncoTargets and Therapy* 11, pp. 2593–2601.

Wu, Y.-H. et al. 2018b. Bortezomib enhances radiosensitivity in oral cancer through inducing autophagy-mediated TRAF6 oncoprotein degradation. *Journal of Experimental & Clinical Cancer Research* 37(1), p. 91.

Xiang, Y. et al. 2015. Targeted inhibition of tumor-specific glutaminase diminishes cell-autonomous tumorigenesis. *Journal of Clinical Investigation* 125(6), pp. 2293–2306.

Xiao, S.H. 2013. Mefloquine, a new type of compound against schistosomes and other helminthes in experimental studies. *Parasitology Research* 112(11), pp. 3723–3740.

Xing, M. et al. 2015. Efficacy and Cardiotoxicity of Liposomal Doxorubicin-Based Chemotherapy in Advanced Breast Cancer: A Meta-Analysis of Ten Randomized Controlled Trials. Lee, J. W. ed. *PLOS ONE* 10(7), p. e0133569.

Xiong, J. et al. 2018. Piperlongumine Induces Apoptosis in Human Melanoma Cells Via Reactive Oxygen Species Mediated Mitochondria Disruption. *Nutrition and Cancer* 70(3), pp. 502–511.

Xu, W.-H. et al. 2012. Doxorubicin-mediated radiosensitivity in multicellular spheroids from a lung cancer cell line is enhanced by composite micelle encapsulation. *International journal of nanomedicine* 7, pp. 2661–71.

Yamaguchi, H. and Wang, H.G. 2004. CHOP is involved in endoplasmic reticulum stress-induced apoptosis by enhancing DR5 expression in human carcinoma cells. *Journal of Biological Chemistry* 279(44), pp. 45495–45502.

Yamaguchi, Y. et al. 2018. Piperlongumine rapidly induces the death of human pancreatic cancer cells mainly through the induction of ferroptosis. *International Journal of Oncology* 52(3), pp. 1011–1022.

Yan, K.H. et al. 2013. Mefloquine exerts anticancer activity in prostate cancer cells via ROS-mediated modulation of Akt, ERK, JNK and AMPK signaling. *Oncology Letters* 5(5), pp. 1541–1545.

Yang, C.-Y. et al. 2015. Interleukin-4 receptor-targeted liposomal doxorubicin as a model for enhancing cellular uptake and antitumor efficacy in murine colorectal cancer. *Cancer Biology & Therapy* 16(11), pp. 1641–1650.

Yang, F. et al. 2018. Uncoupling of ER/Mitochondrial Oxidative Stress in mTORC1 Hyperactivation-Associated Skin Hypopigmentation. *Journal of Investigative Dermatology* 138(3), pp. 669–678.

Yang, Y. et al. 2017. Transcription factor C/EBP homologous protein in health and diseases. *Frontiers in Immunology* 8(NOV).

Yasukawa, K. et al. 1991. Cepharanthine inhibits two-stage tumor promotion by 12-O-tetradecanoylphorbol 13-acetate and mezerein on skin tumor formation in mice initiated with 7,12-dimethylbenz[a]anthracene. *Journal of Cancer Research and Clinical Oncology* 117(5), pp. 421–424.

Yeh, C.-T. et al. 2012. Trifluoperazine, an Antipsychotic Agent, Inhibits Cancer Stem Cell Growth and Overcomes Drug Resistance of Lung Cancer. *American Journal of*

Respiratory and Critical Care Medicine 186(11), pp. 1180–1188.

Yoshida, H. et al. 2014. Significant improvement following combination treatment with mefloquine and mirtazapine in a patient with progressive multifocal leukoencephalopathy after allogeneic peripheral blood stem cell transplantation. *International Journal of Hematology* 99(1), pp. 95–99.

Yu, J. et al. 2001. Chromosome 16 loss of heterozygosity in tuberous sclerosis and sporadic lymphangiomyomatosis. *American Journal of Respiratory and Critical Care Medicine* 164(8 I), pp. 1537–1540.

Yusenko, M. et al. 2018. A novel cell-based screening assay for small-molecule MYB inhibitors identifies podophyllotoxins teniposide and etoposide as inhibitors of MYB activity. *Scientific Reports* 8(1).

Zahedi, P. et al. 2011. Combination Drug Delivery Strategy for the Treatment of Multidrug Resistant Ovarian Cancer. *Molecular Pharmaceutics* 8(1), pp. 260–269.

Zech, R. et al. 2016. Structure of the tuberous sclerosis complex 2 (TSC2) N Terminus provides insight into complex assembly and tuberous sclerosis pathogenesis. *Journal of Biological Chemistry* 291(38), pp. 20008–20020.

Zeng, L.H. et al. 2011. Tsc2 gene inactivation causes a more severe epilepsy phenotype than Tsc1 inactivation in a mouse model of Tuberous Sclerosis Complex. *Human Molecular Genetics* 20(3), pp. 445–454.

Zeynali-Moghaddam, S. et al. 2019. A molecular basis for the synergy between 17-allylamino-17-demethoxy geldanamycin with Capecitabine and Irinotecan in human colorectal cancer cells through VEFG and MMP-9 gene expression. *Gene* 684, pp. 30–38.

Zhang, K.E. et al. 2001. Circulating metabolites of the human immunodeficiency virus protease inhibitor nelfinavir in humans: structural identification, levels in plasma, and antiviral activities. *Antimicrobial agents and chemotherapy* 45(4), pp. 1086–93.

Zhang, L. et al. 2015. Hypoxia-inducible factor-1a contributes to dendritic overgrowth in tuberous sclerosis. *Neuroscience Letters* 612, pp. 43–47.

Zhang, X. et al. 2017. Trifluoperazine, a novel autophagy inhibitor, increases radiosensitivity in glioblastoma by impairing homologous recombination. *Journal of Experimental and Clinical Cancer Research* 36(1).

Zhang, Y. et al. 2014. Coordinated regulation of protein synthesis and degradation by mTORC1. *Nature* 513(7518), pp. 440–3.

Zheng, H.-Y. et al. 2018. 17-(Allylamino)-17-Demethoxygeldanamycin Enhances Etoposide-Induced Cytotoxicity via the Downregulation of Xeroderma Pigmentosum Complementation Group C Expression in Human Lung Squamous Cell Carcinoma Cells. *Pharmacology* 102(1–2), pp. 91–104.

Zhou, L. et al. 2018. Luteolin attenuates Wnt signaling via upregulation of FZD6 to suppress prostate cancer stemness revealed by comparative proteomics. *Scientific Reports* 8(1).

Zhou, P. et al. 2017. Cepharanthine hydrochloride reverses the mdr1 (P-glycoprotein) - mediated esophageal squamous cell carcinoma cell cisplatin resistance through JNK and p53 signals. 8(67), pp. 111144–111160.

Zhu, Q. et al. 2017a. Cepharanthine exerts antitumor activity on choroidal melanoma by reactive oxygen species production and c-Jun N-terminal kinase activation. *Oncology Letters* 13(5), pp. 3760–3766.

Zhu, Y. et al. 2017b. Chelerythrine Inhibits Human Hepatocellular Carcinoma Metastasis *in Vitro*. *Biological & Pharmaceutical BulletinBiological and Pharmaceutical Bulletin* 41(1), pp. 36–46.

Zimmermann, S.C. et al. 2016. Combination therapy with BPTES nanoparticles and metformin targets the metabolic heterogeneity of pancreatic cancer. *Proceedings of the National Academy of Sciences* 113(36), pp. E5328–E5336.

Zordan, P. et al. 2018. Tuberous sclerosis complex – associated CNS abnormalities depend on hyperactivation of mTORC1 and Akt Find the latest version : Tuberous sclerosis complex – associated CNS abnormalities depend on hyperactivation of mTORC1 and Akt. 128(4), pp. 1688–1706.

Zúñiga, M. et al. 2004. Degradation of Proteins from the ER of S. cerevisiae Requires an Intact Unfolded Protein Response Pathway. *Molecular Cell* 5(4), pp. 729–735.

Zuo, Q. et al. 2018. The dietary flavone luteolin epigenetically activates the Nrf2 pathway and blocks cell transformation in human colorectal cancer HCT116 cells. *Journal of Cellular Biochemistry* 119(11), pp. 9573–9582.